DOCTORAL THESIS

Properties of Hyperon Decays

Author:
Nora SALONE

Supervisor:
Andrzej KUPSC
Auxiliary supervisor:
Varvara BATOZSKAYA

A thesis submitted in fulfillment of the requirements
for the degree of Doctor of Philosophy

in the

NATIONAL
CENTRE
FOR NUCLEAR
RESEARCH
ŚWIERK

June 12, 2024

Declaration of Authorship

I, Nora SALONE, declare that this thesis titled, "Properties of Hyperon Decays" and the work presented in it are my own. I confirm that:

- This work was done wholly or mainly while in candidature for a research degree at the National Centre for Nuclear Research.

- Where any part of this thesis has previously been submitted for a degree or any other qualification at the National Centre for Nuclear Research or any other institution, this has been clearly stated.

- Where I have consulted the published work of others, this is always clearly attributed.

- Where I have quoted from the work of others, the source is always given. With the exception of such quotations, this thesis is entirely my own work.

- I have acknowledged all main sources of help.

- Where the thesis is based on work done by myself jointly with others, I have made clear exactly what was done by others and what I have contributed myself.

Signed:

_____

Date:

_____

NATIONAL CENTRE FOR NUCLEAR RESEARCH

Abstract

Properties of Hyperon Decays

Nora SALONE

Hyperons – bound states made of the three lightest quark flavors – play a significant role in our quest to understand the composition of matter. At low energies, where perturbative Quantum Chromodynamics breaks down, baryon interactions are dominated by forces keeping the quarks confined within the hadronic boundary. Hyperons, owing to their similarities to protons and neutrons, offer complementary information on the structure of matter, which can be probed via electromagnetic interaction. On another note, the observed baryonic asymmetry in the Universe has not been explained by the CP violation mechanism assumed in the Standard Model. Strange baryons offer a unique insight into new CP violation effects investigated in this thesis through weak nonleptonic decays.

At electron–positron colliders, hyperon–antihyperon pairs are copiously produced in vector charmonia decays in an inherently polarized state. We study the case where both baryons transition to fully hadronic final states, where the interference of the parity-conserving and parity-violating amplitudes results in an anisotropic distribution of the daughter particles. The related decay asymmetry parameters and the polarization observables can be extracted from the joint angular distribution of the final decay products. Using the spin-correlation terms within the pair, the baryon and antibaryon asymmetries are simultaneously measured, making these observables excellent candidates for testing CP symmetry.

This work presents a feasibility study of CP-violation tests for hyperon pairs produced in an electron–positron collider with a longitudinally polarized electron beam. The information from the production process with this new assumption is encoded in a "production matrix" and successively modified to account for the nonleptonic decays of the pair. Uncertainties of the CP-violation observables built on the decay asymmetries are parametrized in terms of the spin-polarization observables and extracted using an asymptotic maximum likelihood method. It is shown how the uncertainties are reduced in the presence of the beam polarization, identifying hyperon nonleptonic decays as a CP-violation source complementary to the kaon sector.

The spin-entanglement and polarization properties of the produced hyperons are further studied in the semileptonic decays of the pair. The same modular framework is used to derive the "decay matrix" describing a baryon semileptonic transition in a general way. Parameters related to the semileptonic form factors are defined, and their statistical uncertainties are also extracted using the asymptotic maximum likelihood method. The uncertainties depend on the initial baryon polarization and the spin-correlation properties within the produced pair. This dependence on the spin-polarization observables is shown, and the impact of the variables is compared for different semileptonic decays. In parallel, the modular framework is applied to radiative and Dalitz decays of spin-1/2 baryons to obtain their decay matrices.

Streszczenie

Properties of Hyperon Decays

Nora SALONE

Hiperony – hadrony zbudowane z trzech najlżejszych kwarków – odgrywają ważną rolę w naszych próbach zrozumienia struktury materii. Przy niskich energiach nie można opisać oddziaływań silnych przy pomocy rachunku zaburzeń i są one zdominowane przez siły utrzymujące kwarki wewnątrz hadronów. Hiperony, ze względu na ich podobieństwo do protonów i neutronów, mogą uzupełnić naszą wiedzę na temat oddziaływań elektromagnetycznych z materią. Dodatkowo, słabe rozpady hiperonów dają wgląd w mechanizmy naruszenia symetrii CP. Jest to niesłychanie ważne, ponieważ mechanizm łamania CP w Modelu Standardowym jest niewystarczający do wyjaśnienia obserwowanej asymetrii pomiędzy materią i antymaterią we Wszechświecie.

Zderzacze elektronowo-pozytonowych umożliwiają produkcję spinowo spolaryzowanych par hiperon-antyhiperon z dużą częstością w rozpadach charmonium. W słabych hadronowych rozpadach hiperonów interferencja pomiędzy amplitudami dla przejścia zachowującego i dla przejścia naruszającego parzystość prowadzi do niejednorodnego rozkładu cząstek wtórnych. Te rozkłady są opisywane poprzez parametr asymetrii rozpadu oraz parametr rotacji wektora polaryzacji. Polaryzacja oraz korelacja pomiędzy spinami w parze hiperon-antyhiperon pozwala na precyzyjne testy symetrii CP w jednym eksperymencie.

W niniejszej pracy zbadano możliwość przeprowadzenia testów naruszenia CP dla par hiperon-antyhiperon produkowanych w zderzaczach elektron-pozyton ze spolaryzowaną podłużnie wiązką elektronów. Informacja o stanie spinowym w procesie produkcji jest reprezentowana poprzez "macierz produkcji" która jest następnie mnożna poprzez macierze reprezentujące rozpady hiperonu i anty hiperonu.

Błędy parametrów opisujących naruszenie symetrii CP zbudowanych w oparciu o parametry rozpadu słabego są opisane wykorzystując asymptotyczne metody rachunku prawdopodobieństwa. Pozwoliło to na ustaleniu jak błędy statystyczne zmieniają się w zależności od polaryzacji wiązki.

Polaryzacja i korelacje spinowe mogą być także wykorzystane w badaniach rozpadów półleptonowych. Do opisu procesu w podejściu modułowym konieczne jest wyprowadzenia odpowiednich "macierzy rozpadu" zależnych od parametrów związanych z form faktorami półleptonowymi. Niepewności pomiarowe tych parametrów wyznaczyliśmy także przy użyciu asymptotycznych metod statystycznych. Niepewności te zależą od początkowej polaryzacji barionów i od korelacji spinowych pomiędzy hiperonem i antyhiperonem.

Wyznaczyliśmy zależność błędów od tych zmiennych dla różnych rozpadów półleptonowych. Ponadto wyprowadziliśmy w podejściu modułowym ogólne wzory opisujące rozpady radiacyjne i rozpady Dalitza barionów o spinie 1/2.

Acknowledgements

I would like to express my thanks to my supervisor, Andrzej Kupść, for giving me the opportunity to further my studies through different interesting projects, for the fruitful discussions and profound physics knowledge he offered during these years.

I am grateful to my co-supervisor, Varvara Batozskaya, for being a local guide in everything Polish, from navigating through Warsaw to overcoming the language barrier: the first years of my PhD would have been much more difficult without her presence.

Grazie ai miei nonni, Maria e Michele, per il supporto incondizionato a distanza, e a mia zia Robi, per essermi venuta a trovare e per gli immancabili bentornati a base di pizza.

Ai miei genitori, Carlo e Ilaria, per avermi permesso di raggiungere questo obiettivo: non ce l'avrei mai fatta senza il vostro tifo e la vostra expertise accademica. Alle mie sorelle, Bianca ed Emma, per avermi fatta ridere innumerevoli volte, annullando la separazione geografica.

Infine, grazie a Enrico, per riempire le mie giornate e accompagnarmi dovunque, a ogni passo: questa vita sarebbe grigia, senza te al mio fianco.

Contents

*To my family, perché alla fine siamo sempre evvvribbadi töcccinsema,
in un modo o nell'altro*

1

Hyperon phenomenology

In this chapter, I give an introductory account of the main topic of this work, the hyperons. The following presentation assumes the reader has a basic knowledge of particle physics and related mathematical concepts from group theory and quantum field theory. For example, the description of special unitary group, renormalization, or hadronic state will not be given: for details, see e.g. Refs. [1–3].

Most of the visible mass in our Universe is composed of stable nuclei, which in turn are composed of nucleons – bound states of quarks – i.e. protons and neutrons. The Standard Model (SM) describes quark interactions in different energy regimes, understood to a varying degree. In particular, to investigate the structure of matter it is vital to understand hadronic interactions in the regime of confinement, where perturbative Quantum Chromodynamics (QCD) breaks down. Furthermore, the experimental evidence of baryonic asymmetry in our Universe is not fully accounted for by the Charge-conjugation and Parity (CP) violation mechanism formulated in the SM.

Hyperon decays offer a unique insight into a better understanding of the formation of matter. On the one hand, neglecting the mass difference between the three lightest quarks endows QCD with an approximate *SU(3)* flavor symmetry. This implies that hyperons can be obtained from nucleons via the quark flavor replacement u, $d \leftrightarrow s$. The concept of flavor is briefly presented in Section 1.1.1, and is followed by a categorization of composite particles based on their quark flavor content. Section 1.1.2 presents an overview of the strong interaction and other forces in which quarks participate.

The close relation between hyperons and the components of nuclei makes them ideal candidates to supply complementary information about the structure of matter. This is achieved by the extraction of space-like form factors, in processes where baryons are probed via electromagnetic (EM) interaction. Additional insights can be extracted from hyperon time-like form factors (FFs), investigated via electron–positron annihilation into hyperon–antihyperon pairs. When the complex-valued time-like FFs overlap, the result is an inherent polarization of the produced particles. Hyperon FFs, as well as their relation to baryon polarization in the production process, are illustrated in more detail in Section 1.1.3 and in the first part of

Section 1.2.

On the other hand, the polarization is measured via the anisotropic distribution of the final-state particles, via the "self-analyzing" hyperon nonleptonic decays. The resulting decay asymmetry can be defined for both particle and antiparticle and is therefore used to define tests of direct CP violation in the hyperon sector (see Sections 1.3.1, 1.3.2).

1.1 Strange baryons and their interactions

1.1.1 Quark model

Many studies about the "strange" particles have been conducted since their first detection in 1947 (Fig. 1.1). The findings by Rochester and Butler [4] were quickly followed by Powell
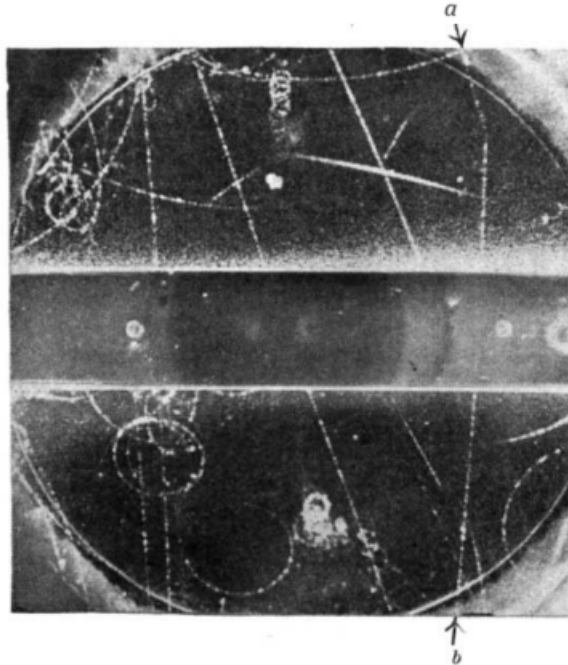
FIGURE 1.1: Early cloud chamber picture of strange particle tracks, where track a (later identified with kaon K^+) decays into the dilepton $\mu^+ + \nu_\mu$ (track b) [4].

[5] and Anderson [6] in observing an unexpected "V" shape in the spatial arrangement of the decay products. We now identify the lighter particles with the kaons and the heavier ones with the hyperons. Later experiments highlighted a peculiar behavior in these particles: they appeared to be produced in very fast processes, with time scales around 10^{-23} s, and to decay with longer lifetimes in the range of 10^{-10} s – as remarked by Pais [7]. Gell-Mann [8] along with Nakano and Nishima [9] developed this "strangeness" into the eponymous quantum number S. To be compatible with experimental observations, the strange particles – always produced in pairs – were assigned opposite values of S, while every other known baryon or lepton had $S = 0$.

At that time, an *SU(2) isospin* symmetry, based on the similar features of the neutron and the proton, had already been proposed. The strangeness quantum number was included in this pattern, generalizing it to a *SU(3) flavor* symmetry. These concepts were the basis for the Eightfold Way by Gell-Mann and Ne'eman [10–12], which finally developed into the quark model by Zweig [13] and, independently, by Gell-Mann [14]. This provided a theory that classified all known hadrons as rearrangements of three elementary "quarks" via their flavor label: *u*-up, *d*-down, and *s*-strange. At present, we know that quarks come in three additional flavors, *c*-charm, *b*-bottom, and *t*-top; given the topic of this thesis, I will restrict the discussion to the three lightest quark flavors.

Historically, the motivation behind the *SU(2)* symmetry lies in the phenomenological findings about the nuclear force, which appeared to be approximately independent of the electric charge. Due to their similar masses, the proton and neutron were thought of as components of an $I = 1/2$ isospin doublet, i.e. "spin-up" ($I_3 = 1/2$) and "spin-down" ($I_3 = -1/2$) states of the *nucleon* in analogy to the spin-1/2 algebra [2]. The inclusion of an additional quark flavor results in the aforementioned *SU(3)* group structure, where the isospin doublet role is assigned to *u* and *d*, while *s* is an isospin singlet of $I_3 = 0$.

In group theory, one can identify a subset of simultaneously diagonalizable generators of a group, which may be represented by a set of matrices. Simultaneous eigenstates may be arranged in an *irreducible* representation of the group, i.e. in a group of matrices that cannot be "reduced" to a block-diagonal shape. These eigenstates can be displayed in a *weight* diagram, label of a given representation, of dimension equal to the number of commuting generators. In the case of *SU(3)*, the weight diagrams are planar, since there are two such generators: the hypercharge Y and the third component of isospin I_3. They are defined as

$$Y = \mathcal{B} + S = \frac{N_u + N_d - 2N_s}{3}, \quad I_3 = Q - \frac{Y}{2} = \frac{N_u - N_d}{2} . \tag{1.1}$$

The above combinations of N_{flavor} reflect the isospin assignments to *u, d* and *s*. In addition, I_3 and Y are linked to the electrical charge Q, baryon number $\mathcal{B}$ and strangeness S. Quark electric charges are fractional, distributed in a way that results in a net integer charge for any hadron. S is assigned to be $S = -1$ for any *s* quark present, and $S = 1$ for any $\bar{s}$. It is conventional to attribute $\mathcal{B} = 1$ to any baryon, and $\mathcal{B} = -1$ to any antibaryon: since these are qqq bound states, it follows that any (anti)quark has $\mathcal{B} = (-)1/3$. This prescription indicates whether a given particle is a baryon. For example, bound states of $q\bar{q}$, the so-called mesons, have baryon number $\mathcal{B} = 0 = 1/3 - 1/3$; the same goes for any non-quark lepton (electrons, neutrinos, etc.).

Before presenting the relevant quark combinations following from the simple three-flavor quark model, some remarks about spin and parity are in order, as they will serve as additional labels of the particle states. For any bound state, the total angular momentum $\vec{J}$ is from the composition of orbital angular momentum $\vec{L}$ and spin $\vec{S}$. Quarks are spin-1/2 particles obeying the Fermi statistics. Therefore, the possible spin configurations for ground-state mesons and baryons are $J = 0$ and $J = 1/2, 3/2$, respectively. For completeness, I also include the vector meson resonances of $J = 1$.

These states may also be categorized using their behavior under the *parity* transformation P, the inversion of the spatial coordinates. Conventionally, the parity eigenvalues for the relevant quarks are

$$P_u \equiv P_d \equiv P_s = 1 \ . \tag{1.2}$$

Under such a prescription, the parity assignments for the lowest-lying mesons and baryons are

$$P_{\text{meson}} = P_q P_{\bar{q}} (-1)^{L_{12}} = -1, \ P_{\text{baryon}} = P_q P_q P_q (-1)^{L_{12}} (-1)^{L_3} = 1 \tag{1.3}$$

with inter-quark orbital angular momenta $L_{12} = L_3 = 0$. Finally, some nomenclature: under a Lorentz transformation, a spin-1 particle behaves like a Lorentz *vector*, hence the name. A spin-0 particle is described by a Lorentz-invariant structure, hence it is called *scalar*; if its intrinsic parity is negative, it is a *pseudoscalar*.

The lightest mesons made of u, d, and s quarks may be organized into the $J^P = 0^-$ pseudoscalar and $J^P = 1^-$ vector nonets according to their minimal quark content and quantum numbers, depicted in Fig. 1.2. A similar diagram may be obtained for the three-flavor qqq
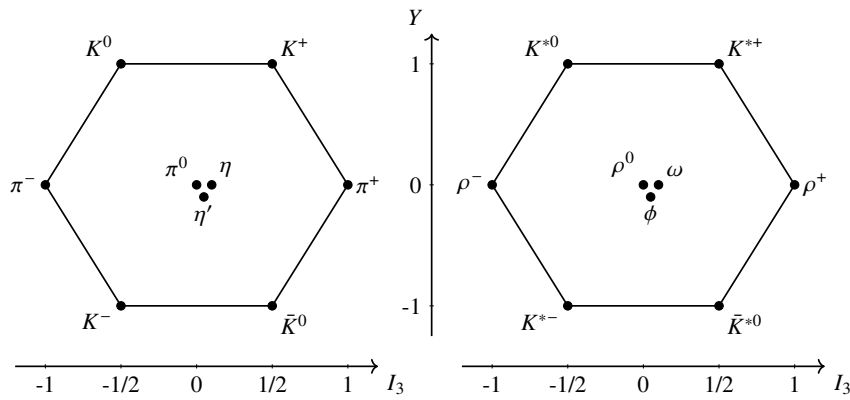

FIGURE 1.2: Weight diagrams for the pseudoscalar (left) and vector (right) meson nonets, in terms of isospin I_3 and hypercharge Y.

configuration: the resulting particles are organized into the $J^P = \frac{1}{2}^+$ baryon octet in Fig. 1.3.
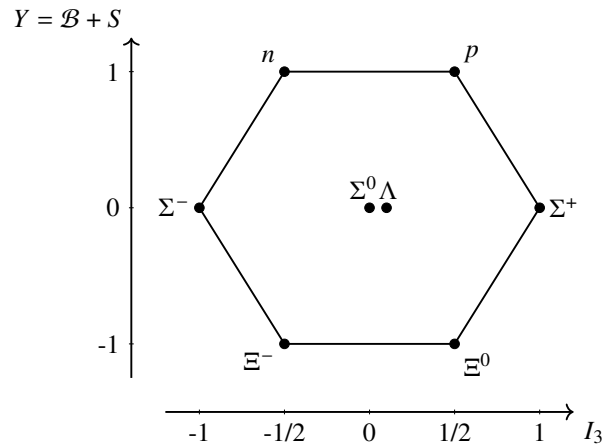

FIGURE 1.3: Weight diagram for the $J^P = \frac{1}{2}^+$ baryon octet.

As quarks are fermions, they must obey the Pauli exclusion principle [15] also within the confinements of baryons, and be described by a totally antisymmetric wavefunction: this must be true for any quark flavor combination. In principle, Gell-Mann and Zweig [13] predicted baryons of equal-flavor quarks: these states are naturally symmetric under $SU(3)_{\text{flavor}}$. In addition, any ground state, i.e. lowest-lying $L = 0$ state, would also be symmetric under spatial inversion. This implies that a ground-state baryon cannot have quarks in a spin-aligned configuration, i.e. with total spin $J = \frac{3}{2}$. This conclusion was challenged by the discovery of the $\Delta^{++}(uuu)$ resonance in proton-pion scattering [6], and of the triply-strange $\Omega^-(sss)$ state [16]. These same-flavor ground-state baryons with spin-parity $\frac{3}{2}^+$ seemed to be totally symmetric under the exchange of any two quarks.

The solution proposed shortly thereafter [17–19] addressed the apparent violation of the Pauli principle and was also the reason behind the naming of Quantum "Chromo" Dynamics: the *color* charge. Each quark possesses a distinct color charge, *r*-red, *b*-blue, or *g*-green – the combination of which gives white, i.e. a colorless hadron. A proper antisymmetric combination of the three color charges, included in the total wavefunction, restores the correct fermionic statistics of baryons. A visual representation of the lowest-lying spin-$\frac{3}{2}^+$ baryon decuplet, including the mentioned Δ^{++} and Ω^-, is presented in Fig. 1.4.
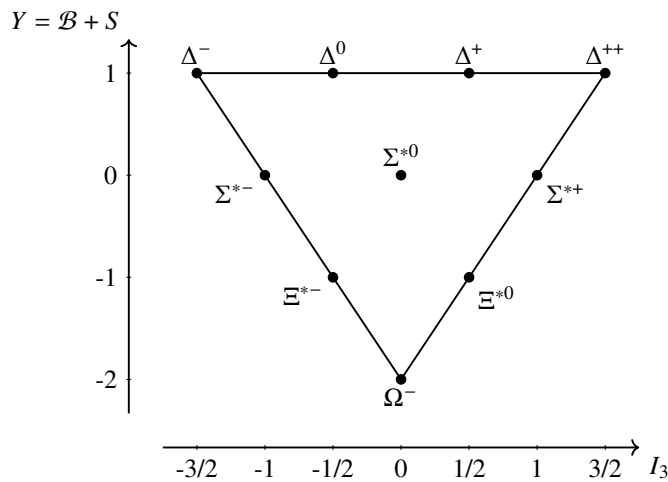
FIGURE 1.4: Weight diagram for the $J^P = \frac{3}{2}^+$ baryon decuplet.

1.1.2 The Standard Model

The study of hyperons is motivated by our inability to directly observe interactions within and between composite particles like the strange baryons. We understand the elementary components of hadrons and their dynamics as asymptotically free particles, i.e. in the higher region of the energy spectrum. However, the same level of insight has not been reached for the mutual interaction of quark bound states at lower energies. In this work, hyperons will be studied in the low-energy regime, irrespective of the underlying quark dynamics: however, it is still worthwhile to present the theories governing quark–quark interactions. For more detail, I refer to Refs. [3, 20], and many other introductory textbooks on quantum field theory.

The previous section includes some examples of how the constituent quarks may be combined to form hadronic structures. In addition to *u, d, s*, quarks may come in three heavier flavors: as a whole, they are arranged in "generations" according to Fig. 1.5. Within the
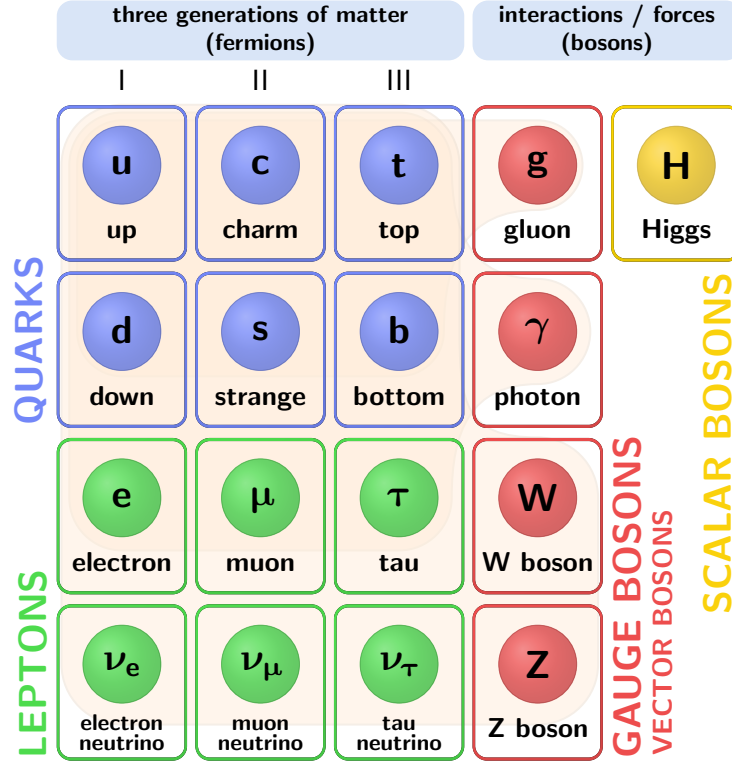
FIGURE 1.5: Elementary particles in the Standard Model of Particles (SM) – picture created with open-source code by I. Neutelings.

hadrons, quarks are "glued" together by spin-1 massless mediators of the strong interaction, the so-called gluons. The Lagrangian describing quark-gluon interactions is

$$\mathcal{L}_{\text{QCD}} = -\frac{1}{4} \overbrace{\left(\partial_\mu A^a_\nu - \partial_\nu A^a_\mu + g f^{abd} A^b_\mu A^d_\nu \right)}^{G^a_{\mu\nu}} G^{\mu\nu}_a \tag{1.4}$$
$$+ \bar{q}_{cfs} \left(i(\gamma_\mu)_{ss'}(\delta_{cc'}\partial^\mu - ig A^\mu_a (t^a)_{cc'}) - \delta_{cc'}\delta_{ss'} m_f \right) q_{c'f's'} \,,$$

where color, flavor, and spinor indices (*c, f* and *s*, respectively) have been written explicitly. The remaining Latin indices label the underlying *SU(3)* color symmetry, appearing in the structure constant f^{abd} and in the generators t^a. Sums over repeated indices are assumed, running over the spinor components $s = 1, ..., 4$, the number of flavors $f = 1, ...6$, the color charges $c = 1, 2, 3$, and the group generators $a = 1, ..., 8$.

The non-Abelian (non-commutative) nature of this theory is highlighted by the $g f^{abd} A^b_\mu A^d_\nu$ term, representing gluon self-interaction. This has deep implications: on the one hand, it clarifies how baryons are described as having three *valence* quarks, immersed in a sea of

continuously created and annihilated quark–antiquark pairs. On the other hand, in the process of renormalizing the gluon propagator, higher-order graphs with four-gluon vertices balance the contributions of fermionic (quark-quark-gluon) loops. This results in the energy-dependent behavior of the strong coupling constant α_s depicted in Fig 1.6, entering Eq. 1.4
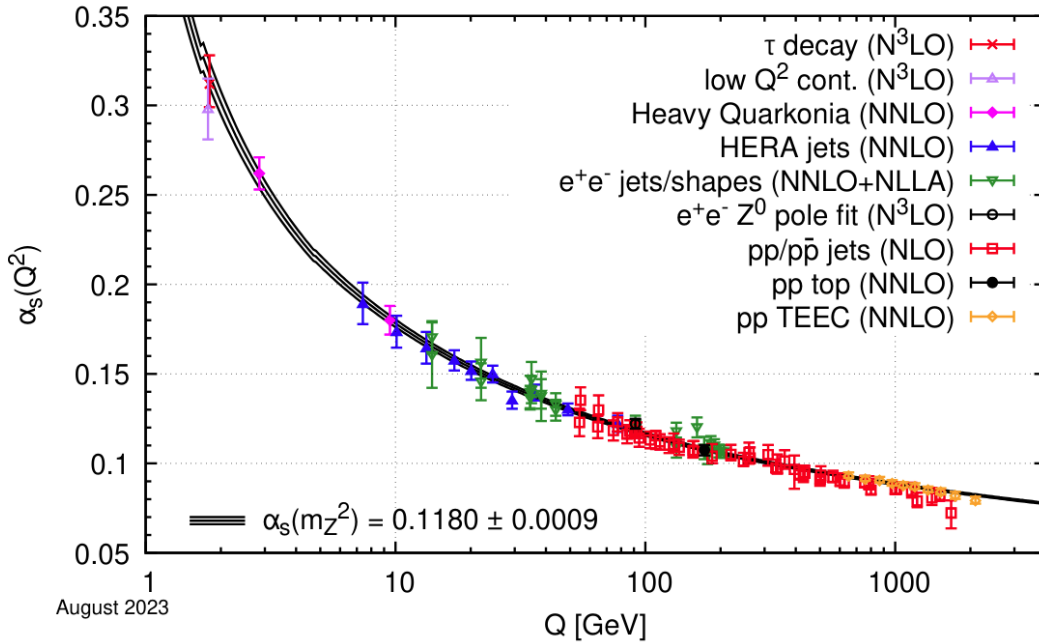
FIGURE 1.6: Strong interaction coupling constant α_s as a function of the energy scale Q [21].

via $\alpha_s = g^2/4\pi$.

At high energies, the coupling constant is small enough to be a proper expansion parameter for the perturbative approach. Quarks are described in terms of their point-like interactions with the force mediators – in the so-called *asymptotic freedom* regime [22, 23]. The opposite behavior is found at low energies: the size of α_s increases, and for a proper dynamical description, one needs to consider the composite particles as the relevant degrees of freedom, which is also known as the quark *confinement* [24] phenomenon. Here lies one of the main issues with hadron nature: despite being well established in theory, the experimental evidence for their quark structure is entirely indirect. It is mainly derived from *a posteriori* deductions based on the processes involving mesons or baryons – be it scattering or decay.

I have briefly covered some basic notions of baryon structure and the force responsible for the binding of the building blocks of matter. The quarks also participate in electromagnetic and weak interactions when coupling to quarks or other leptons. In the spirit of this section, a few introductory remarks about these interactions at the subhadronic level are presented. In later Sections 1.2 and 1.3, I will cover hyperon electromagnetic production and weak decays, respectively, in a qualitative approach that is better suited for their composite nature.

The EM interaction of point-like electrically charged fermions is described by the Quantum Electrodynamics (QED) Lagrangian

$$\mathcal{L}_{\text{QED}} = -\frac{1}{4} \overbrace{(\partial^\mu A^\nu - \partial^\nu A^\mu)}^{F^{\mu\nu}} F_{\mu\nu} + \bar{\psi}(i\slashed{\partial} - m)\psi - e\bar{\psi}\slashed{A}\psi \ . \tag{1.5}$$

The electromagnetic field strength tensor $F^{\mu\nu}$ contains the dynamics of the four-vector potential A^μ, and its interaction strength to a fermion–antifermion pair is quantified by the electric charge e. In this notation, the quark field q_{cfs} in Eq. 1.4 is replaced by the more general spinor ψ, to describe the EM interaction between any two fermions, be it leptons or quarks. The color and flavor indices are absent, as QED does not depend on them, and the matrix products between $\bar{\psi}$ and ψ are performed over spin indices, which are left implicit. As in the strong interaction, the EM force is mediated by a massless spin-1 particle, the photon. Contrary to QCD, QED is an Abelian theory, meaning there is no self-interaction between the mediator bosons – the structure constant f^{abc} is absent. A direct consequence is that the running EM coupling $\alpha_{\text{EM}} = e^2/4\pi$ increases with the energy scale, i.e. is weaker at longer distances, exhibiting the phenomenological characteristics of the EM force.

Strong and EM interactions are both characterized by invariance under P transformation: this is reflected in the Lagrangians of Eq. 1.4 and 1.5. Therefore, when searching for a proper description for nuclear β decays, the first proposal for the neutron-proton-electron vertex was presented by Fermi in complete analogy with QED [25], showing explicit P conservation:

$$\mathcal{L}_\beta = -\frac{G_F}{\sqrt{2}} \left(\bar{\psi}_p \gamma_\mu \psi_n \bar{\psi}_e \gamma^\mu \psi_{\nu_e} + \text{h.c.} \right) \ . \tag{1.6}$$

The discovery of P violation in β decays of ^{60}Co nuclei in 1957 by Wu and collaborators disrupted this picture [26]. The momenta of the produced electrons exhibited a manifest asymmetry incompatible with an isotropic distribution, regardless of the orientation of the magnetic field surrounding the decaying nuclei. In other words, for opposite orientations of the nuclear spin, the electrons were emitted in a preferred direction: had P been conserved, equal emission rates in opposite directions should have been observed.

To account for P violation, a pseudoscalar ($\bar{\psi}\gamma_5\psi$) term was added to the Fermi vertex, and later generalized by Feynman and Gell-Mann [27] and, independently, by Sudarshan and Marshak [28], to the "V–A" structure

$$\mathcal{L} = -\frac{G_F}{2\sqrt{2}} \left(\underbrace{\sum_l \bar{\psi}_l \gamma_\mu (1 - \gamma_5) \psi_{\nu_l}}_{L^\mu} + \overbrace{\bar{D}_C \gamma^\mu (1 - \gamma_5) U}^{H^\mu} \right) \left(L_\mu + H_\mu \right)^\dagger + \text{h.c.} \ . \tag{1.7}$$

The *Vector–Axial-vector* terminology derives from the covariant characteristics of the fermion-fermion terms under Lorentz transformations, i.e. the (polar) vector $\bar{\psi}\gamma^\mu\psi$ and the axial-vector $\bar{\psi}\gamma^\mu\gamma_5\psi$. L^μ and H^μ are the leptonic and hadronic parts of the charged weak current, respectively: they represent the separate interactions between the lepton-neutrino pair and

different quark flavors, symbolized by the operators U, D. The version of the weak current in Eq. 1.7 reflects the current knowledge of the quark model and the later addition by Cabibbo [29]

$$D_C = \cos\theta_C D + \sin\theta_C S \qquad (1.8)$$

of mixing between the three lightest quark flavors to account also for strangeness-changing transitions. Furthermore, Eq. 1.7 displays violation of *charge-conjugation* symmetry C, namely the transformation mapping a particle into its antiparticle. As with P symmetry, the assumption of C conservation followed from analogy with QED and QCD and held until contradicting experimental evidence was found in charged pion decays (see Section 1.3).

The "V−A" effective-field theory already presents all the relevant features that are needed in this work to discuss different types of hyperon decays in Sections 1.3.2, 1.3.3. However, what was recounted until now is far from the current formulation of weak interactions. The phenomenological indication for a short-range force pointed to the presence of a massive mediator, which clashed with the description of the weak theory as a non-Abelian gauge theory. The formulation by Yang and Mills [30] envisaged an underlying local gauge invariance under the symmetry group *SU(2)*, giving rise to three massless spin-1 quanta of electric charges 0, ±1. The explicit addition of a mass term for the gauge fields would have broken the initial gauge invariance and raised issues with renormalization, proven for massless fields by t'Hooft and Veltman [31].

Glashow, Weinberg [32], and Salam [33] ultimately reconciled the presence of massive weak mediators with the gauge invariance of the original theory via spontaneous symmetry breaking. This mechanism happens when the vacuum state of the theory does not exhibit invariance under transformations from the symmetry group of the original Lagrangian. It is also known as the Higgs mechanism [34, 35], where the Higgs field, a complex scalar isodoublet, generates a non-zero vacuum expectation value that breaks the local gauge invariance $SU(2) \times U(1)$ of the Lagrangian. The final result is the appearance of one massless and three massive vector quanta (the EM and weak mediator bosons γ, $W^{\pm}$, Z), and a massive scalar field (the Higgs boson). Consequently, masses of quarks and leptons are generated through a Yukawa-type interaction term with the Higgs scalar field, without losing the initial assumption of local gauge invariance at the Lagrangian level. This also implies that the weak and the electromagnetic forces are formulated as different realizations of the same theory, a concept that goes under the name of *electroweak unification*.

1.1.3 Structure probing and Form Factors

In the previous sections, it was discussed how the current knowledge of the internal structure of baryons is inferred from the Quark Model, finding strong experimental confirmation in hadronic processes of different interactions. This reiterates the message that hadrons, composed of quarks, follow different manifestations of the same laws of nature governing the building blocks. Thus, the point-like interaction vertices must be modified to account for their composite structure.

Form factors (FFs) are scalar functions used to parameterize the deviation of hadronic interaction from the elementary vertices presented in the Lagrangians of Section 1.1.2: a schematic representation of an FF is depicted in Fig. 1.7. More specifically, they depend on
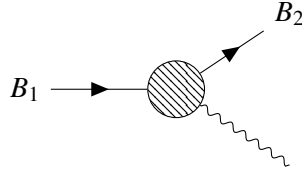

FIGURE 1.7: Decay of baryon B_1 into baryon B_2 and a vector boson, represented by the wiggly line. The blob symbolizes the boson-baryon-baryon vertex modified by the presence of form factors.

the transferred momentum squared q^2 of the reaction they are parameterizing, meaning that they may be investigated in different kinematical regions. For instance, Fig. 1.8 depicts the typical setup of a fixed-target experiment, where the form factors, represented as the blob, are defined in the space-like region $q^2 < 0$. Here, the mediator photon acts as a probe to extract
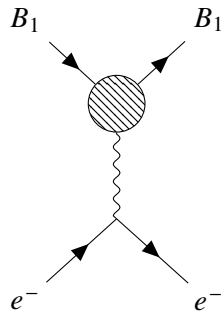
FIGURE 1.8: Diagrammatic description of EM elastic electron-baryon scattering $e^- B_1 \rightarrow e^- B_1$.

information on the intrinsic structure of baryons. Even if a hadron is neutral, the individual quarks carry electric charge, hence electromagnetic scattering is an efficient tool for structure probing at low energies [36]. This is the primary experiment to study the composition of nucleons [37]: however, it cannot be applied directly to unstable particles such as hyperons.

Strange baryons are better suited for investigation through other types of processes such as Dalitz decays or electron–positron annihilation to a hyperon-antihyperon pair (time-like region, $q^2 > 0$, Fig. 1.9). Crossing symmetry and analytic properties are then used to connect the different kinematical regimes of Fig. 1.8 and Fig. 1.9. It is important to note that form factors are labeled differently based on the baryon vertex they parameterize. A process with the same baryon in the initial and final state is described by *elastic* form factors (EFFs) (Fig. 1.8). If the initial and final hadrons are different, *transition* form factors (TFFs) are used. In this work, both types of form factors will be considered: in Section 1.2, I will illustrate the connection between EFFs of hyperon produced in e^+e^- collisions and the polarization features of the final-state pair; they will be useful to understand the hyperon polarization discussed in Chapter 2. In Section 1.3.3, I will discuss how the EM transition matrix element is modified
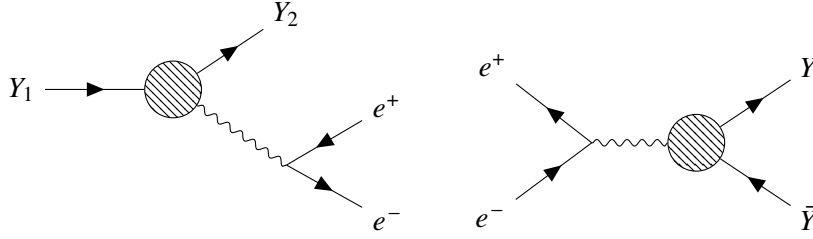
FIGURE 1.9: Dalitz decay $Y_1 \rightarrow Y_2 e^+ e^-$ (left) and EM annihilation $e^+ e^- \rightarrow Y\bar{Y}$ (right). The letter Y is used to denote a hyperon.

according to the conservation laws of the weak interaction: TFFs related to hyperon semileptonic decays are reviewed in Chapter 3, and a feasibility study on their statistical uncertainties is presented.

1.2   Electromagnetic production

As mentioned at the beginning of this chapter, hyperons are produced in processes characterized by zero net strangeness final states, specifically flavor-conserving interactions. Examples of such processes are the strong production of hyperons and kaons in proton-pion interactions or the EM annihilation of $e^+ e^-$ to hyperon–antihyperon pairs. I will focus exclusively on the latter when describing the production of $Y\bar{Y}$ pairs.

The point-like vertex from the QED Lagrangian 1.5 is modified to account for a composite structure by including any EM-allowed term, each weighted by an FF. The matrix element of a P- and C-conserving transition between two spin-1/2 baryons B_1, B_2 is [38]

$$\langle B_2|j^\mu|B_1\rangle = e\left[\left(\gamma^\mu + \frac{M_1 - M_2}{q^2}q^\mu\right)F_1(q^2) + \frac{i\sigma^{\mu\nu}q_\nu}{M_1 + M_2}F_2(q^2)\right] , \qquad (1.9)$$

where $M_{1,2}$ denote the masses of baryons $B_{1,2}$, and $q = p_1 - p_2$ represents the transferred momentum of the transition. To describe a baryonic transition of a different type, e.g. a weak decay, one would need to consider additional Lorentz-invariant structures (and the associated FFs) to keep track of P- or C-violating terms. This will be outlined in Section 1.3.3 and in Chapter 3.

The structure functions $F_1(q^2)$ and $F_2(q^2)$ are called Dirac and Pauli FFs [39], respectively. They may be recombined into the Sachs FFs [40]

$$G_E(q^2) = F_1(q^2) + \frac{q^2}{(M_1 + M_2)^2}F_2(q^2); \qquad G_M(q^2) = F_1(q^2) + F_2(q^2) \qquad (1.10)$$

also called *electric* and *magnetic* FFs to underline their relation to the charge and magnetization densities of the described baryon. The linear combinations in Eq. 1.10 have the added value of simplifying significantly cross-section or decay width formulae. When computing the modulus square of the transition matrix element of Eq. 1.9, any mixed term $F_1 F_2^*$, $F_1^* F_2$ disappears when the Sachs FFs are used, leaving a simpler $|G_{M,E}(q^2)|$ dependence.

Let us now consider the process $e^+e^- \rightarrow \psi(c\bar{c}) \rightarrow Y\bar{Y}$, where the intermediate photon couples to vector charmonia states, producing hyperon–antihyperon ($Y\bar{Y}$) pairs. High-precision spin-polarization studies using J/ψ decay events have been carried out in recent years [41–43] by the BESIII Collaboration [44], and constitute the principal production setting for the $Y\bar{Y}$ pairs investigated in Chapters 2 and 3. This annihilation probes the time-like $q^2 > 4M_Y^2$ region, above the "two-pion threshold", where the hyperons' EFFs are complex-valued. This feature is rooted in the optical theorem [20], where an imaginary part originates if the transferred energy q^2 crosses the threshold for the physical production of a possible intermediate state. To be more precise, let us take our $\gamma^* \rightarrow Y\bar{Y}$ process: the lightest possible intermediate hadronic state would be $\gamma^* \rightarrow \pi^+\pi^- \rightarrow Y\bar{Y}$. If the transferred energy is enough for the physical production of the intermediate pions, $q^2 \geq 4m_\pi^2$, the amplitude gains a non-zero imaginary part.

The relative phase $\Delta\Phi$ is defined as

$$\frac{G_E^\psi}{G_M^\psi} = e^{i\Delta\Phi} \left| \frac{G_E^\psi}{G_M^\psi} \right| \tag{1.11}$$

where the apex ψ stands for "psionic" FFs [45]. Another useful quantity is the ratio $\alpha_\psi \in [-1, 1]$

$$\alpha_\psi = \frac{q^2|G_M^\psi|^2 - 4M_Y^2|G_E^\psi|^2}{q^2|G_M^\psi|^2 + 4M_Y^2|G_E^\psi|^2} \ . \tag{1.12}$$

A complete derivation of the cross-section of this process in the covariant formalism has been provided in Ref. [45]. Without any specific assumption on the spin state of the produced hyperons, one may identify two distinct scenarios: either both final particles are polarized, or neither is. The $Y\bar{Y}$ pair results from the decay of the spin-1 charmonium state. Angular momentum and parity conservation require the spin vectors of the pair to be *spin-correlated*, i.e. aligned in the same direction. They also imply that there are only two partial waves for the final state, $S(L = 0), D(L = 2)$ - exemplified by the G_s, G_d FFs [46].

We can also write the polarization vector of the produced Y ($\bar{Y}$); it has the following dependence on the production parameters α_ψ, $\Delta\Phi$ and the scattering angle θ [45]:

$$\mathbf{P}_Y = \frac{\sqrt{1 - \alpha_\psi^2} \cos\theta \sin\theta}{1 + \alpha_\psi \cos^2\theta} \sin\Delta\Phi \, \hat{\mathbf{y}} \ . \tag{1.13}$$

A relevant feature of Eq. 1.13 is its dependence on the relative phase between electric and magnetic FFs $G_{E,M}^\psi$. It exemplifies how this annihilation process can produce baryon–antibaryon pairs in an inherently polarized state. The $G_{E,M}^\psi$ form factors are linearly related to G_s, G_d [46], implying that the polarization in Eq. 1.13 arises naturally from the interference between the partial waves in the production process.

Notably, Eq. 1.13 is obtained assuming the $Y\bar{Y}$ pair is produced in collisions of beams of unpolarized e^-, e^+. The polarizations $\mathbf{P}_Y$, $\mathbf{P}_{\bar{Y}}$ are aligned and orthogonal to the scattering plane, parallel to the $\hat{\mathbf{y}}$ direction of the center-of-mass (CM) coordinate system, as shown in
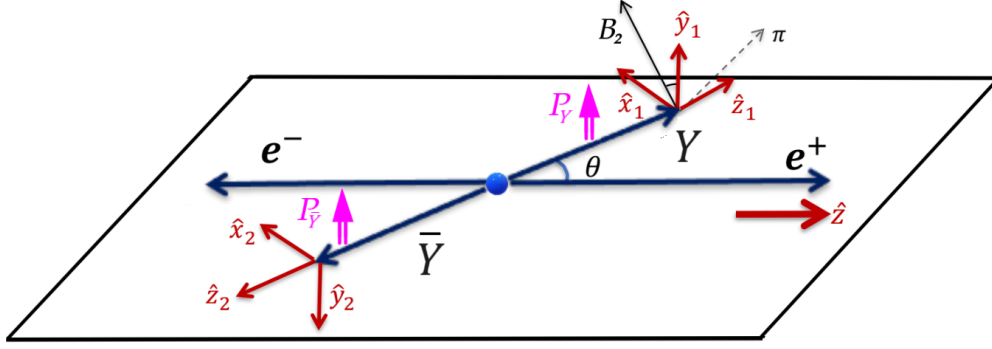
FIGURE 1.10: Orientation of the $Y\bar{Y}$ polarization vectors relative to CM frame ($\{\hat{\mathbf{x}}, \hat{\mathbf{y}}, \hat{\mathbf{z}}\}$) and the rest frame of the produced (anti)hyperon Y ($\bar{Y}$) – picture modified from Ref. [47].

Fig. 1.10. In the presence of a longitudinally polarized e^- beam, $\mathbf{P}_{Y,\bar{Y}}$ acquire two additional components along the remaining directions $\hat{\mathbf{x}}$, $\hat{\mathbf{z}}$ [46]. In Chapter 2, the beam polarization P_e is kept as a variable for our system, and a feasibility study is performed, based on its impact on the polarization vectors of the produced pair.

In the following subsections, I will outline a few definitions regarding the spin-density matrix [48] and the helicity formalisms [49]: their combined application is the pillar of both the analyses in Chapters 2 and 3.

1.2.1 Spin-density matrix

In quantum mechanics, particle states are described by wave functions and may be represented via the state vector "ket" $|\psi\rangle$. Linear combinations of kets and their complex conjugates ($\langle\psi|$, "bra") span the complex vector space where particles live. A set of identical kets describes a pure ensemble. However, most physical ensembles consist of objects in different pure states, each weighted by its probability – the so-called mixed ensembles. In both cases, the density operator ρ contains all the relevant information about the system. For a mixed ensemble,

$$\rho = \sum_k \omega_k |\psi_k\rangle \langle\psi_k| \tag{1.14}$$

is hermitian and $\text{Tr}(\rho) = 1$ - provided that proper normalization is implemented, i.e. $\sum_k \omega_k = 1$. The case of the pure ensemble is obtained from Eq. 1.14 when there is only one state $|\psi\rangle$, i.e. $k = 1$. The expectation value of any observable O measured on a mixed ensemble is defined as

$$\langle O \rangle = \sum_{i,k} \omega_k \langle\psi_k|O|\psi_i\rangle \langle\psi_i|\psi_k\rangle = \text{Tr}(\rho O) . \tag{1.15}$$

The above definitions and properties also encompass the case of a pure ensemble, i.e. $k = 1$. For a particle of arbitrary spin j, its spin-density matrix may be written in this formalism [50]. That is, expressed in a basis of hermitian matrices, as a function of the polarization parameters of such state. The choice of basis depends on the spin of the described particle: in the case of

spin-1/2 baryons [50, 51], Pauli matrices are used in

$$\rho_{1/2} = \frac{1}{2} \sum_{\mu=0}^{3} P_\mu \sigma^\mu \,, \tag{1.16}$$

where P_0 is the cross-section term, $\mathbf{P}$ is the baryon polarization vector and $\sigma^\mu = (\mathbb{1}, \boldsymbol{\sigma})$.

1.2.2   Helicity formalism

In this work, final-state angular distributions for production and decay processes are analyzed using the helicity formalism [49], where the spin of the particles is quantized along the flight direction of the state, rather than along a specific axis. This gives rise to rotationally invariant states, since the helicity operator is defined as the spin projection along the particle momentum direction $\lambda = \mathbf{S} \cdot \hat{\mathbf{p}}$. The quantization along the momentum ensures the states are also invariant under a boost between the CM frame and the rest ("helicity") frames of the produced particles. This framework is particularly suitable to analyze the subsequent decays of the produced $Y\bar{Y}$, typically via the weak interaction, which will be presented in Sections 1.3.2 and 1.3.3.

A two-particle state in the CM frame is defined as

$$|\Omega, \lambda_1, \lambda_2\rangle := R(\phi, \theta, 0) |\lambda_1, \lambda_2\rangle \tag{1.17}$$

where $\lambda_{1,2}$ denote the particle helicities and $R(\phi, \theta, \chi)$ is the rotation matrix. In this definition, I follow closely the notation from Ref. [52], except for leaving implicit the particle momentum p. Eq. 1.17 represents the successive transformations that connect the production frame to the helicity frame of any particle of choice: a rotation to align the particle momentum with the desired axis, followed by a boost. This breaks down into three successive rotations about the coordinate axes, although two are already enough to complete the alignment – hence, $\chi = 0$. In Chapter 3, I will explain in detail how to use the additional free angle to simplify the description of a three-body decay process.

Going back to the production process, the spin-density matrix in this formalism is [52]

$$\rho_{Y,\bar{Y}}^{\lambda_Y, \lambda_{\bar{Y}}; \lambda'_Y, \lambda'_{\bar{Y}}} \propto \sum_{k=\pm 1} \langle \theta, 0, \lambda_Y, \lambda_{\bar{Y}} | S | 0, 0, \lambda, -\lambda \rangle \langle 0, 0, \lambda, -\lambda | S^\dagger | \theta, 0, \lambda'_Y, \lambda'_{\bar{Y}} \rangle \,, \tag{1.18}$$

where $\lambda, \ k, \lambda_Y, \ \lambda_{\bar{Y}}$ represent the positron, vector meson, hyperon and antihyperon helicities, respectively. Helicity states are projected on angular momentum eigenstates using the Wigner rotation matrix [53]

$$\langle J, M, \lambda'_Y, \lambda'_{\bar{Y}} | \Omega, \lambda_Y, \lambda_{\bar{Y}} \rangle = \sqrt{\frac{2J+1}{4\pi}} \mathcal{D}_{M, \lambda_Y - \lambda_{\bar{Y}}}^{J}(\Omega) \delta_{\lambda_Y, \lambda_{\bar{Y}}} \delta_{\lambda'_Y, \lambda'_{\bar{Y}}} \,. \tag{1.19}$$

After further simplifications (see Ref. [52]), the production spin-density matrix reduces to the simple form

$$\rho_{Y,\bar{Y}}^{\lambda_Y, \lambda_{\bar{Y}}; \lambda'_Y, \lambda'_{\bar{Y}}} \propto A_{\lambda_Y, \lambda_{\bar{Y}}} A^*_{\lambda'_Y, \lambda'_{\bar{Y}}} \rho_1^{\lambda_Y - \lambda_{\bar{Y}}, \lambda'_Y - \lambda'_{\bar{Y}}}(\theta) \tag{1.20}$$

i.e. it is described in terms of the transition amplitudes between helicity states $A_{\lambda_Y, \lambda_{\bar{Y}}}$

$$A = \begin{pmatrix} h_1 & h_2 \\ h_2 & h_1 \end{pmatrix} . \tag{1.21}$$

The "helicity amplitudes" $h_{1,2}$ describe the $Y\bar{Y}$ vertex and are related to the psionic FFs $G^{\psi}_{E,M}$. Furthermore, when looking for the un-normalized final angular distribution, the relevant information contained in the two complex FFs can be described using two real parameters α_ψ and $\Delta\Phi$, similarly to Eq. 1.11 and 1.12. The elements of $A_{\lambda_Y, \lambda_{\bar{Y}}}$ are arranged according to the helicity combinations of the produced pairs, with rows numbered $m_1 = 1/2, -1/2$ from top to bottom, and columns $m_2 = 1/2, -1/2$ from left to right.

It is useful to express the spin-density matrix for the $1/2 - \overline{1/2}$ EM production employing [54]

$$\rho_{Y,\bar{Y}} = \frac{1}{4} \sum_{\mu,\bar{\nu}=0}^{3} C_{\mu\bar{\nu}} \sigma^{Y}_{\mu} \otimes \sigma^{\bar{Y}}_{\bar{\nu}} \tag{1.22}$$

where the Pauli matrices represent the spin-1/2 bases for the $Y\bar{Y}$ pair, given in their respective helicity frames. The matrix coefficient $C_{\mu\bar{\nu}}$ can be extracted by projecting Eq. 1.20 on the proper Pauli matrices basis, and summing over the (anti)hyperon helicity indices. The result is a 4×4 matrix of real-valued coefficients containing all the relevant information on the production process polarization observables, encoded via α_ψ and $\Delta\Phi$. Two additional parameters β_ψ and γ_ψ can be defined to express $C_{\mu\nu}$ in a compact way:

$$\beta_\psi = \sqrt{1 - \alpha_\psi^2} \sin(\Delta\Phi), \quad \gamma_\psi = \sqrt{1 - \alpha_\psi^2} \cos(\Delta\Phi) . \tag{1.23}$$

α_ψ, β_ψ, and γ_ψ are functions of the modulus and of the relative phase between the two "helicity amplitudes" h_1, h_2, representing the possible independent helicity configurations of the spin-1/2 pair created in a parity-conserving EM interaction. The rewriting presented in Chapter 2 follows from Ref. [52] and is an alternative option to using the psionic form factors $G^{\psi}_{E,M}$ outlined in Section 1.1.3.

Among the elements of the production matrix $C_{\mu\nu}$, C_{00} represents the cross-section term, C_{0i} and C_{i0} the Cartesian components of the (anti)hyperon polarization vectors, and C_{ij} the spin-correlation terms within the $Y\bar{Y}$ pair. The link to $C_{\mu\bar{\nu}}$ elements in Cartesian components is given directly in Ref. [55]. As mentioned above, a polarized beam affects the polarization vectors of the produced pairs. This implies that the spin-density matrix gains additional components directly dependent on the beam polarization, as presented in Chapter 2.

The discussion so far was specific to the $Y\bar{Y}$ pair, and the indices in the presented formulae reflected this aspect. However, it is important to note that this formalism is completely general and may be applied to any spin-1/2 baryon–antibaryon $B_1\bar{B}_2$ pair produced in e^+e^- annihilation. The polarization observables would differ only by the involved FFs, "elastic" or "transition" depending on whether $B_1 = \bar{B}_2$.
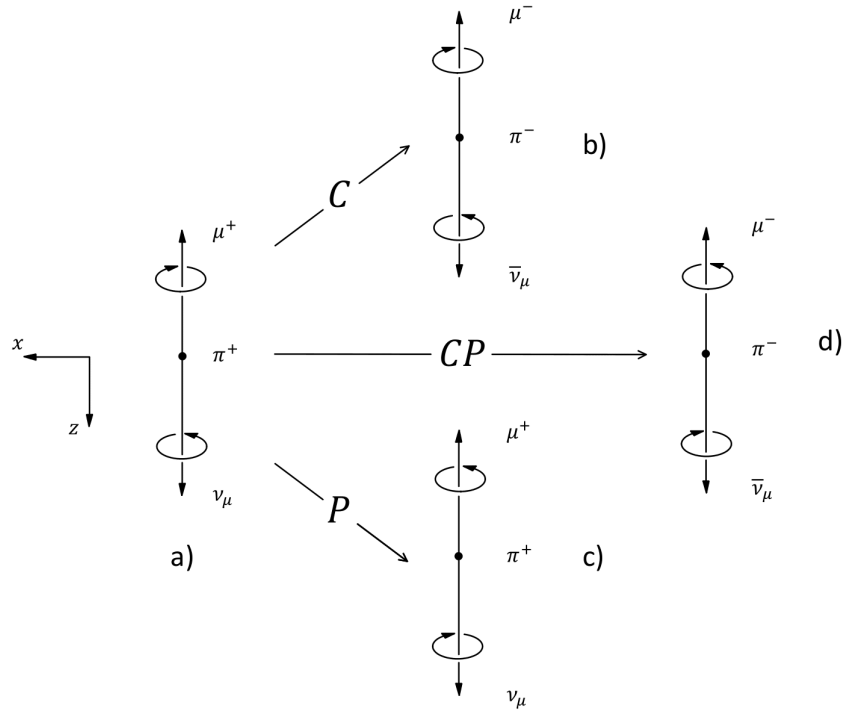
FIGURE 1.11: Charged pion decay $\pi^+ \to \mu^+ \nu_\mu$ (a) and its charge-conjugated (b), parity-reversed (c), and CP-transformed (d) process. The circular arrows represent the handedness of each particle; the straight arrows, their linear momentum.

1.3   Weak decays

After describing the production process, let us move on to the next step: hyperon decays. From their lifetimes, we infer that any decay of a ground-state octet hyperon (except the radiative decay of Σ^0) happens via flavor-changing weak processes. This interaction, as outlined in Section 1.1.2, also violates the spatial inversion P and the charge conjugation C. After the first observation [26], this non-conservation was confirmed in charged pion decays: given the fundamental role of C and P in strong and EM interactions, the effort to restore at least some symmetry came as no surprise. Charged pions decay into muon-neutrino pairs with helicities fixed by angular momentum conservation according to the relation

$$\lambda_\pi = 0 = \underbrace{(\mathbf{S}_\mu + \mathbf{S}_\nu + \mathbf{L})}_{\mathbf{S}_\pi} \cdot \hat{\mathbf{p}}_\nu = -\lambda_\mu + \lambda_\nu \, , \tag{1.24}$$

where λ_π, λ_μ, λ_ν are the pion, muon and neutrino helicities, respectively; $\mathbf{S}_\pi$, $\mathbf{S}_\mu$, $\mathbf{S}_\nu$ are the spin vectors of the involved particles, and $\mathbf{L}$ the relative orbital angular momentum of the muon-neutrino pair.

Both leptons are left-handed – measured with negative helicity – in the decay of, e.g. π^+ (Fig. 1.11a). The C-transformed process conserves the helicity configuration, since charge conjugation leaves momenta and spins unchanged (Fig. 1.11b). Similarly, a spatial inversion

involves the original particles with reversed momenta and untouched spins, due to the axial-vector nature of the latter. By definition, helicities also change sign, which brings the decay of a π^+ into a right-handed lepton pair (positive helicities), depicted in Fig. 1.11c. Although the transformed processes were not observed, experimental findings on the CP-transformed decay, i.e. $\pi^- \to \mu^- \bar{\nu}_\mu$ (Fig. 1.11d), yielded results consistent with the conservation of the combination of charge-conjugation and parity. This was taken as the (premature) confirmation that some level of symmetry would be preserved by the weak interaction, in line with the characteristics of strong and EM forces. In the next sections, I will outline the topic of violation of CP-symmetry in particle physics, followed by a quick overview of the hyperon decays studied in Chapters 2 ("nonleptonic") and 3 ("semileptonic"), with a focus on the attainable information each system offers in this regard.

1.3.1 CP violation

Charged pion decays offered short-lived confirmation of CP-conservation in weak interactions: in the early 1960s its violation (CPV) was observed in kaon decays [56], and confirmed in recent years in B [57–59] and D [60] meson decays. These experimental findings were explained and included in the weak sector of the SM through the Cabibbo-Kobayashi-Maskawa (CKM) matrix [61]

$$V_{\text{CKM}} = \begin{pmatrix} V_{ud} & V_{us} & V_{ub} \\ V_{cd} & V_{cs} & V_{cb} \\ V_{td} & V_{ts} & V_{tb} \end{pmatrix}. \tag{1.25}$$

The matrix above generalized Cabibbo's formulation (Eq. 1.8) to account for charged weak interactions between six quark flavors, and consolidated the pivotal role of CPV in particle interactions. In particular, this phenomenon relates to the formation of matter in the early stages of our Universe: assuming an initial stage of thermal equilibrium, the creation and annihilation of baryon–antibaryon pairs is affected by the expansion process, until the densities of B and $\bar{B}$ reached asymptotic values. CP invariance requires these densities to be the same, but this clashes with the experimental observation from light isotopes formed in Big Bang Nucleosynthesis. According to Sakharov's conditions [62], CPV is a necessary condition for the dynamical generation of baryonic asymmetry, i.e. the abundance of baryonic matter over antimatter in our Universe. So far, all experimental observations are consistent with the SM predictions, and concern only mesons. However, the detected CPV signal is not sufficient to account for the observed asymmetry. This implies that the dominant CPV source may be found in beyond-the-SM (BSM) formulations: to explain baryon asymmetry, the baryon sector is especially relevant to investigate, due to the lack of empirical data.

It should be noted that there are different manifestations of CPV. It is called "direct", when it stems from the direct comparison of particle–antiparticle observables, such as decay rates, or "indirect", when it results from particle–antiparticle mixing, such as $K^0 - \bar{K}^0$ oscillations. The latter is only viable for neutral mesons, as charge conservation forbids hadrons and leptons to mix with their antiparticles. This puts hyperon decays in the roster of direct CPV sources. Furthermore, one may draw a direct comparison between meson and baryon CPV

in the strange sector, by looking at the "nonleptonic" $\Delta S = 1$ decays of kaons and hyperons. This will be discussed in the next sections, where I will give an overview of the hyperon decay modes involved in my research.

1.3.2   Nonleptonic decays

"Nonleptonic" decays are characterized by a fully hadronic final state, e.g. $\Lambda \rightarrow p\pi^-$. For ground-state hyperons, only two-body nonleptonic decays are possible, and the relative transition matrix is [21]

$$\mathcal{M} = G_F m_{\pi^+}^2 \bar{u}_f \left(A - B\gamma_5 \right) u_i . \tag{1.26}$$

The structure of Eq. 1.26 resembles that of Eq. 1.6 with fundamental modifications in the spin structures. Since the pion is a pseudoscalar meson, any baryon–pion final state has negative intrinsic parity, which implies that the dimensionless constants A and B are a pseudoscalar and a scalar, respectively. They correspond to the P-violating S and P-conserving P partial-wave amplitudes. Without making any restrictions on the spin orientations of the initial and final baryons, the transition rate [63]

$$R = 1 + \alpha(\hat{\omega}_f \cdot \hat{\boldsymbol{n}} + \hat{\omega}_i \cdot \hat{\boldsymbol{n}}) + \beta\hat{\boldsymbol{n}} \cdot (\hat{\omega}_f \times \hat{\omega}_i) + \gamma\hat{\omega}_f \cdot \hat{\omega}_i + (1 - \gamma)\hat{\omega}_f \cdot \hat{\boldsymbol{n}}\hat{\omega}_i \cdot \hat{\boldsymbol{n}} \tag{1.27}$$

is written in terms of the final baryon momentum direction $\hat{\boldsymbol{n}}$, the initial and final baryon polarization vectors $\hat{\omega}_{i,f}$, and the decay parameters α, β and γ. They satisfy the constraint $\alpha^2 + \beta^2 + \gamma^2 = 1$ and carry the information about the interference between the P-violating and P-conserving amplitudes, and their moduli:

$$\alpha = \frac{2\Re(S^*P)}{|S|^2 + |P|^2}, \qquad \beta = \frac{2\Im(S^*P)}{|S|^2 + |P|^2}, \qquad \gamma = \frac{|S|^2 - |P|^2}{|S|^2 + |P|^2} . \tag{1.28}$$

In Chapter 2, I present a special case of Eq. 1.27 for polarized hyperons produced in e^+e^- collisions and decaying into final-state baryons which polarization is unmeasured, i.e. its polarizations are summed over. This reflects an experimental setting without a final-state polarimeter, which is the case for the BESIII spectrometer [64]. More importantly, the information about the initial polarization can be extracted from the decay through the α parameter, representing the anisotropy of the distribution of the final-state particles. Since this is done without an external polarimeter to measure the decaying hyperon polarization, this type of decay is also called "self-analyzing".

As mentioned above, hyperon decays are an important source for tests of direct CPV phenomena. The possible CP-symmetry tests built on the observables in Eq. 1.28 are outlined in Chapter 2 and rely on the comparison between particle and antiparticle properties. Also, it is important to note that CPV effects could arise from the interference between ΔI – transition isospin – amplitudes. The term ΔI quantifies the difference in the value of isospin between the initial and final state of a decay – assuming the final state can have more than one value of final isospin I. For example, the final state of the decay $\Sigma^+ \rightarrow n\pi^+$ can have two final isospin values $I = 1/2, 3/2$, resulting from the composition of isospins $I = 1$ (pion), $I = 1/2$
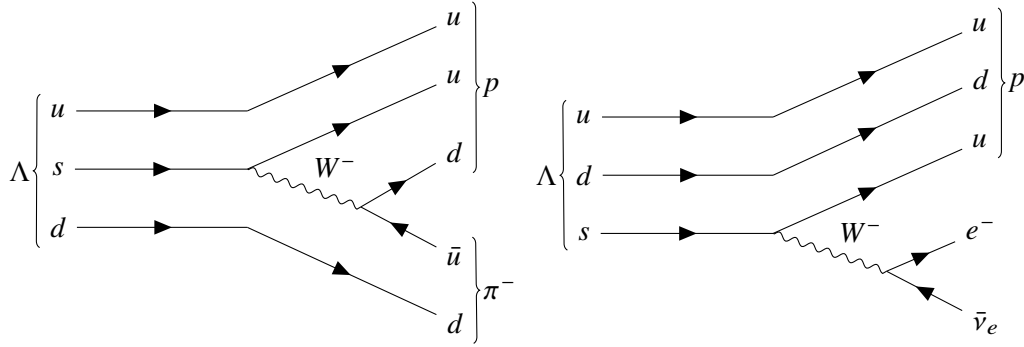
FIGURE 1.12: Feynman diagrams detailing the lepton-lepton interactions for
the nonleptonic (left) and the semileptonic (right) decay of the Λ hyperon.

(nucleon). The Σ^+ hyperon belongs to an isospin triplet of $(I, I_3) = (1, 1)$, meaning that the
possible values of transition isospin are $1/2 \leq \Delta I \leq 5/2$. If we restrict our discussion to the
two lowest amplitudes, we can quantify the hierarchy between the $\Delta I = 1/2$ "leading-order"
(LO) and the sub-leading $\Delta I = 3/2$ amplitudes. The relative size of the subleading amplitudes
is around 3-5% for all the ground-state baryons, and this result was confirmed (Chapter 2) by
the recent results from BESIII [65]. This implies that CPV observables are described, to a
good approximation, by LO ΔI amplitudes. In comparison, CPV effects in the corresponding
$\Delta S = 1$ strange meson decays originate entirely from an interplay of LO and sub-leading
amplitudes, making hyperon CPV effects easier to study – despite the former being the only
hadronic system where the direct $\Delta S = 1$ CPV was properly observed.

1.3.3 Semileptonic decays

Ground-state hyperons may also decay into a baryon and a charged lepton–neutrino pair.
These decays are called "semileptonic" (SL), due to the mixed composition of the final state.
They are the same as neutron β decays, except for the branching fractions: in β decays, a u
quark transitions to a d quark, and this contributes to 100% of the decay width of the neu-
tron. Hyperons exhibit $u - d$ and strangeness-changing SL transitions, but these only amount
to a small fraction ($O(10^{-4})$) of the possible hyperon decay modes. A list of hyperon SL
decays and their properties is given in Chapter 3. From a point-like perspective, an SL tran-
sition involves a charged weak current mediated by a W boson, as in nonleptonic decays; the
difference lies in the type of fermions the W couples to. Only quarks are involved in nonlep-
tonic decays: the W boson is exchanged "internally", while in SL decays the flavor-changing
transition results in the emission of an "external" lepton-neutrino pair (Fig. 1.12).

Despite much smaller yields compared to nonleptonic decays [21], studies of hyperon SL
transitions are important for several reasons. In addition to the measurement of CKM ma-
trix elements [66], the W boson probes the hadronic structure in regions where the involved
baryons can be assumed to be static. One may also be tempted to draw a comparison between
nonleptonic and SL decays in building direct CPV observables, however, replacing a spin-0
pseudoscalar pion with a spin-1 dilepton implies a higher level of complexity in the available
spin combinations of the daughter particles. This is reflected in the expressions for the decay

parameters along the lines of Eq. 1.28. As shown in Ref. [63], such parameters are considerably more complex, and building CPV tests is not straightforward. The aim of Chapter 3 is to study SL transitions of polarized hyperons produced at the BESIII e^+e^- collider.

To analyze these transitions in detail, the approach followed is similar to the study of nonleptonic decays. The transition matrix contains the appropriate structures to account for all the particles involved, in the spirit of Eq. 1.6 and 1.26, and is given explicitly in Chapter 3. Its structure recalls the V-A coupling outlined in Section 1.1.2, replacing the point-like interaction vertices with SL FFs. The dimensionless constants *A, B* (or *S, P*) in the nonleptonic vertex of Eq. 1.26 are replaced by $F_{1,2,3}^{V;A}(q^2)$, functions of the transferred q^2.

In Section 1.2.2, the derivation of the spin-density matrix for the $Y\bar{Y}$ production process was outlined in the helicity formalism. A similar procedure can be applied to express decay transitions of the produced baryon–antibaryon pairs, keeping track of the spin correlations. This modular formalism is presented in detail in Ref. [52], and it consists of a rotation between the mother and daughter particle helicity frames. The information carried by such rotation is encoded in the matrix of coefficients $a_{\mu\nu}$, analogous to $C_{\mu\nu}$ from Eq. 1.22:

$$\sigma_\mu^m \rightarrow \sum_{\mu=0}^{3} a_{\mu\nu}\sigma_\nu^d \ , \tag{1.29}$$

where the Pauli matrices σ_μ^m, σ_ν^d represent the mother and daughter helicity frames, respectively. The explicit shape of the nonleptonic decay matrix is presented and used extensively in Chapter 2. In Chapter 3, the corresponding matrix for SL decays is derived, following the procedure outlined in Ref. [52] – with the modifications imposed by the higher number of spin combinations of the final-state particles.

1.4   My contribution

In this section, I summarize my scientific contributions to the research discussed in the following chapters.

The first work presented in Chapter 2 focuses on analyzing hyperon–antihyperon pairs produced in current and upcoming experimental facilities. A recent update of the Λ hyperon decay asymmetry by the BESIII collaboration served as a driving force for this research work. Using the helicity formalism, I produced the spin-correlation matrix describing $e^+e^- \rightarrow B\bar{B}$ reactions for $J = 1/2$ baryons in the presence of a longitudinally polarized electron beam. This general formalism is applied to the specific case of hyperon production. Specifically, the beam polarization P_e is introduced in the derivation of the production matrix $C_{\mu\nu}$ and kept as a variable to gauge its effects on the various observables: I provided plots of the hyperon polarization as a function of P_e and its comparison to the spin-correlation terms.

I also derived the Fisher information matrix for the CP observables: as it involves the inverse of the probability density function (PDF), this calculation was carried out both analytically and numerically. I determined the Fisher matrix elements using the zeroth term

approximation of the series describing the inverse of the PDF, along with the PDF partial derivatives with respect to the decay parameters contributing to the CP tests (e.g. α_D, ϕ_D). These expressions are later compared to the full numerical integration for the cases of the Σ^+, Λ, and Ξ^- hyperons, and the higher-order terms of the series are shown to have a limited impact on the full PDF. The statistical uncertainties for the CP observables are investigated for varying values of the beam polarization P_e. The precision of the CP tests increases with increasing P_e, reaching a factor-of-four improvement around the realistically achievable $P_e \sim 0.8-0.9$. The feasibility study is carried out on two types of event reconstruction, *single-* (ST) and *double-tag* (DT), and non-zero values of P_e reduce significantly the CP observable uncertainties in both analyses.

Finally, the current status of the CPV phenomenology is reviewed: hyperon nonleptonic decays are expressed in terms of their partial wave-amplitudes *S, P* using isospin decomposition, labeling them via final-state isospin I and transition isospin ΔI. For $\Delta S = 1$ decays, hyperons can be described with the LO amplitudes only: this is checked in light of the updated data, where the $\Delta I = 3/2$ amplitudes are computed for Λ and Ξ decays. I found the corrections to be $\sim 3 - 5\%$ of the size of the LO, implying that hyperon CP observables have a lower level of complexity compared to the analogous $\Delta S = 1$ kaon decays.

In my second work (Chapter 3), an extension of the previous framework is explored. The spin-1/2 baryon–antibaryon pairs are studied in the context of current colliders, such as BE-SIII, where the electron beam is unpolarized. The subsequent semileptonic decays of the spin-entangled pair are investigated in the helicity formalism and encoded in the semileptonic decay matrix – via the "helicity rotation" outlined in Section 1.3.3.

I derived independently the SL transition amplitude and cross-checked the vector and axial-vector helicity amplitudes from previous studies. Employing the residual freedom of rotation when defining helicity frames (Section 1.2.2), I defined the relative orientation of the decay products, so that they are coplanar. Similar to the case of the nonleptonic decay matrix used in Chapter 2, the semileptonic decay matrix is derived. From it, I also extracted its angular dependence on the final baryon spherical angle, in order to isolate the information carried by the helicity amplitudes. This was shown for the specific case of a semileptonic decay and generalized to a spin-1/2 baryon–baryon transition, regardless of the nature of the accompanying boson. The universality of said factorization is explored in detail for the cases of a photon – virtual and real, a pseudoscalar meson, and a vector meson resonance.

Summary of the first chapter

- Hyperons are composite particles closely related to nucleons. Their composite nature is encapsulated in structure functions of the transferred momentum q^2, the so-called form factors.

- Hadrons, such as nucleons and hyperons, interact with other particles according to the interactions described in the SM, i.e. strong, electromagnetic, and weak. The structure of matter is investigated in a low-energy regime using electron–proton scattering in the space-like region. Hyperons have a finite lifetime, and are therefore unsuitable for fixed-target experiments: they are investigated in the time-like region, instead.

- Many such hyperons are produced at e^+e^- experiments, such as BESIII. The produced hyperons can be polarized, and the polarization is caused by a non-vanishing relative phase between the hyperon EM FFs, complex-valued for time-like q^2.

- The produced $Y\bar{Y}$ pairs may decay via flavor-changing transitions. Nonleptonic decays are called self-analyzing, since the polarization is measured by the anisotropic distribution of the decay products – without an external polarimeter. The extracted particle and antiparticle decay asymmetries can be compared to provide CPV observables.

- Semileptonic decays provide additional information about hadron structure via the SL FFs. On the one hand, the spin features are too complex to build CPV observables in the same straightforward manner as with nonleptonic decays. On the other hand, SL decays give access to the measurement of CKM matrix elements.

2

Study of CP violation in hyperon decays at Super Charm-Tau Factories with a polarized electron beam

Abstract

Nonleptonic two-body weak decays of baryons are an important tool to probe the combined charge-conjugation–parity symmetry (CP) violation. We explain why the decays of strange baryons provide complementary information to the decays of kaons. A model-independent parameterization of the nonleptonic decays of the Λ- and Ξ-baryons is reviewed, and the amplitudes are updated according to the latest experimental input. We demonstrate the potential of performing precision tests in strange baryon decays at the next generation electron-positron J/ψ factories with a luminosity of 10^{35} cm^{-2}s^{-1}. The copious production of spin-entangled hyperon–antihyperon pairs via the J/ψ resonance allows for a direct comparison of the baryon and antibaryon decay properties. Using analytic approximations and numerical calculations, we study the quantitative impact of spin correlations and polarization in such CP tests. We show that by using a longitudinally-polarized electron beam, the statistical precision of the CP tests can be significantly improved compared to the experiments without polarized beams. Furthermore, we map out further directions for possible improvements, like analysis of incompletely reconstructed events or a combination of the isospin related processes. Altogether, these methods are promising for the observation of a statistically significant CP-violation signal with a strength corresponding to the standard model predictions. Our conclusions should

encourage more detailed feasibility studies, including optimization of the measurement methods and studies of systematic effects. Finally, our results call for an update of the theory predictions with increased precision.

2.1   Introduction and summary

Although the standard model (SM) of elementary particle physics can describe the subatomic world accurately, there are several theoretical and experimental indications that it needs to be completed. In general, precision tests of symmetries and their violation patterns provide guidelines towards a deeper understanding of elementary particles and their interactions. Here we focus on charge-conjugation parity (CP) violation as a means of teasing out new physics. It is well known that the CP-violating mechanism in the SM is not sufficient to explain the observed imbalance between matter and antimatter in our Universe as a dynamic effect [62]. On the other hand, the processes included in the SM are strong enough to wash out any initial imbalance before the electroweak phase transition [67, 68]. Thus, a CP violation beyond the SM is required. In the quark sector, the existence of CP violation in kaon and beauty meson decays is well established [56, 69, 70] and so far most observations are consistent with the SM expectations. There are tensions like the $B \rightarrow \pi K$ decay puzzle which require further exploration [71]. The first CP-violating signal for charmed mesons, reported by the LHCb experiment [72], is at the upper edge of the SM prediction. As CP-violating effects are subtle, a detailed understanding requires a systematical mapping of various hadronic systems studied with complementary approaches.

In the strange-quark sector, one of the most sensitive probes of non-SM contributions is direct CP violation. The experimental result is given by the value $\mathrm{Re}(\epsilon'/\epsilon) = (16.6 \pm 2.3) \times 10^{-4}$ [73–75] determined from the decay amplitude ratios of K_L and K_S mesons into pion pairs,

$$\frac{\mathcal{A}(K_L \rightarrow \pi^+\pi^-)}{\mathcal{A}(K_S \rightarrow \pi^+\pi^-)} =: \epsilon + \epsilon' \quad \text{and} \quad \frac{\mathcal{A}(K_L \rightarrow \pi^0\pi^0)}{\mathcal{A}(K_S \rightarrow \pi^0\pi^0)} =: \epsilon - 2\epsilon' . \tag{2.1}$$

This direct CP-violating effect arises in the weak part of the transition amplitudes to pions due to the interference between isospin $I = 0$ and $I = 2$ final states ($|\Delta I| = 1/2$ and $|\Delta I| = 3/2$ transitions, respectively). The CP-violation mechanism in the SM requires loop diagrams where all three quark families are involved, the so-called penguin diagrams, like those shown in Fig. 2.1. Predictions for the kaon decays have been a challenge for many years since there are partially cancelling contributions from sub-leading types of the penguin diagrams, where the gluon line is replaced by γ, Z^0, see *e.g.* Ref. [76] and references therein. Recently, a satisfactory understanding was reached using Lattice [77, 78] and effective field theory [79, 80] approaches to Quantum Chromodynamics (QCD). This progress ensures that the kaon decays continue to be an important precision test of the SM.

The subject of our paper is a complementary approach to study CP violation (CPV) in two-body nonleptonic $\Delta S = 1$ transitions of hyperons [81–86]. For such weak two-body decays, one also needs an interference pattern: this time between parity-even and parity-odd decay
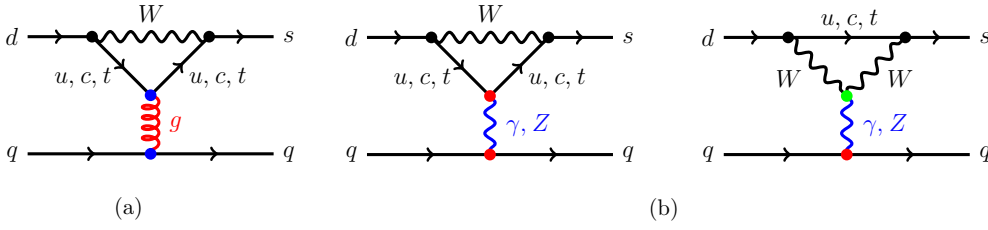
FIGURE 2.1: Quark diagrams relevant for kaon and hyperon decays. Direct CP-violation effects in kaon and hyperon decays in the SM are given by the (a) QCD-penguin operators and (b) electroweak penguin operators. This figure was created using a modified script from Ref. [79].

amplitudes. These emerge from the spin degrees of freedom of the initial and final baryon. Since we will consider decays of a spin-1/2 baryon B to a spin-1/2 baryon b and a pion, the parity-even amplitude leads to a p-wave final state while the parity-odd amplitude to an s-wave final state. The two amplitudes are denoted P and S, respectively. In the following, we will often write the decay generically as $D(B \to b\pi)$. When we need to be more specific, we use indices Λ and Ξ to denote $\Lambda \to p\pi^-$ and $\Xi^- \to \Lambda\pi^-$, respectively. The decay amplitude is

$$\mathcal{A} \sim S\sigma_0 + P\boldsymbol{\sigma} \cdot \hat{\mathbf{n}}, \tag{2.2}$$

where σ_0 is the 2×2 unit matrix, $\boldsymbol{\sigma} := (\sigma_1, \sigma_2, \sigma_3)$ are the Pauli matrices and $\hat{\mathbf{n}} = \mathbf{q}/|\mathbf{q}|$ is the direction of the b-baryon momentum $\mathbf{q}$ in the B-baryon rest frame. It is important to note that these amplitudes depend on the initial (weak) decay, which produces the two final particles, but depend also on the (strong) final-state interaction. These S and P amplitudes are Lorentz scalars, which can depend only on the invariant mass of the two-body system. Yet this quantity is fixed for a two-body decay: if we disregard the unmeasurable overall phase, the two complex amplitudes S and P can be fully specified by the overall normalization $|S|^2 + |P|^2$ and the size and relative phase of the interference term S^*P. These are directly related to the partial decay width and the following two parameters [87]:

$$\alpha_D := \frac{2\,\mathrm{Re}(S^*P)}{|S|^2 + |P|^2} \quad \text{and} \quad \beta_D := \frac{2\,\mathrm{Im}(S^*P)}{|S|^2 + |P|^2}. \tag{2.3}$$

The relation of the parameters to the shape of the angular distribution, including the polarization, of the baryon b will be shown in Sec. 2.2. In the CP-conserving limit, the amplitudes $\overline{S}$ and $\overline{P}$ for the charge-conjugated (c.c.) decay mode of the antibaryon $\overline{D}(\overline{B} \to \overline{b} + \overline{\pi})$ are $\overline{S} = -S$ and $\overline{P} = P$. Therefore, the decay parameters have the opposite values: $\overline{\alpha}_D = -\alpha_D$ and $\overline{\beta}_D = -\beta_D$.

Two independent experimental CPV tests can be defined using these parameters,

$$A_{\mathrm{CP}}^D := \frac{\alpha_D + \overline{\alpha}_D}{\alpha_D - \overline{\alpha}_D} \quad \text{and} \quad B_{\mathrm{CP}}^D := \frac{\beta_D + \overline{\beta}_D}{\alpha_D - \overline{\alpha}_D}, \tag{2.4}$$

where $A_{\mathrm{CP}}^D(B_{\mathrm{CP}}^D) \neq 0$ indicates CP violation in the D decay. The A_{CP}^D test requires measurement of the angular $b(\overline{b})$ distribution from polarized $B(\overline{B})$-baryon decay. The B_{CP}^D test probes

TABLE 2.1: Illustration of the expected statistical uncertainty for the CPV observables $A_{\text{CP}}^{[\Lambda p]}$, $A_{\text{CP}}^{[\Xi-]}$ and $B_{\text{CP}}^{[\Xi-]}$ at BESIII and the proposed SCTF electron–positron collider. The results of the published BESIII measurements are given in the first row [94, 95]. The uncertainties given in the two remaining rows are straightforward re-scaling based on the expected number of events. The SM prediction for $A_{\text{CP}}^{[\Lambda p]}$ is $\sim (1 - 5) \times 10^{-5}$ while for $B_{\text{CP}}^{[\Xi-]}$ it amounts to $O(10^{-4})$ [90].

	$\sigma(A_{\text{CP}}^{[\Lambda p]})$	$\sigma(A_{\text{CP}}^{[\Xi-]})$	$\sigma(B_{\text{CP}}^{[\Xi-]})$	Comment
BESIII	1.0×10^{-2} [1]	1.3×10^{-2}	3.5×10^{-2}	1.3×10^{9} J/ψ [94, 95]
BESIII	3.6×10^{-3}	4.8×10^{-3}	1.3×10^{-2}	1.0×10^{10} J/ψ (projection)
SCTF	2.0×10^{-4}	2.6×10^{-4}	6.8×10^{-4}	3.4×10^{12} J/ψ (projection)

time reversal-odd transitions and can be potentially much more sensitive but it requires in addition a measurement of the $b(\overline{b})$-baryon polarization. In the SM, CPV effects in the hyperon decays are dominated by the QCD-penguin contribution, Fig. 2.1(a).

In the 1960s, hyperon decays were a tool for discrete symmetry tests on equal footing with the kaons. The last dedicated program to observe CP violation in hyperons was performed by the Fermilab experiments E756 [88] and HyperCP [89] at the dawn of this century. In these experiments, the sum of the A_{CP} observables for $\Xi^- \rightarrow \Lambda \pi^-$ ([$\Xi-$]) and $\Lambda \rightarrow p\pi^-$ ([Λp]), $A_{\text{CP}}^{[\Xi-]} + A_{\text{CP}}^{[\Lambda p]}$, was studied. Here, the SM prediction amounts to $-0.5 \times 10^{-4} \leq A_{\text{CP}}^{[\Xi-]} + A_{\text{CP}}^{[\Lambda p]} \leq 0.5 \times 10^{-4}$ [90]. The published result $A_{\text{CP}}^{[\Xi-]} + A_{\text{CP}}^{[\Lambda p]} = 0(7) \times 10^{-4}$ [91] is currently considered to be the most precise test of CP symmetry in the hyperon sector.

The prospect of significantly improving the CPV tests in hyperons is due to a novel method where hyperon–antihyperon pairs are produced in electron–positron collisions at the center-of-mass (c.m.) energy corresponding to the J/ψ resonance. The J/ψ decays into a hyperon–antihyperon pair have relatively large branching fractions of $O(10^{-3})$ [92]. The produced hyperon–antihyperon pair has a well-defined spin-entangled state based on the two possible partial waves (parity symmetry in this strong decay allows for an *s*- and a *d*-wave) [46, 93]. The charge-conjugated decay modes of the hyperon and antihyperon can be measured simultaneously, and their properties compared directly. The uncertainties obtained in the proof-of-concept experiment [94, 95] based on 1.3×10^{9} J/ψ for the $A_{\text{CP}}^{[\Lambda p]}$, $A_{\text{CP}}^{[\Xi-]}$, and $B_{\text{CP}}^{[\Xi-]}$ observables are given in the first row of Table 2.1. With the already available data set of 10^{10} J/ψ collected at BESIII [64], a significantly improved statistical precision is expected, as shown in the second row of the table. However, the uncertainty is still predicted to be two orders of magnitude larger compared to the SM CPV signal.

Crucial improvements are expected at the next-generation electron–positron colliders, the Super Charm-Tau or Super Tau-Charm Factories (SCTF) being under consideration in China [96] and in Russia [97]. Their design luminosity is two orders of magnitude larger than the BEPCII collider [44, 98] allowing for data samples of more than 10^{12} J/ψ events. The projections for the improved statistical uncertainties of the CPV tests, due to the increased data samples, are shown in Table 2.1. This will still not be sufficient to observe an effect if it has a magnitude consistent with the SM predictions. Therefore, besides the increased luminosity, two additional improvements are being discussed to further increase the precision:

1) a c.m. energy spread ΔE compensation and 2) an electron beam polarization. For the first option, a collision scheme is proposed where electrons (positrons) with higher momenta are matched with positrons (electrons) with lower momenta. This promises a ΔE reduction to better match the natural width of J/ψ meson of $\Gamma = 0.09$ MeV, thus up to an order of magnitude increase of the number of J/ψ events for a given integrated luminosity [99–101]. For the second option, an electron beam polarization of 80–90% at J/ψ energies can be obtained with the same beam current [102].

Since the benefits of the first improvement are obvious, we focus on the impact of the use of a polarized electron beam and show that the precision of the CP tests in $e^+e^- \to J/\psi \to \Lambda\overline{\Lambda}$ and $e^+e^- \to J/\psi \to \Xi\overline{\Xi}$ can be significantly improved. The initial findings for $e^+e^- \to J/\psi \to \Lambda\overline{\Lambda}$ have already been reported at the SCTF workshop [103] and independently in Ref. [104]. Here we give a detailed explanation of this result and extend it to sequential hyperon weak decays. In Sec. 2.2 we review the phenomenology and the current experimental status of CP tests in two-body weak decays of hyperons. In Sec. 2.3 we use the formalism based on Jacob–Wick's [49] helicity amplitudes [52] to derive the hyperon–antihyperon production spin-correlation matrix for electron–positron collisions with longitudinal polarization of the electron beam. The asymptotic maximum log-likelihood method from Ref. [105] used for the analysis of uncertainties for the CPV observables is introduced in Sec. 2.3.3. The single-step decays are discussed in Sec. 2.4 and the two-step decays in Sec. 2.5. Further experimental considerations are presented in Sec. 2.6 and Sec. 2.7 contains an outlook.

2.2 CP tests in hyperon decays

2.2.1 General considerations

There are three independent observables that provide a complete description of a weak decay $D(B \to b + \pi)$ with the amplitude given in Eq. (2.2). The first is the partial decay width given by

$$\Gamma = \frac{|\mathbf{q}|}{4\pi M_B} (E_b + M_b)|\mathcal{A}|^2 \,, \tag{2.5}$$

where $|\mathcal{A}|^2 = |S|^2 + |P|^2$ and $E_b = \sqrt{|\mathbf{q}|^2 + M_b^2}$. The M_B and M_b are the masses of the mother and daughter baryon, respectively. The first of the two parameters defined in Eq. (2.3), $-1 < \alpha_D < 1$, can be determined from the angular distribution of the daughter baryon when the mother baryon is polarized. For example, the proton angular distribution from the $\Lambda(\Lambda \to p\pi^-)$ decay in the Λ rest frame is given as

$$\frac{1}{\Gamma}\frac{d\Gamma}{d\Omega} = \frac{1}{4\pi}\left(1 + \alpha_\Lambda \mathbf{P}_\Lambda \cdot \hat{\mathbf{n}}\right) \,, \tag{2.6}$$

where $\mathbf{P}_\Lambda$ is the Λ polarization vector. The second independent decay parameter can be chosen as the angle ϕ_D, $-\pi < \phi_D < \pi$, which gives the rotation of the spin vector between the B and b baryons. To measure ϕ_D, the polarization of both mother and daughter baryons must be determined. For the decay $\Xi(\Xi^- \to \Lambda\pi^-)$, where the cascade is polarized, the ϕ_D parameter

can be determined from the subsequent $\Lambda \to p\pi^-$ decay, which acts as a polarimeter. The relation between the initial Ξ^- polarization $\mathbf{P_\Xi}$ and the daughter Λ polarization $\mathbf{P_\Lambda}$ is given by the Lee–Yang formula [87]:

$$\mathbf{P_\Lambda} = \frac{(\alpha_\Xi + \mathbf{P_\Xi} \cdot \hat{\mathbf{n}})\hat{\mathbf{n}} + \beta_\Xi \mathbf{P_\Xi} \times \hat{\mathbf{n}} + \gamma_\Xi \hat{\mathbf{n}} \times (\mathbf{P_\Xi} \times \hat{\mathbf{n}})}{1 + \alpha_\Xi \mathbf{P_\Xi} \cdot \hat{\mathbf{n}}} \ , \tag{2.7}$$

where the β- and γ-type decay parameters are expressed as

$$\beta_D = \sqrt{1 - \alpha_D^2} \sin \phi_D \ , \quad \gamma_D := \frac{|S|^2 - |P|^2}{|S|^2 + |P|^2} = \sqrt{1 - \alpha_D^2} \cos \phi_D \ , \tag{2.8}$$

implying that $\alpha_D^2 + \beta_D^2 + \gamma_D^2 = 1$. In Table 2.2 the branching fractions ($\mathcal{B}$) and the values of the α_D and ϕ_D parameters for decays of the ground-state octet baryons are listed. When available we report the hyperon–antihyperon average values, defined as

$$\langle \alpha_D \rangle = \frac{\alpha_D - \overline{\alpha}_D}{2} \ , \quad \langle \phi_D \rangle = \frac{\phi_D - \overline{\phi}_D}{2} \ . \tag{2.9}$$

In most cases, the parameters of the antihyperon decays have not been determined yet. The α_D parameter is much easier to measure than ϕ_D, since only the polarization of the initial or final baryon has to be determined. Before 2018 the consensus was that the α_D parameters were known accurately. The BESIII measurement [94, 95] has shown that values for $\Lambda \to p\pi^-$ and $\Xi^- \to \Lambda\pi^-$ were wrong by 17%.

The use of α_D and β_D parameters provides a symmetric description of the real and imaginary parts of the S and P amplitudes. On the other hand, the preferred choice of the α_D and ϕ_D parameters by the Particle Data Group (PDG) is motivated experimentally, as the ϕ_D and α_D uncertainties are approximately uncorrelated. However, the ϕ_D parameter is not directly related to the relative phase between the S and P amplitudes, since it can be written as

$$\phi_D = \arg\{(S + P)(S^* - P^*)\} \ . \tag{2.10}$$

In general, we do not need to know the exact values of the decay parameters to predict the uncertainties of the CPV observables given in Eq. (2.4). Many of our results can be described using approximate analytic formulas where the dependence on parameters is given explicitly. Furthermore, in the proposed measurements the values of the decay parameters are determined directly together with the CPV observables, and are uncorrelated with each other. For specific purposes, such as the estimate of the size of the decay amplitudes in Appendix I, we need the most precise values of the decay parameters and branching ratios or life times. We have made a critical evaluation of the available data, and the preferred values which we have selected are given in bold in Table 2.2. Here, we provide a detailed explanation how some values were determined:

- The $\langle \alpha_{[\Lambda p]} \rangle$ value is the average of the two BESIII measurements [94] and [95]. We

TABLE 2.2: Properties of two-body hadronic decays of the ground-state octet hyperons. Branching fractions $\mathcal{B}$ are rounded to $\pm 0.5\%$ accuracy. In bold are the values assumed in this report. The motivation for the selection of the specific values is given in the main text.

	D	$\mathcal{B}$	$\langle \alpha_D \rangle$	$\langle \phi_D \rangle$ [rad]	A_{CP}	Comment
$\Lambda \to p\pi^-$	$[\Lambda p]$	64%	**0.755(03)**[1]	**−0.113(61)**[2]	**−0.005(10)**[1]	
			0.754(3)(2)	–	−0.006(12)(7)	BESIII [94]
			0.721(6)(5)*	–	–	CLAS [106]
			0.760(6)(3)	–	−0.004(12)(9)	BESIII [95]
$\Lambda \to n\pi^0$	$[\Lambda n]$	36%	**0.692(17)**[3]	–	–	BESIII [94]
$\Sigma^+ \to p\pi^0$	$[\Sigma p]$	52%	**−0.994(04)**[4]	**0.63(59)**[7]	**−0.004(37)**[4]	
$\Sigma^+ \to n\pi^+$	$[\Sigma n]$	48%	**0.068(13)***	**2.91(35)***	–	PDG [92]
$\Sigma^- \to n\pi^-$	$[\Sigma-]$	100%	**−0.068(08)***	**0.17(26)***	–	PDG [92]
$\Xi^0 \to \Lambda\pi^0$	$[\Xi 0]$	100%	**−0.345(08)**[5]	**0.36(21)***	–	AVG [107, 108]
$\Xi^- \to \Lambda\pi^-$	$[\Xi-]$	100%	**−0.379(04)**[6]	−0.042(16)*	–	AVG [92, 109]
			−0.373(5)(2)	0.016(14)(7)	**0.006(13)(6)**	BESIII [95]

---

* Solely based on the result for hyperons (not antihyperons)

[a] Weighted average of the results from [94, 95]

[b] Weighted average of $\phi_{[\Lambda p]}$ from [110–112] the same as in PDG [92]

[c] The $-\overline{\alpha}_{[\Lambda n]}$ value from [94]

[d] Value from [113]

[e] From $\alpha_{[\Xi 0]}\alpha_{[\Lambda p]} = -0.261(6)$ [92] divided by $\alpha_{[\Lambda p]}$[1]

[f] Combination of $\langle \alpha_{[\Xi-]} \rangle$ [95] and $\alpha_{[\Xi-]}\alpha_{[\Lambda p]} = -0.294(5)$ [92] divided by $\alpha_{[\Lambda p]}$[1]

[g] Weighted average of $\phi_{[\Sigma p]}$ from [114, 115]

do not include the result from CLAS experiment [106] since it does not report the measurement of $\langle \alpha_{[\Lambda p]} \rangle$ and would indicate significant violation of the CP symmetry due to the statistically inconsistent value with the BESIII measurement of the antihyperon $\overline{\alpha}_{[\Lambda p]}$. The BESIII results for α_D and $\overline{\alpha}_D$ are correlated and have large uncertainty separately.

• Since the $\langle \phi_{[\Xi-]} \rangle$ measured at BESIII [95] differs by 2.6 standard deviations from $\phi_{[\Xi-]}$ measured by HyperCP [109], we do not provide the average value for $\langle \phi_{[\Xi-]} \rangle$.

Finally, we use other results which do not fit to the format of the table, such as $B_{\mathrm{CP}}^{[\Xi-]}$, $A_{\mathrm{CP}}^{[\Xi-]} + A_{\mathrm{CP}}^{[\Lambda p]}$ or life times of the cascades. They are introduced and referred to when we need to use them. For example, for the determination of the contribution of the $\Delta I = 3/2$ amplitudes we use more precise values of the branching fractions from Ref. [92]: $\mathcal{B}(\Lambda \to p\pi^-) = 0.639(5)$ and $\mathcal{B}(\Lambda \to n\pi^0) = 0.358(5)$.

2.2.2 CP violation phenomenology

Isospin is not conserved in weak transitions, meaning that both the isospin vector length and the third component I_3 change in the decay process. In our hyperon decays of interest, there is effectively a transition from a strange to a down quark: thus, I_3 changes by $-1/2$. For the total isospin, the situation is more involved. It is convenient to classify the weak transition by the isospin ΔI of the transition operator. Starting with the initial isospin I_{ini} of the decaying hyperon, the isospin I of the final state can take values between $|I_{\mathrm{ini}} - \Delta I|$ and $I_{\mathrm{ini}} + \Delta I$. As

TABLE 2.3: Values of the N–π scattering phase shifts δ_{2I}^L relevant for Λ and Σ decays from [117].

	$\lvert\mathbf{q}\rvert$ [MeV/c]	δ_1^S [°]	δ_3^S [°]	δ_1^P [°]	δ_3^P [°]
$\Lambda \to N\pi$	103	6.52(9)	$-4.60(7)$	$-0.79(8)$	$-0.75(4)$
$\Sigma \to N\pi$	190	9.98(23)	$-10.70(13)$	$-0.04(33)$	$-3.27(15)$

a result of these considerations, it is practical to characterize the weak process by the isospin of the final state I and by the change of isospin ΔI. To explain this distinction, let us consider the process $\Xi^- \to \Lambda\pi^-$ where the initial and final isospins are $1/2$ and 1, respectively. This final state can be reached by a transition with $\Delta I = 1/2$, where the isospins are aligned, and a transition with $\Delta I = 3/2$, where the isospins are anti-aligned. Therefore, the transition amplitudes of the decomposition should be labelled by both I and ΔI, and we adopt the notation $S_{2\Delta I, 2I}$ and $P_{2\Delta I, 2I}$.

The transition amplitudes $L = S, P$ can be decomposed as [86]:

$$L = \sum_j L_j \exp\left\{i(\xi_j^L + \delta_j^L)\right\} , \qquad (2.11)$$

where j represents a possible $\{2\Delta I, 2I\}$ combination, while ξ_j^L and δ_j^L denote the weak CP-odd phase and the phase of the combined strong and electromagnetic (e.m.) final state interaction, respectively, and the explicit expressions in the Λ and Ξ cases are written down in Eqs. (2.87) and (2.88). Appendices II and III provide a justification for the decomposition in Eq. (2.11) where the S_j and P_j amplitudes are real numbers. The final-state interaction phase is dominated by the phase shifts of the strong elastic rescattering. The isospin-breaking effects in the rescattering due to hadron mass differences for different charge states are a few percent. Further contributions can be due to $m_d - m_u$ terms in the amplitudes and e.m. interactions of the hadrons, such as radiative corrections or Coulomb interactions. The δ_j^L phase can be written as $\delta_j^L = \delta_{2I}^L + \Delta\delta_j^L$, where the correction term $\Delta\delta_j^L$ includes the isospin-breaking effects due to e.m. interactions in the final state. Here, we will neglect this term, but for future precision studies it should be considered similar to how it was for the kaon to two-pion decays [116].

For the N–π final states, the phases-shifts δ_{2I}^L are well known. We summarize in Table 2.3 the values from Ref. [117] which are relevant for the Λ and Σ decays. The Λ-π scattering phase-shifts, on the other hand, are less precisely determined from experiment. In particular, for $\Xi \to \Lambda\pi$ they can be found via the relation $\tan\left(\delta_2^P - \delta_2^S\right) = \sin\phi_\Xi\sqrt{1 - \alpha_\Xi^2}/\alpha_\Xi$, neglecting the weak-phase difference, where α_Ξ and ϕ_Ξ are obtainable directly from the sequential decays. In doing so, we note that the current ϕ_Ξ data are not all consistent with each other yet, as pointed out in the preceding subsection. On the theoretical side, various analyses have produced different results [118–124], the latest one being $\delta_2^P - \delta_2^S = 8.8(2)°$ [124], which is compatible with one of the earlier predictions [122] and will be used in updating the $A_{\text{CP}}^{[\Xi^-]}$ prediction.

Now we discuss signatures of CP violations in the hyperon decays. They are based on the comparison of the hyperon decay amplitudes, Eq. (2.11), with the ones corresponding to the antihyperon c.c. decay,

$$\overline{S} = - \sum_j S_j \exp\left\{i(-\xi_j^S + \delta_{2I}^S)\right\} \quad \text{and} \quad \overline{P} = \sum_j P_j \exp\left\{i(-\xi_j^P + \delta_{2I}^P)\right\} , \qquad (2.12)$$

where the real-number parameters L_j, ξ_j^L and δ_{2I}^L, $(L = S, P)$, have the same values for the hyperon and antihyperon decays. The isospin-decomposition relations obtained in Appendix I can be applied to the c.c. decays of antihyperons. *A priori*, up to three independent observables can be used to compare properties of a decay to the c.c. one. The first observable is the difference between the partial decay widths

$$\Delta_{\text{CP}} := \frac{\Gamma - \overline{\Gamma}}{\Gamma + \overline{\Gamma}} . \qquad (2.13)$$

In the $\Delta I = 1/2$ limit the Δ_{CP} observable is exactly zero and cannot be used to test CP symmetry. In addition, for $\Xi \to \Lambda\pi$ the isospin of the final Λ–π state is $I = 1$ and there is only one strong phase for each of the S and P amplitudes. This implies that the corresponding Δ_{CP} is zero even if the weak transition includes $|\Delta I| = 3/2$ operators. However, the Δ_{CP} test is possible for $\Lambda \to N\pi$, as the final state can have $I = 1/2$ or $3/2$. For the two Λ-decay modes, to the lowest order in the $\Delta I = 3/2$ amplitudes, starting from Eq. (2.87) we have the relation $2\Delta_{\text{CP}}^{[\Lambda p]} = -\Delta_{\text{CP}}^{[\Lambda n]} = 2\sqrt{2}\Delta_{\text{CP}}$ with

$$\Delta_{\text{CP}} = \frac{P_{1,1}P_{3,3}\sin(\xi_{1,1}^P - \xi_{3,3}^P)\sin(\delta_1^P - \delta_3^P) + S_{1,1}S_{3,3}\sin(\xi_{1,1}^S - \xi_{3,3}^S)\sin(\delta_1^S - \delta_3^S)}{P_{1,1}^2 + S_{1,1}^2} . \qquad (2.14)$$

This requires two weak and two strong phases either in the S amplitude, as in the kaon decays, or in the P amplitude. The precision of the test is suppressed by the small $|\Delta I| = 3/2$ amplitudes and by the term containing sinus of the small strong phases. Therefore, such a test is not competitive and we will not discuss it further.

The remaining two CP tests involve the A_{CP}^D and B_{CP}^D observables defined in Eq. (2.4). If one works to leading order in the weak phases, B_{CP}^D can also be expressed as

$$B_{\text{CP}}^D = \Phi_{\text{CP}}^D \frac{\sqrt{1 - \langle\alpha_D\rangle^2}}{\langle\alpha_D\rangle}\cos\langle\phi_D\rangle - A_{\text{CP}}^D \frac{\langle\alpha_D\rangle}{\sqrt{1 - \langle\alpha_D\rangle^2}}\sin\langle\phi_D\rangle , \qquad (2.15)$$

where $\langle\alpha_D\rangle$ and $\langle\phi_D\rangle$ were defined in Eq. (2.9) and

$$\Phi_{\text{CP}}^D := \frac{\phi_D + \overline{\phi}_D}{2} \qquad (2.16)$$

is based on the spin-rotation decay parameter ϕ_D. In a large acceptance experiment, the decay parameters α and ϕ are uncorrelated, as well as the CPV tests based on the A_{CP}^D and Φ_{CP}^D variables.

Contrary to the CP violation in $K_{L,S} \to \pi\pi$, where $\Delta I = 1/2$ and $\Delta I = 3/2$ amplitudes are both consequential, the dominant effect in hyperons can be studied using only the $\Delta I = 1/2$ amplitudes. The corrections to the CPV effect studied in this approximation will be a few percent, as given by the size of the P_3 and S_3 amplitudes. This is sufficient for the precision expected at SCTF. If a better precision is required, one can construct isospin averages of the observables from different isospin modes to recover the results in the $\Delta I = 1/2$ limit. Such averages are constructed from the isospin decomposition of a given decay process (channel) – for more details, we refer to Appendix I. For Ξ, up to the linear terms in the $\Delta I = 3/2$ amplitudes, they amount to

$$B_{\mathrm{CP}}^{\Xi} := \frac{2B_{\mathrm{CP}}^{[\Xi^-]} + B_{\mathrm{CP}}^{[\Xi^0]}}{3} = \quad \tan(\xi_{1,2}^P - \xi_{1,2}^S)\,, \tag{2.17}$$

$$A_{\mathrm{CP}}^{\Xi} := \frac{2A_{\mathrm{CP}}^{[\Xi^-]} + A_{\mathrm{CP}}^{[\Xi^0]}}{3} = -\tan(\xi_{1,2}^P - \xi_{1,2}^S)\tan(\delta_2^P - \delta_2^S)\,, \tag{2.18}$$

and for Λ

$$B_{\mathrm{CP}}^{\Lambda} := \frac{2B_{\mathrm{CP}}^{[\Lambda p]} + B_{\mathrm{CP}}^{[\Lambda n]}}{3} = \quad \tan(\xi_{1,1}^P - \xi_{1,1}^S)\,, \tag{2.19}$$

$$A_{\mathrm{CP}}^{\Lambda} := \frac{2A_{\mathrm{CP}}^{[\Lambda p]} + A_{\mathrm{CP}}^{[\Lambda n]}}{3} = -\tan(\xi_{1,1}^P - \xi_{1,1}^S)\tan(\delta_1^P - \delta_1^S)\,. \tag{2.20}$$

The leading-order correction for the two isospin states of the cascades is:

$$B_{\mathrm{CP}}^{[\Xi^-]} - B_{\mathrm{CP}}^{[\Xi^0]} = -\frac{3}{2}\left[\frac{P_{3,2}}{P_{1,2}}\sin(\xi_{1,2}^P - \xi_{3,2}^P) - \frac{S_{3,2}}{S_{1,2}}\sin(\xi_{1,2}^S - \xi_{3,2}^S)\right]\,, \tag{2.21}$$

$$A_{\mathrm{CP}}^{[\Xi^-]} - A_{\mathrm{CP}}^{[\Xi^0]} = -\left(B_{\mathrm{CP}}^{[\Xi^-]} - B_{\mathrm{CP}}^{[\Xi^0]}\right)\tan(\delta_2^P - \delta_2^S)\,,$$

which implies that even if the LO $\Delta I = 3/2$ corrections are included, the A and B tests are still connected — giving the same combination of the weak phases. For the Λ decays such a relation is not valid and the A- and B-type variables provide independent information on the weak-phase combinations. We will not discuss this case, since the B-type observables cannot be measured with the standard techniques available at the electron–positron-collider experiments. A combination of the CP tests for the isospin related channels allows for an increased statistical significance of the tests. Such an approach is feasible at SCTF for the Ξ and Λ decays, since all the decay parameters for (anti)cascade and the α parameters for Λ can be measured.

A simpler approach is to treat each decay mode separately when comparing decay parameters for the hyperon and, from the c.c. decay, for the antihyperon. In the $\Delta I = 1/2$ approximation we can write

$$S = |\mathcal{A}|\,\sin\zeta\,\exp(i\xi_S + i\delta_S)\,, \qquad \overline{S} = -|\mathcal{A}|\,\sin\zeta\,\exp(-i\xi_S + i\delta_S)\,, \tag{2.22}$$

$$P = |\mathcal{A}|\,\cos\zeta\,\exp(i\xi_P + i\delta_P)\,, \qquad \overline{P} = \quad |\mathcal{A}|\,\cos\zeta\,\exp(-i\xi_P + i\delta_P)\,,$$

where $0 \le \zeta \le \pi$, $\xi_S(\xi_P)$ is the weak CP-odd phase for the $\Delta I = 1/2$ transition, and $\delta_S(\delta_P)$ is

the strong $s(p)$-wave baryon–pion phase-shift at the c.m. energy corresponding to the hyperon mass. The structure of Eq. (2.22) can be justified, if one assumes that the complete decay process can be split up into the decay itself where one does not resolve the intrinsic structure and a final-state interaction that conserves P and C separately. If one does not resolve the space-time structure of the initial decay, then one can use an effective hermitian Lagrangian to describe the decay and one just reads off the relations $\overline{S}_{\text{ini}} = -S^*_{\text{ini}}$ and $\overline{P}_{\text{ini}} = P^*_{\text{ini}}$. More details are given in Appendix II. The final-state interaction can be described by a 4×4 Omnès-function matrix that is applied to the four initial amplitudes; see also Appendix III. If P (and baryon number) is conserved, then this matrix is diagonal. If C is conserved, then the entries are pairwise the same for particle and antiparticle. Without inelasticities, Watson's theorem [125] identifies the phases with the scattering phase shifts. The decay parameters (α, β, γ) and $\left(\overline{\alpha}, \overline{\beta}, \overline{\gamma}\right)$[1] are then given as

$$\alpha = \sin(2\zeta)\cos(\xi_P - \xi_S + \delta_P - \delta_S)\,, \quad \overline{\alpha} = -\sin(2\zeta)\cos(-\xi_S + \xi_P + \delta_S - \delta_P)\,, \quad (2.23)$$

$$\beta = \sin(2\zeta)\sin(\xi_P - \xi_S + \delta_P - \delta_S)\,, \quad \overline{\beta} = -\sin(2\zeta)\sin(-\xi_P + \xi_S + \delta_P - \delta_S)\,, \quad (2.24)$$

$$\gamma = -\cos(2\zeta)\,, \qquad\qquad\qquad \overline{\gamma} = -\cos(2\zeta)\,. \qquad\qquad\qquad (2.25)$$

Without final-state interactions, $\alpha + \overline{\alpha}$ is always zero and A_{CP} does not constitute an observable that can indicate CP violation, while $B_{\text{CP}} = \tan(\xi_P - \xi_S)$ does. One needs CP violation and final-state interactions to make A_{CP} different from zero. In the presence of final-state interactions, $\beta \neq 0$ does not necessarily indicate CP violation, but B_{CP} still does. The CPV tests based on the A_{CP}, B_{CP} (and Φ_{CP}) observables can be expressed using Eq. (2.22) as

$$A_{\text{CP}} = -\frac{\sqrt{1-\alpha^2}}{\alpha}\sin\phi\tan(\xi_P - \xi_S) \qquad (2.26)$$

$$= -\tan(\delta_P - \delta_S)\tan(\xi_P - \xi_S)\,, \qquad (2.27)$$

$$B_{\text{CP}} = \tan(\xi_P - \xi_S)\,, \qquad (2.28)$$

$$\Phi_{\text{CP}} = \frac{\alpha}{\sqrt{1-\alpha^2}}\cos\phi\tan(\xi_P - \xi_S)\,. \qquad (2.29)$$

Therefore the tests are not independent as they are related to the same $\xi_P - \xi_S$ combination of the CP-odd weak phases. For single-step decays of the singly-strange baryons, measurement of the $B_{\text{CP}}(\Phi_{\text{CP}})$ would require a dedicated detector to determine the daughter-nucleon polarization. Therefore, for the Λ and Σ hyperon decays, we consider only the A_{CP} observable measurements. In this case, the weak phases are determined by Eq. (2.27) using the well known values of the strong N–π phases. Since the strong phases δ_P and δ_S, representing the final state interaction between the baryon and pion, are small, the B_{CP} observable provides much better determination of the weak-phase difference than A_{CP}. This statement assumes that the uncertainties of the A_{CP} and B_{CP} (or Φ_{CP}) measurements are comparable. In Sec. 2.6 we will discuss strategies for the simultaneous measurement of the two observables in the cascade decays.

---

[1]In the remaining part of this section we simplify the notation by omitting subscript D for the decay parameters.

TABLE 2.4: Weak-phase differences in hyperon decays. (left) Standard-model predictions and (right) parameters C_B and C'_B used in Eq. (2.30) to relate the weak-phase differences in hyperon decays to the beyond SM (BSM) constraints from kaon CPV observables. The SM and BSM entries are updates of the corresponding numbers obtained in Refs. [90] and [126], respectively, as explained in the main text.

	$\xi_P - \xi_S$ $(\eta\lambda^5 A^2)$ [10^{-4} rad] SM		C_B C'_B BSM	
$\Lambda \to p\pi^-$	-0.1 ± 1.5	-0.2 ± 2.2	0.9 ± 1.8	0.4 ± 0.9
$\Xi^- \to \Lambda\pi^-$	-1.5 ± 1.2	-2.1 ± 1.7	-0.5 ± 1.0	0.4 ± 0.7

2.2.3   Status of the CPV predictions

In this subsection, we review the estimates of CPV signals for the decay channels $\Lambda \to p\pi^-$ and $\Xi^- \to \Lambda\pi^-$, commonly considered to be the most sensitive modes. In the experimental study of the latter, the former is used as the subsequent process. The SM contributions to $\xi_P - \xi_S$ for the two decay modes are shown in the third column of Table 2.4. These predictions are both $O(10^{-4})$, taking into account the substantial uncertainties which are related to our present lack of ability to explain simultaneously the *s*- and *p*-waves of hyperon nonleptonic decays [90]. The second column of this table contains $\xi_P - \xi_S$ divided by $\eta\lambda^5 A^2$, which is a product of the Wolfenstein parameters for the Cabibbo–Kobayashi–Maskawa matrix and has a value of $1.36(7) \times 10^{-4}$ according to the most recent PDG report [92]. The SM entries in this table are updates of the corresponding numbers found in Ref. [90] and are somewhat modified with respect to the latter, mainly because of our use of the (boldfaced) new α results for $\Lambda \to p\pi^-$ and $\Xi^- \to \Lambda\pi^-$ quoted in Table 2.2.

To compare the theoretical A_{CP} with its most precise measurements to date given in Table 2.2 requires multiplication of the calculated $\xi_P - \xi_S$ by the strong-interaction parameters, as indicated in Eqs. (2.26)-(2.27), an extra step which increases the experimental uncertainty and/or decreases the precision of the predictions. Nevertheless, from Eq. (2.28), we expect that future measurements of B_{CP} can directly determine $\xi_P - \xi_S$ with good precision. For $\Lambda \to p\pi^-$ the strong phases pertaining to Eq. (2.27) are $\delta_1^S = 0.11(2)$ rad and $\delta_1^P = -0.014(1)$ rad from Table 2.3. For $\Xi^- \to \Lambda\pi^-$ the strong-phase difference can be extracted experimentally using the methods discussed in this report. However, since $\beta_{[\Xi^-]}$ is not yet well measured, the $\alpha_{[\Xi^-]}$ data cannot be used to obtain $\delta_2^P - \delta_2^S$ with good precision via $\beta_{[\Xi^-]} = \alpha_{[\Xi^-]} \tan(\delta_2^P - \delta_2^S)$. To update the prediction for $A_{\text{CP}}^{[\Xi^-]}$, we adopt instead the theoretical value $\delta_2^P - \delta_2^S = 8.8(2)$ deg computed in Ref. [124]. Putting together the weak and strong phases, we then arrive at the SM ranges $-3 \times 10^{-5} \le A_{\text{CP}}^{[\Lambda p]} \le 3 \times 10^{-5}$ and $0.5 \times 10^{-5} \le A_{\text{CP}}^{[\Xi^-]} \le 6 \times 10^{-5}$, which are below their respective experimental bounds inferred from Table 2.2 by more than two orders of magnitude.

Measurements on hyperon CPV and its kaon counterpart are complementary to each other because they do not probe the underlying physics in the same way. As mentioned above, in the context of the SM, the direct-CPV parameter ϵ' in the kaon decay $K \to \pi\pi$ arises from both $|\Delta I| = 1/2$ and $|\Delta I| = 3/2$ transitions, where the CP-odd phases come from the QCD,

Fig. 2.1(a), and electroweak, Fig. 2.1(b), penguin contributions, respectively, all of which are induced by effective four-quark operators. There is a delicate balance and cancellation between the two contributions. In the hyperon case, the CPV signal of interest here, such as measured by A_{CP} or B_{CP}, mainly comes from $|\Delta I| = 1/2$ transitions and is dominated by the QCD penguins.

In the presence of physics beyond the SM (BSM), there might be new ingredients causing other types of quark operators to appear and generate effects that are enhanced relative to the SM contributions. This possibility can be realized, for instance, by the so-called chromomagnetic-penguin operators, which contain a *ds* quark bilinear coupled to gluon fields and could be influenced by sizeable new physics in various models [126–131]. The parity-odd and parity-even portions of the operators contribute to ϵ' and the CPV parameter ϵ in neutral-kaon mixing, respectively, and both parts simultaneously affect $\xi_P - \xi_S$. Model independently, one can derive a general relation between the contributions of these operators to the hyperon weak-phase difference and kaon observables [126]:

$$(\xi_P - \xi_S)_{\text{BSM}} = \frac{C'_B}{B_G} \left(\frac{\epsilon'}{\epsilon} \right)_{\text{BSM}} + \frac{C_B}{\kappa} \epsilon_{\text{BSM}} , \qquad (2.30)$$

which further illustrates the complementarity of hyperon and kaon decays. The values of C_B and C'_B, updated from their counterparts evaluated in Ref. [126], are given in Table 2.4, B_G parameterizes the hadronic uncertainty, and κ quantifies the contribution of meson poles. The allowed ranges of $(\epsilon'/\epsilon)_{\text{BSM}}$ and ϵ_{BSM} can be estimated by comparing the experimental values of $\text{Re}(\epsilon'/\epsilon)$ and $|\epsilon|$ with the recent SM predictions [132–134]. Following Ref. [134] we impose

$$\left| \frac{\epsilon'}{\epsilon} \right|_{\text{BSM}} \leq 1 \times 10^{-3} , \qquad |\epsilon|_{\text{BSM}} \leq 2 \times 10^{-4} . \qquad (2.31)$$

Accordingly, using $0.5 < B_G < 2$ and $0.2 < |\kappa| < 1$ [130], we find that the kaon data imply the limits $|\xi_P - \xi_S|^{[\Lambda p]}_{\text{BSM}} \leq 5.3 \times 10^{-3}$ and $|\xi_P - \xi_S|^{[\Xi^-]}_{\text{BSM}} \leq 3.7 \times 10^{-3}$. Additionally, we arrive at $|A^{[\Lambda p]}_{\text{CP}} + A^{[\Xi^-]}_{\text{CP}}|_{\text{BSM}} \leq 11 \times 10^{-4}$, and therefore the upper end of this range is already in tension with the aforementioned HyperCP limit [91]. Clearly, hyperon CPV measurements with much improved precision will provide an independent constraint on the BSM contributions in the strange quark sector. However, a lot also remains to be done on the theory side, as the predictions presently suffer from considerable uncertainties. It is hoped that lattice QCD analyses [135] in the future could help solve this problem.

2.2.4 Experimental status of CPV tests

The dedicated CPV experiment HyperCP (E871) at Fermilab [136], operating between 1996 and 1999, has set the world's best upper limits on hyperon CP violation using the $\Xi^- \to \Lambda\pi \to p\pi^-\pi^-$ decay sequence. A secondary cascade beam was produced by having 800 GeV/c primary protons interacting with a copper target. The sum of the asymmetries $A^{[\Xi^-]}_{\text{CP}} + A^{[\Lambda p]}_{\text{CP}} = 0(5)(4) \times 10^{-4}$ [91] was determined with a data sample of 117×10^6 Ξ^- and 41×10^6 $\overline{\Xi}^+$

using unpolarized cascades. A preliminary result $A_{\text{CP}}^{[\Xi^-]} + A_{\text{CP}}^{[\Lambda p]} = -6(2)(2) \times 10^{-4}$ based on the full data sample of 862×10^6 Ξ and 230×10^6 $\overline{\Xi}$ was presented at the BEACH2008 conference [137]. Since the final result was never published, one can suspect that an inherent problem to understand the systematic effects at the level of 4×10^{-4} was found. The HyperCP has also measured the most precise value of $\phi_{[\Xi^-]}$, see Table 2.2, using 144×10^6 Ξ^- events with average polarization of $\sim 5\%$ [109]. The drawback of the HyperCP experimental method is the charge-conjugation-asymmetric production mechanism and the need to use separate runs with different settings for the baryon and antibaryon measurements. Furthermore, the accuracy of the $\phi_{[\Xi^-]}$ parameter determination was limited by the low value of the Ξ^--beam polarization.

The most recent results, marked by bold fonts in Table 2.2, come from the proof-of-concept measurements [94, 95, 113] at BESIII using a novel method [45, 52, 105]. These results have been obtained using collisions of unpolarized electron and positron beams at the c.m. energy corresponding to the J/ψ resonance. The relevant properties of the $J/\psi \to B\overline{B}$ processes are given in Table 2.5. Given the relatively large branching fractions and low hadronic background, these e^+e^- experiments are well suited for CPV tests. Two different analysis methods can be used: exclusive measurement (double tag, DT) where the decay chains of the baryon and antibaryon are fully reconstructed; inclusive measurement (single tag, ST) where only the decay chain of the baryon or antibaryon is reconstructed. For the ST analysis, the two-body production process is uniquely identifiable, and its kinematics fully determined using missing energy/mass technique. Of importance for all single-step weak decays, *e.g.* $\Lambda \to p\pi^-$, is that the Λ and $\overline{\Lambda}$ are produced with a transverse polarization. The polarization and the spin correlations allow for a simultaneous determination of α and $\overline{\alpha}$, with the method proposed in Ref. [45]. The currently available results for $J/\psi \to \Lambda\overline{\Lambda}$ [94], $J/\psi \to \Sigma^+\overline{\Sigma}^-$ [113] and $J/\psi \to \Xi^-\overline{\Xi}^+$ [95] use 1.3×10^9 J/ψ data with 4.2×10^5 (background 400 events), 8.8×10^4 (background 4.4×10^3 events) and 7.3×10^4 (background 200 events) selected DT candidates, respectively. The final state charged particles are measured in the main drift chamber (and the calorimeter for the photons from the $\Sigma^+ \to p\pi^0(\to \gamma\gamma)$ decay), where a superconducting solenoid provides the magnetic field for momentum determination of the pions and (anti)protons with an accuracy of 0.5% at 1.0 GeV/c [44]. The pions and protons have distinctly different momentum ranges, making particle identification straightforward in the DT-type measurements. The analyses of the already collected 10^{10} J/ψ data by BESIII, have not been finished yet, but one can expect a threefold reduction of the statistical uncertainties as shown in Table 2.1.

2.3   Formalism

2.3.1   Production process

We start from a description of baryon–antibaryon production in electron–positron annihilations with a polarized electron beam. The production process $e^+e^- \to B\overline{B}$, viewed in the c.m. frame, defines the z axis which is chosen along the positron momentum shown in Fig. 2.2.

TABLE 2.5: Properties of the $e^+e^- \rightarrow J/\psi \rightarrow B\overline{B}$ decays to the pairs of ground-state octet hyperons.

Final state	$\mathcal{B}(\times 10^{-4})$	α_ψ	$\Delta\Phi(\text{rad})$	Comment
$\Lambda\overline{\Lambda}$	19.43(3)	0.461(9)	0.740(13)	[94, 138]
$\Sigma^+\overline{\Sigma}^-$	15.0(24)	$-0.508(7)$	$-0.270(15)$	[113, 139]
$\Sigma^-\overline{\Sigma}^+$		— no data —		
$\Sigma^0\overline{\Sigma}^0$	11.64(4)	$-0.449(20)$	–	[138]
$\Xi^0\overline{\Xi}^0$	11.65(43)	0.66(6)	–	[140]
$\Xi^-\overline{\Xi}^+$	9.7(8)	0.586(16)	1.213(48)	[92, 95]

We consider production of spin-1/2 baryon–antibaryon pair in electron–positron annihilation with longitudinally polarized electron beam. Neglecting the electron mass and assuming the one-photon approximation, the helicity of the electron (λ) and positron ($\overline{\lambda}$) has to be opposite since the photon only couples right-handed particles to left-handed antiparticles and vice versa. The number of right-handed (n_R) and left-handed (n_L) electrons in the beam with longitudinal polarization P_e is:

$$n_R = n_- \cdot \frac{1 + P_e}{2} \text{ and } n_L = n_- \cdot \frac{1 - P_e}{2} \, , \tag{2.32}$$

where $n_- = n_R + n_L$ is the total number of electrons. The two helicity configurations where the annihilation is possible are $\lambda = +1/2, \overline{\lambda} = -1/2$ ($\lambda_z = -1$) and $\lambda = -1/2, \overline{\lambda} = +1/2$ ($\lambda_z = 1$). For the collisions with unpolarized positrons, the relative weights of the two configurations are $(1 + P_e)/2$ and $(1 - P_e)/2$, respectively. Therefore, the spin density of the initial electron–positron system can be written as:

$$\rho_1^{i,j}(\theta) := \frac{1 + P_e}{2} d_{-1,i}^{1*}(\theta) \, d_{-1,j}^1(\theta) + \frac{1 - P_e}{2} d_{1,i}^{1*}(\theta) \, d_{1,j}^1(\theta) \tag{2.33}$$

where the quantization axis along the B momentum. The density matrix for the production process is the sum of the contributions from the two helicities, see Eq. (14) in Ref. [52]:

$$\rho_{B\overline{B}}^{\lambda_1,\lambda_2;\lambda_1',\lambda_2'} \propto A_{\lambda_1,\lambda_2} A_{\lambda_1',\lambda_2'}^* \rho_1^{\lambda_1 - \lambda_2, \lambda_1' - \lambda_2'}(\theta) \tag{2.34}$$

with the reduced density matrix ρ_1 given by

$$\frac{1}{2} \begin{pmatrix} \frac{1 + \cos^2\theta}{2} - P_e\cos\theta & \frac{(P_e - \cos\theta)\sin\theta}{\sqrt{2}} & \frac{\sin^2\theta}{2} \\ \frac{(P_e - \cos\theta)\sin\theta}{\sqrt{2}} & \sin^2\theta & \frac{(P_e + \cos\theta)\sin\theta}{\sqrt{2}} \\ \frac{\sin^2\theta}{2} & \frac{(P_e + \cos\theta)\sin\theta}{\sqrt{2}} & \frac{1 + \cos^2\theta}{2} + P_e\cos\theta \end{pmatrix} . \tag{2.35}$$

The four *a priori* possible helicity amplitudes reduce to only two, $h_1 := A_{-1/2,-1/2} = A_{1/2,1/2}$ and $h_2 := A_{1/2,-1/2} = A_{-1/2,1/2}$. If one focuses on the not normalized angular distribution of the production process, the relevant information contained in the two complex form factors
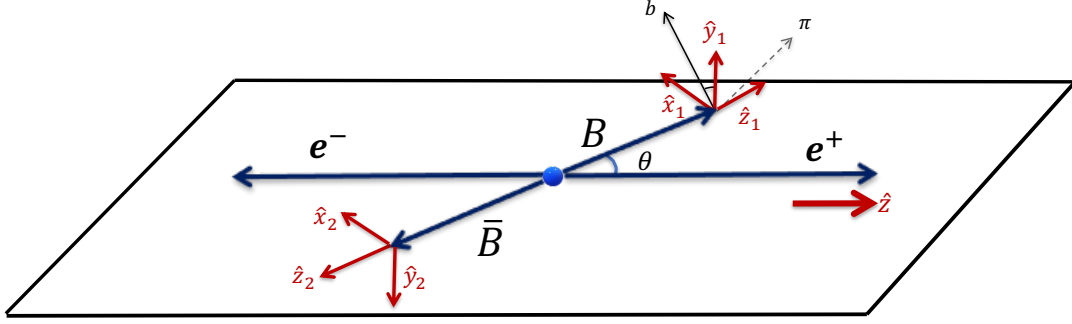
FIGURE 2.2: Orientation of the three coordinate systems used in the analysis. The axes in the baryon B and antibaryon $\overline{B}$ rest (helicity) frames are $(\hat{\mathbf{x}}_1, \hat{\mathbf{y}}_1, \hat{\mathbf{z}}_1)$ and $(\hat{\mathbf{x}}_2, \hat{\mathbf{y}}_2, \hat{\mathbf{z}}_2)$, respectively. They are related as $(\hat{\mathbf{x}}_2, \hat{\mathbf{y}}_2, \hat{\mathbf{z}}_2) = (\hat{\mathbf{x}}_1, -\hat{\mathbf{y}}_1, -\hat{\mathbf{z}}_1)$. In the overall c.m. frame, the $\hat{\mathbf{z}}$ axis is along the positron momentum.

h_1, h_2 can be expressed using only two real parameters. Hence, disregarding the overall normalization, the magnitudes of the two form factors can be represented as $|h_1| = \cos\chi$ and $|h_2| = \sqrt{2}\sin\chi$, where $0 \leq \chi \leq \pi/2$. In addition, the relative phase between the form factors can be defined as $\Delta\Phi := \arg(h_1/h_2)$. The general expression for the joint density matrix of the $B\overline{B}$ pair is:

$$\rho_{B\overline{B}} = \sum_{\mu,\nu=0}^{3} C_{\mu\nu}\, \sigma_\mu^B \otimes \sigma_\nu^{\overline{B}}\,, \tag{2.36}$$

where a set of four Pauli matrices $\sigma_\mu^B(\sigma_\nu^{\overline{B}})$ in the $B(\overline{B})$ rest frame is used and $C_{\mu\nu}$ is a 4×4 real matrix representing polarizations and spin correlations of the baryons. The orientation of the coordinate systems in the baryon rest frames is defined in Fig. 2.2. The axes are denoted $\hat{\mathbf{x}}_1, \hat{\mathbf{y}}_1, \hat{\mathbf{z}}_1$ and $\hat{\mathbf{x}}_2, \hat{\mathbf{y}}_2, \hat{\mathbf{z}}_2$. The elements of the $C_{\mu\nu}$ matrix are functions of the production angle θ of the B baryon:

$$\frac{3}{3+\alpha_\psi} \cdot \begin{pmatrix} 1+\alpha_\psi\cos^2\theta & \gamma_\psi P_e \sin\theta & \beta_\psi\sin\theta\cos\theta & (1+\alpha_\psi)P_e\cos\theta \\ \gamma_\psi P_e\sin\theta & \sin^2\theta & 0 & \gamma_\psi\sin\theta\cos\theta \\ -\beta_\psi\sin\theta\cos\theta & 0 & \alpha_\psi\sin^2\theta & -\beta_\psi P_e\sin\theta \\ -(1+\alpha_\psi)P_e\cos\theta & -\gamma_\psi\sin\theta\cos\theta & -\beta_\psi P_e\sin\theta & -\alpha_\psi-\cos^2\theta \end{pmatrix}, \tag{2.37}$$

where the real parameters α_ψ, β_ψ and γ_ψ are expressed in terms of the previously defined χ and $\Delta\Phi$ as:

$$\alpha_\psi := -\cos(2\chi)\,, \quad \beta_\psi := \sin(2\chi)\sin(\Delta\Phi)\,, \quad \gamma_\psi := \sin(2\chi)\cos(\Delta\Phi) \tag{2.38}$$

and $\alpha_\psi^2 + \beta_\psi^2 + \gamma_\psi^2 = 1$. The B-baryon angular distribution is

$$\frac{1}{\sigma}\frac{d\sigma}{d\Omega_B} = \frac{3}{4\pi}\frac{1+\alpha_\psi\cos^2\theta}{3+\alpha_\psi}\,. \tag{2.39}$$

This relation determines the normalization factor in Eq. (2.37). The B-baryon polarization vector $\mathbf{P}_B$ defined in the rest frame of baryon B, coordinates $(\hat{\mathbf{x}}_1, \hat{\mathbf{y}}_1, \hat{\mathbf{z}}_1)$, is:

$$\mathbf{P}_B := \frac{C_{10}\hat{\mathbf{x}}_1 + C_{20}\hat{\mathbf{y}}_1 + C_{30}\hat{\mathbf{z}}_1}{C_{00}} = \frac{\gamma_\psi P_e \sin\theta\hat{\mathbf{x}}_1 - \beta_\psi \sin\theta\cos\theta\hat{\mathbf{y}}_1 - (1+\alpha_\psi)P_e \cos\theta\hat{\mathbf{z}}_1}{1 + \alpha_\psi \cos^2\theta}.$$
(2.40)

In the chosen helicity frames one has $C_{01} = C_{10}$, $C_{02} = -C_{20}$, $C_{03} = -C_{30}$ and $\mathbf{P}_{\overline{B}} = (C_{01}\hat{\mathbf{x}}_2 + C_{02}\hat{\mathbf{y}}_2 + C_{03}\hat{\mathbf{z}}_2)/C_{00}$. Therefore, the polarization vectors of the baryon and the antibaryon are equal and have the same direction, $\mathbf{P}_{\overline{B}} = \mathbf{P}_B$. In the limit of large c.m. energies (HE), where $\alpha_\psi = 1$ and $\beta_\psi = \gamma_\psi = 0$ [141], the baryon can only have the longitudinal polarization component $\mathbf{P}_B\hat{\mathbf{z}}_1 = 2P_e \cos\theta/(1 + \cos^2\theta)$. In the low energy (LE) limit (close to threshold) $\alpha_\psi = 0$ and $\Delta\Phi = 0$, implying $\beta_\psi = 0$, $\gamma_\psi = 1$ and $\mathbf{P}_B = P_e(\sin\theta\hat{\mathbf{x}}_1 + \cos\theta\hat{\mathbf{z}}_1)$. Therefore, the value of the baryon polarization is equal to the initial electron beam polarization in this case. Fig. 2.3 shows the production-angle dependence of the baryon-polarization magnitude in the $e^+e^- \to J/\psi \to \Lambda\overline{\Lambda}$, $e^+e^- \to J/\psi \to \Xi^-\overline{\Xi}^+$ and $e^+e^- \to J/\psi \to \Sigma^+\overline{\Sigma}^-$ processes for three different values of the electron-beam polarization. The values of the α_ψ and $\Delta\Phi$ parameters from Table 2.5 are used.

For the determination of the uncertainties of the CPV tests, the following tensor $\langle C^2 \rangle_{\mu\nu}$ representing properties of the production process will be needed:

$$\langle C^2 \rangle_{\mu\nu} := \frac{1}{4\pi} \int \frac{C_{\mu\nu}^2}{C_{00}} d\Omega_B = \frac{1}{2} \int_{-1}^{1} \frac{C_{\mu\nu}^2}{C_{00}} d\cos\theta .$$
(2.41)

The production tensor is symmetric and positively defined. In addition $\langle C^2 \rangle_{00} = 1$. For example, it can be used to express the mean-squared polarization $\langle \mathbf{P}_B^2 \rangle$ of the B-baryon defined as:

$$\langle \mathbf{P}_B^2 \rangle = \int \mathbf{P}_B^2 \left(\frac{1}{\sigma} \frac{d\sigma}{d\Omega_B} \right) d\Omega_B = \sum_{i=1}^{3} \langle C_{i0}^2 \rangle .$$
(2.42)

This integral can be calculated exactly, and the result expressed as a linear function of the electron polarization squared P_e^2

$$\langle \mathbf{P}_B^2 \rangle = \mathbb{p}_0 + \mathbb{p}_2 P_e^2 ,$$
(2.43)

where the expression for coefficients $\mathbb{p}_0$ and $\mathbb{p}_2$ are given in Appendix IV. As we will show later, $\langle \mathbf{P}_B^2 \rangle$ determines the uncertainty of the A_{CP} and Φ_{CP} measurement. The results for $\sqrt{\langle \mathbf{P}_B^2 \rangle}$ are shown in Fig. 2.4. We will use the following notation for the polarization and spin-correlation contributions of the production-process tensor:

$$\langle \mathbb{P}_B^2 \rangle := \sum_{i=1}^{3} \left(\langle C^2 \rangle_{i0} + \langle C^2 \rangle_{0i} \right) = 2 \langle \mathbf{P}_B^2 \rangle$$

$$\langle \mathbb{S}_{B\overline{B}}^2 \rangle = \sum_{i,j=1}^{3} \langle C^2 \rangle_{ij} .$$
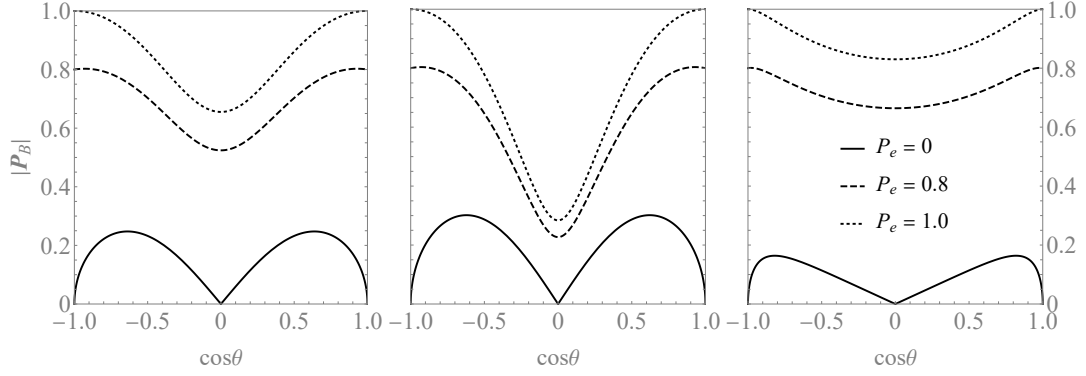(2.44)

FIGURE 2.3: Magnitudes of the hyperon polarization as a function of the production angle for: (a) Λ, (b) Ξ^- and (c) Σ^+ for the electron beam polarizations $P_e = 0, 0.8, 1$ (solid, dashed and dotted lines, respectively). The α_ψ and $\Delta\Phi$ values are taken from Table 2.5.
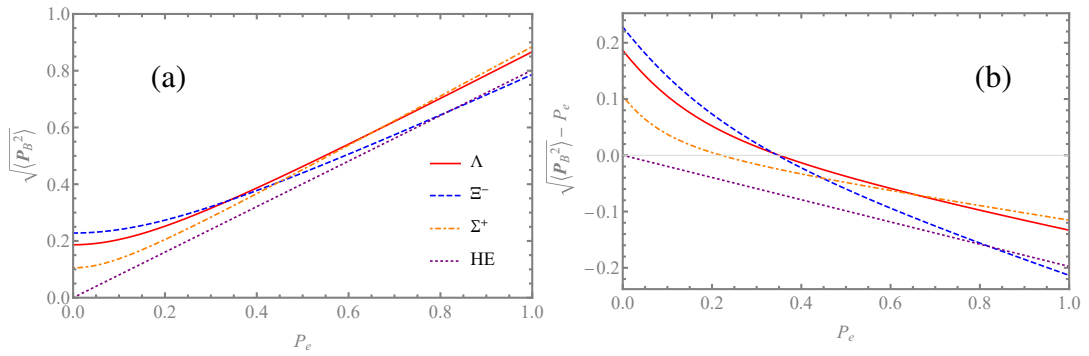

FIGURE 2.4: Average polarization $\sqrt{\langle \mathbf{P}_B^2 \rangle}$ for: Λ (solid line), Ξ^- (dashed line), Σ^+ (dot-dashed line) and high-energy limit (dotted line) as a function of electron beam polarization. In panel (b) the quantity $\sqrt{\langle \mathbf{P}_B^2 \rangle} - P_e$ is plotted to facilitate a more precise comparison. The low-energy limit corresponds to $P_B = P_e$.
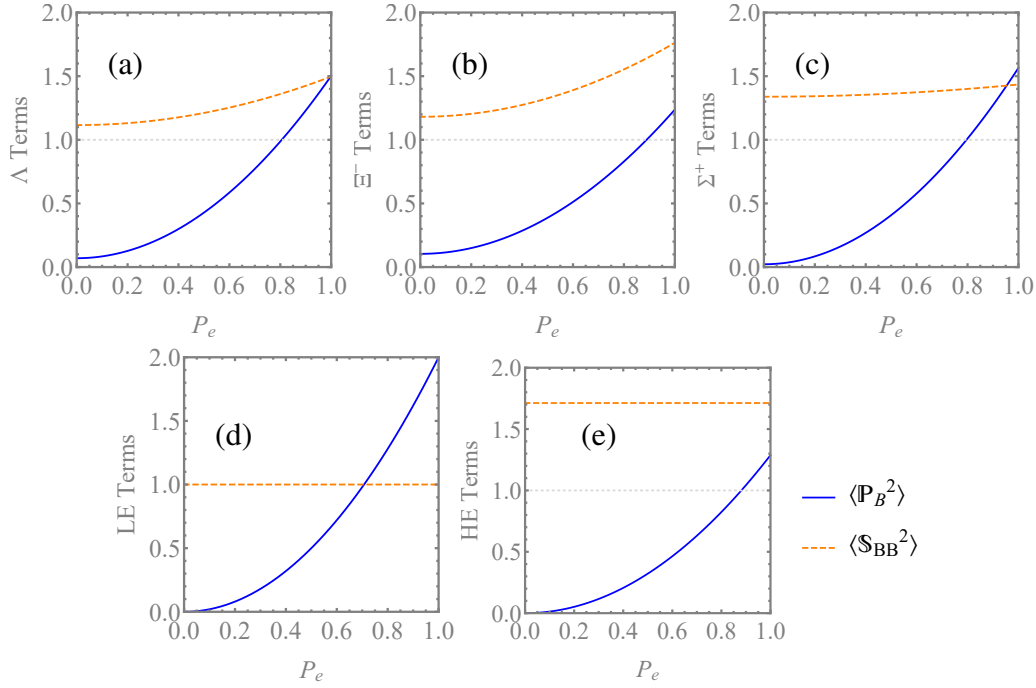
FIGURE 2.5: Polarization $\langle \mathbb{P}_B^2 \rangle$ (solid lines) and spin-correlation terms $\langle \mathbb{S}_{B\overline{B}}^2 \rangle$ (dashed lines) of the $e^+e^- \to B\overline{B}$ processes: (a) $J/\psi \to \Lambda\overline{\Lambda}$, (b) $J/\psi \to \Xi\overline{\Xi}$, (c) $J/\psi \to \Sigma\overline{\Sigma}$, (d) low-energy limit and (e) high-energy limit.

The values of the $\langle \mathbb{P}_B^2 \rangle$ and $\langle \mathbb{S}_{B\overline{B}}^2 \rangle$ terms as function of P_e are shown in Fig. 2.5 for some processes which are discussed later. The dependence on the P_e is much stronger for the polarization terms than for the spin-correlation terms. As we will show in Secs. 2.4 and 2.5 the sizes of the contributions determine the precision of the CPV observables.

2.3.2 Joint angular distributions

The complete joint angular distributions for a production process $e^+e^- \to B\overline{B}$ followed by weak two-body decays of the hyperon B and the antihyperon $\overline{B}$ can be obtained using the modular framework from Ref. [52]. For a single-step decay $D(B \to b\pi)$ and the corresponding c.c. decay mode $\overline{D}(\overline{B} \to \overline{b}\overline{\pi})$, like $e^+e^- \to J/\psi \to \Lambda\overline{\Lambda}$ with $\Lambda \to p\pi^-$ and $\overline{\Lambda} \to \overline{p}\pi^+$, the joint angular distribution,

$$\mathcal{P}^{D\overline{D}}(\xi; \omega) := \frac{1}{\Gamma}\frac{d\Gamma}{d\xi} , \qquad (2.45)$$

is

$$\mathcal{P}^{D\overline{D}}(\xi; \omega) = \frac{1}{(4\pi)^3} \sum_{\mu,\nu=0}^{3} C_{\mu\nu}(\Omega_B; \alpha_\psi, \Delta\Phi, P_e) a_{\mu 0}^D(\Omega_b; \alpha_D) a_{\nu 0}^{\overline{D}}(\Omega_{\overline{b}}; \overline{\alpha}_D) . \qquad (2.46)$$

There are five global parameters to describe the complete angular distribution, and they are represented by the vector $\omega := (\alpha_\psi, \Delta\Phi, P_e, \alpha_D, \overline{\alpha}_D)$. The vector $\xi := (\Omega_B, \Omega_b, \Omega_{\overline{b}})$ represents a complete set of the kinematic variables describing a single-event configuration in the six-dimensional phase space.

We use *helicity angles* to parameterize the multidimensional phase space. These are spherical coordinates in the *helicity reference frames* of the baryons, defined as follows: in the B baryon rest frame with the z axis defined by the unit vector $\hat{\mathbf{z}}_B$, the direction of the b baryon momentum is denoted as $\hat{\mathbf{p}}_b$. The b-baryon helicity system is the b rest frame, where the orientation of the Cartesian coordinate system is given by the unit vectors:

$$\hat{\mathbf{x}}_b = \frac{\hat{\mathbf{z}}_B \times \hat{\mathbf{p}}_b}{|\hat{\mathbf{z}}_B \times \hat{\mathbf{p}}_b|} \times \hat{\mathbf{p}}_b, \quad \hat{\mathbf{y}}_b = \frac{\hat{\mathbf{z}}_B \times \hat{\mathbf{p}}_b}{|\hat{\mathbf{z}}_B \times \hat{\mathbf{p}}_b|} \quad \text{and} \quad \hat{\mathbf{z}}_b = \hat{\mathbf{p}}_b. \tag{2.47}$$

The production is described by the spin-correlation matrix $C_{\mu\nu}(\Omega_B; \alpha_\psi, \Delta\Phi, P_e)$ in Eq. (2.37) and the 4×4 decay matrices $a_{\mu 0}^D := a_{\mu 0}^D(\Omega_b; \alpha_D)$ and $a_{\nu 0}^{\overline{D}} := a_{\nu 0}^{\overline{D}}(\Omega_{\overline{b}}; \overline{\alpha}_D)$. The decay matrices $a_{\mu\nu}^D$ represent the transformations of the spin operators (Pauli matrices) σ_μ^B and σ_ν^b defined in the B and b baryon helicity frames, respectively [52]:

$$\sigma_\mu^B \to \sum_{\nu=0}^{3} a_{\mu\nu}^D \sigma_\nu^b. \tag{2.48}$$

The explicit form of the $a_{\mu\nu}^D(\Omega; \alpha_D, \beta_D, \gamma_D) \leftrightarrow a_{\mu\nu}^D(\{\theta, \varphi\}; \alpha_D, \beta_D, \gamma_D)$ matrix, representing the polarization vector transformation from Eq. (2.7) in our framework, is:

$$\begin{pmatrix} 1 & 0 & 0 & \alpha_D \\ \alpha_D \sin\theta \cos\varphi & \gamma_D \cos\theta \cos\varphi - \beta_D \sin\varphi & -\beta_D \cos\theta \cos\varphi - \gamma_D \sin\varphi & \sin\theta \cos\varphi \\ \alpha_D \sin\theta \sin\varphi & \beta_D \cos\varphi + \gamma_D \cos\theta \sin\varphi & \gamma_D \cos\varphi - \beta_D \cos\theta \sin\varphi & \sin\theta \sin\varphi \\ \alpha_D \cos\theta & -\gamma_D \sin\theta & \beta_D \sin\theta & \cos\theta \end{pmatrix}. \tag{2.49}$$

For the single-step processes only the first column $a_{\mu 0}(\Omega; \alpha_D)$ is used and it depends only on the decay parameter α_D.

For the processes with two-step decays like $e^+e^- \to \Xi\overline{\Xi}$ with $\Xi \to \Lambda\pi$, $\Lambda \to p\pi^-$ + c.c. the joint angular distribution reads:

$$\mathcal{P}^{\Xi\overline{\Xi}}(\xi_{\Xi\overline{\Xi}}; \omega_\Xi) = \frac{1}{(4\pi)^5} \sum_{\mu,\nu=0}^{3} C_{\mu\nu} \left(\sum_{\mu'=0}^{3} a_{\mu\mu'}^\Xi a_{\mu'0}^\Lambda \right) \left(\sum_{\nu'=0}^{3} a_{\nu\nu'}^{\overline{\Xi}} a_{\nu'0}^{\overline{\Lambda}} \right), \tag{2.50}$$

where $\xi_{\Xi\overline{\Xi}} := (\Omega_\Xi, \Omega_\Lambda, \Omega_{\overline{\Lambda}}, \Omega_p, \Omega_{\overline{p}})$ and $\omega_\Xi := (\alpha_\psi, \Delta\Phi, P_e, \alpha_\Xi, \overline{\alpha}_\Xi, \phi_\Xi, \overline{\phi}_\Xi, \alpha_\Lambda, \overline{\alpha}_\Lambda)$ — the phase space has 10 dimensions and there are 9 global parameters.

The single tag (ST) distributions are obtained by integrating out the unmeasured variables. For example, the ST angular distribution of the B baryon measurement for single sequence decays Eq. (2.46) is:

$$\mathcal{P}^D(\xi_b; \omega) = \frac{1}{(4\pi)^2} \sum_{\mu=0}^{3} C_{\mu 0} \cdot a_{\mu 0}^D = \frac{1}{(4\pi)^2} C_{00} \cdot (1 + \alpha_D \mathbf{P}_B \cdot \hat{\mathbf{p}}_b), \tag{2.51}$$

where $\xi_B := (\Omega_B, \Omega_b)$ and $\mathbf{P}_B$ is given by Eq. (2.40). As the reference for comparing the ST uncertainties to the DT measurements with N reconstructed events, we will use a set of two independent ST experiments where the baryon and antibaryon decays are analyzed with

N reconstructed events each.

2.3.3 Asymptotic maximum likelihood method

The importance of the individual parameters ω_k in the joint angular probability density functions (p.d.f.s) of Eqs. (2.46) and (2.50) and their correlations are studied using an ideal asymptotic maximum likelihood method (MLL), discussed in Ref. [105]. The method allows one to reliably estimate the statistical accuracy of the determined global parameters in experiments with large acceptance detectors.

The asymptotic expression of the inverse covariance matrix element kl between parameters ω_k and ω_l of the parameter vector $\boldsymbol{\omega}$ is given by the Fisher information matrix [142]:

$$\mathcal{I}(\omega_k, \omega_l) := N \int \frac{1}{\mathcal{P}} \frac{\partial \mathcal{P}}{\partial \omega_k} \frac{\partial \mathcal{P}}{\partial \omega_l} \mathrm{d}\boldsymbol{\xi} , \qquad (2.52)$$

where N is the number of events in the final selection[2]. The calculated values are used to construct the matrix, which is inverted to obtain the covariance matrix $V = \mathcal{I}^{-1}$ for the parameters. Since asymptotically, in the case of negligible background, the statistical uncertainties given by the standard deviations (s.d.), $\sigma(\omega_k)$, are inversely proportional to the square root of the number of the reconstructed signal events N we will use the product

$$\sigma_C(\omega_k) := \sigma(\omega_k) \times \sqrt{N} , \qquad (2.53)$$

and call it *s.d. coefficient* or normalized statistical uncertainty. It allows for a comparison of the precision of different estimators for a given number of reconstructed events. In most cases, the integral Eq. (2.52) has to be calculated numerically. However, in this approach the explicit dependence on the production and decay parameters is hidden, and the calculations have to be repeated for each parameter set. Therefore, we have constructed analytic approximations, which are presented and discussed in the two following sections.

2.4 Single-step decays

We derive an approximate analytic solution for standard deviation of the A_{CP} measured in a single-step processes described by the p.d.f. in Eq. (2.46). The straightforward method is to determine all elements of the 5×5 inverse covariance matrix corresponding to the parameter vector $\boldsymbol{\omega} = (\alpha_\psi, \Delta\Phi, P_e, \alpha_D, \overline{\alpha}_D)$, invert the matrix and use error propagation to determine the variance $\mathrm{Var}(A_{\mathrm{CP}})$. If the parameter vector can be changed to include the A_{CP} observable and to have the remaining parameters uncorrelated, then the variance $\mathrm{Var}(A_{\mathrm{CP}})$ will be simply given as the inverse of the corresponding information matrix element

$$\frac{1}{\mathrm{Var}(A_{\mathrm{CP}})} = \mathcal{I}(A_{\mathrm{CP}}) := N \int \frac{1}{\mathcal{P}^{D\overline{D}}} \left(\frac{\partial \mathcal{P}^{D\overline{D}}}{\partial A_{\mathrm{CP}}} \right)^2 \mathrm{d}\boldsymbol{\xi} . \qquad (2.54)$$

---

[2]In Appendix V we show how our results should be modified when there is a significant fraction of background events.

Such parameterization can be constructed using the $\langle \alpha_D \rangle$ and A_{CP} parameters and expressing $\alpha_D = \langle \alpha_D \rangle (1 + A_{\text{CP}})$ and $\overline{\alpha}_D = -\langle \alpha_D \rangle (1 - A_{\text{CP}})$. The new parameter set leads to the following expression for the partial derivative of $\mathcal{P}^{D\overline{D}}$ with respect to A_{CP} (taken at $A_{\text{CP}} = 0$)

$$\frac{\partial \mathcal{P}^{D\overline{D}}}{\partial A_{\text{CP}}} = \frac{\langle \alpha_D \rangle}{\mathcal{V}} \sum_{\mu,\nu=0}^{3} C_{\mu\nu} \left(\frac{\partial a_{\mu 0}^{D}}{\partial \alpha_D} a_{\nu 0}^{\overline{D}} + a_{\mu 0}^{D} \frac{\partial a_{\nu 0}^{\overline{D}}}{\partial \overline{\alpha}_D} \right) \tag{2.55}$$

$$= \frac{\alpha_D}{\mathcal{V}} C_{00} \left(\mathbf{P}_B \cdot \hat{\mathbf{p}}_b - \mathbf{P}_{\overline{B}} \cdot \hat{\mathbf{p}}_{\overline{b}} \right) , \tag{2.56}$$

where $\mathcal{V} := \int \mathrm{d}\xi = \int \mathrm{d}\Omega_B \mathrm{d}\Omega_b \mathrm{d}\Omega_{\overline{b}} = (4\pi)^3$ and $\langle \alpha_D \rangle = \alpha_D$ in the $A_{\text{CP}} = 0$ limit. In order to calculate the information $\mathcal{I}(A_{\text{CP}})$, we will use the following representation for the $\mathcal{P}$ p.d.f.

$$\mathcal{P}(\xi; \omega) := C_{00} \frac{1 + \mathcal{G}(\xi; \omega)}{\mathcal{V}} , \tag{2.57}$$

where $\int \mathcal{G} \mathrm{d}\xi = 0$ and $\mathcal{G} \geq -1$. In addition, all terms included in the function $\mathcal{G}$ are multiplied by $\pm \alpha_D$ and for small values of $|\alpha_D|$ are suppressed. Therefore, it is not unreasonable to use the expansion of $1/(1 + \mathcal{G})$ to approximate $1/\mathcal{P}$:

$$\frac{1}{\mathcal{P}} = \frac{\mathcal{V}}{C_{00}} \frac{1}{1 + \mathcal{G}} = \frac{\mathcal{V}}{C_{00}} \sum_{i=0}^{\infty} (-\mathcal{G})^i \tag{2.58}$$

and

$$\mathcal{I}(\omega_k, \omega_l) := \mathcal{I}_0(\omega_k, \omega_l) + \sum_{i=1}^{\infty} (-1)^i \Delta \mathcal{I}_i(\omega_k, \omega_l) \tag{2.59}$$

with

$$\mathcal{I}_0(\omega_k, \omega_l) := N \int \frac{\mathcal{V}}{C_{00}} \frac{\partial \mathcal{P}}{\partial \omega_k} \frac{\partial \mathcal{P}}{\partial \omega_l} \mathrm{d}\xi, \tag{2.60}$$

$$\Delta \mathcal{I}_i(\omega_k, \omega_l) := N \int \frac{\mathcal{V}}{C_{00}} \mathcal{G}^i \frac{\partial \mathcal{P}}{\partial \omega_k} \frac{\partial \mathcal{P}}{\partial \omega_l} \mathrm{d}\xi. \tag{2.61}$$

We can always compare this analytic result using one or more terms of the expansion with the full numerical calculations. The hope is that the analytic approximation reproduces main features of the exact solution. If it does, it will facilitate understanding how the uncertainties depend on the global parameters. We start by considering the 0-th term of the above expansion, $\mathcal{V}/C_{00}$, that leads to the following information:

$$\mathcal{I}_0(A_{\text{CP}}) = N \int \frac{\mathcal{V}}{C_{00}} \left(\frac{\partial \mathcal{P}^{D\overline{D}}}{\partial A_{\text{CP}}} \right)^2 \mathrm{d}\Omega_B \mathrm{d}\Omega_b \mathrm{d}\Omega_{\overline{b}} \tag{2.62}$$

$$= N \frac{\alpha_D^2}{\mathcal{V}} \int C_{00} \left(\mathbf{P}_B \cdot \hat{\mathbf{p}}_b - \mathbf{P}_{\overline{B}} \cdot \hat{\mathbf{p}}_{\overline{b}} \right)^2 \mathrm{d}\Omega_B \mathrm{d}\Omega_b \mathrm{d}\Omega_{\overline{b}} . \tag{2.63}$$
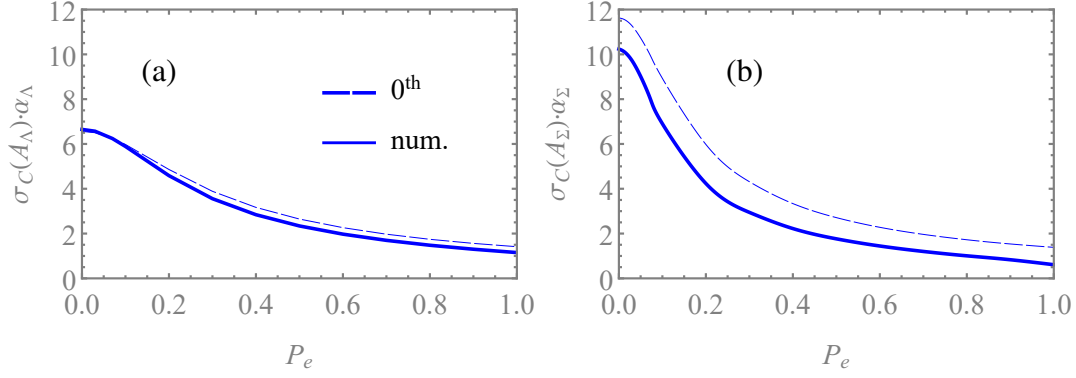
FIGURE 2.6: Standard deviation coefficients for A_{CP}, $\sigma_C(A_{\text{CP}})$, multiplied by the decay parameter value α_D for DT measurements. (a) $e^+e^- \to J/\psi \to \Lambda\overline{\Lambda}$ with decay $\Lambda(\Lambda \to p\pi^-)$, (b) $e^+e^- \to J/\psi \to \Sigma^+\overline{\Sigma}^-$ with decay $\Sigma p(\Sigma^+ \to p\pi^0)$. Dashed lines are the approximations using Eq. (2.65) and solid lines are the exact numerical results.

Integration over Ω_b and $\Omega_{\overline{b}}$ simplifies due to orthonormality

$$\int \left(\mathbf{P}_B \cdot \hat{\mathbf{p}}_b - \mathbf{P}_{\overline{B}} \cdot \hat{\mathbf{p}}_{\overline{b}}\right)^2 \frac{d\Omega_b}{4\pi} \frac{d\Omega_{\overline{b}}}{4\pi} = \int \left(\mathbf{P}_B \cdot \hat{\mathbf{p}}_b\right)^2 \frac{d\Omega_b}{4\pi} + \int \left(\mathbf{P}_{\overline{B}} \cdot \hat{\mathbf{p}}_{\overline{b}}\right)^2 \frac{d\Omega_{\overline{b}}}{4\pi}$$

$$= \frac{\mathbf{P}_B^2}{3} + \frac{\mathbf{P}_{\overline{B}}^2}{3} = \frac{2}{3}\mathbf{P}_B^2 \ .$$

Inserting the result into Eq. (2.56) and Eq. (2.62) we have:

$$\mathcal{I}_0(A_{\text{CP}}) = \frac{N}{4\pi}\alpha_D^2 \frac{2}{3} \int \mathbf{P}_B^2 C_{00} \, d\Omega_B$$

$$= \frac{2N}{3}\alpha_D^2 \int \mathbf{P}_B^2 \left(\frac{1}{\sigma}\frac{d\sigma}{d\Omega_B}\right) d\Omega_B = \frac{2N}{3}\alpha_D^2 \langle \mathbf{P}_B^2 \rangle \ . \tag{2.64}$$

Therefore in this approximation the information is proportional to the B-baryon average squared polarization, as defined in Eq. (2.42). Since A_{CP} is not correlated with other variables, the 0-th approximation for the uncertainty is

$$\sigma(A_{\text{CP}})\sqrt{N} = \sigma_C(A_{\text{CP}}) \approx \sqrt{\frac{3}{2}} \frac{1}{\alpha_D \sqrt{\langle \mathbf{P}_B^2 \rangle}} \ . \tag{2.65}$$

Fig. 2.6(a) shows the s.d. coefficients, $\sigma_C(A_{\text{CP}}^{[\Lambda p]})$, multiplied by the α_Λ parameter value for the $e^+e^- \to J/\psi \to \Lambda\overline{\Lambda}$ processes. The 0-th order result (hereafter we will call it also the analytic approximation) is close to the numerical full result in Eq. (2.52), even if α_Λ is relatively large (0.75). This shows that the influence of the higher order terms is low for the $A_{\text{CP}}^{[\Lambda p]}$ determination.

We also compare the approximate analytic formula to the full numerical calculations for the $e^+e^- \to J/\psi \to \Sigma^+\overline{\Sigma}^-$ process, where both α_ψ and $\Delta\Phi$ have been measured by BESIII [113]. The two Σ^+ decay modes $\Sigma n(\Sigma^+ \to n\pi^+)$ and $\Sigma p(\Sigma^+ \to p\pi^0)$ are interesting as the limiting cases for the expansion since $\alpha_{\Sigma n} = 0.068 \approx 0$ and $\alpha_{\Sigma p} = -0.994 \approx -1$,

respectively. It is worth noting that in the $\Delta I = 1/2$ limit $|\alpha_{\Sigma p}| < \cos(\delta_1^P - \delta_1^S) \approx 0.980$ (see Eq. (2.23) and the values of the strong phase shifts in Table 2.3). We note that the recent BESIII value $\langle \alpha_{\Sigma p} \rangle = -0.994(4)$ (Table 2.2) violates this bound. A proper interpretation of this result requires that all isospin contributions to the Σ^+ decays are considered, but such discussion is beyond the scope of this report. The 0-th approximation for $\sigma_C(A_{\mathrm{CP}}^{\Sigma p}) \cdot |\alpha_{\Sigma p}|$ is given by the dashed line in Fig. 2.6(b). The full numerical result (given by the solid line) differs significantly. The difference comes from the spin-correlation contributions, but the analytic approximation is able to describe the overall trend. From Eq. (2.65) it is clear that the approximation for $\sigma_C(A_{\mathrm{CP}}^{\Sigma n}) \alpha_{\Sigma n}$ is also given by the same dashed line. As expected, the full numerical result coincides with the 0-th approximation in this case. Comparing the trends for Λ and Σ^+, the faster decrease of the uncertainty for Σ^+ is mainly due to the low value of the $\Delta\Phi$ phase for this reaction. In principle, this would make Σp an attractive decay mode for testing CP symmetry with a polarized electron beam. However, we will not discuss further the Σ-baryon decays in this report. The reason is that the predicted CPV effects are significantly smaller, $A_{\mathrm{CP}}^{\Sigma p} \cdot \alpha_{\Sigma p} \approx 3.5 \times 10^{-6}$ and $A_{\mathrm{CP}}^{\Sigma n} \cdot \alpha_{\Sigma n} \approx 2.7 \times 10^{-5}$ [90], and the isospin structure of the amplitudes is more complicated (since also $\Delta I = 5/2$ transitions contribute).

The result for $\sigma_C(A_{\mathrm{CP}}^D)$ in the DT and ST cases is the same when the ST analysis is done under assumption that the $\langle \alpha_D \rangle$ value is known and fixed. In a single-step decay, an ST measurement only allows for a determination of the products $\alpha_D \sqrt{\langle P_B^2 \rangle}$ and $\overline{\alpha}_D \sqrt{\langle P_{\overline{B}}^2 \rangle}$. Therefore, a A_{CP}^D determination using a combination of baryon–antibaryon ST measurements requires knowledge of the polarization through some other means or use a production process where $\langle P_B^2 \rangle = \langle P_{\overline{B}}^2 \rangle$ is assured. For an $e^+e^- \to B\overline{B}$ experiment with an electron beam polarization P_e where the ST data are collected simultaneously and with c.c. symmetric detector acceptance, this condition is fulfilled automatically.

Related to this discussion is a proposal given in Ref. [143] where it is suggested that one could use a triple vector product to determine A_{CP} even if $\Delta\Phi = 0$ and $P_e = 0$, *i.e.* the baryons are unpolarized. For a general baryon–antibaryon state with polarization terms set to zero, the angular distribution after single-step decays reads:

$$\mathcal{P}^{D\overline{D}} \propto C_{00} + \alpha_D \overline{\alpha}_D \sum_{i,j=1}^{3} C_{ij} \left[\frac{a_{i0}^D}{\alpha_D} \right] \left[\frac{a_{j0}^{\overline{D}}}{\overline{\alpha}_D} \right] =: C_{00} + \alpha_D \overline{\alpha}_D \mathcal{F}(\Omega_B, \Omega_b, \Omega_{\overline{b}}) , \qquad (2.66)$$

where $\mathcal{F}(\ldots)$ is a function of the kinematic variables only. Therefore, the p.d.f. is described by a single global parameter $\alpha_{D\overline{D}} := \alpha_D \overline{\alpha}_D = -\langle \alpha_D \rangle^2 (1 - A_{\mathrm{CP}}^2)$. The parameter is related to A_{CP} and can in principle be used to test CP symmetry, but the method has several drawbacks. The information for $\alpha_{D\overline{D}}$ measurement is $\mathcal{I}_0(\alpha_{D\overline{D}}) = N/9 \langle \mathbb{S}^2 \rangle$ and the uncertainty of A_{CP} from the error propagation is:

$$\sigma(A_{\mathrm{CP}}) = \frac{1}{A_{\mathrm{CP}}} \sqrt{\sigma^2(\langle \alpha_D \rangle) + \frac{\sigma^2(\alpha_{D\overline{D}})}{4 \langle \alpha_D \rangle^2}} ,$$

which requires an independent determination of $\langle \alpha_D \rangle$. A meaningful CP test is possible only

if $\sigma(A_{\text{CP}}) < 1$. This requires that the $\sigma(\langle \alpha_D \rangle)$ precision is better than $O(10^{-5})$, since $A_{\text{CP}} \sim O(10^{-5})$ in the SM. If $\sigma(\langle \alpha_D \rangle)$ is not small enough, the $A_{\text{CP}} \neq 0$ value can be interpreted as a A_{CP} null result but with the decay parameters α_D and $\overline{\alpha}_D$ reduced by the factor $\sqrt{1 - A_{\text{CP}}^2}$.

2.5 Two-step decays

In order to study uncertainties of the CP asymmetries in $e^+ e^- \to \Xi^- \overline{\Xi}^+$, we rewrite Eq. (2.50) as

$$\mathcal{P}^{\Xi\overline{\Xi}}(\xi_{\Xi\overline{\Xi}}; \omega_\Xi) = \frac{1}{\mathcal{V}} \sum_{\mu,\nu=0}^{3} C_{\mu\nu} \mathcal{D}_\Xi^\mu \overline{\mathcal{D}}_\Xi^\nu \tag{2.67}$$

using the following notation:

$$\mathcal{D}_\Xi^\mu := \mathcal{D}^\mu(\Omega_\Lambda, \Omega_p; \alpha_\Xi, \phi_\Xi, \alpha_\Lambda) := \sum_{\mu'=0}^{3} a_{\mu\mu'}^\Xi a_{\mu'0}^\Lambda,$$

$$\overline{\mathcal{D}}_\Xi^\mu := \mathcal{D}^\mu(\Omega_{\overline{\Lambda}}, \Omega_{\overline{p}}; \overline{\alpha}_\Xi, \overline{\phi}_\Xi, \overline{\alpha}_\Lambda) := \sum_{\mu'=0}^{3} a_{\mu\mu'}^{\overline{\Xi}} a_{\mu'0}^{\overline{\Lambda}},$$

$$\mathcal{V} := \int \mathrm{d}\xi_{\Xi\overline{\Xi}} = (4\pi)^5 .$$

We use a modified parameter set where α_D and $\overline{\alpha}_D$ are expressed by A_{CP}^D and $\langle \alpha_D \rangle$. For $A_{\text{CP}}^{[\Xi-]}$ and $A_{\text{CP}}^{[\Lambda p]}$, we use a simplified notation A_Ξ and A_Λ, respectively. Similarly, we use $\Phi_{\text{CP}}^{[\Xi-]}$ (denoted as Φ_{CP}) to represent $\phi_\Xi = \Phi_{\text{CP}} + \langle \phi_\Xi \rangle$ and $\overline{\phi}_\Xi = \Phi_{\text{CP}} - \langle \phi_\Xi \rangle$. The vector of the parameters related to the Ξ and Λ decays is $\omega := (\langle \alpha_\Xi \rangle, \langle \phi_\Xi \rangle, \langle \alpha_\Lambda \rangle, A_\Xi, \Phi_{\text{CP}}, A_\Lambda)$. Therefore, the partial derivative *e.g.* with respect to Φ_{CP} is

$$\frac{\partial \mathcal{P}^{\Xi\overline{\Xi}}}{\partial \Phi_{\text{CP}}} = \frac{1}{\mathcal{V}} \sum_{\mu,\nu=0}^{3} C_{\mu\nu} \left(\frac{\partial \mathcal{D}_\Xi^\mu}{\partial \phi_\Xi} \overline{\mathcal{D}}_\Xi^\nu + \mathcal{D}_\Xi^\mu \frac{\partial \overline{\mathcal{D}}_\Xi^\nu}{\partial \overline{\phi}_\Xi} \right) .$$

Due to the orthonormality of the decay and production functions the information matrix elements related to the decay parameters ω_i and ω_j can be written as

$$\mathcal{I}_0(\omega_i, \omega_j) = N \sum_{\mu,\nu=0}^{3} \langle C^2 \rangle_{\mu\nu} \langle \Delta_{\omega_i} \Delta_{\omega_j} \rangle^{\mu\nu} . \tag{2.68}$$

We have checked these orthonormality relations in the explicit calculations. The production tensor is defined in Eq. (2.41). The decay tensor is

$$\langle \Delta_{\omega_i} \Delta_{\omega_j} \rangle^{\mu\nu} := \frac{1}{(4\pi)^4} \int \frac{\partial (\mathcal{D}_\Xi^\mu \overline{\mathcal{D}}_\Xi^\nu)}{\partial \omega_i} \frac{\partial (\mathcal{D}_\Xi^\mu \overline{\mathcal{D}}_\Xi^\nu)}{\partial \omega_j} \mathrm{d}\Omega_\Lambda \mathrm{d}\Omega_p \mathrm{d}\Omega_{\overline{\Lambda}} \mathrm{d}\Omega_{\overline{p}} . \tag{2.69}$$

For example $\mathcal{I}_0(\Phi_{\mathrm{CP}})$ can be expressed as

$$
\begin{aligned}
\mathcal{I}_0(\Phi_{\mathrm{CP}}) &= N \int \frac{\mathcal{V}}{C_{00}} \left(\frac{\partial \mathcal{P}^{\Xi\bar{\Xi}}}{\partial \Phi_{\mathrm{CP}}} \right)^2 \mathrm{d}\xi \\
&= N \sum_{\mu,\nu=0}^{3} \left[\frac{1}{4\pi} \int \frac{C_{\mu\nu}^2}{C_{00}} \mathrm{d}\Omega_\Xi \right] \left[\frac{1}{(4\pi)^4} \int \left(\frac{\partial(\mathcal{D}_\Xi^\mu \overline{\mathcal{D}}_\Xi^\nu)}{\partial \Phi_{\mathrm{CP}}} \right)^2 \mathrm{d}\Omega_\Lambda \mathrm{d}\Omega_p \mathrm{d}\Omega_{\overline{\Lambda}} \mathrm{d}\Omega_{\overline{p}} \right] \\
&=: N \sum_{\mu,\nu=0}^{3} \langle C^2 \rangle_{\mu\nu} \langle \Delta_{\Phi_{\mathrm{CP}}}^2 \rangle^{\mu\nu} \ .
\end{aligned}
$$

The information matrix elements for the decay parameters can be obtained as

$$
\mathcal{I}_0(\omega_i, \omega_j) = N \left[\mathbb{a}_{ij} + \mathbb{b}_{ij} \langle \mathbb{P}_\Xi^2 \rangle + \mathbb{c}_{ij} \langle \mathbb{S}_{\Xi\bar{\Xi}}^2 \rangle \right] \ , \tag{2.70}
$$

where $\langle \mathbb{P}_\Xi^2 \rangle$ $(= 2 \langle \mathbf{P}_\Xi^2 \rangle)$ and $\langle \mathbb{S}_{\Xi\bar{\Xi}}^2 \rangle$ are the sums of the $\langle C^2 \rangle_{\mu\nu}$-matrix polarization and spin-correlation elements, respectively, defined in Eq. (2.44) (and shown for few production processes in Fig. 2.5(b) as the function of electron-beam polarization). Such representation is possible since the decay tensor elements have only three different values $\mathbb{a}_{ij}$, $\mathbb{b}_{ij}$ and $\mathbb{c}_{ij}$. It turns out that the only nonzero elements of the information matrix involving the CP-odd variables for the two-step process are

$$
\mathcal{I}_0(\Phi_{\mathrm{CP}}) = \frac{2N}{27} \left(1 - \alpha_\Xi^2 \right) \alpha_\Lambda^2 \left[\left(3 + \alpha_\Xi^2 \alpha_\Lambda^2 \right) \langle \mathbb{P}_\Xi^2 \rangle + \frac{2}{3} \left(\alpha_\Xi^2 \left(3 - 2\alpha_\Lambda^2 \right) + 3\alpha_\Lambda^2 \right) \langle \mathbb{S}_{\Xi\bar{\Xi}}^2 \rangle \right],
$$
$$\tag{2.71}$$

$$
\mathcal{I}_0(A_\Xi) = \frac{2N}{3} \alpha_\Lambda^2 \alpha_\Xi^2 \left[1 + \frac{3 \left(\alpha_\Lambda^4 + 3 \right) - \alpha_\Xi^2 \left(3 - \alpha_\Lambda^2 \right)^2}{18 \left(1 - \alpha_\Xi^2 \right) \alpha_\Lambda^2} \langle \mathbb{P}_\Xi^2 \rangle + \frac{\alpha_\Xi^2 \left(2\alpha_\Lambda^2 - 3 \right) + 9}{27 \left(1 - \alpha_\Xi^2 \right)} \langle \mathbb{S}_{\Xi\bar{\Xi}}^2 \rangle \right],
$$
$$\tag{2.72}$$

$$
\mathcal{I}_0(A_\Lambda) = \frac{2N}{3} \alpha_\Lambda^2 \alpha_\Xi^2 \left[1 + \frac{\alpha_\Xi^4 - 2\alpha_\Xi^2 + 3}{6\alpha_\Xi^2} \langle \mathbb{P}_\Xi^2 \rangle + \frac{1}{9} (3 - 2\alpha_\Xi^2) \langle \mathbb{S}_{\Xi\bar{\Xi}}^2 \rangle \right], \tag{2.73}
$$

$$
\mathcal{I}_0(A_\Lambda, A_\Xi) = \frac{2N}{3} \alpha_\Lambda^2 \alpha_\Xi^2 \left[1 - \frac{1}{3} \left(\langle \mathbb{P}_\Xi^2 \rangle + \langle \mathbb{S}_{\Xi\bar{\Xi}}^2 \rangle \right) \right] \ . \tag{2.74}
$$

These information matrix elements allows one to determine s.d. and correlations between the CPV observables. The uncertainty for Φ_{CP} is $\sigma(\Phi_{\mathrm{CP}}) = 1/\sqrt{\mathcal{I}(\Phi_{\mathrm{CP}})}$, since the variable is uncorrelated with any other variable. The A_Ξ and A_Λ variables are only correlated with each other and the covariance matrix is obtained by inverting two-dimensional information matrix

$$
\begin{pmatrix} \sigma^2(A_\Xi) & \mathrm{Cov}(A_\Lambda, A_\Xi) \\ \mathrm{Cov}(A_\Lambda, A_\Xi) & \sigma^2(A_\Lambda) \end{pmatrix} = \begin{pmatrix} \mathcal{I}(A_\Xi) & \mathcal{I}(A_\Lambda, A_\Xi) \\ \mathcal{I}(A_\Lambda, A_\Xi) & \mathcal{I}(A_\Lambda) \end{pmatrix}^{-1} \ . \tag{2.75}
$$

The expressions in Eqs. (2.71)–(2.74) have some interesting properties which are valid for any two-step process that can be studied by allowing the α_Λ and α_Ξ parameters to vary. We discuss these properties using a generic notation, where the first decay process is $B \to b\pi$

and the baryon b decays in the sequential weak two-body nonleptonic process.

- The Φ_{CP} uncertainty is not correlated with any other variable, and none of the information matrix elements depend on the $\langle \phi_B \rangle$ value. This is because ϕ_B represents the shift in the φ_b azimuthal angle of the b-baryon, which is integrated out. A dependence on $\langle \phi_B \rangle$ might appear in experiments where the acceptance in the φ_b variable is limited.

- For $\alpha_b = 0$ only $\mathcal{I}_0(A_B) = \frac{1}{3}\alpha_B^2 \langle \mathbb{P}_B^2 \rangle$ is nonzero and the CPV test is the same as in a single-step decay.

- For $\alpha_B \to 0$ two terms are nonzero $\mathcal{I}_0(\Phi_{CP}) = \frac{2}{27}\alpha_b^2 \left[3\langle \mathbb{P}_B^2 \rangle + 2\alpha_b^2 \langle \mathbb{S}_{B\overline{B}}^2 \rangle \right]$ and $\mathcal{I}_0(A_b) = \frac{1}{3}\alpha_b^2 \langle \mathbb{P}_B^2 \rangle$. Therefore, both Φ_{CP} and A_b can be measured. In particular, due to the nonzero $\mathbb{c}$-type term for $\mathcal{I}_0(\Phi_{CP})$ the polarization of the B baryon is not needed. This is an attractive scenario for CPV tests for any baryon decaying into Λ.

- The term $\mathcal{I}_0(A_B)$ is divergent for $|\alpha_B| \to 1$ indicating that $\sigma(A_B)$ vanish in this limit. This is a consequence of the $\sqrt{1 - \alpha_B^2}$ terms in the angular distribution. The validity of such expressions requires that the boundary $|\alpha_B| \leq 1$ must be strictly fulfilled and in the $|\alpha_B| \to 1$ limit there is no linear term in the expansion of the α_B parameter (*i.e.* the linear error is 0). To get a meaningful result, one should use a parameterization which respects this boundary, such as Eq. (2.23) from Sec. 2.2.2. In principle, one can directly investigate the uncertainty of the weak phase difference $\xi_P - \xi_S$. However, as seen from Eq. (2.26) this will introduce correlation with the Φ_{CP} observable (due to the term $\sin\phi$). Instead, one can present results for $\Delta\zeta_B := \alpha_B/\sqrt{1 - \alpha_B^2}A_B$, which do not introduce such correlation. The information matrix elements are modified due to the Jacobian of the variable transformation to

$$\mathcal{I}_0(\Delta\zeta_B) = \frac{(1 - \alpha_B^2)}{\alpha_B^2}\mathcal{I}_0(A_B),$$

$$\mathcal{I}_0(A_b, \Delta\zeta_B) = \frac{\sqrt{1 - \alpha_B^2}}{\alpha_B}\mathcal{I}_0(A_b, A_B) \,.$$

We first discuss uncertainties for the production tensors corresponding to the simplest cases. Unpolarized and uncorrelated sources of B and $\overline{B}$ correspond to $\langle C^2 \rangle_{\mu\nu} = \text{diag}(1, 0, 0, 0)$. The only nonzero elements of the information matrix are

$$\mathcal{I}_0(A_B) = \mathcal{I}_0(A_b) = \mathcal{I}_0(A_b, A_B) = N\frac{2}{3}\alpha_b^2\alpha_B^2 \,,$$

where we have assumed samples of N events each for the cascade and anticascade decays. Since the information matrix corresponding to the A_Ξ and A_Λ is singular, the asymmetries are fully correlated and cannot be determined separately, but the sum $A_\Xi + A_\Lambda$ can and the uncertainty is $\sigma_C(A_\Xi + A_\Lambda) = \sqrt{3/2}/(\alpha_\Lambda\alpha_\Xi)$.

As the next example, we consider two independent ST experiments with N events each using polarized cascades and anticascades having the same average polarization $\langle \mathbf{P}_B^2 \rangle$. In the

0-th approximation, the expressions for the uncertainties depend on the production mechanism only via the average $\langle \mathbf{P}_B^2 \rangle$. For example, in the HyperCP-type experiments, where the initial hyperon polarization is considered to be a fixed vector that does not depend on the kinematic variables of the production process, the average reduces to the square of the vector $\sqrt{\langle \mathbf{P}_B^2 \rangle} \to |\mathbf{P}_B|$. The Fisher information matrix is the sum of the matrices for the two ST experiments

$$\mathcal{I}_0(\omega_i, \omega_j) = 2N \left[\mathbb{a}_{ij} + \mathbb{b}_{ij} \langle \mathbf{P}_B^2 \rangle \right] \tag{2.76}$$

and the elements of the information matrix for the CP-test observables read

$$\mathcal{I}_0(\Phi_{\mathrm{CP}}) = N \frac{4}{27} \left(1 - \alpha_B^2 \right) \alpha_b^2 \left(3 + \alpha_B^2 \alpha_b^2 \right) \langle \mathbf{P}_B^2 \rangle ,$$

$$\mathcal{I}_0(A_B) = N \frac{4}{3} \alpha_b^2 \alpha_B^2 \left[1 + \frac{3 \left(\alpha_b^4 + 3 \right) - \alpha_B^2 \left(3 - \alpha_b^2 \right)^2}{18 \left(1 - \alpha_B^2 \right) \alpha_b^2} \langle \mathbf{P}_B^2 \rangle \right] ,$$

$$\mathcal{I}_0(A_b) = N \frac{4}{3} \alpha_b^2 \alpha_B^2 \left[1 + \frac{\alpha_B^4 - 2 \alpha_B^2 + 3}{6 \alpha_B^2} \langle \mathbf{P}_B^2 \rangle \right] , \tag{2.77}$$

$$\mathcal{I}_0(A_b, A_B) = N \frac{4}{3} \alpha_b^2 \alpha_B^2 \left[1 - \frac{1}{3} \langle \mathbf{P}_B^2 \rangle \right] .$$

For two HyperCP-type experiments with $|\mathbf{P}_B| = |\mathbf{P}_{\overline{B}}|$ and N events each the formulas are the same. The resulting uncertainties $\sigma_C = \sigma \sqrt{N}$ for the A_Λ, A_Ξ and $A_\Lambda + A_\Xi$ observables measured using the $\Xi^-/\overline{\Xi}^+$ decay chains are shown in Fig. 2.7(a), while for Φ_{CP} they are shown in Fig. 2.7(b). The uncertainty of the sum $A_\Lambda + A_\Xi$ is nearly independent of the average polarization. Due to the large correlation term $\mathcal{I}(A_\Lambda, A_\Xi)$ in Eq. (2.77) the relation between the information and uncertainties is not straightforward. However, the 2×2 information matrix for A_Λ and A_Ξ can be diagonalized. The new uncorrelated variables $A_\pm$ are

$$A_\pm := \frac{1}{\sqrt{2}} \left[\sqrt[4]{\frac{\mathcal{I}(A_\Lambda)}{\mathcal{I}(A_\Xi)}} A_\Xi \pm \sqrt[4]{\frac{\mathcal{I}(A_\Xi)}{\mathcal{I}(A_\Lambda)}} A_\Lambda \right] , \tag{2.78}$$

where we have chosen an orthonormal transformation. If the polarization $|\mathbf{P}_\Xi|$ is zero, $A_+ = (A_\Lambda + A_\Xi)/\sqrt{2}$ is the only CP-violating variable that can be measured. Since the definition of the variables $A_\pm$ depends on the polarization (and on detection efficiencies in an experiment) we will not use or discuss them further. Since only two weak phases $\Delta \xi^\Xi := (\xi_P - \xi_S)^{[\Xi-]}$ and $\Delta \xi^\Lambda := (\xi_P - \xi_S)^{[\Lambda p]}$ describe CP-violation in the $[\Xi-]$ and $[\Lambda p]$ decays we provide the corresponding 2×2 Fisher information matrix, that is based on Eq. (2.52) and does not require the analytic approximation:

$$\mathcal{I}(\Delta \xi^\Xi) = \mathcal{I}(\Phi_{\mathrm{CP}}) \frac{1 - \langle \alpha_\Xi \rangle^2}{\langle \alpha_\Xi \rangle^2} \cos^2 \langle \phi_\Xi \rangle + \mathcal{I}(A_\Xi) \frac{\langle \alpha_\Xi \rangle^2}{1 - \langle \alpha_\Xi \rangle^2} \sin^2 \langle \phi_\Xi \rangle ,$$

$$\mathcal{I}(\Delta \xi^\Lambda) = \mathcal{I}(A_\Lambda) \frac{\langle \alpha_\Lambda \rangle^2}{1 - \langle \alpha_\Lambda \rangle^2} \sin^2 \langle \phi_\Lambda \rangle , \tag{2.79}$$

$$\mathcal{I}(\Delta \xi^\Lambda, \Delta \xi^\Xi) = \frac{\langle \alpha_\Xi \rangle}{\sqrt{1 - \langle \alpha_\Xi \rangle^2}} \sin \langle \phi_\Xi \rangle \frac{\langle \alpha_\Lambda \rangle}{\sqrt{1 - \langle \alpha_\Lambda \rangle^2}} \sin \langle \phi_\Lambda \rangle \mathcal{I}(A_\Lambda, A_\Xi)$$
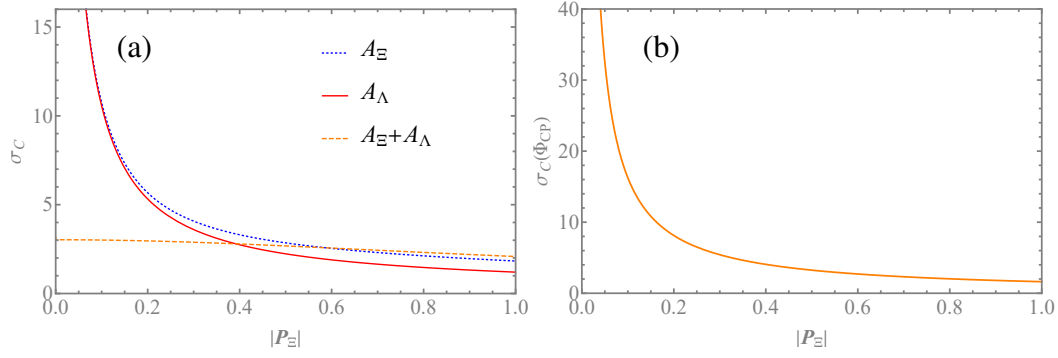
FIGURE 2.7: Uncertainties σ_C for CP tests in HyperCP-type experiment using analytic approximation: (a) A_Λ (solid line), A_Ξ (dotted line) and $A_\Xi + A_\Lambda$ (dashed line), (b) Φ_{CP}.

However, since $\langle \phi_\Xi \rangle \approx 0$, the Φ_{CP} measurement gives the dominating contribution to the $\Delta \xi^\Xi$ uncertainty.

Our next case is the decay of a (pseudo)scalar meson like η_c or χ_{c0} into a $B\bar{B}$ pair with the production tensor $\langle C^2 \rangle_{\mu\nu} = \text{diag}(1, 1, 1, 1)$. There are no polarization terms, $\langle \mathbb{P}_B^2 \rangle = 0$, and $\langle \mathbb{S}_{B\bar{B}}^2 \rangle = 3$. The information matrix element $\mathcal{I}_0(A_b, A_B)$ is zero, which means that all three CPV observables are uncorrelated. The diagonal terms of the information matrix are functions of α_b and α_B only:

$$\mathcal{I}_0(\Phi_{CP}) = N \frac{4}{27} \left(1 - \alpha_B^2 \right) \alpha_b^2 \left[\alpha_B^2 \left(3 - 2\alpha_b^2 \right) + 3\alpha_b^2 \right],$$

$$\mathcal{I}_0(A_B) = N \frac{2}{3} \alpha_b^2 \alpha_B^2 \left[1 + \frac{\alpha_B^2 \left(2\alpha_b^2 - 3 \right) + 9}{9 \left(1 - \alpha_B^2 \right)} \right],$$

$$\mathcal{I}_0(A_b) = N \frac{2}{3} \alpha_b^2 \alpha_B^2 \left[1 + \frac{1}{3} (3 - 2\alpha_B^2) \right] .$$

Fig. 2.8 shows the uncertainties σ_C for this case as a function of α_B and α_b decay parameters. This case is interesting since all production parameters are fixed and CP-test uncertainties depend only on α_b and α_B.

To understand the relative importance of the polarization and spin-correlation terms for the CP tests, one can compare the two above extreme cases. For example, the polarization in two ST experiments with N events that would lead to the same uncertainty of the Φ_{CP} measurement as in the DT approach with N events is:

$$|\mathbf{P}_B|^2 = \frac{\alpha_B^2 \left(3 - 2\alpha_b^2 \right) + 3\alpha_b^2}{3 + \alpha_B^2 \alpha_b^2} .$$

For $\Xi \to \Lambda\pi$ this gives $|\mathbf{P}_B| = 0.80$.

Now we will discuss the results specific for the $e^+ e^- \to J/\psi \to \Xi\bar{\Xi}$ process. The relations for the ST experiment, realized as two independent measurements with N events each
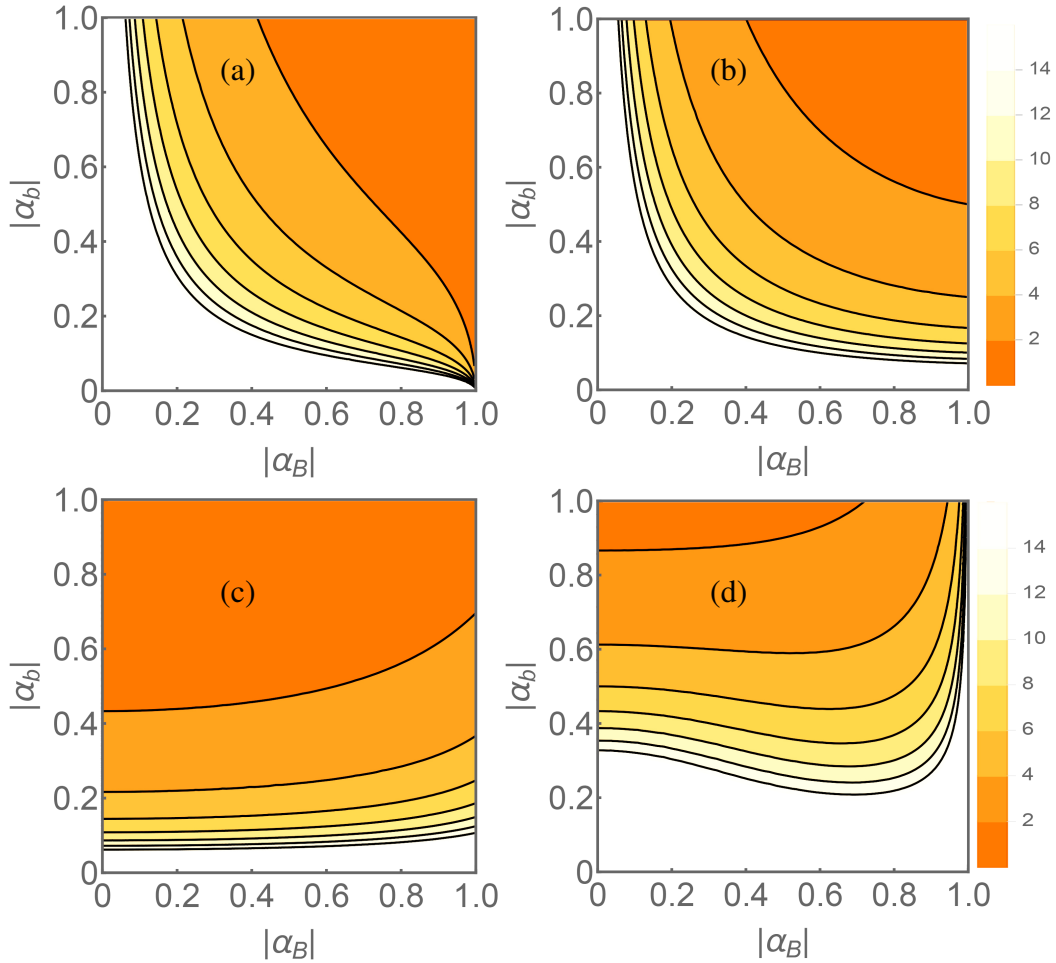
FIGURE 2.8: (Color online) Statistical uncertainties σ_C of (a) A_B, (b) A_b, (c) $\Delta\zeta_B$ and (d) Φ_{CP} measurement in a (pseudo)scalar meson decay to $B\bar{B}$ as a function of α_B and α_b treated as free parameters. The white regions in the bottom of the plots correspond to the uncertainties $\sigma_C(\ldots) > 15$.

[3], are still valid. The only difference is that now the results can be represented as a function of the electron-beam polarization P_e, and the average cascade polarization $|\mathbf{P}_\Xi|$ is calculated using Eq. (2.43). The results in the analytic approximation for the A-type observables corresponding to the ones in Fig. 2.7(a) are shown in Fig. 2.9(a). Since even for the $P_e = 0$ the average polarization of the cascades is not zero, all the three CP tests are possible. For the average values of the decay parameters we do not provide approximate analytic results since the corresponding information matrix elements are correlated and in general multidimensional matrices have to be inverted to obtain uncertainties. Therefore, likely such analytic solution will not provide better understanding of the interrelations between the parameters. The numeric results for uncertainties of $\langle\alpha_\Xi\rangle$, $\langle\phi_\Xi\rangle$ and $\langle\alpha_\Lambda\rangle$ are shown in Fig. 2.10(a)–(c) both for ST- and DT-type experiments. For the ST experiments, the uncertainty improves much more than for DT experiments. It is understood by the fact that the spin-correlation terms contribute only to the DT experiments and the dependence on the P_e is weaker. The

---

[3]Of course this is not the way one does the experiment since both the baryon and antibaryon decays can be measured simultaneously.
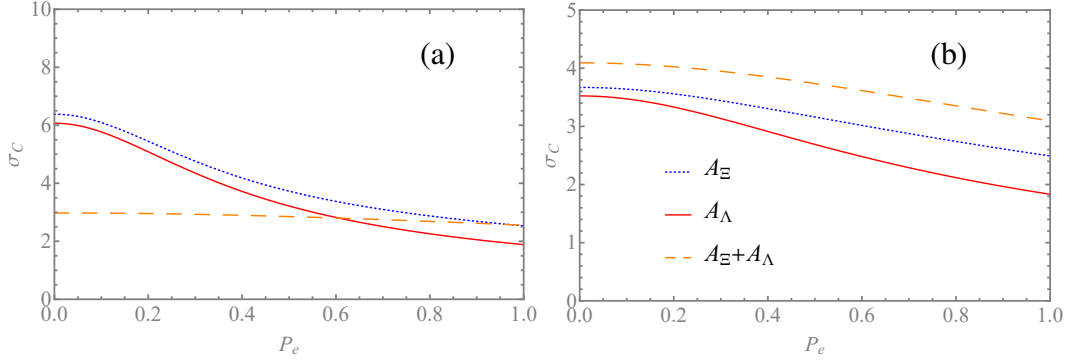
FIGURE 2.9: Uncertainties, σ_C, for the $e^+e^- \rightarrow J/\psi \rightarrow \Xi\bar{\Xi}$ (a) two ST and (b) DT experiments with N events each: A_Λ (solid line), A_Ξ (dotted line) and $A_\Lambda + A_\Xi$ (dashed line).

TABLE 2.6: Correlation matrix for the asymmetries and averages in the $e^+e^- \rightarrow J/\psi \rightarrow \Xi\bar{\Xi}$ process with $P_e = 0.8$ for DT. Input parameters are $\langle\alpha_\Xi\rangle = -0.373$, $\langle\phi_\Xi\rangle = 0.016$ and $\langle\alpha_\Lambda\rangle = 0.760$. The error is the last significant digit unless specified explicitly, and only the results statistically different from zero are shown.

	$\Delta\Phi$	$\langle\alpha_\Xi\rangle$	$\langle\phi_\Xi\rangle$	$\langle\alpha_\Lambda\rangle$	A_Ξ	A_Λ	Φ_{CP}	P_e
α_ψ	−0.128	–	0.011	-0.008	–	-0.017(2)	–	-0.031
$\Delta\Phi$		0.009	0.009	-0.071(2)	–	–	–	0.191(3)
$\langle\alpha_\Xi\rangle$			-0.021(4)	0.078(3)	–	–	–	0.037
$\langle\phi_\Xi\rangle$				-0.032	–	–	–	−0.005
$\langle\alpha_\Lambda\rangle$					–	–	–	−0.455

numerical results for the A_Ξ, Φ_{CP} and A_Λ are given in Fig. 2.10(d)–(f) and compared to the analytic approximations, which represent well the results specially for the Ξ decay CPV tests. As a cross-check of the calculations, we provide in Table 2.6 the full correlation matrix of all parameters using the full numerical calculations for $P_e = 0.8$. Significant values of some correlation terms, like $\Delta\Phi$–α_ψ or $\langle\alpha_\Lambda\rangle$–$P_e$, indicate that it might be difficult to provide an intuitive picture of the relations between all the parameters. However, the numerical results confirm that the CP-violation variables are almost uncorrelated with the other variables and support our assumption that they can be analyzed separately.

Finally, it is interesting to consider a general two-step process $B \rightarrow b\pi$ in the low- and high-energy limits (LE- and HE limits, respectively, introduced in Sec. 2.3) for a single photon $e^+e^- \rightarrow B\bar{B}$ annihilation process. These cases might be of interest for close to threshold charm baryon studies or baryon–antibaryon production experiments at high energies. In the LE limit ($\alpha_\psi = 0$, $\beta_\psi = 0$, $\gamma_\psi = 1$) the terms $\langle\mathbb{P}_B^2\rangle$ and $\langle\mathbb{S}_{B\bar{B}}^2\rangle$ are $2P_e^2$ and 1, respectively. In the HE limit ($\alpha_\psi = 1$, $\beta_\psi = 0$, $\gamma_\psi = 0$) they are equal to $6(1 - \pi/4)P_e^2$ and $3(\pi/2 - 1)$, respectively. In both cases the spin-correlation terms do not depend on the electron polarization and the $\langle\mathbb{P}_B^2\rangle$ terms are proportional to P_e^2. A comparison of the uncertainties for $P_e = 0$ and $P_e = 1$ in the DT-experiment setting is presented in Fig. 2.11. The conclusion is that the polarization helps to reach better precision in both cases, and the improvement is qualitatively similar.
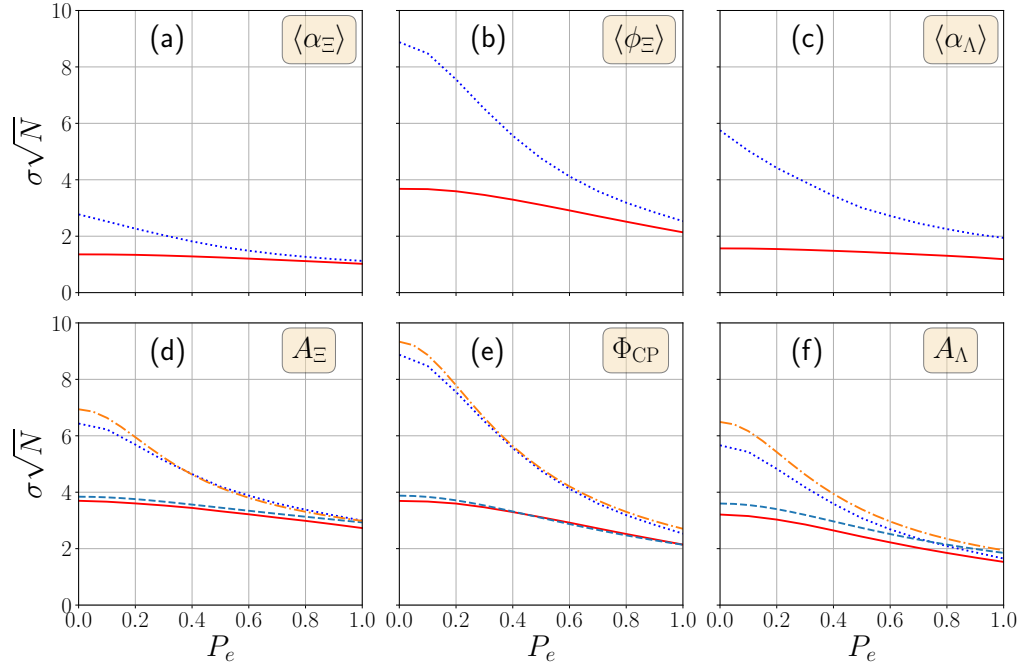
FIGURE 2.10: Numerical estimate of the uncertainty $\sigma\sqrt{N}$ of (a)–(c) average decay parameters and (d)–(f) CPV observables in $e^+e^- \rightarrow J/\psi \rightarrow \Xi^-\overline{\Xi}^+$. The dotted lines and the solid lines are the results for ST and DT experiments, respectively. For the asymmetries A_Ξ, Φ_{CP} and A_Λ also the analytic approximation is given: dashed-dotted lines and dashed are ST and DT results, respectively.

2.6   Experimental considerations

The benefits of a large electron-beam polarization for CP-violation studies should be clear by now. Here we discuss three additional aspects related to the detection technique which should be considered when planning such an experiment,

(a) Combination of the ST and DT data sets including detection efficiency and background aspects.

(b) Polar angle dependence of uncertainty and the detection efficiency.

(c) Implications of the discussed collision scheme with large-crossing angle.

Combination of ST and DT measurements   In general, the best precision can be achieved by combining three non-overlapping event sets. The first set includes the DT events, where both the B and $\overline{B}$ decay chains are reconstructed. The remaining events can be divided into two ST sets where $B(\overline{B})$ decay is fully reconstructed but not the corresponding $\overline{B}(B)$. The efficiencies of the B, $\overline{B}$ and $B\overline{B}$ sets are denoted as ϵ_B, $\epsilon_{\overline{B}}$ and $\epsilon_{B\overline{B}}$, respectively. The efficiencies can depend on the vector ξ of the kinematic variables, but not on the global reaction parameters given by the ω vector. Since we discuss improvements with respect to the DT-type experiment, ϵ_B is given by the ratio between the detection efficiencies of the DT and ST cases.
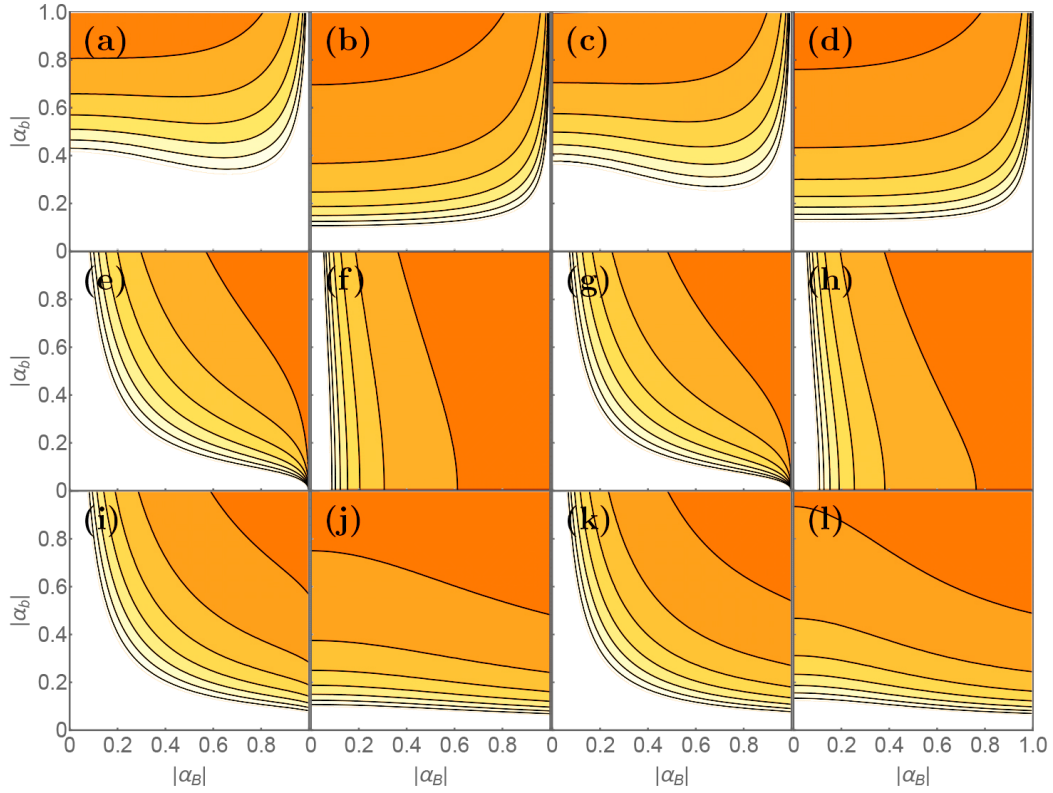
FIGURE 2.11: (Color online) Statistical uncertainties σ_C of: (a)–(d) Φ_{CP}, (e)–(h) A_B and (i)–(l) A_b measurements in the $e^+e^- \rightarrow \gamma^* \rightarrow B\overline{B}$ process with two-step B-baryon decays in the low-energy (LE) limit ($\alpha_\psi = 0$ and $\Delta\Phi = 0$) and high-energy (HE) limit ($\alpha_\psi = 1$) as the function of α_B and α_b treated as free parameters. The columns from left are: (LE limit, $P_e = 0$), (LE limit, $P_e = 1$), (HE limit, $P_e = 0$) and (HE limit, $P_e = 1$). The same color scale as in Fig. 2.8 is used. The white regions in the plots correspond to uncertainties $\sigma_C(\dots) > 15$.

We also neglect any efficiency dependence on the kinematic variables. We recollect that the information in the DT experiment, based on N reconstructed events, is given by Eq. (2.70):

$$\mathcal{I}_0^{\mathrm{DT}}(\omega_i, \omega_j) = N \left[\mathbb{a}_{ij} + \mathbb{b}_{ij} \langle \mathbb{P}_B^2 \rangle + \mathbb{c}_{ij} \langle \mathbb{S}_{B\overline{B}}^2 \rangle \right] \ .$$

For the two-step process $\mathbb{a}_{ij}$, $\mathbb{b}_{ij}$ and $\mathbb{c}_{ij}$ can be read from Eq. (2.71)–(2.74). For the single-step process only A_B can be measured $\mathbb{a}_{A_B} = \mathbb{c}_{A_B} = 0$ and $\mathbb{b}_{A_B} = 1/3$:

$$\mathcal{I}_0(A_B) = N \frac{1}{3} \langle \mathbb{P}_B^2 \rangle \ .$$

The information provided by the two additional ST sets is

$$\mathcal{I}_0^{\mathrm{ST}}(\omega_i, \omega_j) = N \frac{1 - \epsilon_B \mathcal{B}}{\epsilon_B \mathcal{B}} \left[2\mathbb{a}_{ij} + \mathbb{b}_{ij} \langle \mathbb{P}_B^2 \rangle \right] \ , \tag{2.80}$$

where the branching fraction product of the decay sequence is $\mathcal{B}$ and equal detection efficiencies $\epsilon_B = \epsilon_{\overline{B}}$ are assumed. The interpretation of the above equation is that an additional $2N/(\epsilon_B \mathcal{B})$ events are added from the two ST sets. Therefore, the information of the combined ST and DT experiment (ST&DT) is the sum of the two independent measurements

$$\mathcal{I}_0^{\mathrm{ST\&DT}}(\omega_i, \omega_j) = N \left[\frac{2 - \epsilon_B \mathcal{B}}{\epsilon_B \mathcal{B}} \mathbb{a}_{ij} + \frac{1}{\epsilon_B \mathcal{B}} \mathbb{b}_{ij} \langle \mathbb{P}_B^2 \rangle + \mathbb{c}_{ij} \langle \mathbb{S}_{B\overline{B}}^2 \rangle \right] \ . \tag{2.81}$$

In the single-step decays the $\sigma_C(A_{\mathrm{CP}})$ dependence on the electron-beam polarization for both ST and DT experiments is approximately given by Eq. (2.65). The A_Λ uncertainties for ST, DT and the combined $e^+ e^- \to J/\psi \to \Lambda\overline{\Lambda}$ measurement are plotted in Fig. 2.12 as the function of P_e. Two cases of the detection efficiencies $\epsilon_B = 1$ and $\epsilon_B = 0.5$ are considered and $\mathcal{B}(\Lambda \to p\pi^-) = 0.64$ is used. For the case with the reconstruction efficiency of 0.5 a two-times improvement of σ_C is achieved for the combination, compared to the DT measurement only. Of course, a detailed feasibility study which includes the detector response will be needed to determine the efficiency which can be obtained for the combined DT and ST measurement.

An important background contribution which should be considered for the ST analysis of the $J/\psi \to \Lambda\overline{\Lambda}$ events is $J/\psi \to pK^-\overline{\Lambda} + \mathrm{c.c}$ with $\mathcal{B} = (8.6 \pm 1.1) \times 10^{-4}$ [92] as it will have a similar final state topology as the signal channel. Similar experimental considerations will also hold for the $J/\psi \to \Sigma\overline{\Sigma}$ two-body decay channels.

The results for A_Ξ and Φ_{CP} in the $e^+ e^- \to J/\psi \to \Xi\overline{\Xi}$ are shown in Fig. 2.13. For the two-step decays, the increasing beam polarization improves the ST uncertainties much faster compared to the corresponding DT uncertainties. For the polarization of $P_e = 0.8$ the uncertainty of the ST experiment is better if we assume realistic efficiency of 50% deduced from a comparison of the BESIII ST [144] and DT [95] analyses.

Furthermore, the non-reducible backgrounds for the ST event samples are also expected to be low. The background channels to be considered are $J/\psi \to \gamma\eta_c(\to \Xi^-\overline{\Xi}^+)$, $J/\psi \to$
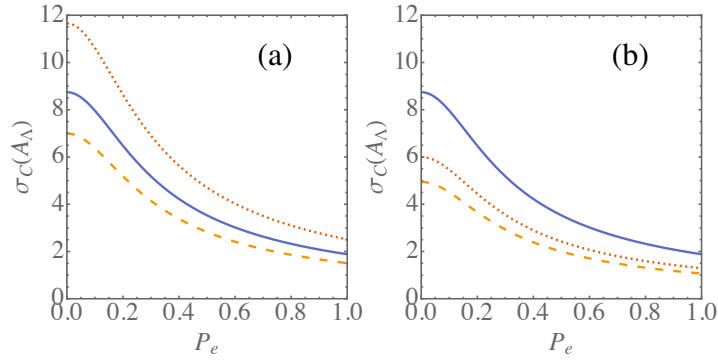
FIGURE 2.12: Statistical uncertainties $\sigma_C(A_\Lambda)$ for the $e^+e^- \to J/\psi \to \Lambda\overline{\Lambda}$ process as a function of the electron-beam polarization P_e. The solid-blue lines represent DT measurement. The dotted-red lines represent contribution from ST events which do not contribute to the DT event class (statistically independent ST events). The orange-dashed lines represent the result from the combination of the two event classes. The decay branching fraction is $\mathcal{B} = 0.64$ [92]. The detection efficiency of the Λ decay was assumed to be (a) $\epsilon_\Lambda = \overline{\epsilon}_\Lambda = 1$ and (b) $\epsilon_\Lambda = \overline{\epsilon}_\Lambda = 0.5$. The results are normalized to the number of the DT events.
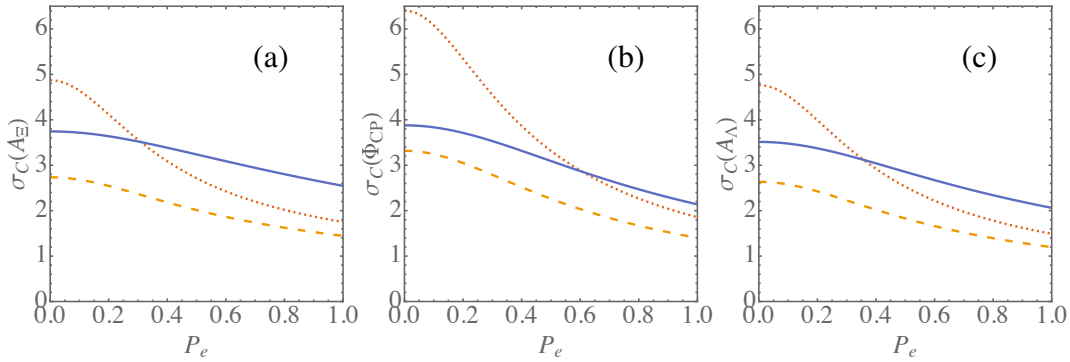
FIGURE 2.13: Statistical uncertainties σ_C for the CP-violation observables in the $\Xi^- \to \pi^-\Lambda(\to p\pi^-) + $ c.c. decay sequences from the $e^+e^- \to J/\psi \to \Xi\overline{\Xi}$ process: (a) $\sigma_C(A_\Xi)$, (b) $\sigma_C(\Phi_{CP})$ and (c) $\sigma_C(A_\Lambda)$ as a function of electron beam polarization P_e. The solid-blue lines represent DT measurement. The dotted-red lines represent contribution from ST events which do not contribute to the DT event class (statistically independent ST events). The orange-dashed lines represent the result from the combination of the two event classes. The detection efficiency of the Ξ-decay sequence was assumed $\epsilon_\Xi = \overline{\epsilon}_\Xi = 0.5$ and branching fraction of the complete decay chain $\mathcal{B} = 0.64$. The results are normalized to the number of the DT events.
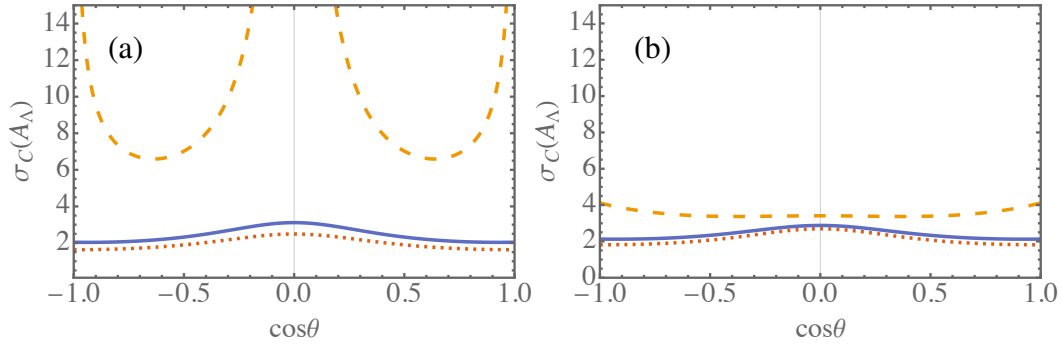
FIGURE 2.14: Uncertainties $\sigma_C(A_\Lambda)$ in the DT measurement in (a) $e^+e^- \to J/\psi \to \Lambda\overline{\Lambda}$ and (b) $e^+e^- \to J/\psi \to \Xi\overline{\Xi}$ processes as a function of the production angle $\cos\theta$ where dashed line shows $P_e = 0$, solid line is for $P_e = 0.8$ and dotted line representes $P_e = 1$.

$\Xi(1530)^-\overline{\Xi}^+ \to \Xi^-\pi^0\overline{\Xi}^+$ and $J/\psi \to \Lambda\pi^-\overline{\Lambda}\pi^+$. While the first two channels can be suppressed using event kinematics variables, the third can be reduced by requiring a non-zero decay length for the $\Xi \to \Lambda\pi$ decay candidates. For the DT method the background contribution is 0.25% and for ST the background is at the percent level, while roughly three times more ST events can be reconstructed compared to DT.

Polar-angle efficiency dependence Detectors at electron-positron colliders experiments have approximate cylindrical symmetry with axis along the beam directions (considerations for large-crossing angle are discussed in a separate paragraph) and uniform detection efficiency in the azimuthal angle. However, the polar-angle coverage is limited. For example, in the BESIII experiment $|\cos\theta| < 0.93$ for tracks of charged particles. The hyperons decay some centimeters away from the interaction point and the final state particles with large $|\cos\theta|$ values have low transverse momenta, which are more difficult to reconstruct. These effects reduce the reconstruction efficiency at large values of $|\cos\theta|$.

The event yield is a product of the efficiency and the differential cross-section of the $e^+e^- \to B\overline{B}$ process $d\Gamma/d\Omega \propto (1+\alpha_\psi \cos^2\theta)$ as shown in Eq. (2.39). Since both $J/\psi \to \Lambda\overline{\Lambda}$ and $J/\psi \to \Xi^-\overline{\Xi}^+$ have $\alpha_\psi > 0$ (Table 2.5) the (anti)hyperons and the decay (anti)nucleons are more likely emitted in the forward and backward directions. The uncertainty as a function of the production angle $\cos\theta$ can be obtained by replacing the production tensor $\langle C^2\rangle_{\mu\nu}$ by the normalized spin correlation matrix $C_{\mu\nu}^2/C_{00}^2$. The numerical expressions for the functions $\mathbb{P}_B^2(\cos\theta)$ and $\mathbb{S}_{B\overline{B}}^2(\cos\theta)$ are given in Appendix IV. The results are shown in Fig. 2.14 for $\sigma_C(A_\Lambda)$ in DT experiments in $e^+e^- \to J/\psi \to \Lambda\overline{\Lambda}$ and $e^+e^- \to J/\psi \to \Xi\overline{\Xi}$ for different values of the electron beam polarization. Corresponding plots for $\sigma_C(\Phi_{CP})$ in the $e^+e^- \to J/\psi \to \Xi\overline{\Xi}$ DT and combined DT&ST measurements are shown in Fig. 2.15.

Large-angle collision scheme The SCTF will use crab-waist collision scheme, meaning larger crossing angle than at BEPCII (22 mrad). The presently considered crossing angle is 60 mrad [96, 97]. However, in Ref. [101] much larger crossing angles, up to 500 mrad, are considered in conjunction with a novel c.m. energy monochromatization scheme. The
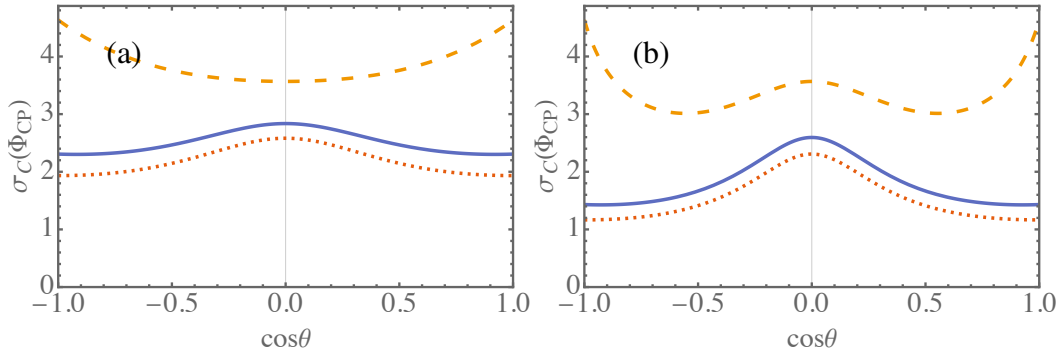
FIGURE 2.15: Uncertainties $\sigma_C(\Phi_{CP})$ as a function of the production angle $\cos\theta$ for (a) DT and (b) DT&ST with 50% efficiency experiment where dashed line (orange) shows $P_e = 0$, solid line (blue) is for $P_e = 0.8$ and dotted line (red) represents $P_e = 1$.

monochromatization could increase the number of the J/ψ events and therefore it is worthwhile to discuss some consequences of such collision arrangement for the acceptance in the hyperon CP-violation tests.

In such a collision scheme, the detector reference frame is significantly different from the electron–positron c.m. system. This has impact on both angular acceptance and the detection efficiency as a function of the measured-particles momenta and it has to be considered in the detector design. For example, the polar-angle, θ_{LAB}, distribution of Ξ^- in the detector rest frame is given in Fig. 2.16(a) for the 0.0, 0.3 and 0.5 rad crossing angles. If the decay particles are measured only in the $|\cos\theta_{LAB}| < 0.93$ range as in the BESIII detector, the observed Ξ production-angle distribution in the electron–positron c.m. system is as in Fig. 2.16(b). A large beam-crossing angle will also significantly affect the azimuthal-angle distribution in the detector reference system, as shown in Fig. 2.17(a). Therefore, the detection acceptance will be not symmetrical in the azimuthal angle what should be corrected for in the analysis. However, the acceptance effects should be easy to disentangled from the process angular distributions since in the electron–positron collision rest frame the azimuthal distribution has to be flat. In addition, an improved particle identification algorithm will be needed since the momentum distributions of the final-state protons and pions will overlap with each other, as shown in Fig. 2.17(b), while for the electron–positron rest frame collision scheme a momentum range separation was sufficient.

2.7 Outlook

We have advocated the importance of CPV studies in hyperon decays as a complementary tool to the studies in kaon decays. Using recent experimental results, we have revised and updated the amplitudes of the Λ and Ξ hadronic two-body decays.

The main part of this report discusses the implications of the polarized-electron beams for CPV tests in the nonleptonic hyperon decays at SCTF, using entangled baryon–antibaryon pairs from J/ψ decays with data sets of 10^{12} J/ψ events. The use of the polarization, together with additional improvements of the analysis techniques, shows the potential to reach
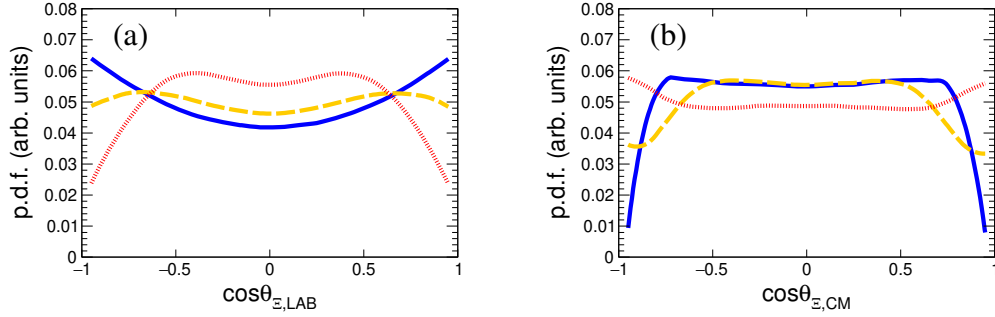
FIGURE 2.16: (color online) Production angle distribution for beam-crossing angles 0 rad (blue solid), 0.3 rad (orange dashed) and 0.5 rad (red dotted). (a) The Ξ production angle in the detector frame. (b) The Ξ production angle in the electron–positron c.m. frame for the events where all six charged tracks are accepted in the detector $|\cos\theta_{\mathrm{LAB}}| < 0.93$.
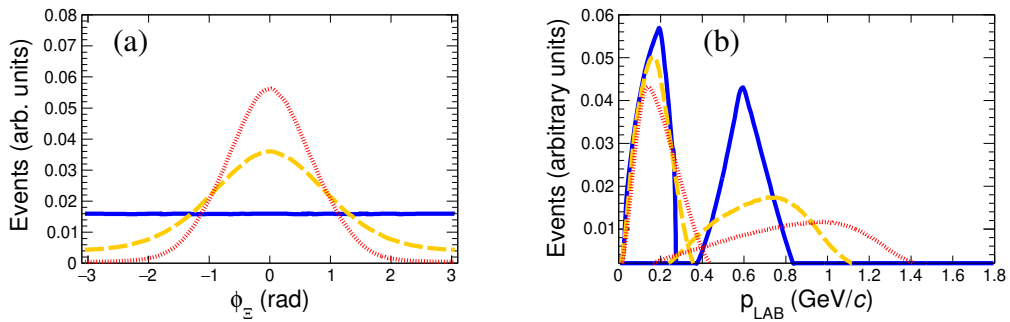

FIGURE 2.17: (color online) (a) Azimuthal distribution of Ξ_{LAB} and (b) momentum distributions for all final state particles for beam scattering angles 0 rad (blue solid), 0.3 rad (orange dashed) and 0.5 rad (red dotted).

a precision compatible with the size of the predicted SM signal.

Using an analytical approximation for the Fisher information matrices of the CPV observables, we can understand how the precision of such measurements depends on the polarization and spin-correlation terms in the production processes. Some of the obtained analytical results can be directly extended to charm baryon CPV studies. At SCTF, they can be studied in close-to-threshold $e^+e^- \to B\overline{B}$ processes. For such processes, the analytic results of Sec. 2.4 and Sec. 2.5 can be taken as a starting point. The main difference in the strategy for charmed baryons is due to the fact that the branching fractions for two-body nonleptonic decays are small, and the DT analysis likely will not be feasible.

In addition to the $e^+e^- \to B\overline{B}$ processes, the HyperCP-type experiments can be an interesting option for CP tests and decay parameter determination, provided that sources of (anti)baryons with large initial polarization are available. Possible candidate processes are semileptonic decays of charmed baryons $\Xi_c^0 \to \Xi^- \ell^+ \nu_\ell$ or two-body hadronic decays like $\Xi_c^0 \to \Xi^- \pi^+$ with large value of the decay parameter $\alpha = 0.63(3)$ [145] and relatively large branching fraction 1.2 % [92]. For such studies, unpolarized charmed baryons that are abundantly produced at the LHC in pp collisions can be used. Again, our analytic formulas can be used to provide a first estimate of the statistical uncertainties for such experiments.

We have left out a potentially interesting discussion of the uncertainties of the decay parameters α_D and ϕ_D. The α_D parameter is correlated with production parameters and extraction of uncertainties and correlation coefficients requires inverting information matrices with larger dimensions and the analytical results might be difficult to interpret. The same is valid for the production parameters α_ψ and $\Delta\Phi$ that are relevant for the experiments where the goal is to study the properties of the production process. Usually such experiments have a limited number of the collected events and analysis is done assuming the decay parameters are known.

I   Isospin decomposition

Here, we evaluate the $\Delta I = 1/2$ and $\Delta I = 3/2$ components of the $\Lambda \to N\pi$ and $\Xi \to \Lambda\pi$ amplitudes. As in the main text, we *assume* isospin symmetry for the elementary weak decay process but take into account the impact of isospin-violating mass splittings in the kinematics. The basic parameters in the Feynman matrix element $\overline{u}_b(g_S - \gamma_5 g_P)u_B$ of the weak decay of a spin-1/2 baryon B into another spin-1/2 baryon b and a pion are related to the partial-wave amplitudes S and P via

$$g_S = S, \qquad g_P = P\,\frac{E+M}{|\mathbf{q}|}\,, \tag{2.82}$$

where $|\mathbf{q}|$, E, and M stand for the momentum, energy, and mass, respectively, of b in the rest frame of B. Further considerations on $g_{S,P}$ are provided in Appendix II (see also mini-review 79.2., "Hyperon nonleptonic decays", in Ref. [92]). The isospin breaking mentioned above arises from the p-wave kinematical factor $|\mathbf{q}|/(E+M)$ as well as the phase space volume.

Suppose we have two decay modes, labelled I and II, connected by isospin symmetry (*e.g.*, $\Lambda \to p\pi^-$ and $\Lambda \to n\pi^0$). Our isospin-symmetry assumption for the basic parameters is then expressible as

$$(g_S)_\text{I} = (g_S)_\text{II}\,, \qquad\qquad (g_P)_\text{I} = (g_P)_\text{II}\,. \qquad\qquad (2.83)$$

In view of Eqs. (2.82) and (2.83), the S and P amplitudes $S_\text{I,II}$ and $P_\text{I,II}$, respectively, for the two processes, including corrections Δ_I and Δ_II due to different masses in the kinematical factors, can be written as

$$S_\text{I} = S_\text{II}\,, \qquad P_\text{I}(1 + \Delta_\text{I}) =: P_\text{I}\frac{E_\text{I} + M_\text{I}}{|\mathbf{q}_\text{I}|}\frac{|\overline{\mathbf{q}}|}{\overline{E} + \overline{M}} = P_\text{II}(1 + \Delta_\text{II})\,, \qquad (2.84)$$

where $|\overline{\mathbf{q}}|/(\overline{E} + \overline{M})$ contains only isospin-averaged masses,[4] which ensures that $|\Delta_\text{I,II}| \ll 1$. For $\Lambda \to p\pi^-$ ($[\Lambda p]$), $\Lambda \to n\pi^0$ ($[\Lambda n]$), $\Xi^- \to \Lambda\pi^-$ ($[\Xi-]$), and $\Xi^0 \to \Lambda\pi^0$ ($[\Xi 0]$), the Δs are calculated to be at most a couple of percents in size, specifically

$$\Delta_{[\Lambda p]} = 0.007769(3)\,, \qquad \Delta_{[\Lambda n]} = -0.023631(6)\,, \qquad (2.85)$$

$$\Delta_{[\Xi-]} = -0.0201(9)\,, \qquad \Delta_{[\Xi 0]} = 0.011(1)\,. \qquad (2.86)$$

The isospin decomposition, in notation similar to Ref. [146], of the $L = S, P$ amplitudes for $\Lambda \to N\pi$ into their $\Delta I = 1/2, 3/2$ components reads

$$L_{[\Lambda p]} = -\sqrt{\frac{2}{3}}L_{1,1}\exp(i\xi_1^L + i\delta_1^L) + \sqrt{\frac{1}{3}}L_{3,3}\exp(i\xi_3^L + i\delta_3^L)\,,$$

$$L_{[\Lambda n]} = \sqrt{\frac{1}{3}}L_{1,1}\exp(i\xi_1^L + i\delta_1^L) + \sqrt{\frac{2}{3}}L_{3,3}\exp(i\xi_3^L + i\delta_3^L)\,, \qquad (2.87)$$

where in the $L = P$ case $P_{[\Lambda p]}$ and $P_{[\Lambda n]}$ on the left-hand sides are to be replaced by $(1 + \Delta_{[\Lambda p]})P_{[\Lambda p]}$ and $(1 + \Delta_{[\Lambda n]})P_{[\Lambda n]}$, respectively, as per the discussion in the previous paragraph. Analogously, for the $\Xi \to \Lambda\pi$ channels one has

$$L_{[\Xi-]} = L_{1,2}\exp(i\xi_{1,2}^L + i\delta_2^L) + \frac{1}{2}L_{3,2}\exp(i\xi_{3,2}^L + i\delta_2^L)\,,$$

$$L_{[\Xi 0]} = \frac{1}{\sqrt{2}}L_{1,2}\exp(i\xi_{1,2}^L + i\delta_2^L) - \frac{1}{\sqrt{2}}L_{3,2}\exp(i\xi_{3,2}^L + i\delta_2^L)\,, \qquad (2.88)$$

with $P_{[\Xi-]} \to (1 + \Delta_{[\Xi-]})P_{[\Xi-]}$ and $P_{[\Xi 0]} \to (1 + \Delta_{[\Xi 0]})P_{[\Xi 0]}$. Incorporating Eqs. (2.87) and (2.88) into Eqs. (2.3) and (2.5), employing the experimental values of the pertinent α parameters, partial rates, phase shifts, and masses, and dropping the tiny weak phases ξ_j^L, we can then extract $L_{2\Delta I,2I}$ for the Λ and Ξ modes.

In the Ξ case, due to the fact that only one phase-shift difference, $\delta_2^P - \delta_2^S$, is involved, it turns out to be possible to derive $L_{1,2}$ and $L_{3,2}$ analytically in terms of empirically known quantities, but we will not include the lengthy expressions in this paper. To evaluate them

---

[4]Explicitly, these are $\overline{M}_N = (M_p + M_n)/2$, $\overline{M}_\Xi = (M_{\Xi^-} + M_{\Xi^0})/2$, and $\overline{M}_\pi = (2M_{\pi^+} + M_{\pi^0})/3$ for the isospin nonsinglets.

TABLE 2.7: Amplitudes, in dimensionless units of $G_\mathrm{F} m_{\pi^+}^2$, for the $\Delta I = 1/2$ and $\Delta I = 3/2$ transitions, and the corresponding $(\Delta I = 3/2)/(\Delta I = 1/2)$ amplitude ratios, in the Λ- and Ξ-hyperon nonleptonic decays.

Decay	$\Delta I = 1/2$		$\Delta I = 3/2$		$(\Delta I = 3/2)/(\Delta I = 1/2)$	
mode	S	P	S	P	S ratio	P ratio
$\Xi \to \Lambda\pi$	$-2.05(1)$	$0.386(5)$	$0.11(2)$	$-0.002(8)$	$-0.05(1)$	$-0.005(21)$
$\Lambda \to N\pi$	$-1.718(8)$	$-0.759(2)$	$-0.050(9)$	$0.036(9)$	$0.029(6)$	$-0.05(1)$

numerically, we adopt the boldfaced $\alpha_{[\Xi-]}$ and $\alpha_{[\Xi0]}$ numbers quoted in Table 2.2 as well as the appropriate masses and partial rates from Ref. [92]. As for the strong phases, after combining the relation $\tan\left(\delta_2^P - \delta_2^S\right) = \sin\phi \sqrt{1 - \alpha^2}/\alpha$ with the measured α and ϕ parameters for the Ξ decays listed in Table 2.2, we find the average experimental value $\delta_2^P - \delta_2^S = 1(4)°$, which is consistent with zero and perhaps suggestive of it being considerably smaller than the pion–nucleon phase shifts relevant to the Λ and Σ decays (given in Table 2.3).[5] Putting things together, we collect the resulting $L_{1,2}$, $L_{3,2}$, and $L_{3,2}/L_{1,2}$ in Table 2.7, all the Ls written in units of the Fermi constant G_F times the charged pion's squared mass. Evidently, the size of $S_{3,2}$ relative to $S_{1,2}$ is 5%, while $P_{3,2}$ is consistent with zero (less than 3% of $P_{1,2}$ within one standard deviation).

Compared to their Ξ counterparts, the Λ decay amplitudes are more complicated, having four different strong phases, and consequently it does not seem feasible to arrive at analytical formulas for $L_{1,1}$ and $L_{3,3}$. Nevertheless, one can still determine them by means of numerical computation. Thus, with the boldfaced $\alpha_{[\Lambda p]}$ and $\alpha_{[\Lambda n]}$ entries in Table 2.2, the $\Lambda \to N\pi$ phases in Table 2.3, and masses and partial rates from Ref. [92], we obtain the numbers displayed in the bottom row of Table 2.7. It shows that the $\Delta I = 3/2$ components of S and P are 3% and 5% of the corresponding $\Delta I = 1/2$ ones in size.

If one is interested merely in the relative size of the different amplitudes, it is possible to infer their ratios approximately from the αs and squared amplitudes upon expanding them to linear order in the $\Delta I = 3/2$ components or the Δ_D parameters, which have effects of comparable size on the $\Delta I = 1/2$ contributions. This complementary procedure also helps cross-check Table 2.7.

In this approximation, for the Ξ modes we have the α combinations

$$\alpha_{[\Xi]} := \frac{2\alpha_{[\Xi-]} + \alpha_{[\Xi0]}}{3} = 2\hat{s}_1 \hat{P}_1 \cos\left(\delta_2^P - \delta_2^S\right)\left[1 + \frac{1}{3}\left(1 - 2\hat{s}_1^2\right)\left(2\Delta_{[\Xi-]} + \Delta_{[\Xi0]}\right)\right] \tag{2.89}$$
$$\overset{\text{exp}}{=} -0.368(4)\,,$$

$$\frac{\alpha_{[\Xi-]} - \alpha_{[\Xi0]}}{\alpha_{[\Xi]}} = \left(1 - 2\hat{s}_1^2\right)\left(\frac{3}{2}\frac{\hat{s}_3}{\hat{s}_1} - \frac{3}{2}\frac{\hat{P}_3}{\hat{P}_1} + \Delta_{[\Xi-]} - \Delta_{[\Xi0]}\right) \tag{2.90}$$
$$\overset{\text{exp}}{=} 0.092(25)\,,$$

---

[5]By contrast, as remarked in Sec. 2.2.2, recent theoretical studies have predicted that $\delta_2^P - \delta_2^S$ might be significantly bigger [122, 124], as much as $9°$.

where $\hat{L}_k = L_{k,2}/(S_{1,2}^2 + P_{1,2}^2)^{1/2}$ for $L = S, P$ and $k = 1, 3$, implying that $\hat{s}_1^2 + \hat{P}_1^2 = 1$. We also have the squared amplitudes

$$|\mathcal{A}_{[\Xi-]}|^2 = S_{1,2}^2 + (1 - 2\Delta_{[\Xi-]})P_{1,2}^2 + S_{1,2}S_{3,2} + P_{1,2}P_{3,2},$$
$$|\mathcal{A}_{[\Xi0]}|^2 = \tfrac{1}{2}S_{1,2}^2 + \tfrac{1}{2}(1 - 2\Delta_{[\Xi0]})P_{1,2}^2 - S_{1,2}S_{3,2} - P_{1,2}P_{3,2}, \qquad (2.91)$$

where the left-hand sides are connected via Eq. (2.5) to the observed rates $\Gamma(\Xi^- \to \Lambda\pi^-)$ and $\Gamma(\Xi^0 \to \Lambda\pi^0)$, respectively, leading to

$$\frac{1}{2}\frac{\Gamma(\Xi^- \to \Lambda\pi^-) - 2\Gamma(\Xi^0 \to \Lambda\pi^0)\,r_\Xi}{\Gamma(\Xi^- \to \Lambda\pi^-) + \Gamma(\Xi^0 \to \Lambda\pi^0)\,r_\Xi} = \hat{s}_1\hat{s}_3 + \hat{P}_1\hat{P}_3 - \frac{2}{3}(\Delta_{[\Xi-]} - \Delta_{[\Xi0]})\hat{P}_1^2 \qquad (2.92)$$
$$\stackrel{\text{exp}}{=} -0.050(11),$$

where $r_\Xi = 1.0270(18)$ is the ratio of phase space volumes of the two modes. From Eq. (2.89) we extract $\hat{s}_1 = -0.9827(4)$ and hence $\hat{P}_1 = (1 - \hat{s}_1^2)^{1/2} = 0.185(2)$, with which we solve Eqs. (2.90) and (2.92) for $\hat{s}_3 = 0.05(1)$ and $\hat{P}_3 = -0.001(4)$, and so we get $\hat{s}_3/\hat{s}_1 = -0.05(1)$ and $\hat{P}_3/\hat{P}_1 = -0.007(20)$. These results can be seen to be compatible with the $\Xi \to \Lambda\pi$ entries in Table 2.7.

Similarly, in the Λ case, we have

$$\alpha_{[\Lambda]} := \frac{2\alpha_{[\Lambda p]} + \alpha_{[\Lambda n]}}{3} = 2\tilde{s}_1\tilde{P}_1\cos(\delta_1^P - \delta_1^S)\left[1 + \frac{1}{3}(1 - 2\tilde{s}_1^2)(2\Delta_{[\Lambda p]} + \Delta_{[\Lambda n]})\right] \qquad (2.93)$$
$$\stackrel{\text{exp}}{=} 0.734(6),$$

$$\frac{\alpha_{[\Lambda p]} - \alpha_{[\Lambda n]}}{\alpha_{[\Lambda]}} = \frac{-3}{\sqrt{2}}\left[\frac{\tilde{s}_3}{\tilde{s}_1}\frac{\cos(\delta_1^P - \delta_3^S)}{\cos(\delta_1^P - \delta_1^S)} + \frac{\tilde{P}_3}{\tilde{P}_1}\frac{\cos(\delta_1^S - \delta_3^P)}{\cos(\delta_1^P - \delta_1^S)}\right]$$
$$+ 3\sqrt{2}\left[\tilde{s}_1\tilde{s}_3\cos(\delta_1^S - \delta_3^S) + \tilde{P}_1\tilde{P}_3\cos(\delta_1^P - \delta_3^P)\right]$$
$$+ (1 - 2\tilde{s}_1^2)(\Delta_{[\Lambda p]} - \Delta_{[\Lambda n]}) \qquad (2.94)$$
$$\stackrel{\text{exp}}{=} 0.086(24),$$

$$\frac{\Gamma(\Lambda \to p\pi^-) - 2\Gamma(\Lambda \to n\pi^0)\,r_\Lambda}{\Gamma(\Lambda \to p\pi^-) + 2\Gamma(\Lambda \to n\pi^0)\,r_\Lambda} = -\sqrt{8}\left[\tilde{s}_1\tilde{s}_3\cos(\delta_1^S - \delta_3^S) + \tilde{P}_1\tilde{P}_3\cos(\delta_1^P - \delta_3^P)\right]$$
$$- \frac{4}{3}(\Delta_{[\Lambda p]} - \Delta_{[\Lambda n]})\tilde{P}_1^2$$
$$\qquad (2.95)$$
$$\stackrel{\text{exp}}{=} -0.053(13),$$

where $\tilde{L}_k = L_{k,k}/(S_{1,1}^2 + P_{1,1}^2)^{1/2}$ for $L = S, P$ and $k = 1, 3$ and $r_\Lambda = 0.965815(8)$ is the ratio of $\Lambda \to N\pi$ phase-space volumes. From Eq. (2.93) we obtain $\tilde{s}_1 = -0.915(2)$ and hence $\tilde{P}_1 = -(1 - \tilde{s}_1^2)^{1/2} = -0.404(4)$, with which we find $\tilde{s}_3 = -0.027(5)$ and $\tilde{P}_3 = 0.019(6)$ from Eqs. (2.94) and (2.95) and consequently $\tilde{s}_3/\tilde{s}_1 = 0.029(6)$ and $\tilde{P}_3/\tilde{P}_1 = -0.05(1)$. As expected, these are in line with the $\Lambda \to N\pi$ numbers in Table 2.7.

Finally, we illustrate how the knowledge about the $\Delta I = 1/2, 3/2$ components could improve the accuracy of estimating the β and ϕ parameters, which are linked to α by Eq. (2.8) and not all of which have been measured. Focusing on the Λ channels, for the βs we can write, to first order in the $\Delta I = 3/2$ amplitudes,

$$\frac{\beta_{[\Lambda p]}}{\alpha_{[\Lambda p]}} = \tan\left(\delta_1^P - \delta_1^S\right) + \frac{\tilde{P}_3 \sin\left(\delta_1^P - \delta_3^P\right)}{\sqrt{2}\,\tilde{P}_1 \cos^2\left(\delta_1^P - \delta_1^S\right)} - \frac{\tilde{s}_3 \sin\left(\delta_1^S - \delta_3^S\right)}{\sqrt{2}\,\tilde{s}_1 \cos^2\left(\delta_1^P - \delta_1^S\right)} \,,$$

$$\frac{\beta_{[\Lambda n]}}{\alpha_{[\Lambda n]}} = \tan\left(\delta_1^P - \delta_1^S\right) - \frac{\sqrt{2}\,\tilde{P}_3 \sin\left(\delta_1^P - \delta_3^P\right)}{\tilde{P}_1 \cos^2\left(\delta_1^P - \delta_1^S\right)} + \frac{\sqrt{2}\,\tilde{s}_3 \sin\left(\delta_1^S - \delta_3^S\right)}{\tilde{s}_1 \cos^2\left(\delta_1^P - \delta_1^S\right)} \,, \tag{2.96}$$

as the contributions linear in the Δ_D's cancel in the ratios. Upon applying these formulas and Eq. (2.8), with the boldfaced $\alpha_{[\Lambda p]}$ and $\alpha_{[\Lambda n]}$ values in Table 2.2, the $\Lambda \to N\pi$ strong phases in Table 2.3, and the above calculation of $\tilde{s}_{1,3}$ and $\tilde{P}_{1,3}$, we arrive at

$$\beta_{[\Lambda p]} = -0.100(2)\,, \qquad\qquad \phi_{[\Lambda p]} = -0.153(3)\,, \tag{2.97}$$

$$\beta_{[\Lambda n]} = -0.083(3)\,, \qquad\qquad \phi_{[\Lambda n]} = -0.115(7)\,. \tag{2.98}$$

If the $\Delta I = 3/2$ terms in Eq. (2.96) were neglected, we would instead get $\beta_{[\Lambda p]} = -0.097(2)$, $\phi_{[\Lambda p]} = -0.148(3)$, $\beta_{[\Lambda n]} = -0.089(3)$, and $\phi_{[\Lambda n]} = -0.123(6)$, which differ from their counterparts in Eqs. (2.97) and (2.98) by 3% and 7%, respectively. It is interesting to notice that the $\phi_{[\Lambda p]}$ prediction in Eq. (2.97) is 20 times more precise than the direct measurement of $-0.113(61)$ quoted in Table 2.2.

II Effective Lagrangian and parameterization of amplitudes

A hermitian effective Lagrangian for the initial decay $B \to b\pi$ where all baryons have spin-1/2 is given by

$$\mathcal{L} = g_S\, i\bar{b}B\pi - g_S^*\, i\overline{B}b\,\overline{\pi} - g_P\, \bar{b}i\gamma_5 B\pi - g_P^*\, \overline{B}i\gamma_5 b\,\overline{\pi}\,. \tag{2.99}$$

The g_S terms lead to s-waves for the decay products, the g_P terms lead to p-waves and the g_S terms break parity (P) symmetry while the g_P terms do not. If g_S is real, then the g_S terms break P and C, but conserve CP symmetry. If g_P is real, then the g_P terms conserve C symmetry and therefore also CP. One can make g_P real and positive by moving its phase into a redefinition of the B-baryon field (and a redefinition of the discrete transformations by an additional phase). The CP symmetry is then conserved, if the parameter g_S is real.

Except for an irrelevant overall phase, one might write the decay matrix elements as

$$\mathcal{M}_{B \to b\pi} \sim \bar{u}_b\left(g_S - g_P\gamma_5\right)u_B\,, \qquad \mathcal{M}_{\overline{B} \to \overline{b}\overline{\pi}} \sim \bar{v}_B\left(-g_S^* - g_P^*\gamma_5\right)v_b\,. \tag{2.100}$$

This fits to the conventions of the Particle Data Group. Then one reads off: $S_{\rm ini} \sim g_S$, $\overline{S}_{\rm ini} \sim -g_S^*$, $P_{\rm ini} \sim g_P$, $\overline{P}_{\rm ini} \sim g_P^*$ where the p-waves pick up an additional phase space factor that we have not displayed explicitly. The relations between partial-wave amplitudes and parameters

from the Lagrangian suggest writing for the initial amplitudes

$$
\begin{aligned}
S_{\text{ini}} &= \quad |S|\, e^{i\xi_S}\,, \qquad P_{\text{ini}} = |P|\, e^{i\xi_P}\,,\\
\overline{S}_{\text{ini}} &= -|S|\, e^{-i\xi_S}\,, \qquad \overline{P}_{\text{ini}} = |P|\, e^{-i\xi_P}\,.
\end{aligned}
\tag{2.101}
$$

Strictly speaking, ξ_P is not needed. What matters is the relative phase between S and P, which can be expressed via $\xi_S - \xi_P$ but equally well via ξ_S if one puts $\xi_P = 0$. In principle, phases can vary between 0 and 2π or $-\pi$ and π. However, an overall minus sign for all amplitudes would not lead to an observable consequence. Therefore, it is sufficient to consider $\xi_S - \xi_P \in [0, \pi)$ or $\in [-\pi/2, +\pi/2)$. If (2.101) were the complete amplitudes, then one would always find $\overline{\alpha} = -\alpha$ and $\overline{\beta} = \beta$, irrespective of CP violation or conservation. For the case of CP symmetry, one would find $\beta = 0$.

This whole analysis leaves out final-state interactions. Rescattering is a non-local phenomenon that cannot be treated by a tree-level calculation using a local, hermitian Lagrangian. Instead, one can use explicit loop calculations if one has a microscopic picture of the reaction, or one can use an Omnès-function matrix that parameterizes the final-state interactions. This is discussed in more detail in Appendix III.

III   Treatment of final-state interactions

In the following, we discuss in some detail the treatment of final-state interactions for the main decays of the Λ and $\overline{\Lambda}$ baryons. The case of $\Xi^{0,-}$ decays is just simpler. Concerning the general treatment of final-state interactions, see also [147–151]. The hyperon decays that we study in the present work do not allow for many intermediate inelastic channels, since the decaying strange quark is not very heavy. Decays of charm or bottom baryons would provide much more phase space and correspondingly contain many more open channels. Kinematically closed channels might become important if they are strong (e.g. resonance enhanced) and if their threshold is close to the studied invariant mass (e.g. this happens for the $f_0(980)$ and the kaon–antikaon threshold [152]). There are no non-strange resonances close to the Λ mass and no single-strange resonances close to the Ξ mass.

The relevant decay channels of Λ are $(p\pi^-)_S$, $(p\pi^-)_P$, $(n\pi^0)_S$, $(n\pi^0)_P$ where the subscript denotes the partial wave. It is more convenient to build linear combinations with respect to the isospin of the final states. Then the four decay channels are $(N\pi)_{S,I=1/2}$, $(N\pi)_{S,I=3/2}$, $(N\pi)_{P,I=1/2}$, $(N\pi)_{P,I=3/2}$. Following the conventions of the main text, we denote the corresponding decay amplitudes by $L_{1,1}$ for $I = 1/2$ and by $L_{3,3}$ for $I = 3/2$; here $L = S, P$. The initial decay amplitudes that emerge from the weak process are denoted by $L^{\text{ini}}_{\ldots}$. For the corresponding antiparticle decays, we use $\overline{L}_{\ldots}$. We assume baryon number conservation. Then there are no oscillations between Λ and its antiparticle $\overline{\Lambda}$. But the final-state interactions (FSI) might allow for transitions between the 4 final states $(N\pi)_{S,I=1/2}$, $(N\pi)_{S,I=3/2}$, $(N\pi)_{P,I=1/2}$, and $(N\pi)_{P,I=3/2}$. This defines a coupled-channel problem. We assume that the weak process is of short-distance nature such that no structure is resolved. Therefore, the discontinuity of

a decay amplitude is solely given by the FSI. This defines an Omnès problem [153]; for an analogous situation, see *e.g.* [152].

In general, one has a 4×4 Omnès-function matrix Ω that parameterizes the FSI. This matrix maps the "bare" amplitudes of the initial decay onto the "full" amplitudes that contain the FSI:

$$
\begin{pmatrix} S_{1,1} \\ S_{3,3} \\ P_{1,1} \\ P_{3,3} \end{pmatrix} = \Omega \begin{pmatrix} S_{1,1}^{\text{ini}} \\ S_{3,3}^{\text{ini}} \\ P_{1,1}^{\text{ini}} \\ P_{3,3}^{\text{ini}} \end{pmatrix}.
\tag{2.102}
$$

The corresponding equation for the antiparticle sector reads

$$
\begin{pmatrix} \overline{S}_{1,1} \\ \overline{S}_{3,3} \\ \overline{P}_{1,1} \\ \overline{P}_{3,3} \end{pmatrix} = \overline{\Omega} \begin{pmatrix} \overline{S}_{1,1}^{\text{ini}} \\ \overline{S}_{3,3}^{\text{ini}} \\ \overline{P}_{1,1}^{\text{ini}} \\ \overline{P}_{3,3}^{\text{ini}} \end{pmatrix}.
\tag{2.103}
$$

Next, we assume that parity and charge conjugation are both conserved by the FSI. This is true for strong and electromagnetic FSI. In this case, the FSI are the same in the particle and antiparticle sector, *i.e.* $\Omega = \overline{\Omega}$, and there is no cross talk between the parity-even p-waves and the parity-odd s-waves:

$$
\Omega = \overline{\Omega} = \begin{pmatrix} \Omega_S & 0 \\ 0 & \Omega_P \end{pmatrix}
\tag{2.104}
$$

with 2×2 matrices Ω_S and Ω_P.

Finally, we assume isospin symmetry. Then the 2×2 matrices become diagonal. Watson's theorem [125] ensures that the phase of the pertinent Omnès function agrees with the scattering phase shift $\delta_{L,2I}$ of the corresponding N-π scattering:

$$
\Omega_L = \text{diag} \left(|\Omega_{L,2I=1}| \, e^{i \delta_{L,1}}, |\Omega_{L,2I=3}| \, e^{i \delta_{L,3}} \right)
\tag{2.105}
$$

with $L = S, P$. Here it is of advantage that we changed from the particle basis ($p\pi^-$ and $n\pi^0$) to the isospin basis ($I = 1/2$ and $I = 3/2$). In the particle basis, the 2×2 Omnès matrices would not be diagonal.

Of course, if required by precision, the assumptions that lead from more general 4×4 matrices in (2.102) and (2.103) to (2.104) and (2.105) can be relaxed one by one.

IV   Average polarization and spin-correlation terms

Expression for average polarization squared

$$\langle \mathbf{P}_B^2 \rangle = \int \mathbf{P}_B^2 \left(\frac{1}{\sigma} \frac{d\sigma}{d\Omega_B} \right) d\Omega_B = \frac{3}{2} \int \mathbf{P}_B^2 \frac{1 + \alpha_\psi \cos^2\theta}{3 + \alpha_\psi} d\cos\theta \,, \tag{2.106}$$

where $\mathbf{P}_B$ is given by Eq. (2.40). The integral can be calculated exactly, and the result is expressed as

$$\langle \mathbf{P}_B^2 \rangle = \mathbb{p}_0 + \mathbb{p}_2 P_e^2 \,, \tag{2.107}$$

where

$$\mathbb{p}_0 = \frac{\left(1 - \alpha_\psi^2\right) \sin^2(\Delta\Phi)}{\alpha_\psi^2 (3 + \alpha_\psi)} \left\{ 3 + 2\alpha_\psi - 3(1 + \alpha_\psi) F(\alpha_\psi) \right\} \,, \tag{2.108}$$

$$\mathbb{p}_2 = \frac{3(1 + \alpha_\psi)^2}{\alpha_\psi (3 + \alpha_\psi)} \left\{ 1 - \frac{1 - \alpha_\psi}{1 + \alpha_\psi} \cos^2(\Delta\Phi) - \left(1 - (1 - \alpha_\psi) \cos^2(\Delta\Phi) \right) F(\alpha_\psi) \right\} \,. \tag{2.109}$$

The function $F(\alpha)$ is

$$F(\alpha) := \int_0^1 \frac{dx}{1 + \alpha x^2} = \begin{cases} \frac{\arctan\sqrt{\alpha}}{\sqrt{\alpha}} & 0 < \alpha \le 1 \\ 1 & \alpha = 0 \\ \frac{\operatorname{arctanh}\sqrt{|\alpha|}}{\sqrt{|\alpha|}} & -1 < \alpha < 0 \end{cases} \,. \tag{2.110}$$

Properties of the function $F(1) = \frac{\pi}{4}$ and $\lim_{\alpha \to -1} F(\alpha) = \infty$. The function is drawn in Fig. 2.18. For $\alpha_\psi = 1$ the coefficients are

$$\mathbb{p}_0 = 0 \quad \text{and} \quad \mathbb{p}_2 = \frac{3(4 - \pi)}{4} \approx 0.6438 \tag{2.111}$$

and for $\alpha_\psi = 0$

$$\mathbb{p}_0 = \frac{2}{15} \sin^2(\Delta\Phi) \quad \text{and} \quad \mathbb{p}_2 = \frac{2 + \cos(2\Delta\Phi)}{3} \,. \tag{2.112}$$

One derives similar expressions for the sum of the squares of the spin-correlation terms. The result can be expressed as

$$\langle \mathbb{S}_{B\overline{B}}^2 \rangle = \mathbb{s}_0 + \mathbb{s}_2 P_e^2 \,, \tag{2.113}$$

where

$$\mathbb{s}_0 = \frac{1}{\alpha_\psi^2 (3 + \alpha_\psi)} \left\{ \left(1 - \alpha_\psi^2 \right) (2\alpha_\psi + 3) \cos(2\Delta\Phi) - 7\alpha_\psi^3 - 2\alpha_\psi - 3 \right.$$
$$\left. -3(\alpha_\psi + 1)^2 F(\alpha_\psi) \left[(1 - \alpha_\psi) \cos(2\Delta\Phi) + \alpha_\psi - 2\alpha_\psi^2 - 1 \right] \right\} \,, \tag{2.114}$$

$$\mathbb{s}_2 = \frac{6(1 - \alpha_\psi^2) \sin^2(\Delta\Phi)}{\alpha_\psi (3 + \alpha_\psi)} \left\{ (1 + \alpha_\psi) F(\alpha_\psi) - 1 \right\} \,. \tag{2.115}$$
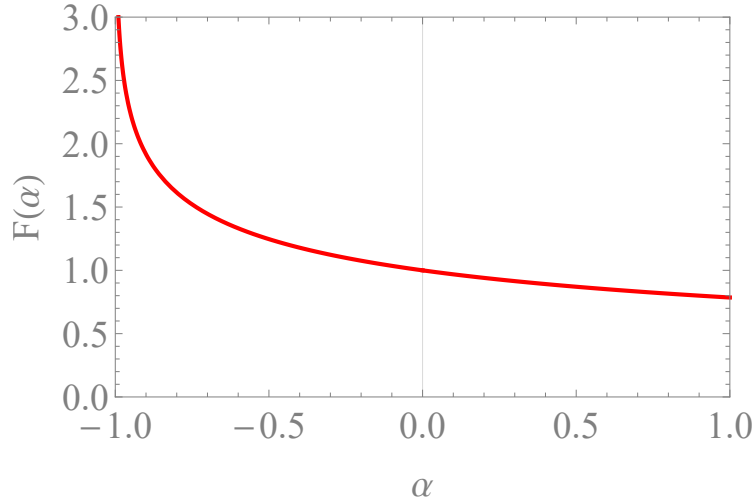
FIGURE 2.18: Function $F(\alpha)$ defined in Eq. (2.110). The function is divergent for $\alpha \to -1$.

For the $e^+ e^- \to B\overline{B}$ process specified by the parameters α_ψ, β_ψ and γ_ψ the polarization and spin-correlation terms as a function of the B-baryon production angle θ are

$$\mathbb{P}_B^2(\cos\theta) = 2 \frac{(\alpha_\psi + 1)^2 P_e^2 \cos^2\theta + \sin^2\theta \left(\beta_\psi^2 \cos^2\theta + P_e^2 \gamma_\psi^2\right)}{\left(1 + \alpha_\psi \cos^2\theta\right)^2}, \tag{2.116}$$

$$\mathbb{S}_{B\overline{B}}^2(\cos\theta) = \frac{\left(\alpha_\psi^2 + 1\right)\sin^4\theta + \left(\alpha_\psi + \cos^2\theta\right)^2 + 2\sin^2\theta \left(\gamma_\psi^2 \cos^2\theta + P_e^2 \beta_\psi^2\right)}{\left(1 + \alpha_\psi \cos^2\theta\right)^2} . \tag{2.117}$$

V   Modification of the Fisher information matrices to include background

Neglecting resolution effect for the $\boldsymbol{\xi}$ variables the overall probability density function including background term, $\mathcal{P}^B(\boldsymbol{\xi})$, and relative detection efficiency $\epsilon(\boldsymbol{\xi})$ is

$$\mathcal{P}^T(\boldsymbol{\xi}; \boldsymbol{\omega}) = p\mathcal{P}(\boldsymbol{\xi}; \boldsymbol{\omega})\epsilon(\boldsymbol{\xi}) + (1 - p)\mathcal{P}^B(\boldsymbol{\xi}) . \tag{2.118}$$

We impose the normalization $\int \mathcal{P}^B(\boldsymbol{\xi})\mathrm{d}\boldsymbol{\xi} = 1$ for the background and $\int \mathcal{P}(\boldsymbol{\xi}; \boldsymbol{\omega})\epsilon(\boldsymbol{\xi})\mathrm{d}\boldsymbol{\xi} = 1$ for the signal. The last condition implies that the relative efficiency $\epsilon(\boldsymbol{\xi})$ must be equal to one if it is constant. The coefficient $p = S/N$ represents the ratio of the number of the signal events, S, to the total number of the signal and background events N. It is assumed that the ratio is fixed and has a known value. The Fisher information matrix Eq. (2.52) now reads:

$$\mathcal{I}(\omega_k, \omega_l) := N \int \frac{1}{\mathcal{P}^T} \frac{\partial \mathcal{P}^T}{\partial \omega_k} \frac{\partial \mathcal{P}^T}{\partial \omega_l} \mathrm{d}\boldsymbol{\xi}$$

$$= Np^2 \int \frac{1}{\mathcal{P}^T} \frac{\partial \mathcal{P}}{\partial \omega_k} \frac{\partial \mathcal{P}}{\partial \omega_l} \epsilon^2(\boldsymbol{\xi})\mathrm{d}\boldsymbol{\xi} . \tag{2.119}$$

We rewrite the background distribution as

$$\mathcal{P}^B(\boldsymbol{\xi}) =: \frac{1 + \mathcal{G}^B(\boldsymbol{\xi})}{\mathcal{V}} \tag{2.120}$$

and use Eq. (2.57) representation for the signal with $C_{00} = 1$. The term $1/\mathcal{P}^T$ can be therefore written as

$$\frac{1}{\mathcal{P}^T} = \frac{\mathcal{V}}{1 + p(\epsilon - 1) + p\mathcal{G}\epsilon + (1 - p)\mathcal{G}^B} \tag{2.121}$$

$$\approx \frac{\mathcal{V}}{1 + p\mathcal{G}} , \tag{2.122}$$

where the approximate form is obtained by setting $\epsilon(\boldsymbol{\xi}) = const. \equiv 1$ and $\mathcal{G}^B = 0$. Therefore, the analytical 0-th order approximations for experiments with background can be obtained by replacing $N \to S^2/N$ in our expressions.

Summary of the second chapter

- Hyperon-antihyperon pairs are produced in e^+e^- annihilation via charmonia decays. The effect of the beam polarization in the production process is explored in the context of upcoming facilities such as STCFs.

- The spin-correlation matrix for the production of spin-1/2 baryon–antibaryon pairs is derived: the polarization vectors of the pair gain additional components directly proportional to the beam polarization, which also affects the spin-correlation within the pair.

- The joint angular distribution (JAD) including the nonleptonic decays of the $B\bar{B}$ pair is obtained and used in an approximate maximum likelihood method to derive the Fisher information matrix for the CP observables. The PDF is approximated analytically to derive compact expressions for the uncertainties for the CP observables. The impact of higher-order terms in the approximating series is explored by comparison with the exact numerical results, and found to be small: the zeroth order term provides a good description of the uncertainties for the examined hyperon decays.

- The statistical uncertainties are also investigated for varying values of beam polarization P_e, on ST and DT analyses. The CP tests show improved precision with increasing P_e, with a factor of four reduction of the uncertainties size around the attainable value $P_e \sim 0.8 - 0.9$.

- The current status of CPV phenomenology is reviewed, expressing hyperon nonleptonic decays in terms of partial wave-amplitudes S, P using isospin decomposition. An updated estimate of the relative size between LO and first-order correction was provided in light of recent decay asymmetry measurements.

3

Semileptonic decays of spin-entangled baryon–antibaryon pairs

This chapter originally appeared as "Semileptonic decays of spin-entangled baryon–antibaryon pairs" by V. Batozskaya, A. Kupsc, N. Salone and J. Wiechnik, Physical Review D 108, 1, 016011, 2023. Copyright (2023) by the American Physical Society.

Abstract

A modular representation for the semileptonic decays of baryons originating from spin polarized and correlated baryon–antibaryon pairs is derived. The complete spin information of the decaying baryon is propagated to the daughter baryon via a real-valued matrix. It allows to obtain joint differential distributions in sequential processes involving the semileptonic decay in a straightforward way. The formalism is suitable for extraction of the semileptonic form factors in experiments where strange-baryon–antibaryon pairs are produced in electron–positron annihilation or in charmonia decays. We give examples such as the complete angular distributions in the $e^+e^- \to \Lambda\bar{\Lambda}$ process, where $\Lambda \to pe^-\bar{\nu}_e$ and $\bar{\Lambda} \to \bar{p}\pi^+$. The formalism can also be used to describe the distributions in semileptonic decays of charm and bottom baryons. Using the same principles, the modules to describe electromagnetic and neutral current weak baryon decay processes involving a charged lepton–antilepton pair can be obtained. As an example, we provide the decay matrix for the Dalitz transition between two spin-1/2 baryons.

3.1   Introduction

Baryon semileptonic (SL) decays are an important tool to study transitions between ground state baryons. Comparing to the nonleptonic baryon decays where at least three hadronic currents are involved, the SL transition involves only a two-point hadronic vertex and the external W-boson field coupled to the leptonic current. The properties of the hadronic vertices

are described by a set of scalar functions, *form factors*, that depend on the invariant mass squared of the emitted virtual W-boson. In particular, the semileptonic processes allow to probe the kinematic regions of the form factors that are dominated by the static properties of the baryons. The recent progress in the lattice quantum chromodynamics gives a hope to determine the properties of the form factors from the first principles with the accuracy sufficient for a comparison with precise experimental data [154]. Once the hadronic effects are well understood, the SL decays will provide a complementary method to determine Cabbibo–Kobayashi–Maskawa matrix elements [66] and to search for beyond the Standard Model effects such as violation of lepton flavor and charge-conjugation–parity symmetries [155]. In this article, we provide a modular description of the semileptonic decays that can be used to extract properties of the form factors in the experiments using spin entangled baryon–antibaryon pairs.

The helicity amplitude method [156–158] that is commonly used in the analyses of semileptonic decays allows to express the angular distributions in an efficient and compact way. The complete process is described as a sequence of two-body decays, where each of them is analyzed in the rest frame of the subsequent decaying particle. For a semileptonic decay $B_1 \rightarrow B_2 + \ell^- \bar{\nu}_\ell$, the first decay step $B_1 \rightarrow B_2 W^-_{\text{off-shell}}$ is analyzed in the B_1 rest frame, whereas $W^-_{\text{off-shell}} \rightarrow \ell^- \bar{\nu}_\ell$ is analyzed in the $W^-_{\text{off-shell}}$ rest frame. The resulting expressions for the differential distributions are compact and can be written in a quasi-factorized form. The formalism also describes joint angular distributions in the semileptonic decays of a spin polarized baryons.

A novel approach to study strange baryon decays is to use hyperon–antihyperon pairs from J/ψ resonances produced in electron–positron annihilations [45]. The complete angular distribution in such processes can be conveniently represented using a product of real-valued matrices that describe the initial spin-entangled baryon–antibaryon state and chains of two-body weak decays. These matrices can be rearranged to describe many decay scenarios in the $e^+e^- \rightarrow \Lambda\bar{\Lambda}$, $e^+e^- \rightarrow \Xi\bar{\Xi}$ and similar processes [45, 47, 52, 105]. Several high-profile analyses using multidimensional maximum likelihood fits to angular distributions were performed by the electron–positron collider experiment BESIII [65, 159] using this modular formalism. These multidimensional analyses have demonstrated increased precision of the decay parameters measurements and enabled to observe effects that were averaged out in previous studies, such as a polarization of the hyperon–antihyperon pair from charmonia decays.

The same spin-entangled hyperon–antihyperon system can be used to study semileptonic decays such as $\Lambda \rightarrow p e^- \bar{\nu}_e$ or $\Xi^- \rightarrow \Lambda e^- \bar{\nu}_e$. The processes are relatively rare with the branching fractions (BFs) $8.32(14) \times 10^{-4}$ and $5.63(31) \times 10^{-4}$, respectively [160]. In the reactions $e^+e^- \rightarrow J/\psi \rightarrow \Lambda\bar{\Lambda}$ and $e^+e^- \rightarrow J/\psi \rightarrow \Xi^-\bar{\Xi}^+$ the hyperon semileptonic decay is tagged via a common decay of the antihyperon: $\bar{\Lambda} \rightarrow \bar{p}\pi^+$ and $\bar{\Xi}^+ \rightarrow \bar{\Lambda}\pi^+$, respectively. The tagging processes involve only charged particles in the final state, therefore their momenta can be precisely determined. This allows one to reconstruct the momentum of the antineutrino in the semileptonic process and to determine the four-momentum squared of the lepton pair that is needed to study the dynamics of the process. The polarization of the hyperons is given

by the angular distributions in their decays, but usually the polarization of the leptons is not measured. Such double-tag (DT) technique is often used to determine absolute branching fractions in electron–positron collider experiments [161]. With large number of collected events in experiments such as BESIII [162] studies of decay distributions in the semileptonic hyperon decays are possible. A formalism that uses spin correlations and polarization of the produced baryon–antibaryon system is needed to determine the decay parameters with the best precision. The purpose of this report is to extend the approach from Refs. [47, 52] to include decay matrices representing the three-body semileptonic processes. Our starting point is the helicity formalism for semileptonic decays from Ref. [158]. We construct a real-valued decay matrix relating the initial and final baryons' spin states, represented by the Pauli matrices. The obtained decay matrix is used to construct the full joint decay distributions of the spin-entangled baryon–antibaryon pair in a modular way.

The paper is organized as follows: in Sec. 3.2 and Sec. 3.4 we review the formalism to describe baryon–antibaryon production process and semileptonic decays, respectively. In Sec. 3.5 the main result is derived — the spin-density matrix of the daughter baryon in the semileptonic decay. Sec. 3.6 presents modular formulas to describe the angular distributions of the semileptonic hyperon decays. Finally, in Sec. 3.7 we collect some numerical results.

3.2 Production process

In general a state of two spin-1/2 particles e.g. a baryon–antibaryon pair $B_1 \bar{B}_1$ can be written as [52]

$$\rho_{B_1 \bar{B}_1} = \sum_{\mu, \bar{\nu}=0}^{3} C_{\mu \bar{\nu}} \sigma_{\mu}^{B_1} \otimes \sigma_{\bar{\nu}}^{\bar{B}_1}, \tag{3.1}$$

where a set of four Pauli matrices $\sigma_{\mu}^{B_1}(\sigma_{\bar{\nu}}^{\bar{B}_1})$ acting in the rest frame of a baryon $B_1(\bar{B}_1)$ is used and $C_{\mu \bar{\nu}}$ is a 4×4 real matrix representing polarizations and spin correlations of the baryons. Here we consider mainly baryon–antibaryon systems created in the $e^+ e^- \rightarrow B_1 \bar{B}_1$ process. However, the formalism can be applied for the pairs from decays of (pseudo)scalar or tensor particles such as $\psi(2S), \eta_c, \chi_{c0}, \chi_{c2} \rightarrow B_1 \bar{B}_1$ or in a fact to any pair of spin-1/2 particles (for example baryon–baryon, muon–antimuon and others). The spin matrices $\sigma_{\mu}^{B_1}$ and $\sigma_{\bar{\nu}}^{\bar{B}_1}$ are given in the coordinate systems with the axes denoted $\hat{\mathbf{x}}_1, \hat{\mathbf{y}}_1, \hat{\mathbf{z}}_1$ and $\hat{\mathbf{x}}_3, \hat{\mathbf{y}}_3, \hat{\mathbf{z}}_3$ as shown in Fig. 3.1. The directions of the two right-handed coordinate systems are related as $(\hat{\mathbf{x}}_3, \hat{\mathbf{y}}_3, \hat{\mathbf{z}}_3) = (\hat{\mathbf{x}}_1, -\hat{\mathbf{y}}_1, -\hat{\mathbf{z}}_1)$. The spin correlation matrix $C_{\mu \bar{\nu}}$ for the reaction $e^+ e^- \rightarrow B_1 \bar{B}_1$ depends in the lowest order on two parameters, $\alpha_{\psi} \in [-1, 1]$ and $\Delta \Phi \in [-\pi, \pi)$. The elements of the $C_{\mu \bar{\nu}}$ matrix are functions of the baryon B_1 production angle θ_1 in the electron–positron center-of-momentum (c.m.) system. The matrix for the single photon annihilation
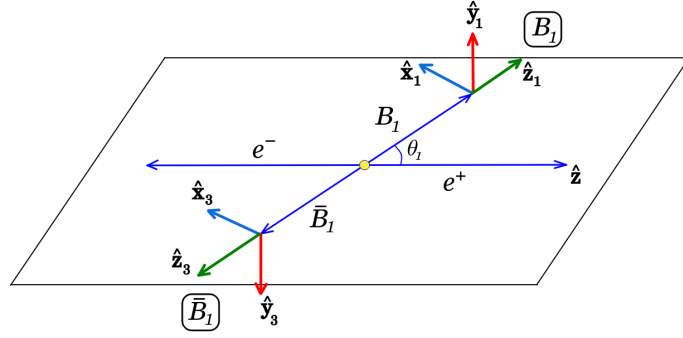
FIGURE 3.1: Definition of the three coordinate systems used to describe the spin-entangled $B_1\bar{B}_1$ state. The overall c.m. frame with $\hat{\mathbf{z}}$ axis (e.g. for $e^+e^- \to B_1\bar{B}_1$ it is defined along the positron momentum). The axes in baryon B_1 and antibaryon $\bar{B}_1$ rest frames (helicity frames) are denoted $(\hat{\mathbf{x}}_1, \hat{\mathbf{y}}_1, \hat{\mathbf{z}}_1)$ and $(\hat{\mathbf{x}}_3, \hat{\mathbf{y}}_3, \hat{\mathbf{z}}_3)$, respectively.

of unpolarized electrons and positrons is [52]:

$$
C_{\mu\bar{\nu}} \propto
\begin{pmatrix}
1 + \alpha_\psi \cos^2\theta_1 & 0 & \beta_\psi \sin\theta_1 \cos\theta_1 & 0 \\
0 & \sin^2\theta_1 & 0 & \gamma_\psi \sin\theta_1 \cos\theta_1 \\
-\beta_\psi \sin\theta_1 \cos\theta_1 & 0 & \alpha_\psi \sin^2\theta_1 & 0 \\
0 & -\gamma_\psi \sin\theta_1 \cos\theta_1 & 0 & -\alpha_\psi - \cos^2\theta_1
\end{pmatrix},
\quad (3.2)
$$

where the parameters β_ψ and γ_ψ are expressed via α_ψ and $\Delta\Phi$ as $\beta_\psi = \sqrt{1 - \alpha_\psi^2}\,\sin(\Delta\Phi)$ and $\gamma_\psi = \sqrt{1 - \alpha_\psi^2}\,\cos(\Delta\Phi)$. We will also use a more general formula from Ref. [47] that describes the annihilation processes with polarized electron beams.

3.3   Invariant form factors

Let us consider a semileptonic decay of a $1/2^+$ hyperon B_1 into a $1/2^+$ baryon B_2 and an off-shell W^--boson decaying to the lepton pair $l^-\bar{\nu}_l$ with the momenta and masses denoted as $B_1(p_1, M_1) \to B_2(p_2, M_2) + l^-(p_l, m_l) + \bar{\nu}_l(p_\nu, 0)$. The matrix elements due to the vector J_μ^V and axial-vector J_μ^A currents in notation from Ref. [158] are:

$$
\langle B_2|J_\mu^V + J_\mu^A|B_1\rangle = \bar{u}(p_2)\left[\gamma_\mu\left(F_1^V(q^2) + F_1^A(q^2)\gamma_5 \right) + \frac{i\sigma_{\mu\nu}q^\nu}{M_1}\left(F_2^V(q^2) + F_2^A(q^2)\gamma_5 \right) \right.
$$
$$
\left. + \frac{q_\mu}{M_1}\left(F_3^V(q^2) + F_3^A(q^2)\gamma_5 \right) \right] u(p_1) ,
$$

$$(3.3)$$

where $q_\mu := (p_1 - p_2)_\mu = (p_l + p_\nu)_\mu$ is the fourmomentum transfer. The fourmomentum squared q^2 ranges from m_l^2 to $(M_1 - M_2)^2$. The form factors $F_{1,2,3}^{V,A}(q^2)$ are complex functions of q^2 that describe hadronic effects in the transition. Neglecting possible CP-odd weak phases, the corresponding form factors are the same for the $(l^-, \bar{\nu}_l)$ and (l^+, ν_l) transitions. To fully determine the hadronic part of a semileptonic decay, the six involved form factors should be extracted as a function of q^2. The form factors are usually parameterized by the axial-vector

to vector g_{av} coupling, the weak-magnetism g_w coupling and the pseudoscalar g_{av3} coupling. They are obtained by normalizing to $F_1^V(0)$:

$$g_{av} = \frac{F_1^A(0)}{F_1^V(0)}, \qquad g_w = \frac{F_2^V(0)}{F_1^V(0)}, \qquad g_{av3} = \frac{F_3^A(0)}{F_1^V(0)}. \tag{3.4}$$

For experiments with a limited number of events, the q^2-dependence of the form factors is assumed using a model. The standard approach is to include one or more poles of the mesons that have the correct quantum numbers to mix with the W boson and have the masses close to the q^2 range in the decay. Traditionally one pole is explicitly included together with an effective contribution from other poles [163] such as in the Becirevic–Kaidalov (BK) [164] parameterization:

$$F_i(q^2) = \frac{F_i(0)}{1 - \frac{q^2}{M^2}} \frac{1}{1 - \alpha_{\mathrm{BK}} \frac{q^2}{M^2}}, \tag{3.5}$$

where the dominant pole mass M is outside the kinematic region and the parameter α_{BK} represent an effective contribution from the meson poles with higher messes. Here the case $\alpha_{\mathrm{BK}} = 0$ represents the dominant pole contribution. This parameterization gives real-valued form factors. If more data is available, one or more extra parameters can be added to describe the q^2 distribution. In the hyperon decays the range of $q^2 \leq (M_1 - M_2)^2$ is limited and in the first order can completely neglect the q^2 dependence using the values of the couplings at the $q^2 = 0$ point. A better approximation is to include an effective-range parameter r_i that represent linear dependence on q^2:

$$F_i(q^2) = F_i(0) \left[1 + r_i q^2 + ... \right]. \tag{3.6}$$

For example, using (3.5) the effective-range parameter is $r_i = (1 + \alpha_{\mathrm{BK}})/M^2$. The main take-away message from the above discussion is that, for practical purposes, the q^2 dependence of an SL form factor can be represented by one or two parameters. In experiments, these parameters can be determined from the observed distributions. The optimal method for such parametric estimation is the maximum likelihood method using multidimensional unbinned data. We will first construct modular formulas for the angular distributions and then in Sec. 3.7 discuss the attainable statistical uncertainties for the SL form factors parameters as the function of the number of observed events.

3.4 Helicity amplitudes

We will describe the $B_1 \rightarrow B_2 + W_{\mathrm{off\text{-}shell}}^-$ process using three coordinate systems attached to the three involved particles. In the baryon B_1 rest frame $\mathbb{R}_1$, with the $(\hat{\mathbf{x}}_1, \hat{\mathbf{y}}_1, \hat{\mathbf{z}}_1)$ Cartesian coordinate system shown in Fig. 3.1, the B_1-spin projection on the quantization axis $\hat{\mathbf{z}}_1$ is $\kappa = \pm 1/2$. The daughter baryon B_2 is emitted in the direction given by the spherical coordinates θ_2, ϕ_2 in $\mathbb{R}_1$ and the B_2-helicity is $\lambda_2 = \pm 1/2$. The off-shell W^- boson is emitted in the direction $\theta_W = \pi - \theta_2$, $\phi_W = \pi + \phi_2$ in the $\mathbb{R}_1$ frame. It has helicity $\underline{\lambda}_W = \{t, -1, 0, +1\}$ where the time component, $\underline{\lambda}_W = t$, corresponds to $J_W = 0$ and the remaining three components

to $J_W = 1$. Therefore, $\underline{\lambda}_W$ uniquely defines both spin J_W and helicity λ_W as $J_W(\underline{\lambda}_W) = \{0, 1, 1, 1\}$ and $\lambda_W(\underline{\lambda}_W) = \{0, -1, 0, 1\}$, respectively. The fourmomentum vector of the off-shell W^- is $q_\mu = (q_0, p \sin\theta_W \cos\phi_W, p \sin\theta_W \sin\phi_W, p \cos\theta_W)$ in the $\mathbb{R}_1$ system. The energy q_0 of the off-shell W^- boson and the magnitude of the three-momentum p are the following functions of the q^2 invariant

$$q_0(q^2) = \frac{1}{2M_1}(M_1^2 - M_2^2 + q^2) \tag{3.7}$$

and

$$p(q^2) = |\mathbf{p}_2| = \frac{1}{2M_1}\sqrt{Q_+ Q_-}, \tag{3.8}$$

where

$$Q_\pm = (M_1 \pm M_2)^2 - q^2. \tag{3.9}$$

The spin direction and subsequent decays of the baryon B_2 and boson $W^-_{\text{off-shell}}$ are described in two helicity systems denoted $\mathbb{R}_2$ and $\mathbb{R}_W$, respectively. The helicity frame $\mathbb{R}_2$ is obtained by performing three active rotations: (a) around the $\hat{\mathbf{z}}_1$–axis by $-\phi_2$; (b) a rotation around the new $\hat{\mathbf{y}}$–axis by $-\theta_2$; (c) a rotation around the $\hat{\mathbf{z}}_2$-axis by $+\chi_2$, see Fig. 3.2 [49]. The first two rotations are sufficient to align $\mathbf{p}_2$ with the z-axis and such two-rotations prescription is used e.g. in Ref. [52]. Here we allow for an additional rotation that can be e.g. used to bring the momenta $\mathbf{p}_2$, $\mathbf{p}_l$ and $\mathbf{p}_\nu$ to one plane. Initially, we consider the angle χ_2 of this rotation as an arbitrary parameter. The combined (a)–(c) three-dimensional rotation is given by the product of three axial rotations $\mathcal{R}(\chi_2, -\theta_2, -\phi_2) = R_z(\chi_2)R_y(-\theta_2)R_z(-\phi_2)$. Subsequently, one then boosts to the B_2 rest frame. The $\mathbb{R}_W$ frame is defined using the same procedure with the rotation matrix $\mathcal{R}(\chi_W, -\theta_W, -\phi_W)$ and the subsequent boost to the $W^-_{\text{off-shell}}$ rest frame. Since the $W^-_{\text{off-shell}}$ direction is opposite to B_2 in $\mathbb{R}_1$, one has $\phi_W = \pi + \phi_2$ and $\theta_W = \pi - \theta_2$. In order to assure that the coordinate systems in $\mathbb{R}_2$ and $\mathbb{R}_W$ are related as $(\hat{\mathbf{x}}_2, \hat{\mathbf{y}}_2, \hat{\mathbf{z}}_2) = (\hat{\mathbf{x}}_W, -\hat{\mathbf{y}}_W, -\hat{\mathbf{z}}_W)$ we set $\chi_W = -\chi_2$.

The matching transition amplitude between B_1 and the two daughter particles expressed using the defined above helicity frames is [49, 52]:

$$\langle \Omega_2, \lambda_2, \underline{\lambda}_W | S | J = 1/2, \kappa \rangle = \sqrt{\frac{2J+1}{8\pi^2}} \langle \lambda_2, \underline{\lambda}_W | S | J = 1/2, \kappa \rangle \mathcal{D}^{1/2*}_{\kappa, \lambda_2 - \lambda_W}(\Omega_2)$$

$$= \frac{1}{2\pi} H_{\lambda_2, \underline{\lambda}_W}(q^2) \mathcal{D}^{1/2*}_{\kappa, \lambda_2 - \lambda_W}(\Omega_2), \tag{3.10}$$

where $\mathcal{D}^J_{m_1, m_2}(\Omega_2) := \mathcal{D}^J_{m_1, m_2}(\phi_2, \theta_2, -\chi_2)$ is the Wigner rotation matrix, where the convention $\mathcal{D}^J_{m_1, m_2}(\phi, \theta, \chi) = e^{-im_1\phi - im_2\chi} \mathcal{D}^J_{m_1, m_2}(0, \theta, 0) = e^{-im_1\phi - im_2\chi} d^J_{m_1, m_2}(\theta)$ is used (see Appendix I). The order and the signs of the angles $\Omega_2 = \{\phi_2, \theta_2, -\chi_2\}$ in the Wigner functions are opposite to the used in the rotations to define the helicity reference frames. In addition, the normalization factor is different since we allow for three independent rotation angles. The helicity amplitudes $H_{\lambda_2, \underline{\lambda}_W}(q^2)$ are functions of q^2 and depend on the helicities of the daughter particles. The vector and axial-vector helicity amplitudes $H_{\lambda_2, \underline{\lambda}_W} = H^V_{\lambda_2, \underline{\lambda}_W} + H^A_{\lambda_2, \underline{\lambda}_W}$ are
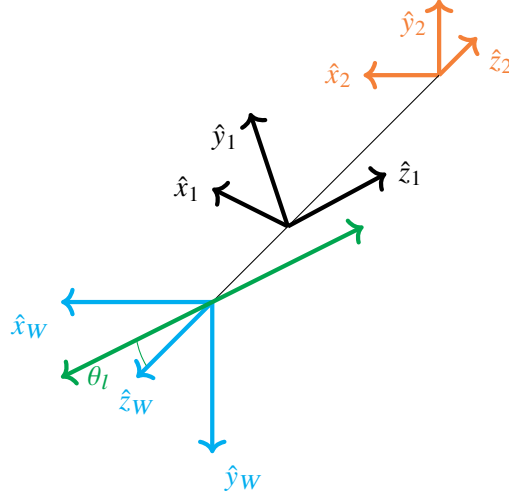
FIGURE 3.2: Definition of the three coordinate systems used to describe the semileptonic decay $B_1 \rightarrow B_2 + W^-_{\text{off-shell}}$. The axes in the B_1, B_2 and $W^-_{\text{off-shell}}$ rest frames (helicity frames: $\mathbb{R}_1$, $\mathbb{R}_2$ and $\mathbb{R}_W$) are denoted $(\hat{\mathbf{x}}_1, \hat{\mathbf{y}}_1, \hat{\mathbf{z}}_1)$, $(\hat{\mathbf{x}}_2, \hat{\mathbf{y}}_2, \hat{\mathbf{z}}_2)$ and $(\hat{\mathbf{x}}_W, \hat{\mathbf{y}}_W, \hat{\mathbf{z}}_W)$, respectively.

related to the invariant form factors in the following way:

$$
\begin{aligned}
H^V_{\frac{1}{2}t} &= \frac{\sqrt{Q_+}}{\sqrt{q^2}}\left[(M_1 - M_2)F^V_1 + \frac{q^2}{M_1}F^V_3\right], \\
H^V_{\frac{1}{2}1} &= \sqrt{2Q_-}\left[-F^V_1 - \frac{M_1 + M_2}{M_1}F^V_2\right], \\
H^V_{\frac{1}{2}0} &= \frac{\sqrt{Q_-}}{\sqrt{q^2}}\left[(M_1 + M_2)F^V_1 + \frac{q^2}{M_1}F^V_2\right], \\
H^A_{\frac{1}{2}t} &= \frac{\sqrt{Q_-}}{\sqrt{q^2}}\left[-(M_1 + M_2)F^A_1 + \frac{q^2}{M_1}F^A_3\right], \\
H^A_{\frac{1}{2}1} &= \sqrt{2Q_+}\left[F^A_1 - \frac{M_1 - M_2}{M_1}F^A_2\right], \\
H^A_{\frac{1}{2}0} &= \frac{\sqrt{Q_+}}{\sqrt{q^2}}\left[-(M_1 - M_2)F^A_1 + \frac{q^2}{M_1}F^A_2\right],
\end{aligned}
\tag{3.11}
$$

where the remaining helicity amplitudes are obtained by applying the parity operator:

$$
H^V_{-\lambda_2,-\lambda_W} = H^V_{\lambda_2,\lambda_W}, \qquad H^A_{-\lambda_2,-\lambda_W} = -H^A_{\lambda_2,\lambda_W}.
\tag{3.12}
$$

The decay $W^- \rightarrow l^- \bar{\nu}_l$ is described in $\mathbb{R}_W$ where the emission angles of the l^- lepton are θ_l and ϕ_l. The value of the lepton momentum in this frame is

$$
|\mathbf{p}_l| = \frac{q^2 - m_l^2}{2q}.
\tag{3.13}
$$

The decay amplitude reads

$$\langle \Omega_l, \lambda_l, \lambda_\nu | S_l | J_W, q^2, \lambda_W \rangle = \sqrt{\frac{2J_W + 1}{4\pi}} (-1)^{J_W} h^l_{\lambda_l \lambda_\nu}(q^2) \mathcal{D}^{J_W*}_{\lambda_W, \lambda_l - \lambda_\nu}(\Omega_l) \,, \qquad (3.14)$$

where $\Omega_l = \{\phi_l, \theta_l, 0\}$. The helicity amplitudes $h^l_{\lambda_l \lambda_\nu}$ for the elementary transition to the final lepton pair can be calculated directly by evaluating the Feynman diagrams. The neutrino helicities are $\lambda_\nu = 1/2$ and $\lambda_\nu = -1/2$ for $(l^-, \bar{\nu}_l)$ and (l^+, ν_l), respectively. The moduli squared of $h^l_{\lambda_l \lambda_\nu}$ are [158]:

$$\text{nonflip}(\underline{\lambda}_W = \mp 1) : \; |h^l_{\lambda_l = \mp \frac{1}{2}, \lambda_\nu = \pm \frac{1}{2}}|^2 = 8\delta(\lambda_l + \lambda_\nu)(q^2 - m_l^2), \qquad (3.15)$$

$$\text{flip}(\underline{\lambda}_W = 0, t) : \; |h^l_{\lambda_l = \pm \frac{1}{2}, \lambda_\nu = \pm \frac{1}{2}}|^2 = 8\delta(\lambda_l - \lambda_\nu)\frac{m_l^2}{2q^2}(q^2 - m_l^2), \qquad (3.16)$$

where here and in the following the upper and lower signs refer to the configurations $(l^-, \bar{\nu}_l)$ and (l^+, ν_l), respectively.

The representations in Eqs. (3.10) and (3.14) imply that the complete amplitude for the $B_1(\kappa) \to B_2(\lambda_2)$ transition reads:

$$\sum_{\underline{\lambda}_W} \langle \Omega_l, \lambda_l, \lambda_\nu | S_l | q^2, \underline{\lambda}_W \rangle \langle \Omega_2, \lambda_2, \underline{\lambda}_W | S | 1/2, \kappa \rangle \,, \qquad (3.17)$$

where the $\underline{\lambda}_W$ sum runs over the four W-boson helicity components $\{t, -1, 0, +1\}$. An explicit representation of the amplitude with the angular part separated is

$$\sum_{\underline{\lambda}_W} (-1)^{J_W} h^l_{\lambda_l \lambda_\nu} \mathcal{D}^{J_W*}_{\lambda_W, \lambda_l - \lambda_\nu}(\Omega_l) H_{\lambda_2, \underline{\lambda}_W} \mathcal{D}^{1/2*}_{\kappa, \lambda_2 - \lambda_W}(\Omega_2) =$$

$$\sum_{\underline{\lambda}_W} (-1)^{J_W} h^l_{\lambda_l \lambda_\nu} d^{J_W}_{\lambda_W, \lambda_l - \lambda_\nu}(\theta_l) H_{\lambda_2, \underline{\lambda}_W} d^{1/2}_{\kappa, \lambda_2 - \lambda_W}(\theta_2) \exp\left[i\kappa\phi_2 + i\lambda_2\chi_2 - i\lambda_W(\chi_2 - \phi_l)\right] ,$$

$$(3.18)$$

where the final expression combines all azimuthal-angle rotations in one term. One can consider two options for selecting χ_2 to define the transversal orientation of the $\mathbb{R}_2$ and $\mathbb{R}_W$ helicity frames. The first option is to set $\chi_2 = 0$ as in Ref. [52] where the corresponding azimuthal angle of the charged lepton in the $\mathbb{R}_W$ system is ϕ_l^0. An alternative is to select $\chi_2^{3\text{-b}}$ so that $\hat{x}_2$ is in the decay plane of the semileptonic decay. In this case the momenta of the leptons are in this plane which corresponds to $\phi_l^{3\text{-b}} = 0$ and the $\chi_2^{3\text{-b}} = \phi_l^0$ relation holds.

The amplitude can be rearranged by inserting a complete spin basis for the baryon B_2 to represent transition between $B_1(\kappa)$ and $B_2(\lambda_2)$:

$$\sum_{\lambda'=-1/2}^{1/2} \sum_{\underline{\lambda}_W} \langle \Omega_l, \lambda_l, \lambda_\nu | S_l | q^2, \underline{\lambda}_W \rangle \langle \lambda_2, \underline{\lambda}_W | \lambda' \rangle \langle \Omega_2, \lambda' | S | 1/2, \kappa \rangle \tag{3.19}$$

$$= \frac{1}{2\pi} \sum_{\lambda'=-1/2}^{1/2} \mathcal{D}_{\kappa,\lambda'}^{1/2*}(\Omega_2) \left\{ \sum_{\underline{\lambda}_W} \langle \Omega_l, \lambda_l, \lambda_\nu | S_l | q^2, \underline{\lambda}_W \rangle \langle \lambda_2, \underline{\lambda}_W | \lambda' \rangle H_{\lambda_2, \underline{\lambda}_W}(q^2) \right\} \tag{3.20}$$

$$= \frac{1}{2\pi} \sum_{\lambda'=-1/2}^{1/2} \mathcal{D}_{\kappa,\lambda'}^{1/2*}(\Omega_2) \mathcal{H}_{\lambda', \lambda_2}(\Omega_l, q^2, \lambda_l, \lambda_\nu) . \tag{3.21}$$

Therefore the angular dependence on Ω_2 can be separated in the amplitude of the complete process. Since usually experiments do not measure polarization of the leptons, it is useful to consider a tensor that describes the $W^\pm$-boson decay with the lepton helicities summed over:

$$L_{\underline{\lambda}_W, \underline{\lambda}'_W}(q^2, \Omega_l) := \sum_{\lambda_l=-1/2}^{1/2} \langle \Omega_l, \lambda_l, \lambda_\nu | S_l |, q^2, \underline{\lambda}'_W \rangle^* \langle \Omega_l, \lambda_l, \lambda_\nu | S_l | q^2, \underline{\lambda}_W \rangle \tag{3.22}$$

$$= \frac{3}{4\pi} \sum_{\lambda_l=-1/2}^{1/2} |h_{\lambda_l \lambda_\nu}^l(q^2)|^2 (-1)^{J_W + J'_W} \mathcal{D}_{\lambda_W, \lambda_l - \lambda_\nu}^{J_W*}(\Omega_l) \mathcal{D}_{\lambda'_W, \lambda_l - \lambda_\nu}^{J'_W}(\Omega_l) \tag{3.23}$$

$$= \frac{3}{4\pi} e^{i(\lambda_W - \lambda'_W)\phi_l} \sum_{\lambda_l=-1/2}^{1/2} |h_{\lambda_l \lambda_\nu}^l(q^2)|^2 (-1)^{J_W + J'_W} d_{\lambda_W, \lambda_l - \lambda_\nu}^{J_W}(\theta_l) d_{\lambda'_W, \lambda_l - \lambda_\nu}^{J'_W}(\theta_l) . \tag{3.24}$$

The interference contribution from $\underline{\lambda}_W = t$ and $\underline{\lambda}_W = 0$ gives an extra minus sign. We write the tensor as:

$$L_{\underline{\lambda}_W, \underline{\lambda}'_W}(q^2, \Omega_l) = \frac{6}{\pi}(q^2 - m_l^2) \left[\ell_{\underline{\lambda}_W, \underline{\lambda}'_W}^{\mathrm{nf}}(\Omega_l) + \varepsilon \ell_{\underline{\lambda}_W, \underline{\lambda}'_W}^{\mathrm{f}}(\Omega_l) \right] , \tag{3.25}$$

where $\varepsilon = m_l^2/(2q^2)$. The hermitian matrix for the nonflip transition reads

$$\ell_{\underline{\lambda}_W, \underline{\lambda}'_W}^{\mathrm{nf}}(\Omega_l) = \begin{pmatrix} 0 & 0 & 0 & 0 \\ 0 & \frac{(1\pm\cos\theta_l)^2}{4} & \mp\frac{e^{-i\phi_l}\sin\theta_l(1\pm\cos\theta_l)}{2\sqrt{2}} & \frac{1}{4}e^{-2i\phi_l}\sin^2\theta_l \\ 0 & \mp\frac{e^{i\phi_l}\sin\theta_l(1\pm\cos\theta_l)}{2\sqrt{2}} & \frac{1}{2}\sin^2\theta_l & \mp\frac{e^{-i\phi_l}\sin\theta_l(1\mp\cos\theta_l)}{2\sqrt{2}} \\ 0 & \frac{1}{4}e^{2i\phi_l}\sin^2\theta_l & \mp\frac{e^{i\phi_l}\sin\theta_l(1\mp\cos\theta_l)}{2\sqrt{2}} & \frac{(1\mp\cos\theta_l)^2}{4} \end{pmatrix} , \tag{3.26}$$

while for the flip transition

$$
\ell^{\mathrm{f}}_{\underline{\lambda}_W,\underline{\lambda}'_W}(\Omega_l) = \begin{pmatrix} 1 & -\dfrac{e^{i\phi_l}\sin\theta_l}{\sqrt{2}} & -\cos\theta_l & \dfrac{e^{-i\phi_l}\sin\theta_l}{\sqrt{2}} \\ -\dfrac{e^{-i\phi_l}\sin\theta_l}{\sqrt{2}} & \dfrac{\sin^2\theta_l}{2} & \dfrac{e^{-i\phi_l}\sin\theta_l\cos\theta_l}{\sqrt{2}} & -\dfrac{1}{2}e^{-2i\phi_l}\sin^2\theta_l \\ -\cos\theta_l & \dfrac{e^{i\phi_l}\sin\theta_l\cos\theta_l}{\sqrt{2}} & \cos^2\theta_l & -\dfrac{e^{-i\phi_l}\sin\theta_l\cos\theta_l}{\sqrt{2}} \\ \dfrac{e^{i\phi_l}\sin\theta_l}{\sqrt{2}} & -\dfrac{1}{2}e^{2i\phi_l}\sin^2\theta_l & -\dfrac{e^{i\phi_l}\sin\theta_l\cos\theta_l}{\sqrt{2}} & \dfrac{1}{2}\sin^2\theta_l \end{pmatrix}.
$$

$$(3.27)$$

3.5 Decay matrix

Here, we derive a matrix that relates the spin of the baryon B_2 to the spin of the baryon B_1 in $B_1 \to B_2\ell\nu_\ell$ where the state of the lepton pair with the summed spin projections is given by the $L_{\underline{\lambda}_W,\underline{\lambda}'_W}(q^2,\Omega_l)$ tensor in Eq. (3.23). The transition can be represented by a tensor $T^{\kappa\kappa',\lambda_2\lambda'_2}$ that describes how the initial spin-density matrix $\rho_1^{\kappa\kappa'}$ of the baryon B_1 transforms to the density matrix $\rho_2^{\lambda_2\lambda'_2}$ of the baryon B_2:

$$
\rho_2^{\lambda_2\lambda'_2} = T^{\kappa\kappa',\lambda_2\lambda'_2}\rho_1^{\kappa\kappa'} \ . \tag{3.28}
$$

Using Eq. (3.10) the transition tensor is given as

$$
T^{\kappa\kappa',\lambda_2\lambda'_2} = \frac{1}{4\pi^2}\sum_{\underline{\lambda}_W,\underline{\lambda}'_W} H_{\lambda_2\underline{\lambda}_W}H^*_{\lambda'_2\underline{\lambda}'_W}\mathcal{D}^{1/2*}_{\kappa,\lambda_2-\lambda_W}(\Omega_2)\mathcal{D}^{1/2}_{\kappa',\lambda'_2-\lambda'_W}(\Omega_2)L_{\lambda_W,\lambda'_W}(q^2,\Omega_l) \tag{3.29}
$$

$$
\equiv \frac{1}{4\pi^2}\sum_{\underline{\lambda}_W,\underline{\lambda}'_W} T^{\kappa\kappa',\lambda_2\lambda'_2}_{\underline{\lambda}_W,\underline{\lambda}'_W}(q^2,\Omega_2)L_{\underline{\lambda}_W,\underline{\lambda}'_W}(q^2,\Omega_l) \ . \tag{3.30}
$$

The explicit expression for the phases of the hadronic tensor due to the azimuthal rotations is

$$
\begin{aligned}
T^{\kappa\kappa',\lambda_2\lambda'_2}_{\underline{\lambda}_W,\underline{\lambda}'_W}(q^2,\Omega_2) = {}& H_{\lambda_2\underline{\lambda}_W}H^*_{\lambda'_2\underline{\lambda}'_W}d^{1/2}_{\kappa,\lambda_2-\lambda_W}(\theta_2)d^{1/2}_{\kappa',\lambda'_2-\lambda'_W}(\theta_2) \\
& \times \exp\left[i\kappa\phi_2 + i\lambda_2\chi_2 - i\lambda_W\chi_2\right] \\
& \times \exp\left[-i\kappa'\phi_2 - i\lambda'_2\chi_2 + i\lambda'_W\chi_2\right] \ ,
\end{aligned} \tag{3.31}
$$

where we use the generic case with $\Omega_2 = \{\phi_2,\theta_2,\chi_2\}$ and $\Omega_l = \{\phi_l,\theta_l,0\}$. The overall phases of the contraction of the above hadronic tensor and the leptonic tensor in Eq. (3.24) for the two choices of the orientations of the coordinate systems $\mathbb{R}_2$ and $\mathbb{R}_W$ are:

$$
(\chi_2 = 0) \to \exp\left[i(\kappa - \kappa')\phi_2 + i(\lambda_W - \lambda'_W)\phi_l^0\right], \tag{3.32}
$$

$$
(\phi_l^{\text{3-b}} = 0) \to \exp\left[i(\kappa - \kappa')\phi_2 + i(\lambda_2 - \lambda'_2)\chi_2^{\text{3-b}}\right] \tag{3.33}
$$

$$
= \exp\left[i(\kappa - \kappa')\phi_2 + i(\lambda_2 - \lambda'_2)\phi_l^0\right] \ . \tag{3.34}
$$

The two representations are not equivalent but can be written in terms of the tensors evaluated for $\Omega_2^0 := \{\phi_2,\theta_2,0\}$ and $\Omega_l^0 = \{0,\theta_l,0\}$ as

$$T^{\kappa\kappa',\lambda_2\lambda_2'}(\chi_2 = 0) = \frac{1}{4\pi^2} \sum_{\underline{\lambda}_W,\underline{\lambda}_W'} \exp\left[i(\lambda_W - \lambda_W')\phi_l^0\right] T_{\underline{\lambda}_W,\underline{\lambda}_W'}^{\kappa\kappa',\lambda_2\lambda_2'}(\Omega_2^0) L_{\underline{\lambda}_W,\underline{\lambda}_W'}(\Omega_l^0), \quad (3.35)$$

$$T^{\kappa\kappa',\lambda_2\lambda_2'}(\phi_l^{3\text{-b}} = 0) = \frac{1}{4\pi^2} \exp\left[i(\lambda_2 - \lambda_2')\phi_l^0\right] \sum_{\underline{\lambda}_W,\underline{\lambda}_W'} T_{\underline{\lambda}_W,\underline{\lambda}_W'}^{\kappa\kappa',\lambda_2\lambda_2'}(\Omega_2^0) L_{\underline{\lambda}_W,\underline{\lambda}_W'}(\Omega_l^0) . \quad (3.36)$$

Instead of the helicities, the transition can be written as in Ref. [52] using spin base vectors $\sigma_\mu^{B_1}$ and $\sigma_\nu^{B_2}$ in the mother and daughter reference systems $\mathbb{R}_1$ and $\mathbb{R}_2$, respectively. The 4×4 matrix $\mathcal{B}_{\mu\nu}$ describes how the decay process transforms the base Pauli matrices:

$$\sigma_\mu^{B_1} \rightarrow \frac{3(q^2 - m_l^2)}{4\pi^3} \sum_{\nu=0}^{3} \mathcal{B}_{\mu\nu}\sigma_\nu^{B_2} . \quad (3.37)$$

The real coefficients $\mathcal{B}_{\mu\nu}$ can be obtained by inserting Pauli σ_μ matrices for the mother and the daughter baryons in the expression for the tensor $T^{\kappa\kappa',\lambda_2\lambda_2'}$:

$$\mathcal{B}_{\mu\nu} := \frac{2\pi^3}{3(q^2 - m_l^2)} \sum_{\lambda_2,\lambda_2'=-1/2}^{1/2} \sum_{\kappa,\kappa'=-1/2}^{1/2} T^{\kappa\kappa',\lambda_2\lambda_2'}\sigma_\mu^{\kappa,\kappa'}\sigma_\nu^{\lambda_2',\lambda_2} . \quad (3.38)$$

However, as we show in Appendix II the coefficients can be represented as

$$\mathcal{B}_{\mu\nu} = \sum_{\kappa=0}^{3} \mathcal{R}_{\mu\kappa}^{(4)}(\Omega_2)b_{\kappa\nu}(q^2,\Omega_l) , \quad (3.39)$$

where $\mathcal{R}_{\mu\kappa}^{(4)}(\Omega_2)$ is the 4×4 space-like rotation matrix obtained as the direct sum of identity and 3D rotation $\mathcal{R}(\Omega_2)$: $\mathcal{R}^{(4)}(\Omega_2) = \text{diag}(1, \mathcal{R}(\Omega_2))$. The argument $\Omega_2 = \{\phi_2, \theta_2, -\chi_2\}$ assures that the rotation is the inverse of the rotation $\mathcal{R}(\{\chi_2, -\theta_2, -\phi_2\})$ that was used to define the helicity frame $\mathbb{R}_2$. The coefficients $b_{\mu\nu}$ correspond to the $B_1 \rightarrow B_2$ transition where the orientations of the axes of the reference systems are aligned $\Omega_2 = \{0, 0, 0\}$. They can be obtained by inserting Pauli σ_μ matrices for the mother and the daughter baryons in the expression for the tensor $T^{\kappa\kappa',\lambda_2\lambda_2'}$ with Ω_2 set to $\{0, 0, 0\}$ what implies replacement $\mathcal{D}_{m_1,m_2}^{1/2}(\{0, 0, 0\}) = \delta(m_1 - m_2)$:

$$b_{\mu\nu} := \frac{\pi}{6(q^2 - m_l^2)} \sum_{\underline{\lambda}_W,\underline{\lambda}_W'} \sum_{\lambda_2,\lambda_2'=-1/2}^{1/2} H_{\lambda_2\underline{\lambda}_W} H_{\lambda_2'\underline{\lambda}_W'}^* \underbrace{\sigma_\mu^{\lambda_2-\lambda_W,\lambda_2'-\lambda_W'}\sigma_\nu^{\lambda_2',\lambda_2} L_{\underline{\lambda}_W,\underline{\lambda}_W'}(q^2,\Omega_l)}_{\mathcal{T}_{\mu\nu}^{\underline{\lambda}_W,\underline{\lambda}_W',\lambda_2,\lambda_2'}} ,$$

$$(3.40)$$

$$b_{\mu\nu} = \sum_{\underline{\lambda}_W, \underline{\lambda}'_W} \sum_{\lambda_2, \lambda'_2 = -1/2}^{1/2} H_{\lambda_2 \underline{\lambda}_W} H^*_{\lambda'_2 \underline{\lambda}'_W} \mathcal{T}_{\mu\nu}^{\underline{\lambda}_W, \underline{\lambda}'_W, \lambda_2, \lambda'_2}$$

$$= \sum_{\underline{\lambda}_W} \sum_{\lambda_2 = -1/2}^{1/2} \left\{ |H_{\lambda_2 \underline{\lambda}_W}|^2 \, \mathcal{T}_{\mu\nu}^{\underline{\lambda}_W, \underline{\lambda}_W, \lambda_2, \lambda_2} \right.$$

$$\left. + 2 \sum_{\underline{\lambda}'_W < \underline{\lambda}_W} \sum_{\lambda'_2 < \lambda_2} \left[\Re(H_{\lambda_2 \underline{\lambda}_W} H^*_{\lambda'_2 \underline{\lambda}'_W}) \Re\mathcal{T}_{\mu\nu}^{\underline{\lambda}_W, \underline{\lambda}'_W, \lambda_2, \lambda'_2} + \Im(H_{\lambda_2 \underline{\lambda}_W} H^*_{\lambda'_2 \underline{\lambda}'_W}) \Im\mathcal{T}_{\mu\nu}^{\underline{\lambda}_W, \underline{\lambda}'_W, \lambda_2, \lambda'_2} \right] \right\}. \tag{3.41}$$

The last form involves only real valued tensors $\mathcal{T}_{\mu\nu}^{\underline{\lambda}_W, \underline{\lambda}_W, \lambda_2, \lambda_2}$, $\Re\mathcal{T}_{\mu\nu}^{\underline{\lambda}_W, \underline{\lambda}'_W, \lambda_2, \lambda'_2}$ and $\Im\mathcal{T}_{\mu\nu}^{\underline{\lambda}_W, \underline{\lambda}'_W, \lambda_2, \lambda'_2}$. The hadronic part is encoded in the real-valued functions of q^2: $|H_{\lambda_2 \underline{\lambda}_W}|^2$, $\Re(H_{\lambda_2 \underline{\lambda}_W} H^*_{\lambda'_2 \underline{\lambda}'_W})$ and $\Im(H_{\lambda_2 \underline{\lambda}_W} H^*_{\lambda'_2 \underline{\lambda}'_W})$, where $\underline{\lambda}'_W < \underline{\lambda}_W$ and $\lambda'_2 < \lambda_2$. Moreover, the form factors $H_{-\frac{1}{2}1} = H_{\frac{1}{2}-1} = 0$ reducing number of the functions.

We will represent the $b_{\mu\nu}$ matrix as the sum of the non-flip and flip contributions $b_{\mu\nu} = b_{\mu\nu}^{\mathrm{nf}} + \varepsilon b_{\mu\nu}^{\mathrm{f}}$. The cross-section term is written as $b_{00} = b_{00}^{\mathrm{nf}} + \varepsilon b_{00}^{\mathrm{f}}$ where

$$b_{00}^{\mathrm{nf}} = \frac{1}{4}(1 \mp \cos\theta_l)^2 |H_{\frac{1}{2}1}|^2 + \frac{1}{4}(1 \pm \cos\theta_l)^2 |H_{-\frac{1}{2}-1}|^2 + \frac{1}{2}\sin^2\theta_l(|H_{-\frac{1}{2}0}|^2 + |H_{\frac{1}{2}0}|^2), \tag{3.42}$$

$$b_{00}^{\mathrm{f}} = |H_{\frac{1}{2}t}|^2 + |H_{-\frac{1}{2}t}|^2 + \frac{1}{2}\sin^2\theta_l(|H_{\frac{1}{2}1}|^2 + |H_{-\frac{1}{2}-1}|^2) + \cos^2\theta_l(|H_{\frac{1}{2}0}|^2 + |H_{-\frac{1}{2}0}|^2) \tag{3.43}$$
$$- 2\cos\theta_l \Re(H^*_{\frac{1}{2}0} H_{\frac{1}{2}t} + H^*_{-\frac{1}{2}0} H_{-\frac{1}{2}t}),$$

define the angular distributions for the decay of unpolarized baryon B_1 when the spins of all final particles are summed over. The differential decay rate is obtained by multiplying by the kinematic and spinor normalization factors that depend on q^2

$$d\Gamma = \frac{G_F^2}{(2\pi)^5} |V_{us}|^2 \frac{|\mathbf{p}_l||\mathbf{p}_2|}{16 M_1^2} (q^2 - m_l^2) b_{00} dq d\Omega_2 d\Omega_l \tag{3.44}$$

$$= G_F^2 |V_{us}|^2 V_{Ph}(q^2)(q^2 - m_l^2) b_{00} dq d\Omega_2 d\Omega_l, \tag{3.45}$$

where $V_{Ph}(q^2) = (2\pi)^{-5}(4M_1)^{-2}|\mathbf{p}_l||\mathbf{p}_2|$ is the three-body phase space density factor [160]. The momenta $|\mathbf{p}_2|$ and $|\mathbf{p}_l|$ of the baryon B_2 and the lepton are given in Eqs. (3.8) and (3.13), respectively.

The first row of the b_{0i} matrix, where $i = 1, 2, 3$ (x, y, z), gives the polarization vector $\mathbf{P} = (P_x, P_y, P_z)$ of the baryon B_2 in the reference frame $\mathbb{R}_2$ corresponding to the decay of unpolarized baryon B_1. These elements are:

$$b_{01} = -\Re(\mathcal{I}_{01})\cos\phi_l + \Im(\mathcal{I}_{01})\sin\phi_l = P_x b_{00},$$
$$b_{02} = \Re(\mathcal{I}_{01})\sin\phi_l + \Im(\mathcal{I}_{01})\cos\phi_l = P_y b_{00}, \tag{3.46}$$
$$b_{03} = b_{03}^{\mathrm{nf}} + \varepsilon b_{03}^{\mathrm{f}} = P_z b_{00},$$

where $\mathcal{I}_{\mu\nu}$ are complex. We use notation $\mathcal{I}_{\mu\nu} = \mathcal{I}_{\mu\nu}^{\mathrm{nf}} + \varepsilon \mathcal{I}_{\mu\nu}^{\mathrm{f}}$ and

$$
\begin{aligned}
\mathcal{I}_{01}^{\mathrm{nf}} &= \pm \frac{1}{\sqrt{2}} \sin \theta_l \left[(1 \pm \cos \theta_l) H^*_{-\frac{1}{2}-1} H_{\frac{1}{2}0} + (1 \mp \cos \theta_l) H^*_{-\frac{1}{2}0} H_{\frac{1}{2}1} \right] , \\
\mathcal{I}_{01}^{\mathrm{f}} &= \sqrt{2} \sin \theta_l \left[(H^*_{-\frac{1}{2}-1} H_{\frac{1}{2}t} - H^*_{-\frac{1}{2}t} H_{\frac{1}{2}1}) + \cos \theta_l (H^*_{-\frac{1}{2}0} H_{\frac{1}{2}1} - H^*_{-\frac{1}{2}-1} H_{\frac{1}{2}0}) \right] , \\
b_{03}^{\mathrm{nf}} &= \frac{1}{4}(1 \mp \cos \theta_l)^2 |H_{\frac{1}{2}1}|^2 - \frac{1}{4}(1 \pm \cos \theta_l)^2 |H_{-\frac{1}{2}-1}|^2 - \frac{1}{2} \sin^2 \theta_l (|H_{-\frac{1}{2}0}|^2 - |H_{\frac{1}{2}0}|^2), \\
b_{03}^{\mathrm{f}} &= |H_{\frac{1}{2}t}|^2 - |H_{-\frac{1}{2}t}|^2 + \frac{1}{2} \sin^2 \theta_l (|H_{\frac{1}{2}1}|^2 - |H_{-\frac{1}{2}-1}|^2) - \cos^2 \theta_l (|H_{-\frac{1}{2}0}|^2 - |H_{\frac{1}{2}0}|^2) \\
&\quad - 2 \cos \theta_l \Re (H^*_{\frac{1}{2}0} H_{\frac{1}{2}t} - H^*_{-\frac{1}{2}0} H_{-\frac{1}{2}t}) .
\end{aligned}
\tag{3.47}
$$

The first column b_{i0} of the matrix corresponds to the decay of the spin polarized baryon B_1. The element $b_{30} = b_{30}^{\mathrm{nf}} + \varepsilon b_{30}^{\mathrm{f}}$ is:

$$
\begin{aligned}
b_{30}^{\mathrm{nf}} &= \frac{1}{4}(1 \pm \cos \theta_l)^2 |H_{-\frac{1}{2}-1}|^2 - \frac{1}{4}(1 \mp \cos \theta_l)^2 |H_{\frac{1}{2}1}|^2 - \frac{1}{2} \sin^2 \theta_l (|H_{-\frac{1}{2}0}|^2 - |H_{\frac{1}{2}0}|^2) , \\
b_{30}^{\mathrm{f}} &= |H_{\frac{1}{2}t}|^2 - |H_{-\frac{1}{2}t}|^2 - \frac{1}{2} \sin^2 \theta_l (|H_{\frac{1}{2}1}|^2 - |H_{-\frac{1}{2}-1}|^2) - \cos^2 \theta_l (|H_{-\frac{1}{2}0}|^2 - |H_{\frac{1}{2}0}|^2) \\
&\quad - 2 \cos \theta_l \Re (H^*_{\frac{1}{2}0} H_{\frac{1}{2}t} - H^*_{-\frac{1}{2}0} H_{-\frac{1}{2}t}) .
\end{aligned}
\tag{3.48}
$$

The elements b_{10} and b_{20} are

$$
\begin{aligned}
b_{10} &= -\cos \phi_l \Re(\mathcal{I}_{10}) + \sin \phi_l \Im(\mathcal{I}_{10}) , \\
b_{20} &= \sin \phi_l \Re(\mathcal{I}_{10}) + \cos \phi_l \Im(\mathcal{I}_{10}) ,
\end{aligned}
\tag{3.49}
$$

where

$$
\begin{aligned}
\mathcal{I}_{10}^{\mathrm{nf}} &= \pm \frac{1}{\sqrt{2}} \sin \theta_l \left[(1 \pm \cos \theta_l) H^*_{-\frac{1}{2}-1} H_{-\frac{1}{2}0} + (1 \mp \cos \theta_l) H^*_{\frac{1}{2}0} H_{\frac{1}{2}1} \right] , \\
\mathcal{I}_{10}^{\mathrm{f}} &= \sqrt{2} \sin \theta_l \left[(H^*_{-\frac{1}{2}-1} H_{-\frac{1}{2}t} - H^*_{\frac{1}{2}t} H_{\frac{1}{2}1}) + \cos \theta_l (H^*_{\frac{1}{2}0} H_{\frac{1}{2}1} - H^*_{-\frac{1}{2}-1} H_{-\frac{1}{2}0}) \right] .
\end{aligned}
\tag{3.50}
$$

The decay plane representation which requires three rotation angles for baryon B_2 gives simple formulas for the remaining terms of the decay matrix. The terms of the non-flip contributions for the aligned (with $\phi_l = 0$) decay matrix $b_{\mu\nu}^{\mathrm{nf}}$ are:

$$
b_{\mu\nu}^{\mathrm{nf}} = \begin{pmatrix}
b_{00}^{\mathrm{nf}} & -\Re(\mathcal{I}_{01}^{\mathrm{nf}}) & \Im(\mathcal{I}_{10}^{\mathrm{nf}}) & b_{03}^{\mathrm{nf}} \\
-\Re(\mathcal{I}_{10}^{\mathrm{nf}}) & \Re(\mathcal{E}_{00}^{\mathrm{nf}} + \mathcal{E}_{11}^{\mathrm{nf}}) & -\Im(\mathcal{E}_{00}^{\mathrm{nf}} + \mathcal{E}_{11}^{\mathrm{nf}}) & \Re(\mathcal{I}_{13}^{\mathrm{nf}}) \\
\Im(\mathcal{I}_{10}^{\mathrm{nf}}) & \Im(\mathcal{E}_{00}^{\mathrm{nf}} - \mathcal{E}_{11}^{\mathrm{nf}}) & \Re(\mathcal{E}_{00}^{\mathrm{nf}} - \mathcal{E}_{11}^{\mathrm{nf}}) & -\Im(\mathcal{I}_{13}^{\mathrm{nf}}) \\
b_{30}^{\mathrm{nf}} & -\Re(\mathcal{I}_{31}^{\mathrm{nf}}) & \Im(\mathcal{I}_{31}^{\mathrm{nf}}) & b_{33}^{\mathrm{nf}}
\end{pmatrix} ,
\tag{3.51}
$$

where

$$
b_{33}^{\mathrm{nf}} = \frac{1}{2} \sin^2 \theta_l (|H_{-\frac{1}{2}0}|^2 + |H_{\frac{1}{2}0}|^2) - \frac{1}{4}(1 \mp \cos \theta_l)^2 |H_{\frac{1}{2}1}|^2 - \frac{1}{4}(1 \pm \cos \theta_l)^2 |H_{-\frac{1}{2}-1}|^2
\tag{3.52}
$$

and

$$\mathcal{I}_{13}^{\mathrm{nf}} = \pm\frac{1}{\sqrt{2}}\sin\theta_l\left\{(1\pm\cos\theta_l)H^*_{-\frac{1}{2}-1}H_{-\frac{1}{2}0} - (1\mp\cos\theta_l)H^*_{\frac{1}{2}0}H_{\frac{1}{2}1}\right\},$$

$$\mathcal{I}_{31}^{\mathrm{nf}} = \pm\frac{1}{\sqrt{2}}\sin\theta_l\left\{(1\pm\cos\theta_l)H^*_{-\frac{1}{2}-1}H_{\frac{1}{2}0} - (1\mp\cos\theta_l)H^*_{-\frac{1}{2}0}H_{\frac{1}{2}1}\right\},$$

$$\mathcal{E}_{00}^{\mathrm{nf}} = \sin^2\theta_l H^*_{-\frac{1}{2}0}H_{\frac{1}{2}0},$$

$$\mathcal{E}_{11}^{\mathrm{nf}} = \frac{1}{2}\sin^2\theta_l H^*_{-\frac{1}{2}-1}H_{\frac{1}{2}1}. \tag{3.53}$$

The terms of the flip contributions for the aligned decay matrix $b_{\mu\nu}^{\mathrm{f}}$ are:

$$b_{\mu\nu}^{\mathrm{f}} = \begin{pmatrix} b_{00}^{\mathrm{f}} & -\mathfrak{R}(\mathcal{I}_{01}^{\mathrm{f}}) & \mathfrak{I}(\mathcal{I}_{10}^{\mathrm{f}}) & b_{03}^{\mathrm{f}} \\ -\mathfrak{R}(\mathcal{I}_{10}^{\mathrm{f}}) & \mathfrak{R}(\mathcal{E}_{00}^{\mathrm{f}} - \mathcal{E}_{11}^{\mathrm{f}}) & -\mathfrak{I}(\mathcal{E}_{00}^{\mathrm{f}} - \mathcal{E}_{11}^{\mathrm{f}}) & \mathfrak{R}(\mathcal{I}_{13}^{\mathrm{f}}) \\ \mathfrak{I}(\mathcal{I}_{10}^{\mathrm{f}}) & \mathfrak{I}(\mathcal{E}_{00}^{\mathrm{f}} + \mathcal{E}_{11}^{\mathrm{f}}) & \mathfrak{R}(\mathcal{E}_{00}^{\mathrm{f}} + \mathcal{E}_{11}^{\mathrm{f}}) & -\mathfrak{I}(\mathcal{I}_{13}^{\mathrm{f}}) \\ b_{30}^{\mathrm{f}} & -\mathfrak{R}(\mathcal{I}_{31}^{\mathrm{f}}) & \mathfrak{I}(\mathcal{I}_{31}^{\mathrm{f}}) & b_{33}^{\mathrm{f}} \end{pmatrix}, \tag{3.54}$$

where

$$b_{33}^{\mathrm{f}} = |H_{-\frac{1}{2}t}|^2 + |H_{\frac{1}{2}t}|^2 + \cos^2\theta_l(|H_{-\frac{1}{2}0}|^2 + |H_{\frac{1}{2}0}|^2) - \frac{1}{2}\sin^2\theta_l(|H_{\frac{1}{2}1}|^2 + |H_{-\frac{1}{2}-1}|^2)$$

$$- 2\cos\theta_l\mathfrak{R}(H^*_{\frac{1}{2}0}H_{\frac{1}{2}t} + H^*_{-\frac{1}{2}0}H_{-\frac{1}{2}t}) \tag{3.55}$$

and

$$\mathcal{I}_{13}^{\mathrm{f}} = \sqrt{2}\sin\theta_l\left\{H^*_{-\frac{1}{2}-1}H_{-\frac{1}{2}t} + H^*_{\frac{1}{2}1}H_{\frac{1}{2}t} - \cos\theta_l(H^*_{\frac{1}{2}0}H_{\frac{1}{2}1} + H^*_{-\frac{1}{2}-1}H_{-\frac{1}{2}0})\right\},$$

$$\mathcal{I}_{31}^{\mathrm{f}} = \sqrt{2}\sin\theta_l\left\{H^*_{-\frac{1}{2}-1}H_{\frac{1}{2}t} + H^*_{-\frac{1}{2}t}H_{\frac{1}{2}1} - \cos\theta_l(H^*_{-\frac{1}{2}0}H_{\frac{1}{2}1} + H^*_{-\frac{1}{2}-1}H_{\frac{1}{2}0})\right\},$$

$$\mathcal{E}_{00}^{\mathrm{f}} = 2\left\{H^*_{-\frac{1}{2}t}H_{\frac{1}{2}t} + \cos^2\theta_l H^*_{-\frac{1}{2}0}H_{\frac{1}{2}0} - \cos\theta_l(H^*_{-\frac{1}{2}0}H_{\frac{1}{2}t} + H^*_{-\frac{1}{2}t}H_{\frac{1}{2}0})\right\},$$

$$\mathcal{E}_{11}^{\mathrm{f}} = \sin^2\theta_l H^*_{-\frac{1}{2}-1}H_{\frac{1}{2}1}. \tag{3.56}$$

If the form factors have no complex phases, meaning the $\mathcal{I}_{\mu\nu}$ terms are real functions, the decay matrix reads as

$$b_{\mu\nu} = \begin{pmatrix} b_{00} & -\mathcal{I}_{01} & 0 & \mathcal{I}_{03} \\ -\mathcal{I}_{10} & b_{11} & 0 & \mathcal{I}_{13} \\ 0 & 0 & b_{22} & 0 \\ -\mathcal{I}_{30} & \mathcal{I}_{31} & 0 & b_{33} \end{pmatrix}. \tag{3.57}$$

The terms of the $b_{\mu\nu}$ matrix in general form for an arbitrary ϕ_l value are given in Appendix III. They should be used if two rotation angle representation as in Ref. [52] was applied.

3.6 Joint angular distributions

Here, we provide examples how to construct modular expressions for the angular distributions of semileptonic decays of baryons. First, using our formalism, we rewrite the results from Ref. [158] for the single baryon B_2 decay. The simplest case is the decay of a spin polarized baryon $B_1 \rightarrow B_2 l^-\bar{\nu}_l$. If the polarization of the final particles is not measured, the fully

differential angular distribution $d\Gamma \propto \mathcal{W} = V_{Ph}(q^2)(q^2 - m_l^2)\mathrm{Tr}\rho_{B_2}$, where

$$\mathrm{Tr}\rho_{B_2} \propto \sum_{\mu=0}^{3} C_{\mu 0}\mathcal{B}_{\mu 0}^{B_1 B_2} = \sum_{\mu=0}^{3} C_{\mu 0} \sum_{\kappa=0}^{3} \mathcal{R}_{\mu\kappa}^{(4)}(\Omega_2) b_{\kappa 0}^{B_1 B_2}(q^2, \Omega_l) , \qquad (3.58)$$

with the baryon B_1 spin state in its rest frame described by the polarization vector $C_{\mu 0} = (1, P_x, P_y, P_z)$. The elements of the decay matrix $b_{\mu 0}^{B_1 B_2}(q^2, \Omega_l) := b_{\mu 0}(q^2, \Omega_l; \omega_{B_1 B_2})$ are given in Eq. (3.49). For example, if the initial polarization has only P_z component the joint angular distribution for the decay process $B_1 \rightarrow B_2 l^- \bar\nu_l$ is:

$$\mathcal{W}(\xi; \omega) = V_{Ph}(q^2)(q^2 - m_l^2) \left[b_{00}(q^2, \Omega_l; \omega_{B_1 B_2}) + P_z b_{30}(q^2, \Omega_l; \omega_{B_1 B_2}) \cos\theta_2 \right] , \qquad (3.59)$$

where the vector $\xi := (\theta_2, \phi_2, q^2, \Omega_l)$ represents a complete set of the kinematic variables describing an event configuration and the parameter vector $\omega_{B_1 B_2}$ represents the polarization P_z, the semileptonic couplings in Eq. (3.4) and the range parameters in Eq. (3.6). If the baryon B_2 decays weakly as $B_2 \rightarrow B_4 \pi$ the complete angular distribution is $\mathcal{W} = V_{Ph}(q^2)(q^2 - m_l^2)\mathrm{Tr}\rho_{B_4}$ with

$$\mathrm{Tr}\rho_{B_4} \propto \sum_{\mu, \nu=0}^{3} C_{\mu 0}\mathcal{B}_{\mu\nu}^{B_1 B_2} a_{\nu 0}^{B_2 B_4} = \sum_{\mu=0}^{3} C_{\mu 0} \sum_{\kappa, \nu=0}^{3} \mathcal{R}_{\mu\kappa}^{(4)}(\Omega_2) b_{\kappa\nu}^{B_1 B_2}(q^2, \Omega_l) a_{\nu 0}(\theta_4, \phi_4; \alpha_{B_2}) . \qquad (3.60)$$

The decay matrix $a_{\nu 0}(\theta_4, \phi_4; \alpha_{B_2})$ [52] describes the nonleptonic decay $B_2 \rightarrow B_4 \pi$ and using the representation from Appendix IV is given as:

$$\begin{bmatrix} a_{00} \\ a_{10} \\ a_{20} \\ a_{30} \end{bmatrix} = \mathcal{R}^{(4)}(\{0, \theta_4, \phi_4\}) \begin{bmatrix} 1 \\ 0 \\ 0 \\ \alpha_{B_2} \end{bmatrix} = \begin{bmatrix} 1 \\ \alpha_{B_2} \sin\theta_4 \cos\phi_4 \\ \alpha_{B_2} \sin\theta_4 \sin\phi_4 \\ \alpha_{B_2} \cos\theta_4 \end{bmatrix} , \qquad (3.61)$$

where θ_4 and ϕ_4 are the helicity angles of B_4 in the $\mathbb{R}_2$ frame and α_{B_2} is the decay asymmetry parameter. The corresponding angular distribution for charge-conjugated decay mode is obtained by the replacements $H_{\lambda_2 \lambda_W}^{B_1} \rightarrow H_{\lambda_2 \lambda_W}^{\bar B_1}$, $g_{av/w}^{B_1} \rightarrow g_{av/w}^{\bar B_1}$ and swapping between $(l^-, \bar\nu_l)$ and (l^+, ν_l). Neglecting hadronic CP-violating effects, one has $H_{\lambda_2, \lambda_W}^{V(\bar B_1)} = H_{\lambda_2, \lambda_W}^{V(B_1)}$ and $H_{\lambda_2, \lambda_W}^{A(\bar B_1)} = -H_{\lambda_2, \lambda_W}^{A(B_1)}$ Eq. (3.12) meaning that $g_w^{\bar B_1} = g_w^{B_1}$ and $g_{av}^{\bar B_1} = -g_{av}^{B_1}$ [165, 166].

Now we consider a decay of a spin-entangled baryon–antibaryon system $B_1 \bar B_1$, where the initial state is given by the spin correlation matrix $C_{\mu\nu}^{B_1 \bar B_1}$ defined in Eq. (3.1) with $B_1 \rightarrow B_2 l^- \bar\nu_l$. The semileptonic decay is tagged by a common decay of the antibaryon $\bar B_1$. For hyperon decay studies, a nonleptonic decay $\bar B_1 \rightarrow \bar B_3 \bar\pi$ is used. One obvious advantage of the studies using baryon–antibaryon pairs is that the charge-conjugated decays, corresponding to the $\bar B_1 \rightarrow \bar B_2 l^+ \nu_l$ and $B_1 \rightarrow B_3 \pi$ scenario, can be studied simultaneously. A common practice is to implicitly combine events corresponding to the charge-conjugated channels in the analyses to determine the decay properties in the CP-symmetry limit. In such analyses, the quantities that are even (odd) with respect to the parity operation have the same (opposite

TABLE 3.1: Properties of selected semileptonic decays of the ground-state-octet hyperons. The column labelled $M_1 - M_2$ gives the upper range of the $\sqrt{q^2}$ variable.

Decay	Transition	$\mathcal{B}(\times 10^{-4})$	g_{av}	g_w	$M_1 - M_2$ [MeV]	Comment
$\Lambda \to p e^- \bar{\nu}_e$	V_{us}	8.32(14)	0.718(15)	1.066	177	[66, 160]
$\Sigma^+ \to \Lambda e^+ \nu_e$[1]	V_{ud}	0.20(05)	0.01(10)	2.4(17)	74	[160]
$\Xi^- \to \Lambda e^- \bar{\nu}_e$	V_{us}	5.63(31)	0.25(5)	0.085	206	[66, 167]
$\Xi^- \to \Sigma^0 e^- \bar{\nu}_e$	V_{us}	0.87(17)	1.25(15)	2.609	129	[66, 167]
$\Xi^0 \to \Sigma^+ e^- \bar{\nu}_e$	V_{us}	2.52(8)	1.22(5)	2.0(9)	125	[160]

[a]Since for Σ^+ $F_1 = 0$, the coupling constants g_{av} and g_w are defined as F_1^V/F_1^A and F_2^V/F_1^A, respectively.

sign) values when combining the two cases. At the same time, the CP-symmetry can be tested by comparing values of the separately determined parameters for the baryon and antibaryon decays. Using as a building block the semileptonic decay matrix one constructs the angular distribution for the case when polarization of baryons B_2 and $\bar{B}_3$ is not measured:

$$\mathrm{Tr}\rho_{B_2\bar{B}_3} \propto \sum_{\mu,\bar{\nu}=0}^{3} C_{\mu\bar{\nu}}^{B_1\bar{B}_1} \mathcal{B}_{\mu 0}^{B_1 B_2} a_{\bar{\nu}0}^{\bar{B}_1\bar{B}_3}. \tag{3.62}$$

The matrix $\mathcal{B}_{\mu 0}^{B_1 B_2} := \mathcal{B}_{\mu 0}(\theta_2, \phi_2, q^2, \Omega_l; \omega_{B_1 B_2})$ describes the semileptonic decay and $a_{\bar{\nu}0}^{\bar{B}_1\bar{B}_3} := a_{\bar{\nu}0}(\theta_3, \phi_3; \bar{\alpha}_{B_1})$ [52] describes the nonleptonic decay $\bar{B}_1 \to \bar{B}_3\pi$, where θ_3 and ϕ_3 are the helicity angles of $\bar{B}_3$ in the $\bar{B}_1$ rest frame and $\bar{\alpha}_{B_1}$ is the decay asymmetry parameter. The joint angular distribution for the process is $\mathcal{W}(\xi; \omega) = V_{Ph}(q^2)(q^2 - m_l^2)\mathrm{Tr}\rho_{B_2\bar{B}_3}$, where:

$$\begin{aligned}
\mathrm{Tr}\rho_{B_2\bar{B}_3} =& C_{00}^{B_1\bar{B}_1}(\theta_1)b_{00}(\xi') + \sum_{i,j=1}^{3} C_{ij}^{B_1\bar{B}_1}(\theta_1)\mathcal{B}_{i0}(\xi')a_{j0}(\theta_3,\phi_3;\bar{\alpha}_{B_1}) \\
& + \sum_{i=1}^{3} C_{i0}^{B_1\bar{B}_1}(\theta_1)\mathcal{B}_{i0}(\xi') + b_{00}(\xi')\sum_{j=1}^{3} C_{0j}^{B_1\bar{B}_1}(\theta_1)a_{j0}(\theta_3,\phi_3;\bar{\alpha}_{B_1})
\end{aligned} \tag{3.63}$$

with $C_{\mu\bar{\nu}}^{B_1\bar{B}_1}$ given in Eq. (3.2) for the annihilation of the unpolarized electron–positron beams. The vectors of the kinematic variables are $\xi = (\theta_1, \theta_2, \phi_2, q^2, \Omega_l, \theta_3, \phi_3)$ while $\xi' = (\theta_2, \phi_2, q^2, \Omega_l)$. The full vector of parameters is denoted as $\omega := (\alpha_\psi, \Delta\Phi, g_{av}^{B_1}, g_w^{B_1}, \bar{\alpha}_{B_1})$.

3.7   Sensitivities for SL form factors parameters

Here we present estimates for the statistical uncertainties of the parameters describing form factors of selected semileptonic hyperon decays. The derived angular distributions are used to construct the normalized multidimensional probability density function for an event configuration. They are functions of q^2 and the helicity angles, and depend on the form factor parameters such as g_{av} and g_w (3.4). The parameters can be determined in an experiment

TABLE 3.2: Properties of the $e^+e^- \to J/\psi \to B_1\overline{B}_1$ decays to the pairs of ground-state octet hyperons.

	$\mathcal{B}(\times 10^{-4})$	α_ψ	$\Delta\Phi$ [rad]	Comment
$\Lambda\overline{\Lambda}$	19.43(33)	0.475(4)	0.752(8)	[43, 65]
$\Sigma^+\overline{\Sigma}^-$	15.0(24)	−0.508(7)	−0.270(15)	[139, 171]
$\Xi^-\overline{\Xi}^+$	9.7(8)	0.586(16)	1.213(49)	[159, 160]
$\Xi^0\overline{\Xi}^0$	11.65(4)	0.514(16)	1.168(26)	[172, 173]

using maximum likelihood (ML) method, which guarantees consistency and efficiency properties. We provide uncertainties of the parameters in the large number of events limit and assuming the detection efficiency does not depend on the kinematic variables as described in Refs. [47, 105]. Since the ML estimators are asymptotically normal, the product of their standard deviations, σ, and $\sqrt{N}$, where N is the number of the observed events, does not depend on N. The uncertainties are obtained by calculating elements of the Fisher information matrix that is inverted to obtain the covariance matrix for the parameters.

We consider the semileptonic decays of hyperons listed in Table 3.1. We neglect form factors F_3^V and F_2^A which vanish in the limit of the SU(3) flavor symmetry [168]. Equation (3.11) allows one to estimate the relative contribution of different form factors to the angular distributions. Based on the g_{av} and g_w values from Table 3.1 the q^2 dependence of the six helicity amplitudes for the Λ semileptonic decays is shown in Fig. 3.3(a). To allow a better comparison, the amplitudes are multiplied by $\sqrt{q^2}$. Close to the lower boundary, $q^2 = m_e^2$, the longitudinal and scalar helicity amplitudes dominate, with $H_{\frac{1}{2}0}^{V(A)} \approx H_{\frac{1}{2}t}^{V(A)}$. Close to the upper boundary at the zero recoil point, $q^2 = (M_1 - M_2)^2$, the contributions $H_{\frac{1}{2}t}^V$ and $H_{\frac{1}{2}1}^A = -\sqrt{2}H_{\frac{1}{2}0}^A$ are dominant with $H_{\frac{1}{2}t}^V = -H_{\frac{1}{2}0}^A/g_{av}$. We do not consider the decay $\Sigma^- \to ne^-\bar{\nu}_e$ since the final state includes two neutral particles, neutron and neutrino, making it impossible to fully reconstruct the events. In addition, no measurements exist for the production parameters in the $e^+e^- \to \Sigma^-\bar{\Sigma}^+$ process.

The first case is the decay $\Lambda \to pe^-\bar{\nu}_e$ studied in the exclusive process $e^+e^- \to J/\psi \to \Lambda\overline{\Lambda}$, where $\overline{\Lambda} \to \bar{p}\pi^+$ is used for tagging. The angular distribution is given by Eq. (3.62) where the parameters of the production process $e^+e^- \to J/\psi \to \Lambda\overline{\Lambda}$ needed to define the spin-correlation–polarization matrix $C_{\mu\nu}$ are given in Table 3.2. The properties of $\overline{\Lambda} \to \bar{p}\pi^+$ decay and the charge conjugated process that is used to tag the SL decay are given in Table 3.3. We assume the production parameters and the decay parameters of the nonleptonic decays used for the tagging to be well known and fixed. Since the coupling g_{av3} is multiplied by m_e in the transition amplitude [169], we set it to zero because it cannot be determined from experiment with a reasonable uncertainty. In addition, the parameters $r_{v,w}$ and r_{av} defined in Eq. (3.6) are fixed to the values deduced from the ansatz for the $s \to u$ transition of Refs. [66, 170] and listed in Table 3.4. The statistical uncertainties $\sigma(g_{av})$ and $\sigma(g_w)$ for the coupling constants g_{av} and g_w, respectively, are given in the first row of Table 3.4. The main feature is that the uncertainty for the g_{av} coupling is nearly one order of magnitude less than for g_w since the latter is suppressed by the $q^2/M_1^2 < (M_1 - M_2)^2/M_1^2 \approx 0.025$ factor (3.11). The second row

(a)
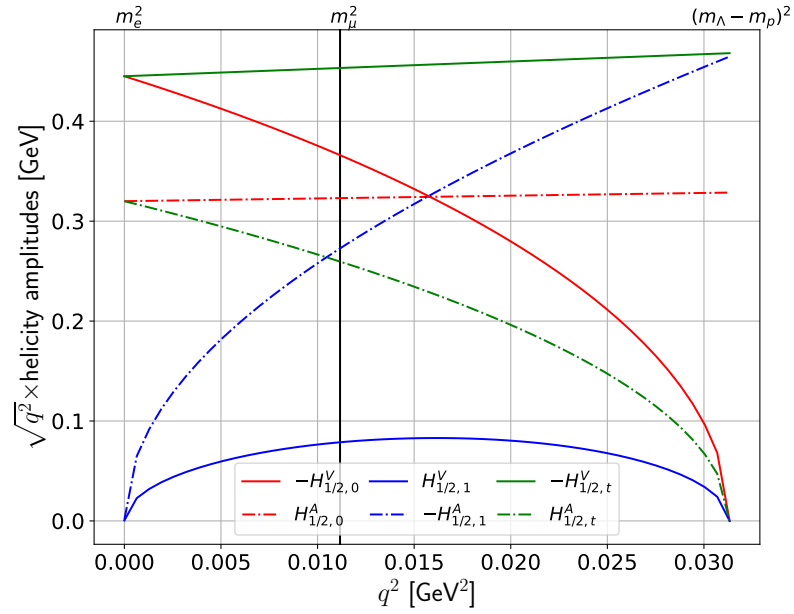
(b)
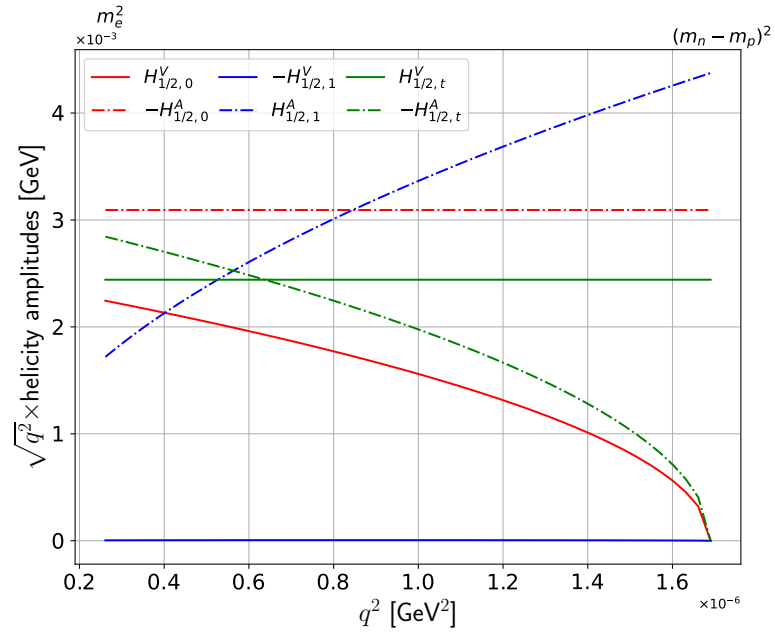
FIGURE 3.3: The q^2-dependence of the six helicity amplitudes for (a) $\Lambda \rightarrow p l^- \bar{\nu}_l$ and (b) $n \rightarrow p e^- \bar{\nu}_e$ decays. For the Λ decay, the kinematic range for the μ-mode is to the right of the vertical line $q^2 = m_\mu^2$.

TABLE 3.3: Properties of the main decays of the ground-state octet hyperons that can be used to tag the SL decays. The decay asymmetry $\bar{\alpha}_D$ for the charge conjugated decay modes in the CP-symmetry conservation limit is $\bar{\alpha}_D = -\alpha_D$.

D	$\mathcal{B}(\%)$	α_D	Comment
$\Lambda \to p\pi^-$	64	0.755(3)	[159, 174]
$\Sigma^+ \to p\pi^0$	52	$-0.994(4)$	[171]
$\Xi^- \to \Lambda\pi^-$	100	$-0.379(4)$	[159, 160]
$\Xi^0 \to \Lambda\pi^0$	96	$-0.375(3)$	[160, 173]

TABLE 3.4: Statistical uncertainties for the g_{av} and g_w couplings for some semileptonic decays reconstructed using double-tag method Eq. (3.62).

Decay	$\sigma(g_{av})\sqrt{N}$	$\sigma(g_w)\sqrt{N}$	$r_{v,w}$ [GeV^{-2}]	r_a [GeV^{-2}]
$\Lambda \to pe^-\bar{\nu}_e$	1.8	12		
$\Xi^- \to [\Lambda \to pe^-\bar{\nu}_e]\pi^-$	1.8	12		
$\Xi^- \to [\Lambda \to p\pi^-]e^-\bar{\nu}_e$	0.6	9	1.94	1.28
$\Xi^- \to [\Sigma^0 \to [\Lambda \to p\pi^-]\gamma]e^-\bar{\nu}_e$	5.0	29		
$\Xi^0 \to [\Sigma^+ \to p\pi^0]e^-\bar{\nu}_e$	4.0	28		
$\Sigma^+ \to [\Lambda \to p\pi^-]e^+\nu_e$	0.5	19	2.83	1.71

corresponds to an independent method to study $\Lambda \to pe^-\bar{\nu}_e$ using the $e^+e^- \to J/\psi \to \Xi^-\bar{\Xi}^+$ process with the $\Xi^- \to [\Lambda \to pe^-\bar{\nu}_e]\pi^-$ sequence and $\bar{\Xi}^+ \to [\bar{\Lambda} \to \bar{p}\pi^+]\pi^-$ for the tagging. The modular expression for the angular distribution of such process reads

$$\text{Tr}\rho_{p\bar{p}} \propto \sum_{\mu,\bar{\nu}=0}^{3} C_{\mu\bar{\nu}}^{\Xi\bar{\Xi}} \sum_{\mu'=0}^{3} a_{\mu\mu'}^{\Xi\Lambda} \mathcal{B}_{\mu'0}^{\Lambda p} \sum_{\bar{\nu}'=0}^{3} a_{\bar{\nu}\bar{\nu}'}^{\bar{\Xi}\bar{\Lambda}} a_{\bar{\nu}'0}^{\bar{\Lambda}\bar{p}} . \tag{3.64}$$

The polarization of the Λ originating from the nonleptonic weak decay $\Xi^- \to \Lambda\pi^-$, is $\sim 40\%$, to be compared to the root-mean-squared value of the Λ polarization in $e^+e^- \to J/\psi \to \Lambda\bar{\Lambda}$ of 11% [47]. However, the uncertainties of the weak couplings are the same for both methods. To further investigate dependence on the initial polarization of Λ we set $\Delta\Phi = 0$ to have the zero polarization, while to obtain maximally polarized Λ we include the longitudinal polarization of the electron beam and use the production matrix $C_{\mu\bar{\nu}}$ from Ref. [47]. The impact of the spin correlations for the uncertainties can be studied by comparing the results using the angular distributions (3.62) or (3.64) with full production matrices $C_{\mu\bar{\nu}}$ to the ones where all elements except $C_{\mu 0}$ are set to zero. This arrangement assures that the spin correlation terms are excluded. In all these tests the uncertainties of $\sigma(g_{av})$ and $\sigma(g_w)$ remain unchanged, meaning that the polarization and the spin correlations of the mother hyperon in the decay play almost no role for the measurements of properties of the semileptonic decays to baryons whose polarization is not measured.

The entries from the third row and below in Table 3.4 correspond to the decays where the polarization of the daughter baryon is measured and the angular distributions include the complete $\mathcal{B}_{\mu\mu'}$ matrices. For example, the angular distribution for $\Xi^- \to \Lambda e^-\bar{\nu}_e$ measurement in

$e^+e^- \to J/\psi \to \Xi^-\bar{\Xi}^+$ is

$$\mathrm{Tr}\rho_{p\bar{p}} \propto \sum_{\mu,\bar{\nu}=0}^{3} C_{\mu\bar{\nu}}^{\Xi\bar{\Xi}} \sum_{\mu'=0}^{3} \mathcal{B}_{\mu\mu'}^{\Xi\Lambda} a_{\mu'0}^{\Lambda p} \sum_{\bar{\nu}'=0}^{3} a_{\bar{\nu}\bar{\nu}'}^{\bar{\Xi}\bar{\Lambda}} a_{\bar{\nu}'0}^{\bar{\Lambda}\bar{p}} . \tag{3.65}$$

Since the uncertainties depend on the values of the weak couplings it is difficult to compare the results for different decays in Table 3.4. By repeating the studies with variation of $\Delta\Phi$ and the electron beam polarization some impact is seen for the uncertainties, specially for the g_w parameter in $\Sigma^+ \to \Lambda e^+\nu_e$. In addition, we study the uncertainties for single spin polarized baryon decays with the angular distributions given by Eq. (3.58). The baryon B_1 polarization vector is set to $C_{\mu 0} = (1, 0, P_y, 0)$. The results for $\sigma(g_{av})$ and $\sigma(g_w)$ are shown in Fig. 3.4. The uncertainty for large P_y decreases typically by 20% comparing to the unpolarized case.

Our formalism applies also to the $n \to pe^-\bar{\nu}_e$ decay and it should be equivalent to the approach from Ref. [175] for the single neutron decay. However, we can also describe decay correlations for a spin entangled neutron–neutron pair. As an example, we take nn spin singlet state given by the spin correlation matrix $C_{\mu\nu} = \mathrm{diag}(1, -1, 1, 1)$. The coupling constants g_{av} and g_w are 1.2754(13) and 1.853, respectively [160, 175]. The q^2 dependence of the form factors is neglected due to the tiny range, $m_e < \sqrt{q^2} < M_n - M_p$, of the variable. The corresponding helicity amplitudes for the neutron beta decay are shown in Fig. 3.3(b). The resulting uncertainty of the g_{av} measurement in the double beta decay of the singlet pair is $\sigma(g_{av})\sqrt{N} = 4.3$. It should be compared to the uncertainties in the measurements with single neutrons that are shown in Fig. 3.4(a) as a function of the neutron polarization. For unpolarized neutron $\sigma(g_{av})\sqrt{N} = 7.4$ and it decreases to 4.1 when the polarization is equal to one. The flip-contribution to the helicity amplitudes (3.54) of about 8% was neglected in the estimates. The g_w coupling cannot be determined since its contribution to the helicity amplitude $H_{\frac{1}{2}0}^V$ is suppressed by a factor q^2/M_n^2. Moreover, the second amplitude that includes g_w, $H_{\frac{1}{2}1}^V$, is suppressed by $\sqrt{q^2}$ and as seen in Fig. 3.3(b) it is consistent with zero.

3.8 Conclusions

We have constructed a modular description of the differential distributions for baryon semileptonic decays where the baryons are originating from entangled baryon–antibaryon pairs produced in the electron–positron annihilations or in charmonia decays. The formalism allows to extract the weak form factors using complete information available in such experiments. The lepton mass effects as well as polarization effects of the decaying parent hyperon are included in the formalism. The presented modular expressions are applicable to various sequential processes like $B_1 \to B_2(\to B_3 + \pi) + l + \nu_l$ that involve a semileptonic decay. Two conventions for defining transversal directions of the helicity frames were considered. The daughter baryon spin-density matrix in a semileptonic decay takes the simplest form when expressed using the angles in the decay plane. The two representations are equivalent, provided that one uses the matching set of rotations to define the helicity angles.

(a)
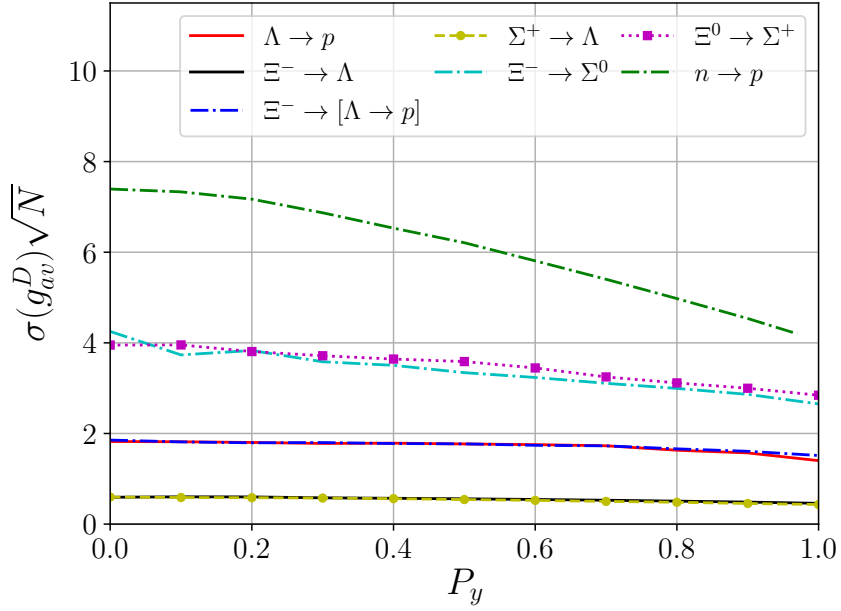
(b)
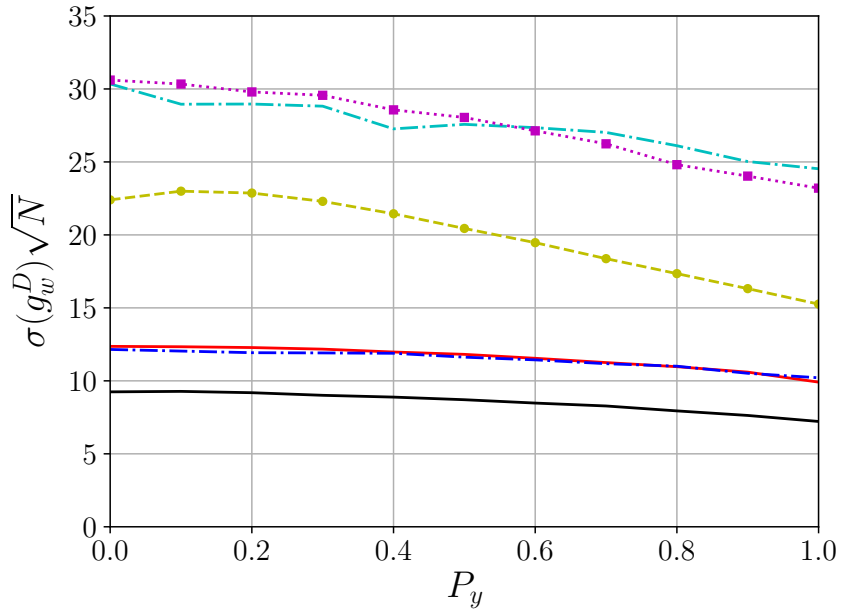
FIGURE 3.4: Statistical uncertainties (a) $\sigma(g_{av})\sqrt{N}$ and (b) $\sigma(g_w)\sqrt{N}$ for semileptonic decays as a function of the initial baryon polarization. Note that there is no estimate of $\sigma(g_w)$ for $n \to pe^- \nu_e$ in panel (b) as explained in the text.

We have not included radiative corrections in our estimates but they have to be considered in the experimental analyses. Over the years, the radiative corrections to hadronic β-decays have been extensively studied [176] and the specific applications to the hyperon semileptonic decays are discussed in Ref. [177]. The state-of-the-art in experimental analyses is to use PHOTOS program [178] that is based on leading-logarithmic (collinear) approximation. The procedure is applied to all final particles, but the electron (positron) tracks are most affected.

The BESIII experiment has collected 10^{10} J/ψ [162] meaning that for semileptonic decays data samples of less than 10^4 events are available. Therefore, a rough estimate of the achievable uncertainties with this data set is given by dividing the values in Table 3.4 by 100. The J/ψ decays into a hyperon–antihyperon pair can provide a clean setting with low systematic uncertainties for the CP-symmetry conservation tests in semileptonic decays, since the decays of the charge conjugated modes can be done simultaneously.

A similar modular approach with decay matrices might be useful for studies of radiative and Dalitz decays. As a cross-check and illustration in Appendix IV we provide formulas for the Dalitz transition $B_1 \to B_2 l^+ l^-$ between baryons with spin 1/2 as well as decay matrix for a weak radiative decay with real photon $B_1 \to B_2 \gamma$.

For the studies of semileptonic decays of heavy baryons induced by the quark transitions $c \to s + l^+ + \nu_l$ or $b \to c + l^- + \bar{\nu}_l$ the previously available formalism [158] is likely sufficient if only beams of polarized baryons are used. This might change in the near future with BESIII and Belle II experiments, where entangled charmed baryon–antibaryon pairs will be available. One difference would be a measurement of the polarization for the tagging reactions which probably has to use three-body hadronic weak decays. However, even for the case of single baryon decays, our approach provides an easy and flexible way to implement different decay sequences in the event generators that propagate spin information of the decaying baryons.

I   Conventions for Wigner functions and Pauli matrices

Conventions for Pauli matrices: rows $m_1 = 1/2, -1/2$ are numbered from top to bottom and columns $m_2 = 1/2, -1/2$ are numbered from left to right:

$$
\sigma_0^{m_1,m_2} = \begin{pmatrix} 1 & 0 \\ 0 & 1 \end{pmatrix}, \; \sigma_1^{m_1,m_2} = \begin{pmatrix} 0 & 1 \\ 1 & 0 \end{pmatrix}, \; \sigma_2^{m_1,m_2} = \begin{pmatrix} 0 & -i \\ i & 0 \end{pmatrix}, \; \sigma_3^{m_1,m_2} = \begin{pmatrix} 1 & 0 \\ 0 & -1 \end{pmatrix}.
\tag{3.66}
$$

The corresponding Wigner functions $\mathcal{D}_{m_1,m_2}^J(0,\theta,0) = d_{m_1,m_2}^J(\theta)$ are for $J = 1/2$

$$
\mathcal{D}_{m_1,m_2}^{1/2}(0,\theta,0) = \begin{pmatrix} \cos\theta/2 & -\sin\theta/2 \\ \sin\theta/2 & \cos\theta/2 \end{pmatrix},
\tag{3.67}
$$

with the columns and rows expressed using the same convention. For $J = 1$ the functions are

$$\mathcal{D}^1_{m_1,m_2}(0,\theta,0) = \begin{pmatrix} \frac{1}{2}(1+\cos\theta) & \frac{1}{\sqrt{2}}\sin\theta & \frac{1}{2}(1-\cos\theta) \\ -\frac{1}{\sqrt{2}}\sin\theta & \cos\theta & \frac{1}{\sqrt{2}}\sin\theta \\ \frac{1}{2}(1-\cos\theta) & -\frac{1}{\sqrt{2}}\sin\theta & \frac{1}{2}(1+\cos\theta) \end{pmatrix}, \qquad (3.68)$$

where the rows (m_1) and columns (m_2) are labeled in the order $(-1,0,1)$ from left to right and top to bottom, respectively. This convention matches the complete Wigner $\mathcal{D}$ functions given as $\mathcal{D}^J_{m_1,m_2}(\phi,\theta,\chi) = \exp(-im_1\phi)\mathcal{D}^J_{m_1,m_2}(0,\theta,0)\exp(-im_2\chi)$. The Pauli matrices are related to the 3D rotation matrices $R_{jk}(\Omega)$ for $\Omega \equiv \{\phi,\theta,\chi\}$ in the following way :

$$R_{jk}(\Omega) = \frac{1}{2}\sum_{\kappa,\kappa'}\sum_{\zeta,\zeta'}(\sigma_j)^{\kappa,\kappa'}(\sigma_k)^{\zeta',\zeta}\mathcal{D}^{1/2*}_{\kappa,\zeta}(\Omega)\mathcal{D}^{1/2}_{\kappa',\zeta'}(\Omega)$$

$$= \begin{pmatrix} \cos\theta\cos\chi\cos\phi - \sin\chi\sin\phi & -\cos\theta\sin\chi\cos\phi - \cos\chi\sin\phi & \sin\theta\cos\phi \\ \cos\theta\cos\chi\sin\phi + \sin\chi\cos\phi & \cos\chi\cos\phi - \cos\theta\sin\chi\sin\phi & \sin\theta\sin\phi \\ -\sin\theta\cos\chi & \sin\theta\sin\chi & \cos\theta \end{pmatrix},$$

$$(3.69)$$

where the columns (k) and rows (j) are labeled $k, j = 1, 2, 3$ (x, y, z) from left to right and from top to bottom, respectively.

II Derivation of the decay matrix decomposition

Starting from the amplitude representation in Eq. (3.21) we derive expression Eq. (3.39). Multiplying the amplitude in Eq. (3.21) by its conjugate to obtain spin-density matrix and by inserting basis Pauli matrices for the mother and the daughter baryon:

$$\mathcal{B}^D_{\mu\nu} = \frac{1}{8\pi^2}\sum_{\lambda,\lambda'}\sum_{\kappa,\kappa'}\sum_{\zeta,\zeta'}\mathcal{H}_{\zeta,\lambda}\mathcal{H}^*_{\zeta',\lambda'}(\sigma_\mu)^{\kappa,\kappa'}(\sigma_\nu)^{\lambda',\lambda}\mathcal{D}^{1/2*}_{\kappa,\zeta}(\Omega)\mathcal{D}^{1/2}_{\kappa',\zeta'}(\Omega)$$

$$= \frac{1}{8\pi^2}\sum_{\zeta,\zeta'}\underbrace{\left[\sum_{\lambda,\lambda'}(\sigma_\nu)^{\lambda',\lambda}\mathcal{H}_{\zeta,\lambda}\mathcal{H}^*_{\zeta',\lambda'}\right]}_{I^{\zeta,\zeta'}_\nu}\underbrace{\left[\sum_{\kappa,\kappa'}(\sigma_\mu)^{\kappa,\kappa'}\mathcal{D}^{1/2*}_{\kappa,\zeta}(\Omega)\mathcal{D}^{1/2}_{\kappa',\zeta'}(\Omega)\right]}_{R^{\zeta,\zeta'}_\mu(\Omega)} \qquad (3.70)$$

$$= \frac{1}{8\pi^2}\sum_{\zeta,\zeta'}R^{\zeta,\zeta'}_\mu(\Omega)I^{\zeta,\zeta'}_\nu,$$

where the running indices in all sums $\kappa, \kappa', \lambda', \lambda$ and ζ, ζ' are $-1/2$ and $+1/2$. Despite $\mathcal{B}^D_{\mu\nu}$ being a real-value matrix, the matrices $I^{\zeta,\zeta'}_\nu$ and $R^{\zeta,\zeta'}_\mu(\Omega)$ are not real-valued. We would like to rewrite Eq. (3.70) as a product of a 4D rotation matrix and a 4×4 matrix $b_{\rho\nu}$ in the form given in Eq. (3.39):

$$\mathcal{B}^D_{\mu\nu} = \frac{1}{8\pi^2}\sum_{\rho=0}^{3}\mathcal{R}^{(4)}_{\mu\rho}(\Omega)b_{\rho\nu}.$$

In order to derive the form of $\mathcal{R}^{(4)}_{\mu\rho}(\Omega)$ we set the matrix $b_{\mu\nu}$ to the identity 4×4 matrix. This can be achieved by setting $\mathcal{H}_{\zeta,\lambda} = \delta_{\zeta\lambda}$ since

$$\sum_{\zeta,\zeta'}\sum_{\lambda,\lambda'}(\sigma_\nu)^{\lambda',\lambda}\delta_{\zeta,\lambda}\delta_{\zeta',\lambda'}(\sigma_\mu)^{\zeta,\zeta'} = 2\delta_{\nu\mu}\,. \tag{3.71}$$

Such replacement in Eq. (3.70) gives:

$$\begin{aligned}
\mathcal{R}^{(4)}_{\mu\nu}(\Omega) &= \frac{1}{2}\sum_{\lambda,\lambda'}\sum_{\kappa,\kappa'}\sum_{\zeta,\zeta'}\delta_{\zeta,\lambda}\delta_{\zeta',\lambda'}\,(\sigma_\mu)^{\kappa,\kappa'}(\sigma_\nu)^{\lambda',\lambda}\mathcal{D}^{1/2*}_{\kappa,\zeta}(\Omega)\mathcal{D}^{1/2}_{\kappa',\zeta'}(\Omega) \\
&= \frac{1}{2}\sum_{\kappa,\kappa'}\sum_{\zeta,\zeta'}(\sigma_\mu)^{\kappa,\kappa'}(\sigma_\nu)^{\zeta',\zeta}\,\mathcal{D}^{1/2*}_{\kappa,\zeta}(\Omega)\mathcal{D}^{1/2}_{\kappa',\zeta'}(\Omega)\,.
\end{aligned} \tag{3.72}$$

By evaluating the above expression one gets the explicit form for $\mathcal{R}^{(4)}_{\mu\nu}(\Omega)$:

$$\begin{pmatrix}
1 & 0 & 0 & 0 \\
0 & \cos\theta\cos\chi\cos\phi - \sin\chi\sin\phi & -\cos\theta\sin\chi\cos\phi - \cos\chi\sin\phi & \sin\theta\cos\phi \\
0 & \cos\theta\cos\chi\sin\phi + \sin\chi\cos\phi & \cos\chi\cos\phi - \cos\theta\sin\chi\sin\phi & \sin\theta\sin\phi \\
0 & -\sin\theta\cos\chi & \sin\theta\sin\chi & \cos\theta
\end{pmatrix}, \tag{3.73}$$

which is the 4D rotation where the spatial part $\mathcal{R}_{jk}(\Omega)$ corresponds to the product of the following three axial rotations:

$$\begin{aligned}
\mathcal{R}_{jk}(\Omega) &= R_z(\phi)R_y(\theta)R_z(\chi) \\
&= \begin{pmatrix} \cos\phi & -\sin\phi & 0 \\ \sin\phi & \cos\phi & 0 \\ 0 & 0 & 1 \end{pmatrix}\begin{pmatrix} \cos\theta & 0 & \sin\theta \\ 0 & 1 & 0 \\ -\sin\theta & 0 & \cos\theta \end{pmatrix}\begin{pmatrix} \cos\chi & -\sin\chi & 0 \\ \sin\chi & \cos\chi & 0 \\ 0 & 0 & 1 \end{pmatrix}\,.
\end{aligned} \tag{3.74}$$

The expression for $b_{\mu\nu}$ can be deduced by setting $\mathcal{R}^{(4)}_{\mu\rho}(\Omega)$ to the 4×4 identity matrix i.e. by setting $\Omega = \{0,0,0\}$:

$$\begin{aligned}
b_{\mu\nu} = \mathcal{B}^D_{\mu\nu}(\Omega \equiv 0) &= \sum_{\zeta,\zeta'}\left[\sum_{\lambda,\lambda'}(\sigma_\nu)^{\lambda',\lambda}\mathcal{H}_{\zeta,\lambda}\mathcal{H}^*_{\zeta',\lambda'}\right]\left[\sum_{\kappa,\kappa'}(\sigma_\mu)^{\kappa,\kappa'}\delta_{\kappa,\zeta}\delta_{\kappa',\zeta'}\right] \\
&= \sum_{\zeta,\zeta'}\sum_{\lambda,\lambda'}(\sigma_\nu)^{\lambda',\lambda}\mathcal{H}_{\zeta,\lambda}\mathcal{H}^*_{\zeta',\lambda'}(\sigma_\mu)^{\zeta,\zeta'}\,.
\end{aligned} \tag{3.75}$$

The elements of the real-valued matrix $b_{\rho\nu}$ expressed in terms of amplitudes $\mathcal{H}$ are:

$$b_{\rho 0} = \begin{pmatrix}
|\mathcal{H}_{--}|^2 + |\mathcal{H}_{+-}|^2 + |\mathcal{H}_{-+}|^2 + |\mathcal{H}_{++}|^2 \\
2\Re\left(\mathcal{H}_{++}\mathcal{H}^*_{-+} + \mathcal{H}_{--}\mathcal{H}^*_{+-}\right) \\
2\Im\left(\mathcal{H}_{++}\mathcal{H}^*_{-+} - \mathcal{H}_{--}\mathcal{H}^*_{+-}\right) \\
-|\mathcal{H}_{--}|^2 + |\mathcal{H}_{++}|^2 + |\mathcal{H}_{+-}|^2 - |\mathcal{H}_{-+}|^2
\end{pmatrix}, \tag{3.76}$$

$$
b_{\rho 1} = \begin{pmatrix} 2\Re\left(\mathcal{H}_{++}\mathcal{H}_{+-}^* + \mathcal{H}_{--}\mathcal{H}_{-+}^*\right) \\ 2\Re\left(\mathcal{H}_{++}\mathcal{H}_{--}^* + \mathcal{H}_{-+}\mathcal{H}_{+-}^*\right) \\ 2\Im\left(\mathcal{H}_{++}\mathcal{H}_{--}^* - \mathcal{H}_{-+}\mathcal{H}_{+-}^*\right) \\ 2\Re\left(\mathcal{H}_{++}\mathcal{H}_{+-}^* - \mathcal{H}_{--}\mathcal{H}_{-+}^*\right) \end{pmatrix}, \tag{3.77}
$$

$$
b_{\rho 2} = \begin{pmatrix} -2\Im\left(\mathcal{H}_{++}\mathcal{H}_{+-}^* - \mathcal{H}_{--}\mathcal{H}_{-+}^*\right) \\ -2\Im\left(\mathcal{H}_{++}\mathcal{H}_{--}^* + \mathcal{H}_{-+}\mathcal{H}_{+-}^*\right) \\ 2\Re\left(\mathcal{H}_{++}\mathcal{H}_{--}^* - \mathcal{H}_{-+}\mathcal{H}_{+-}^*\right) \\ -2\Im\left(\mathcal{H}_{++}\mathcal{H}_{+-}^* + \mathcal{H}_{--}\mathcal{H}_{-+}^*\right) \end{pmatrix}, \tag{3.78}
$$

$$
b_{\rho 3} = \begin{pmatrix} -|\mathcal{H}_{--}|^2 - |\mathcal{H}_{+-}|^2 + |\mathcal{H}_{-+}|^2 + |\mathcal{H}_{++}|^2 \\ 2\Re\left(\mathcal{H}_{++}\mathcal{H}_{-+}^* - \mathcal{H}_{--}\mathcal{H}_{+-}^*\right) \\ 2\Im\left(\mathcal{H}_{++}\mathcal{H}_{-+}^* + \mathcal{H}_{--}\mathcal{H}_{+-}^*\right) \\ |\mathcal{H}_{--}|^2 + |\mathcal{H}_{++}|^2 - |\mathcal{H}_{+-}|^2 - |\mathcal{H}_{-+}|^2 \end{pmatrix}. \tag{3.79}
$$

The matrix elements $b_{\mu\nu}$ are interrelated since they are expressed by the four complex amplitudes $\mathcal{H}_{\lambda,\lambda'}$. Therefore, neglecting the unobservable overall phase there are up to six independent real-valued functions in addition to the unpolarized cross-section term b_{00}. The b-matrix can be considered as a generalization of Lee-Yang baryon polarization formula [87] which has maximum two independent parameters (see example in Appendix IV.b). The terms b_{i0}/b_{00} are discussed in [179] in the context of hadronic decays and are called aligned polarimeter fields $\alpha_{x,y,z}$. In Appendix IV we give the b matrices for few example processes.

III Complete decay matrix for SL decays

The terms of the non-flip contributions for the unaligned (with arbitrary ϕ_l) decay matrix $b_{\mu\nu}^{\mathrm{nf}}$ are (the term b_{33}^{nf} does not depend on the angle and it is not repeated):

$$
\begin{aligned}
b_{11}^{\mathrm{nf}} &= \Re(\mathcal{E}_{00}^{\mathrm{nf}}) + \left\{\Re(\mathcal{E}_{11}^{\mathrm{nf}})\cos 2\phi_l - \Im(\mathcal{E}_{11}^{\mathrm{nf}})\sin 2\phi_l\right\}, \\
b_{12}^{\mathrm{nf}} &= -\Im(\mathcal{E}_{00}^{\mathrm{nf}}) - \left\{\Re(\mathcal{E}_{11}^{\mathrm{nf}})\sin 2\phi_l + \Im(\mathcal{E}_{11}^{\mathrm{nf}})\cos 2\phi_l\right\}, \\
b_{13}^{\mathrm{nf}} &= \Re(\mathcal{I}_{13}^{\mathrm{nf}})\cos \phi_l - \Im(\mathcal{I}_{13}^{\mathrm{nf}})\sin \phi_l, \\
b_{21}^{\mathrm{nf}} &= \Im(\mathcal{E}_{00}^{\mathrm{nf}}) - \left\{\Re(\mathcal{E}_{11}^{\mathrm{nf}})\sin 2\phi_l + \Im(\mathcal{E}_{11}^{\mathrm{nf}})\cos 2\phi_l\right\}, \\
b_{22}^{\mathrm{nf}} &= \Re(\mathcal{E}_{00}^{\mathrm{nf}}) - \left\{\Re(\mathcal{E}_{11}^{\mathrm{nf}})\cos 2\phi_l - \Im(\mathcal{E}_{11}^{\mathrm{nf}})\sin 2\phi_l\right\}, \\
b_{23}^{\mathrm{nf}} &= -(\Re(\mathcal{I}_{13}^{\mathrm{nf}})\sin \phi_l + \Im(\mathcal{I}_{13}^{\mathrm{nf}})\cos \phi_l), \\
b_{31}^{\mathrm{nf}} &= -(\Re(\mathcal{I}_{31}^{\mathrm{nf}})\cos \phi_l - \Im(\mathcal{I}_{31}^{\mathrm{nf}})\sin \phi_l), \\
b_{32}^{\mathrm{nf}} &= \Re(\mathcal{I}_{31}^{\mathrm{nf}})\sin \phi_l + \Im(\mathcal{I}_{31}^{\mathrm{nf}})\cos \phi_l \,.
\end{aligned} \tag{3.80}
$$

The remaining terms of the flip contributions for the decay matrix $b^{\mathrm{f}}_{\mu\nu}$ are:

$$
\begin{aligned}
b^{\mathrm{f}}_{11} &= \mathfrak{R}(\mathcal{E}^{\mathrm{f}}_{00}) - \left\{\mathfrak{R}(\mathcal{E}^{\mathrm{f}}_{11}) \cos 2\phi_l - \mathfrak{I}(\mathcal{E}^{\mathrm{f}}_{11}) \sin 2\phi_l\right\}, \\
b^{\mathrm{f}}_{12} &= -\mathfrak{I}(\mathcal{E}^{\mathrm{f}}_{00}) + \left\{\mathfrak{R}(\mathcal{E}^{\mathrm{f}}_{11}) \sin 2\phi_l + \mathfrak{I}(\mathcal{E}^{\mathrm{f}}_{11}) \cos 2\phi_l\right\}, \\
b^{\mathrm{f}}_{13} &= \mathfrak{R}(\mathcal{I}^{\mathrm{f}}_{13}) \cos \phi_l - \mathfrak{I}(\mathcal{I}^{\mathrm{f}}_{13}) \sin \phi_l, \\
b^{\mathrm{f}}_{21} &= \mathfrak{I}(\mathcal{E}^{\mathrm{f}}_{00}) + \left\{\mathfrak{R}(\mathcal{E}^{\mathrm{f}}_{11}) \sin 2\phi_l + \mathfrak{I}(\mathcal{E}^{\mathrm{f}}_{11}) \cos 2\phi_l\right\}, \\
b^{\mathrm{f}}_{22} &= \mathfrak{R}(\mathcal{E}^{\mathrm{f}}_{00}) + \left\{\mathfrak{R}(\mathcal{E}^{\mathrm{f}}_{11}) \cos 2\phi_l - \mathfrak{I}(\mathcal{E}^{\mathrm{f}}_{11}) \sin 2\phi_l\right\}, \\
b^{\mathrm{f}}_{23} &= -(\mathfrak{R}(\mathcal{I}^{\mathrm{f}}_{13}) \sin \phi_l + \mathfrak{I}(\mathcal{I}^{\mathrm{f}}_{13}) \cos \phi_l), \\
b^{\mathrm{f}}_{31} &= -(\mathfrak{R}(\mathcal{I}^{\mathrm{f}}_{31}) \cos \phi_l - \mathfrak{I}(\mathcal{I}^{\mathrm{f}}_{31}) \sin \phi_l), \\
b^{\mathrm{f}}_{32} &= \mathfrak{R}(\mathcal{I}^{\mathrm{f}}_{31}) \sin \phi_l + \mathfrak{I}(\mathcal{I}^{\mathrm{f}}_{31}) \cos \phi_l .
\end{aligned}
\tag{3.81}
$$

IV Examples of aligned decay matrices

IV.a $B_1 \to B_2\gamma$

The amplitude of Eq. (3.10) for the weak decay $B_1 \to B_2\gamma$ simplifies by replacing $\underline{\lambda}_W \to \lambda_\gamma$ where $\lambda_\gamma = \{-1, 1\}$. For the hadronic tensor, only terms $H_{\frac{1}{2}1}$ and $H_{-\frac{1}{2}-1}$ are non-zero. The transition tensor for decay with real photon in helicity representation reads:

$$
T^{\kappa\kappa',\lambda_2\lambda'_2} = \frac{1}{4\pi} \sum_{\lambda_\gamma} H_{\lambda_2\lambda_\gamma} H^*_{\lambda'_2\lambda_\gamma} \mathcal{D}^{1/2*}_{\kappa,\lambda_2-\lambda_\gamma}(\Omega_2) \mathcal{D}^{1/2}_{\kappa',\lambda'_2-\lambda_\gamma}(\Omega_2) .
\tag{3.82}
$$

The decay matrix $b^\gamma_{\mu\nu}$ is following:

$$
\begin{aligned}
b^\gamma_{\mu\nu} &:= \sum_{\lambda_\gamma} \sum_{\lambda_2,\lambda'_2=-1/2}^{1/2} H_{\lambda_2\lambda_\gamma} H^*_{\lambda'_2\lambda_\gamma} \sigma^{\lambda_2-\lambda_\gamma,\lambda'_2-\lambda_\gamma}_\mu \sigma^{\lambda'_2,\lambda_2}_\nu \\
&= |H_{-1/2,-1}|^2 \sigma^{1/2,1/2}_\mu \sigma^{-1/2,-1/2}_\nu + |H_{1/2,+1}|^2 \sigma^{-1/2,-1/2}_\mu \sigma^{1/2,1/2}_\nu
\end{aligned}
\tag{3.83}
$$

or

$$
b^\gamma_{\mu\nu} \propto \begin{pmatrix} 1 & 0 & 0 & \alpha_\gamma \\ 0 & 0 & 0 & 0 \\ 0 & 0 & 0 & 0 \\ -\alpha_\gamma & 0 & 0 & -1 \end{pmatrix}
\tag{3.84}
$$

where

$$
\alpha_\gamma = |H_{1/2,+1}|^2 - |H_{-1/2,-1}|^2; \quad |H_{1/2,+1}|^2 + |H_{-1/2,-1}|^2 = 1 .
\tag{3.85}
$$

IV.b $B_1 \to B_2\pi$

For the weak nonleptonic decay $D(B_1 \to B_2\pi)$ we present the results from Ref. [52] as a product of rotation matrix and the aligned decay matrix:

$$T^{\kappa\kappa',\lambda_2\lambda_2'} = \frac{1}{4\pi} H_{\lambda_2,0} H^*_{\lambda_2',0} \mathcal{D}^{1/2*}_{\kappa,\lambda_2}(\Omega_2) \mathcal{D}^{1/2}_{\kappa',\lambda_2'}(\Omega_2) \, . \tag{3.86}$$

The decay matrix $b^D_{\mu\nu}$ is rewritten as

$$
\begin{aligned}
b^D_{\mu\nu} &:= \sum_{\lambda_2,\lambda_2'=-1/2}^{1/2} H_{\lambda_2,0} H^*_{\lambda_2',0} \sigma_\mu^{\lambda_2,\lambda_2'} \sigma_\nu^{\lambda_2',\lambda_2} \\
&= |H_{-1/2,0}|^2 \sigma_\mu^{-1/2,-1/2} \sigma_\nu^{-1/2,-1/2} + |H_{1/2,0}|^2 \sigma_\mu^{1/2,1/2} \sigma_\nu^{1/2,1/2} \\
&\quad + H_{1/2,0} H^*_{-1/2,0} \sigma_\mu^{1/2,-1/2} \sigma_\nu^{-1/2,1/2} + H_{-1/2,0} H^*_{1/2,0} \sigma_\mu^{-1/2,1/2} \sigma_\nu^{1/2,-1/2}
\end{aligned}
\tag{3.87}
$$

or

$$
b^D_{\mu\nu} \propto \begin{pmatrix} 1 & 0 & 0 & \alpha_D \\ 0 & \gamma_D & -\beta_D & 0 \\ 0 & \beta_D & \gamma_D & 0 \\ \alpha_D & 0 & 0 & 1 \end{pmatrix}
\tag{3.88}
$$

where

$$\alpha_D = |H_{1/2,0}|^2 - |H_{-1/2,0}|^2; \quad |H_{1/2,0}|^2 + |H_{-1/2,0}|^2 = 1, \tag{3.89}$$

$$\beta_D = 2\Im(H_{1/2,0} H^*_{-1/2,0}); \quad \gamma_D = 2\Re(H_{1/2,0} H^*_{-1/2,0}) \, . \tag{3.90}$$

IV.c $B_1 \to B_2\gamma^* \to B_2 l^+ l^-$

The decay matrices for the $B_1 \to B_2\gamma^* \to B_2 l^+ l^-$ electromagnetic decay can be obtained by simplifying the hadronic tensor by setting to zero all form factors except for $H^V_{\frac{1}{2}1} = H^V_{-\frac{1}{2}-1}$ and $H^V_{\frac{1}{2}0} = H^V_{-\frac{1}{2}0}$ that are non-zero in this parity-conserving process. The decay $\gamma^* \to l^- l^+$ is described in the $\mathbb{R}_\gamma$ frame where the emission angles of the l^- lepton are θ_l and ϕ_l. The value of the lepton momentum in this frame is

$$|\mathbf{p}_l| = \frac{\sqrt{q^2 - 4m_l^2}}{2} \, . \tag{3.91}$$

The leptonic tensor for the γ^* decay $\lambda_\gamma = \{-1, 0, 1\}$ with the lepton helicities summed over is:

$$L_{\lambda_\gamma, \lambda_\gamma'}(q^2, \Omega_l) := \sum_{\lambda_+ = -1/2}^{1/2} \sum_{\lambda_- = -1/2}^{1/2} \langle \Omega_-, \lambda_-, \lambda_+ | S_l |, q^2, \lambda_\gamma' \rangle^* \langle \Omega_-, \lambda_-, \lambda_+ | S_l | q^2, \lambda_\gamma \rangle \quad (3.92)$$

$$= \sum_{\lambda_+ = -1/2}^{1/2} \sum_{\lambda_- = -1/2}^{1/2} |h^l_{\lambda_+ \lambda_-}(q^2)|^2 \mathcal{D}^{1*}_{\lambda_\gamma, \lambda_- - \lambda_+}(\Omega_l) \mathcal{D}^1_{\lambda_\gamma', \lambda_- - \lambda_+}(\Omega_l) \quad (3.93)$$

$$= e^{i(\lambda_\gamma - \lambda_\gamma')\phi_l} \sum_{\lambda_+ = -1/2}^{1/2} \sum_{\lambda_- = -1/2}^{1/2} |h^l_{\lambda_+ \lambda_-}(q^2)|^2 d^1_{\lambda_\gamma, \lambda_- - \lambda_+}(\theta_l) d^1_{\lambda_\gamma', \lambda_- - \lambda_+}(\theta_l) .$$
$$(3.94)$$

The moduli squared of $h^l_{\lambda_- \lambda_+}$ corresponding to the vertex $\bar{u}(p_z, \lambda_-)\gamma^\mu v(-p_z, \lambda_+)\epsilon_\mu$ calculated using the charged-lepton spinor representation from Appendix in Ref. [180] are:

$$\text{nonflip}(\lambda_\gamma = \mp 1) : \ |h^l_{\lambda_- = \mp\frac{1}{2}, \lambda_+ = \pm\frac{1}{2}}|^2 = 2q^2, \quad (3.95)$$

$$\text{flip}(\lambda_\gamma = 0) : \ |h^l_{\lambda_- = \pm\frac{1}{2}, \lambda_+ = \pm\frac{1}{2}}|^2 = 4m_l^2. \quad (3.96)$$

The resulting leptonic tensor reads

$$L_{\lambda_\gamma, \lambda_\gamma'}(q^2, \Omega_l) =$$

$$= \left(q^2 - 4m_l^2\right) \begin{pmatrix} \cos^2\theta_l & -\sqrt{2}e^{-i\phi_l}\sin\theta_l\cos\theta_l & e^{-2i\phi_l}\sin^2\theta_l \\ -\sqrt{2}e^{i\phi_l}\sin\theta_l\cos\theta_l & -\cos 2\theta_l & \sqrt{2}e^{-i\phi_l}\sin\theta_l\cos\theta_l \\ e^{2i\phi_l}\sin^2\theta_l & \sqrt{2}e^{i\phi_l}\sin\theta_l\cos\theta_l & \cos^2\theta_l \end{pmatrix}$$

$$+ \left(q^2 + 4m_l^2\right)\text{diag}(1, 1, 1) .$$
$$(3.97)$$

The differential decay rate of the unpolarized baryon B_1 in the electromagnetic conversion process where the spins of all final particles are summed is

$$d\Gamma \propto \frac{\alpha_{\text{em}}^2}{q^2} V_{Ph}(q^2) \left(1 - \frac{4m_l^2}{q^2}\right) b_{00}^{\text{em}} dq d\Omega_2 d\Omega_l , \quad (3.98)$$

where $V_{Ph}(q^2)$ is the three-body phase space density factor given by the product of the momenta $|\mathbf{p}_2|$ and $|\mathbf{p}_l|$ of the baryon B_2 and the lepton, given in Eqs. (3.8) and (3.91), respectively. The unrotated decay matrix can be obtained adapting (3.40):

$$b_{\mu\nu}^{\text{em}} := \frac{1}{2(q^2 - 4m_l^2)} \sum_{\lambda_\gamma, \lambda_\gamma' = -1,0} \sum_{\lambda_2, \lambda_2' = -1/2}^{1} H_{\lambda_2 \lambda_\gamma} H^*_{\lambda_2' \lambda_\gamma'} \mathcal{T}_{\mu\nu}^{\lambda_\gamma, \lambda_\gamma', \lambda_2, \lambda_2'} . \quad (3.99)$$

Its elements are

$$
b_{\mu\nu}^{\text{em}} = \begin{pmatrix}
b_{00}^{\text{em}} & b_{01}^{\text{em}} & b_{02}^{\text{em}} & 0 \\
b_{01}^{\text{em}} & b_{11}^{\text{em}} & b_{12}^{\text{em}} & b_{13}^{\text{em}} \\
b_{02}^{\text{em}} & b_{12}^{\text{em}} & b_{22}^{\text{em}} & b_{23}^{\text{em}} \\
0 & -b_{13}^{\text{em}} & -b_{23}^{\text{em}} & b_{33}^{\text{em}}
\end{pmatrix},
\tag{3.100}
$$

where

$$
\begin{aligned}
b_{00}^{\text{em}} &= \left[\cos^2\theta_l + \frac{q^2 + 4m_l^2}{q^2 - 4m_l^2} \right] |H_{\frac{1}{2}1}^V|^2 + 2 \left[\sin^2\theta_l + \frac{4m_l^2}{q^2 - 4m_l^2} \right] |H_{\frac{1}{2}0}^V|^2, \\
b_{33}^{\text{em}} &= -\left[\cos^2\theta_l + \frac{q^2 + 4m_l^2}{q^2 - 4m_l^2} \right] |H_{\frac{1}{2}1}^V|^2 + 2 \left[\sin^2\theta_l + \frac{4m_l^2}{q^2 - 4m_l^2} \right] |H_{\frac{1}{2}0}^V|^2, \\
b_{01}^{\text{em}} &= -\sqrt{2} \sin 2\theta_l \sin\phi_l \, \Im(H_{\frac{1}{2}1}^V H_{\frac{1}{2}0}^{V*}), \\
b_{02}^{\text{em}} &= -\sqrt{2} \sin 2\theta_l \cos\phi_l \, \Im(H_{\frac{1}{2}1}^V H_{\frac{1}{2}0}^{V*}), \\
b_{11}^{\text{em}} &= \cos 2\phi_l \sin^2\theta_l |H_{\frac{1}{2}1}^V|^2 + 2 \left[\sin^2\theta_l + \frac{4m_l^2}{q^2 - 4m_l^2} \right] |H_{\frac{1}{2}0}^V|^2, \\
b_{22}^{\text{em}} &= -\cos 2\phi_l \sin^2\theta_l |H_{\frac{1}{2}1}^V|^2 + 2 \left[\sin^2\theta_l + \frac{4m_l^2}{q^2 - 4m_l^2} \right] |H_{\frac{1}{2}0}^V|^2, \\
b_{12}^{\text{em}} &= -\sin 2\phi_l \sin^2\theta_l |H_{\frac{1}{2}1}^V|^2, \\
b_{23}^{\text{em}} &= -\sqrt{2} \sin 2\theta_l \sin\phi_l \, \Re(H_{\frac{1}{2}1}^V H_{\frac{1}{2}0}^{V*}), \\
b_{13}^{\text{em}} &= \sqrt{2} \sin 2\theta_l \cos\phi_l \, \Re(H_{\frac{1}{2}1}^V H_{\frac{1}{2}0}^{V*}) .
\end{aligned}
\tag{3.101}
$$

Decay plane aligned parameters reduce to the following form

$$
b_{\mu\nu}^{\text{em}} = \begin{pmatrix}
b_{00}^{\text{em}} & 0 & b_{02}^{\text{em}} & 0 \\
0 & b_{11}^{\text{em}} & 0 & b_{13}^{\text{em}} \\
b_{02}^{\text{em}} & 0 & b_{22}^{\text{em}} & 0 \\
0 & -b_{13}^{\text{em}} & 0 & b_{33}^{\text{em}}
\end{pmatrix},
\tag{3.102}
$$

where in the real form factors limit additionally the term b_{02}^{em} vanishes. Thus, no polarization is induced, but the initial polarization and spin correlations of the baryon B_1 are transferred to the daughter baryon.

IV.d $B_1 \to B_2[V^* \to P_1 P_2]$

Here we consider a decay of a spin-1/2 baryon to a spin-1/2 baryon and a pair of pseudoscalar mesons P_1 and P_2 via an intermediate vector meson, V e.g. $B_1 \to B_2\rho^0 \to \pi^+\pi^-$. The decay matrices are obtained as in Appendix IV.c by replacing the dilepton with the pseudoscalars, and the virtual photon with a massive vector meson decaying strongly. Since the initial baryon decays weakly into the intermediate state $B_1 \to B_2 V^*$, all vector and axial vector form factors should be used. The decay $V^*(q) \to P_1(m_1, \mathbf{p}_\pi)P_2(m_2, -\mathbf{p}_\pi)$ is described in the $\mathbb{R}_V$ frame where the emission angles of the P_1 pseudoscalar are θ_π and ϕ_π. The value of the momentum

$\mathbf{p}_\pi$ is

$$|\mathbf{p}_\pi| = \sqrt{\frac{q^4 + m_2^4 + m_1^4 - 2q^2 m_1^2 - 2q^2 m_2^2 - 2m_1^2 m_2^2}{4q^2}} \ . \tag{3.103}$$

The tensor for the $V^* \to P_1 P_2$ decay for the helicities $\lambda_V, \lambda'_V = \{-1, 0, 1\}$ is:

$$\mathfrak{H}_{\lambda_V \lambda'_V}(\Omega_\pi) := e^{i(\lambda_V - \lambda'_V)\phi_\pi}|h^V|^2 d^1_{\lambda_V,0}(\theta_\pi) d^1_{\lambda'_V,0}(\theta_\pi) \ , \tag{3.104}$$

where h^V is a constant and it can be absorbed as a normalization factor. The resulting tensor reads

$$\mathfrak{H}_{\lambda_V \lambda'_V}(\Omega_\pi) = \begin{pmatrix} \frac{\sin^2 \theta_\pi}{2} & \frac{e^{-i\phi_\pi}\sin\theta_\pi \cos\theta_\pi}{\sqrt{2}} & -\frac{e^{-2i\phi_\pi}}{2}\sin^2\theta_\pi \\ \frac{e^{i\phi_\pi}\sin\theta_\pi \cos\theta_\pi}{\sqrt{2}} & \cos^2\theta_\pi & -\frac{e^{-i\phi_\pi}\sin\theta_\pi \cos\theta_\pi}{\sqrt{2}} \\ -\frac{e^{2i\phi_\pi}}{2}\sin^2\theta_\pi & -\frac{e^{i\phi_\pi}\sin\theta_\pi \cos\theta_\pi}{\sqrt{2}} & \frac{\sin^2\theta_\pi}{2} \end{pmatrix} . \tag{3.105}$$

The unrotated decay matrix can be obtained by replacing the leptonic tensor with the tensor $\mathfrak{H}_{\lambda_V, \lambda'_V}$ in (3.40):

$$b^V_{\mu\nu} := \sum_{\lambda_V, \lambda'_V = -1}^{1} H_{\lambda_2 \lambda_V} H^*_{\lambda'_2 \lambda'_V} \mathcal{T}^{\lambda_V, \lambda'_V, \lambda_2, \lambda'_2}_{\mu\nu} \ . \tag{3.106}$$

Its elements are

$$b^V_{00} = \left(|H_{\frac{1}{2}0}|^2 + |H_{-\frac{1}{2}0}|^2\right)\cos^2\theta_\pi + \frac{1}{2}\left(|H_{\frac{1}{2}1}|^2 + |H_{-\frac{1}{2}-1}|^2\right)\sin^2\theta_\pi,$$

$$b^V_{01} = \mathfrak{R}(\mathcal{A})\cos\phi_\pi + \mathfrak{I}(\mathcal{A})\sin\phi_\pi,$$

$$b^V_{02} = \mathfrak{I}(\mathcal{A})\cos\phi_\pi - \mathfrak{R}(\mathcal{A})\sin\phi_\pi,$$

$$b^V_{03} = \left(|H_{\frac{1}{2}0}|^2 - |H_{-\frac{1}{2}0}|^2\right)\cos^2\theta_\pi + \frac{1}{2}\left(|H_{\frac{1}{2}1}|^2 - |H_{-\frac{1}{2}-1}|^2\right)\sin^2\theta_\pi,$$

$$b^V_{10} = \mathfrak{R}(\mathcal{B})\cos\phi_\pi + \mathfrak{I}(\mathcal{B})\sin\phi_\pi,$$

$$b^V_{20} = \mathfrak{I}(\mathcal{B})\cos\phi_\pi - \mathfrak{R}(\mathcal{B})\sin\phi_\pi,$$

$$b^V_{11} = \mathfrak{R}(\mathcal{C}) - \mathfrak{R}(\mathcal{D})\cos 2\phi_\pi - \mathfrak{I}(\mathcal{D})\sin 2\phi_\pi,$$

$$b^V_{12} = \mathfrak{I}(\mathcal{C}) - \mathfrak{I}(\mathcal{D})\cos 2\phi_\pi + \mathfrak{R}(\mathcal{D})\sin 2\phi_\pi,$$

$$b^V_{21} = -\mathfrak{I}(\mathcal{C}) - \mathfrak{I}(\mathcal{D})\cos 2\phi_\pi + \mathfrak{R}(\mathcal{D})\sin 2\phi_\pi, \tag{3.107}$$

$$b^V_{22} = \mathfrak{R}(\mathcal{C}) + \mathfrak{R}(\mathcal{D})\cos 2\phi_\pi + \mathfrak{I}(\mathcal{D})\sin 2\phi_\pi,$$

$$b^V_{13} = -\mathfrak{R}(\mathcal{E})\cos\phi_\pi - \mathfrak{I}(\mathcal{E})\sin\phi_\pi,$$

$$b^V_{23} = -\mathfrak{I}(\mathcal{E})\cos\phi_\pi + \mathfrak{R}(\mathcal{E})\sin\phi_\pi,$$

$$b^V_{30} = \left(|H_{\frac{1}{2}0}|^2 - |H_{-\frac{1}{2}0}|^2\right)\cos^2\theta_\pi - \frac{1}{2}\left(|H_{\frac{1}{2}1}|^2 - |H_{-\frac{1}{2}-1}|^2\right)\sin^2\theta_\pi,$$

$$b^V_{31} = \mathfrak{R}(\mathcal{F})\cos\phi_\pi + \mathfrak{I}(\mathcal{F})\sin\phi_\pi,$$

$$b^V_{32} = \mathfrak{I}(\mathcal{F})\cos\phi_\pi - \mathfrak{R}(\mathcal{F})\sin\phi_\pi,$$

$$b^V_{33} = \left(|H_{\frac{1}{2}0}|^2 + |H_{-\frac{1}{2}0}|^2\right)\cos^2\theta_\pi - \frac{1}{2}\left(|H_{\frac{1}{2}1}|^2 + |H_{-\frac{1}{2}-1}|^2\right)\sin^2\theta_\pi,$$

with

$$\mathcal{A} = \sqrt{2}\cos\theta_\pi\sin\theta_\pi\left(H^*_{\frac{1}{2}0}H_{-\frac{1}{2}-1} - H^*_{\frac{1}{2}1}H_{-\frac{1}{2}0}\right), \tag{3.108}$$

$$\mathcal{B} = \sqrt{2}\cos\theta_\pi\sin\theta_\pi\left(H^*_{-\frac{1}{2}0}H_{-\frac{1}{2}-1} - H^*_{\frac{1}{2}1}H_{\frac{1}{2}0}\right), \tag{3.109}$$

$$C = 2H^*_{\frac{1}{2}0}H_{-\frac{1}{2}0}\cos^2\theta_\pi, \tag{3.110}$$

$$\mathcal{D} = H^*_{\frac{1}{2}1}H_{-\frac{1}{2}-1}\sin^2\theta_\pi, \tag{3.111}$$

$$\mathcal{E} = \sqrt{2}\cos\theta_\pi\sin\theta_\pi\left(H^*_{-\frac{1}{2}0}H_{-\frac{1}{2}-1} + H^*_{\frac{1}{2}1}H_{\frac{1}{2}0}\right), \tag{3.112}$$

$$\mathcal{F} = \sqrt{2}\cos\theta_\pi\sin\theta_\pi\left(H^*_{\frac{1}{2}0}H_{-\frac{1}{2}-1} + H^*_{\frac{1}{2}1}H_{-\frac{1}{2}0}\right). \tag{3.113}$$

Decay plane aligned parameters reduce to the following form

$$b^V_{\mu\nu} = \begin{pmatrix} b^V_{00} & \Re(\mathcal{A}) & \Im(\mathcal{A}) & b^V_{03} \\ \Re(\mathcal{B}) & \Re(C-\mathcal{D}) & \Im(C-\mathcal{D}) & -\Re(\mathcal{E}) \\ \Im(\mathcal{B}) & -\Im(C+\mathcal{D}) & \Re(C+\mathcal{D}) & -\Im(\mathcal{E}) \\ b^V_{30} & \Re(\mathcal{F}) & \Im(\mathcal{F}) & b^V_{33} \end{pmatrix}. \tag{3.114}$$

The differential decay rate of the process with unpolarized baryon B_1 and the spins of B_2 summed over is

$$d\Gamma \propto V_{Ph}(q^2)b^V_{00}dq\,d\Omega_2\,d\Omega_\pi\,, \tag{3.115}$$

where $V_{Ph}(q^2)$ is the three-body phase space density factor given by the product of the momenta $|\mathbf{p}_2|$ and $|\mathbf{p}_\pi|$.

Summary of the third chapter

- Semileptonic decay of $Y\bar{Y}$ pairs are investigated. This analysis refers to the potential signal using the data statistics collected by current e^+e^- colliders with an unpolarized beam of electrons (e.g. BESIII).

- The semileptonic transition amplitude between spin-1/2 baryons, with a final-state dilepton, is derived in the helicity formalism. Using the helicity rotation, the complete semileptonic decay matrix for a $J = 1/2$ $B\bar{B}$ pair is presented.

- The JAD for the semileptonic transition of the spin-entangled $Y\bar{Y}$ is obtained. This is a first-time result, as previously this formalism had been applied only to hadronic decays.

- The JAD is employed in the approximate maximum likelihood method to compute the statistical uncertainties for the SL form factors. Several hyperon decays are studied, using the most recent results on hyperon–antihyperon production from BESIII.

- The spin correlation within the pair significantly affects the extracted uncertainties, offering a new approach to semileptonic decay studies. In particular, including the information from the production process shows a better precision for the SL FFs, for a similar number of events.

- The angular dependence of the semileptonic decay matrix on the final baryon spherical angle is isolated and generalized to spin-1/2 baryon–baryon transitions with various final-state bosons.

4

Summary and Outlook

This thesis collects my research work on hyperon decays and their properties. This chapter outlines the findings of this research and includes discussions of future directions.

Hyperons are three-quark bound states made of combinations of the three lightest flavors, *u, d,* and *s*, with at least one *s* quark. That is to say, any baryon with a non-zero value of the "strangeness" quantum number, by definition. The descriptor 'strange particles' originates at the time of their discovery, being long-lived particles created in strong flavor-conserving processes. Both interactions are relevant to the discussion carried out in this thesis.

Electromagnetism has been vastly utilized as a probe for investigating the structure of matter, e.g., in fixed-target experiments involving the nucleons. In this setup, the nucleon EM form factors have been widely studied in the space-like q^2 regime. The shorter lifetimes of hyperons make them unsuitable for such an investigation: instead, they offer complementary information via e^+e^- annihilation into $Y\bar{Y}$ pairs. There, hyperon EM form factors are investigated in the time-like kinematical region, which can be linked to the space-like form factors exploiting analyticity and crossing symmetry. Such FFs are complex-valued, and the relative phase between them results in the polarization of the produced pair. The baryon and antibaryon are also spin-entangled, a feature that improves the uncertainty determination of observables deriving from the weak decays of the pair. The research included in this dissertation is focused on weak hyperon decays, when the mother particles are produced in spin-entangled pairs through electron–positron annihilation.

The polarization of the EM-produced $Y\bar{Y}$ is retrieved by studying the subsequent decays of the hyperons. It is measured via the anisotropic distribution of the final-state particles, in nonleptonic decays. Independent measurements of baryon and antibaryon decay asymmetries are accessible by employing the spin-correlation of the pair. The asymmetries are then compared to construct tests of direct CP violation.

The first study, in Chapter 2, describes the impact of a longitudinally polarized beam of electrons on the decay studies. The spin-correlation matrix for the $e^+e^- \rightarrow Y\bar{Y}$ reaction gains additional elements directly proportional to the beam polarization, particularly for the

(anti)hyperon polarization vector. The statistical uncertainties of the CPV observables are significantly reduced for hyperons produced with a longitudinally polarized electron beam. With this improvement, envisioned at the next-generation e^+e^- colliders, the observed CPV signal has the potential to reach the strength of the SM predictions.

Next-generation electron–positron colliders, known as Super τ-charm factories (STCF), offer higher statistics at J/ψ energies. As an increased luminosity is not enough to reach the SM CPV signal, the electron beam polarization has also been discussed as an additional improvement to these facilities. This is the starting point of our feasibility study, where we assume a dataset of 10^{12} J/ψ events and evaluate the effects of a longitudinally polarized beam of electrons on the statistical uncertainties of the hyperon CPV observables.

This research involves the use of a modular framework to describe the production process and the decay chains: with the appropriate modifications, it can be applied to other sources of polarized hyperons. For example, charm baryons nonleptonic or semileptonic decays involving a daughter hyperon are produced in large numbers in proton–proton collisions at the LHC. This situation would be the case of single polarized (anti)hyperons, also discussed in Chapter 2. Here, the polarization vectors are assumed to have a fixed magnitude.

Charm baryons can also be produced in e^+e^- colliders. The beam polarization-dependent production matrix is extracted without any assumptions on the flavor content of the produced pair, only on their spin. This formalism would apply to charm baryon–antibaryon pairs in a straightforward manner, provided that they are spin-1/2 baryons. Charm pairs are being produced at the BEPCII collider, with the world's first threshold data on the $\Lambda_c^+\bar{\Lambda}_c^-$ pair collected in 2014 [181]. However, as I show in Chapter 2, the viability of such an inquiry hinges on the spin-correlation information, retrievable via the DT reconstruction method. Nonleptonic decays of charm baryons have too small branching fractions to be employed successfully in a similar analysis. A focused strategy incorporating the envisioned enhancements for STCFs may effectively tackle the issue, providing a framework for the direct application of our results.

Chapter 3 focuses on the semileptonic decays of spin-correlated baryon–antibaryon produced at e^+e^- colliders with an unpolarized electron beam. The derived SL "decay" matrix represents the transition between two $J = 1/2$ baryons, where the mother particle decays into the daughter semileptonically. That is combined with the information from the production process to obtain the joint angular distribution, in the same manner as in Chapter 2. Using the asymptotic maximum likelihood method, the Fisher information matrix for the SL form factor parameters is obtained.

The spin-correlation effects are shown to have a non-negligible influence on the extracted uncertainties, a conclusion shared by the work in Chapter 2. Currently, our results are being employed in the extraction of the hyperon SL FFs from the data collected by the BESIII collaboration. A significant increase in the number of events, e.g. from the luminosity enhancement planned in STCFs, will improve the statistical precision of the SL form factor parameters. As in the previous study, an extension would entail the inclusion of a longitudinally polarized e^- beam and studies of the impact of beam polarization on the SL FF parameter uncertainties. Moreover, the generic nature of this approach enables its direct application to spin-entangled

$J = 1/2$ charm baryon–antibaryon pairs.

Finally, the decay matrix is decomposed to isolate its dependence from the spherical angle defined in the mother helicity frame. The remaining amplitude contains information on the SL transition, that can be easily modified to depict scenarios of $J = 1/2 \rightarrow 1/2$ baryon decays emitting different final-state bosons. Among the detailed examples, the case of nonleptonic decay (a final pseudoscalar) is obtained, along with the matrix for a pseudoscalar pair production via a vector meson resonance. Radiative and Dalitz decays are also discussed, with the latter being currently utilized in a BESIII analysis of transitions between Σ^0 and Λ hyperons with a dilepton pair.

The main feature of both works is the generic nature of the formulae derived therein. Possible extensions of both works would involve spin-3/2 baryons, by changing the spin basis in which to expand the production matrix for one or both (anti)baryons with $J = 3/2$. This would entail expanding the already derived production matrices [52] for processes with a longitudinally polarized electron beam. Likewise, the SL decay matrix would be derived after replacing the initial baryon with a spin-3/2 mother particle – keeping the final state to a spin-1/2 baryon and a virtual W boson. From there, the aforementioned examples of aligned decay matrices should be obtained with a similar procedure as in Chapter 3.

Studies on nonleptonic hyperon decays are worth mentioning as an extension of the decays investigated in Chapter 2. The revised value of the Λ decay asymmetry [65] calls for an update of the nonleptonic transition amplitudes. From the new hyperon data, one can extract the latest values for the two contributions to the decay amplitude, of opposite behavior under parity transformation. These partial-wave amplitudes have been previously calculated in chiral perturbation theory (χPT), up to one-loop corrections in the non-relativistic limit. Since the first publication on the topic in the 1980s [182], different approaches to deriving such corrections have been taken, and the theoretical framework has been updated to favor a relativistic approach. I am currently working on producing first-time calculations of such l-wave amplitudes in relativistic χPT, including contributions from the spin-3/2 decuplet baryons and resonance saturation effects, to provide the best fitting description of hyperon nonleptonic decays.

The works presented in this thesis differ in the used methodology or the investigated case study, however, they share the common aim to showcase the potential of hyperon studies. Overall, in this era of increasing interest in hadron physics and high-precision measurements, hyperon decays have proved to be an invaluable tool in providing a deeper insight into our understanding of the laws of nature and the structure of matter.

Bibliography

[1] W.K. Tung. *Group Theory in Physics*. World Scientific, 1985. ISBN: 978-9-971-96656-0.

[2] D. Griffiths. *Introduction to Elementary Particles*. Wiley, 2008. ISBN: 978-3-527-40601-2.

[3] M. Srednicki. *Quantum field theory*. Cambridge University Press, 2007.

[4] G. D. Rochester and C. C. Butler. Evidence for the Existence of New Unstable Elementary Particles. *Nature* 160 (1947), pp. 855–857. DOI: 10.1038/160855a0.

[5] C. F. Powell. Mesons. *Reports on Progress in Physics* 13.1 (Jan. 1950), p. 350. DOI: 10.1088/0034-4885/13/1/309. URL: https://dx.doi.org/10.1088/0034-4885/13/1/309.

[6] H. L. Anderson et al. Total Cross-sections of Positive Pions in Hydrogen. *Phys. Rev.* 85 (1952), p. 936. DOI: 10.1103/PhysRev.85.936.

[7] A. Pais. Some Remarks on the V-Particles. *Phys. Rev.* 86 (1952), pp. 663–672. DOI: 10.1103/PhysRev.86.663.

[8] M. Gell-Mann. Isotopic Spin and New Unstable Particles. *Phys. Rev.* 92 (1953), pp. 833–834. DOI: 10.1103/PhysRev.92.833.

[9] T. Nakano and K. Nishijima. Charge Independence for V-particles. *Prog. Theor. Phys.* 10 (1953), pp. 581–582. DOI: 10.1143/PTP.10.581.

[10] M. Gell-Mann. The Eightfold Way: A Theory of strong interaction symmetry. *Report No. CTSL-20, TID-12608* (1961). DOI: 10.2172/4008239.

[11] Y. Ne'eman. Derivation of strong interactions from a gauge invariance. *Nucl. Phys.* 26 (1961), pp. 222–229. DOI: 10.1016/0029-5582(61)90134-1.

[12] M. Gell-Mann. Symmetries of baryons and mesons. *Phys. Rev.* 125 (1962), pp. 1067–1084. DOI: 10.1103/PhysRev.125.1067.

[13] G. Zweig. An SU(3) model for strong interaction symmetry and its breaking. *Report No. CERN-TH-401* (1964).

[14] M. Gell-Mann. A Schematic Model of Baryons and Mesons. *Phys. Lett.* 8 (1964), pp. 214–215. DOI: 10.1016/S0031-9163(64)92001-3.

[15] W. Pauli. Über den Zusammenhang des Abschlusses der Elektronengruppen im Atom mit der Komplexstruktur der Spektren. *Z. Phys.* 31.1 (1925), pp. 765–783. DOI: 10.1007/BF02980631.

[16] V. E. Barnes et al. Observation of a Hyperon with Strangeness Minus Three. *Phys. Rev. Lett.* 12 (1964), pp. 204–206. DOI: 10.1103/PhysRevLett.12.204.

[17]   O. W. Greenberg. Spin and Unitary Spin Independence in a Paraquark Model of Baryons and Mesons. *Phys. Rev. Lett.* 13 (1964), pp. 598–602. DOI: `10.1103/PhysRevLett.13.598`.

[18]   O. W. Greenberg and D. Zwanziger. Saturation in Triplet Models of Hadrons. *Phys. Rev.* 150 (1966), pp. 1177–1180. DOI: `10.1103/PhysRev.150.1177`.

[19]   H. Fritzsch, M. Gell-Mann, and H. Leutwyler. Advantages of the Color Octet Gluon Picture. *Phys. Lett. B* 47 (1973), pp. 365–368. DOI: `10.1016/0370-2693(73)90625-4`.

[20]   M. E. Peskin and D. V. Schroeder. *An Introduction to quantum field theory*. Addison-Wesley, 1995.

[21]   R. L. Workman et al. Review of Particle Physics. *PTEP* 2022 (2022), p. 083C01. DOI: `10.1093/ptep/ptac097`.

[22]   D.J. Gross and F. Wilczek. Ultraviolet Behavior of Nonabelian Gauge Theories. *Phys. Rev. Lett.* 30 (1973). Ed. by J. C. Taylor, pp. 1343–1346. DOI: `10.1103/PhysRevLett.30.1343`.

[23]   H.D. Politzer. Reliable Perturbative Results for Strong Interactions? *Phys. Rev. Lett.* 30 (1973). Ed. by J. C. Taylor, pp. 1346–1349. DOI: `10.1103/PhysRevLett.30.1346`.

[24]   R. Alkofer and J. Greensite. Quark Confinement: The Hard Problem of Hadron Physics. *J. Phys. G* 34 (2007), S3. DOI: `10.1088/0954-3899/34/7/S02`.

[25]   E. Fermi. An attempt of a theory of beta radiation. *Z. Phys.* 88 (1934), pp. 161–177. DOI: `10.1007/BF01351864`.

[26]   C. S. Wu et al. Experimental Test of Parity Conservation in β Decay. *Phys. Rev.* 105 (1957), pp. 1413–1414. DOI: `10.1103/PhysRev.105.1413`.

[27]   R. P. Feynman and M. Gell-Mann. Theory of Fermi interaction. *Phys. Rev.* 109 (1958), pp. 193–198. DOI: `10.1103/PhysRev.109.193`.

[28]   E. C. G. Sudarshan and R. e. Marshak. Chirality invariance and the universal Fermi interaction. *Phys. Rev.* 109 (1958), pp. 1860–1860. DOI: `10.1103/PhysRev.109.1860.2`.

[29]   N. Cabibbo. Unitary Symmetry and Leptonic Decays. *Phys. Rev. Lett.* 10 (1963), pp. 531–533. DOI: `10.1103/PhysRevLett.10.531`.

[30]   C.N. Yang and Robert L. Mills. Conservation of Isotopic Spin and Isotopic Gauge Invariance. *Phys. Rev.* 96 (1954), pp. 191–195. DOI: `10.1103/PhysRev.96.191`.

[31]   Gerard 't Hooft and M. J. G. Veltman. Regularization and Renormalization of Gauge Fields. *Nucl. Phys. B* 44 (1972), pp. 189–213. DOI: `10.1016/0550-3213(72)90279-9`.

[32]   S. Weinberg. A Model of Leptons. *Phys. Rev. Lett.* 19 (1967), pp. 1264–1266. DOI: `10.1103/PhysRevLett.19.1264`.

[33]   A. Salam. Weak and Electromagnetic Interactions. *Conf. Proc. C* 680519 (1968), pp. 367–377. DOI: `10.1142/9789812795915_0034`.

[34]   P. W. Higgs. Broken Symmetries and the Masses of Gauge Bosons. *Phys. Rev. Lett.* 13 (1964), pp. 508–509. DOI: `10.1103/PhysRevLett.13.508`.

[35] F. Englert and R. Brout. Broken Symmetry and the Mass of Gauge Vector Mesons. *Phys. Rev. Lett.* 13 (1964), pp. 321–323. DOI: 10.1103/PhysRevLett.13.321.

[36] C. E. Carlson. Electromagnetic $N - \Delta$ transition at high Q^2. *Phys. Rev. D* 34 (1986), p. 2704. DOI: 10.1103/PhysRevD.34.2704.

[37] V. Punjabi et al. The Structure of the Nucleon: Elastic Electromagnetic Form Factors. *Eur. Phys. J. A* 51 (2015), p. 79. DOI: 10.1140/epja/i2015-15079-x.

[38] B. Kubis and U. G. Meissner. Baryon form-factors in chiral perturbation theory. *Eur. Phys. J. C* 18 (2001), pp. 747–756. DOI: 10.1007/s100520100570.

[39] D.R. Yennie, M.M. Lévy, and D.G. Ravenhall. Electromagnetic Structure of Nucleons. *Rev. Mod. Phys.* 29.1 (1957), p. 144. DOI: 10.1103/RevModPhys.29.144.

[40] R.G. Sachs. High-Energy Behavior of Nucleon Electromagnetic Form Factors. *Phys. Rev.* 126 (1962), pp. 2256–2260. DOI: 10.1103/PhysRev.126.2256.

[41] J.Z. Bai et al. Decays of the J/ψ to $\Lambda\overline{\Lambda}$, $\Lambda\overline{\Lambda}\gamma$ and $\Lambda\overline{\Lambda}\pi^0$ final states. *Phys. Lett. B* 424 (1998). [Erratum: Phys.Lett.B 438, 447–448 (1998)], pp. 213–218. DOI: 10.1016/S0370-2693(98)00171-3.

[42] M. Ablikim et al. Measurement of J/psi decays into Lambda anti-Lambda pi+ pi-. *Chin. Phys. C* 36 (2012), pp. 1031–1039. DOI: 10.1088/1674-1137/36/11/001.

[43] M. Ablikim et al. Study of J/ψ and $\psi(3686)$ decay to $\Lambda\bar{\Lambda}$ and $\Sigma^0\bar{\Sigma}^0$ final states. *Phys. Rev. D* 95.5 (2017), p. 052003. DOI: 10.1103/PhysRevD.95.052003.

[44] M. Ablikim et al. Design and Construction of the BESIII Detector. *Nucl. Instrum. Meth. A* 614 (2010), pp. 345–399. DOI: 10.1016/j.nima.2009.12.050.

[45] G. Fäldt and A. Kupsc. Hadronic structure functions in the $e^+e^- \to \bar{\Lambda}\Lambda$ reaction. *Phys. Lett. B* 772 (2017), pp. 16–20. DOI: 10.1016/j.physletb.2017.06.011.

[46] A. Z. Dubnickova, S. Dubnicka, and M. P. Rekalo. Investigation of the nucleon electromagnetic structure by polarization effects in e+ e- —> N anti-N processes. *Nuovo Cim. A* 109 (1996), pp. 241–256. DOI: 10.1007/BF02731012.

[47] N. Salone et al. Study of CP violation in hyperon decays at super-charm-tau factories with a polarized electron beam. *Phys. Rev. D* 105.11 (2022), p. 116022. DOI: 10.1103/PhysRevD.105.116022.

[48] J.J. Sakurai and J. Napolitano. *Modern Quantum Mechanics*. Quantum physics, quantum information and quantum computation. Cambridge University Press, Oct. 2020. ISBN: 978-1-108-47322-4. DOI: 10.1017/9781108587280.

[49] M. Jacob and G. C. Wick. On the General Theory of Collisions for Particles with Spin. *Annals Phys.* 7 (1959), pp. 404–428. DOI: 10.1006/aphy.2000.6022.

[50] M.G. Doncel et al. Properties of polarization density matrix in Regge pole models. *Phys. Rev. D* 7 (1973), pp. 815–835. DOI: 10.1103/PhysRevD.7.815.

[51] M.G. Doncel, L. Michel, and P. Minnaert. Rigorous spin tests from usual strong decays. *Nucl. Phys. B* 38 (1972), pp. 477–528. DOI: 10.1016/0550-3213(72)90321-5.

[52] E. Perotti et al. Polarization observables in e^+e^- annihilation to a baryon-antibaryon pair. *Phys. Rev. D* 99.5 (2019), p. 056008. DOI: 10.1103/PhysRevD.99.056008.

[53] E. Wigner. Einige Folgerungen aus der Schrödingerschen Theorie für die Termstrukturen. *Z. Phys.* 43 (1927), pp. 624–652. DOI: 10.1007/BF01397327.

[54] F. Tabakin and R.A. Eisenstein. Meson Exchange Calculation of the $\bar{p}p \to \bar{\Lambda}\Lambda$ Reaction. *Phys. Rev. C* 31 (1985), p. 1857. DOI: 10.1103/PhysRevC.31.1857.

[55] G. Fäldt. Polarization observables in the $e^+e^- \to \bar{\Lambda}\Lambda$ reaction. *Eur. Phys. J. A* 52.5 (2016), p. 141. DOI: 10.1140/epja/i2016-16141-y.

[56] J.H. Christenson et al. Evidence for the 2π Decay of the K_2^0 Meson. *Phys. Rev. Lett.* 13 (1964), pp. 138–140. DOI: 10.1103/PhysRevLett.13.138.

[57] B. Aubert et al. Observation of CP violation in the B^0 meson system. *Phys. Rev. Lett.* 87 (2001), p. 091801. DOI: 10.1103/PhysRevLett.87.091801.

[58] K. Abe et al. Observation of large CP violation in the neutral B meson system. *Phys. Rev. Lett.* 87 (2001), p. 091802. DOI: 10.1103/PhysRevLett.87.091802.

[59] A. Poluektov et al. Evidence for direct CP violation in the decay $B\pm \to D^{(*)}K\pm$, $D \to K_S^0\pi^+\pi^-$ and measurement of the CKM phase phi3. *Phys. Rev. D* 81 (2010), p. 112002. DOI: 10.1103/PhysRevD.81.112002.

[60] R. Aaij et al. Observation of CP Violation in Charm Decays. *Phys. Rev. Lett.* 122.21 (2019), p. 211803. DOI: 10.1103/PhysRevLett.122.211803.

[61] M. Kobayashi and T. Maskawa. CP Violation in the Renormalizable Theory of Weak Interaction. *Prog. Theor. Phys.* 49 (1973), pp. 652–657. DOI: 10.1143/PTP.49.652.

[62] A.D. Sakharov. Violation of CP Invariance, C asymmetry, and baryon asymmetry of the universe. *Pisma Zh. Eksp. Teor. Fiz.* 5 (1967), pp. 32–35. DOI: 10.1070/PU1991v034n05ABEH002497.

[63] E.D. Commins and P.H. Bucksbaum. *Weak Interactions of Leptons and Quarks*. Cambridge University Press, 1983. ISBN: 978-0-521-27370-1.

[64] C.-Z. Yuan and S.L. Olsen. The BESIII physics programme. *Nature Rev. Phys.* 1.8 (2019), pp. 480–494. DOI: 10.1038/s42254-019-0082-y.

[65] M. Ablikim et al. Polarization and Entanglement in Baryon-Antibaryon Pair Production in Electron-Positron Annihilation. *Nature Phys.* 15 (2019), pp. 631–634. DOI: 10.1038/s41567-019-0494-8.

[66] N. Cabibbo, E.C. Swallow, and R. Winston. Semileptonic hyperon decays. *Ann. Rev. Nucl. Part. Sci.* 53 (2003), pp. 39–75. DOI: 10.1146/annurev.nucl.53.013103.155258.

[67] V.A. Kuzmin, V.A. Rubakov, and M.E. Shaposhnikov. On the Anomalous Electroweak Baryon Number Nonconservation in the Early Universe. *Phys. Lett. B* 155 (1985), p. 36. DOI: 10.1016/0370-2693(85)91028-7.

[68] M.E. Shaposhnikov. Standard model solution of the baryogenesis problem. *Phys. Lett. B* 277 (1992). [Erratum: Phys.Lett.B 282, 483 (1992)], pp. 324–330. DOI: 10.1016/0370-2693(92)90753-Q.

[69] B. Aubert et al. Observation of CP violation in the B^0 meson system. *Phys. Rev. Lett.* 87 (2001), p. 091801. DOI: 10.1103/PhysRevLett.87.091801.

[70] K. Abe et al. Observation of large CP violation in the neutral B meson system. *Phys. Rev. Lett.* 87 (2001), p. 091802. DOI: 10.1103/PhysRevLett.87.091802.

[71] A.J. Buras et al. The $B \rightarrow piK$ puzzle and its relation to rare B and K decays. *Eur. Phys. J. C* 32 (2003), pp. 45–54. DOI: `10.1140/epjc/s2003-01379-9`.

[72] R. Aaij et al. Observation of CP Violation in Charm Decays. *Phys. Rev. Lett.* 122.21 (2019), p. 211803. DOI: `10.1103/PhysRevLett.122.211803`.

[73] J.R. Batley et al. A Precision measurement of direct CP violation in the decay of neutral kaons into two pions. *Phys. Lett. B* 544 (2002), pp. 97–112. DOI: `10.1016/S0370-2693(02)02476-0`.

[74] A. Alavi-Harati et al. Measurements of direct CP violation, CPT symmetry, and other parameters in the neutral kaon system. *Phys. Rev. D* 67 (2003). [Erratum: Phys.Rev.D 70, 079904 (2004)], p. 012005. DOI: `10.1103/PhysRevD.70.079904`.

[75] E. Abouzaid et al. Precise Measurements of Direct CP Violation, CPT Symmetry, and Other Parameters in the Neutral Kaon System. *Phys. Rev. D* 83 (2011), p. 092001. DOI: `10.1103/PhysRevD.83.092001`.

[76] A.J. Buras. The ε/ε-story: 1976–2021. *Acta Physica Polonica B* 52.1 (2021), p. 7. ISSN: 1509-5770. DOI: `10.5506/aphyspolb.52.7`. URL: `http://dx.doi.org/10.5506/APhysPolB.52.7`.

[77] Z. Bai et al. Standard Model Prediction for Direct CP Violation in K→$\pi\pi$ Decay. *Phys. Rev. Lett.* 115.21 (2015), p. 212001. DOI: `10.1103/PhysRevLett.115.212001`.

[78] R. Abbott et al. Direct CP violation and the $\Delta I = 1/2$ rule in $K \rightarrow \pi\pi$ decay from the standard model. *Phys. Rev. D* 102.5 (2020), p. 054509. DOI: `10.1103/PhysRevD.102.054509`.

[79] H. Gisbert and A. Pich. Direct CP violation in $K^0 \rightarrow \pi\pi$: Standard Model Status. *Rept. Prog. Phys.* 81.7 (2018), p. 076201. DOI: `10.1088/1361-6633/aac18e`.

[80] J. Aebischer, C. Bobeth, and A.J. Buras. ε'/ε in the Standard Model at the Dawn of the 2020s. *Eur. Phys. J. C* 80.8 (2020), p. 705. DOI: `10.1140/epjc/s10052-020-8267-1`.

[81] S. Okubo. Decay of the Sigma+ Hyperon and its Antiparticle. *Phys. Rev.* 109 (1958), pp. 984–985. DOI: `10.1103/PhysRev.109.984`.

[82] A. Pais. Notes on Antibaryon Interactions. *Phys. Rev. Lett.* 3 (1959), pp. 242–244. DOI: `10.1103/PhysRevLett.3.242`.

[83] T. Brown, S.F. Tuan, and S. Pakvasa. CP Nonconservation in Hyperon Decays. *Phys. Rev. Lett.* 51 (1983), p. 1823. DOI: `10.1103/PhysRevLett.51.1823`.

[84] L.-L. Chau and H.-Y. Cheng. Partial Rate Differences From CP Violation in Hyperon Nonleptonic Decays. *Phys. Lett. B* 131 (1983), pp. 202–208. DOI: `10.1016/0370-2693(83)91121-8`.

[85] J.F. Donoghue and S. Pakvasa. Signals of CP Nonconservation in Hyperon Decay. *Phys. Rev. Lett.* 55 (1985), p. 162. DOI: `10.1103/PhysRevLett.55.162`.

[86] J.F. Donoghue, X.-G. He, and S. Pakvasa. Hyperon Decays and CP Nonconservation. *Phys. Rev. D* 34 (1986), p. 833. DOI: `10.1103/PhysRevD.34.833`.

[87] T. D. Lee and C.-N. Yang. General Partial Wave Analysis of the Decay of a Hyperon of Spin 1/2. *Phys. Rev.* 108 (1957), pp. 1645–1647. DOI: `10.1103/PhysRev.108.1645`.

[88]   P.M. Ho et al. Measurement of the polarization and magnetic moment of Anti-xi+
        anti-hyperons produced by 800-GeV/c protons. *Phys. Rev. D* 44 (1991), pp. 3402–
        3418. DOI: 10.1103/PhysRevD.44.3402.

[89]   R.A. Burnstein et al. HyperCP: A High-rate spectrometer for the study of charged
        hyperon and kaon decays. *Nucl. Instrum. Meth. A* 541 (2005), pp. 516–565. DOI: 10.
        1016/j.nima.2004.12.031.

[90]   J. Tandean and G. Valencia. CP violation in hyperon nonleptonic decays within the
        standard model. *Phys. Rev. D* 67 (2003), p. 056001. DOI: 10.1103/PhysRevD.67.
        056001.

[91]   T. Holmstrom et al. Search for CP violation in charged-Xi and Lambda hyperon de-
        cays. *Phys. Rev. Lett.* 93 (2004), p. 262001. DOI: 10.1103/PhysRevLett.93.
        262001.

[92]   P.A. Zyla et al. Review of Particle Physics. *PTEP* 2020.8 (2020), p. 083C01. DOI:
        10.1093/ptep/ptaa104.

[93]   N. Cabibbo and R. Gatto. Electron Positron Colliding Beam Experiments. *Phys. Rev.*
        124 (1961), pp. 1577–1595. DOI: 10.1103/PhysRev.124.1577.

[94]   M. Ablikim et al. Polarization and Entanglement in Baryon-Antibaryon Pair Produc-
        tion in Electron-Positron Annihilation. *Nature Phys.* 15 (2019), pp. 631–634. DOI:
        10.1038/s41567-019-0494-8.

[95]   M. Ablikim et al. Weak phases and CP-symmetry tests in sequential decays of entan-
        gled double-strange baryons. *Nature* 606 (2022), pp. 64–69. DOI: 10.1038/s41586-
        022-04624-1.

[96]   Q. Luo and D. Xu. Progress on Preliminary Conceptual Study of HIEPA, a Super
        Tau-Charm Factory in China. *9th International Particle Accelerator Conference*. June
        2018. DOI: 10.18429/JACoW-IPAC2018-MOPML013.

[97]   E.B. Levichev et al. Electron–positron beam collision studies at the Budker Institute
        of Nuclear Physics. *Phys. Usp.* 61.5 (2018), pp. 405–423. DOI: 10.3367/UFNe.
        2018.01.038300.

[98]   M.-H. Ye and Z.-P. Zheng. BEPC, THE BEIJING ELECTRON POSITRON COL-
        LIDER. *Int. J. Mod. Phys. A* 2 (1987), pp. 1707–1725. DOI: 10.1142/S0217751X87000880.

[99]   A. Renieri. Possibility of Achieving Very High-Energy Resolution in electron-Positron
        Storage Rings. LNF-75/6-R. Feb. 1975.

[100]   A.A. Avdienko et al. THE PROJECT OF MODERNIZATION OF THE VEPP-4
        STORAGE RING FOR MONOCHROMATIC EXPERIMENTS IN THE ENERGY
        RANGE OF PSI AND UPSILON MESONS. *Conf. Proc. C* 830811 (1983). Ed. by
        F.T. Cole and R. Donaldson. Contribution to: HEACC83, pp. 186–189.

[101]   V.I. Telnov. Monochromatization of e^+e^- colliders with a large crossing angle. Aug.
        2020. arXiv: 2008.13668 [physics.acc-ph].

[102]   I.A. Koop, A.V. Bogomyagkov, and A.V. Otboev. Longitudinal Polarization in Novosi-
        birsk c-tau factory. *Joint Workshop on Future charm-tau Factory*. Sept. 2019. URL:
        https://c-tau.ru/indico/event/3/contributions/206/.

[103] A. Kupsc. Hyperon physics at SCTF with polarized beams. *Joint Workshop on Future charm-tau Factory*. Sept. 2019. URL: https://c-tau.ru/indico/event/3/contributions/206/.

[104] A. Bondar et al. Measurement of the weak mixing angle at a Super Charm-Tau factory with data-driven monitoring of the average electron beam polarization. *JHEP* 03 (2020), p. 076. DOI: 10.1007/JHEP03(2020)076.

[105] P. Adlarson and A. Kupsc. CP symmetry tests in the cascade-anticascade decay of charmonium. *Phys. Rev. D* 100.11 (2019), p. 114005. DOI: 10.1103/PhysRevD.100.114005.

[106] D.G. Ireland et al. Kaon Photoproduction and the Λ Decay Parameter α_-. *Phys. Rev. Lett.* 123.18 (2019), p. 182301. DOI: 10.1103/PhysRevLett.123.182301.

[107] R. Handler et al. PRECISE MEASUREMENT OF THE ASYMMETRY PARAMETER IN THE DECAY XI0 —> LAMBDA PI0. *Phys. Rev. D* 25 (1982), pp. 639–651. DOI: 10.1103/PhysRevD.25.639.

[108] J.R. Batley et al. New Precise Measurements of the $\Xi^0 -> \Lambda\gamma$ and $\Xi^0 -> \Sigma^0\gamma$ Decay Asymmetries. *Phys. Lett. B* 693 (2010), pp. 241–248. DOI: 10.1016/j.physletb.2010.08.046.

[109] M. Huang et al. New measurement of Xi- —> Lambda pi- decay parameters. *Phys. Rev. Lett.* 93 (2004), p. 011802. DOI: 10.1103/PhysRevLett.93.011802.

[110] W.E. Cleland et al. A measurement of the beta-parameter in the charged nonleptonic decay of the lambda0 hyperon. *Nucl. Phys. B* 40 (1972), pp. 221–254. DOI: 10.1016/0550-3213(72)90544-5.

[111] O.E. Overseth and R.F. Roth. Time Reversal Invariance in Lambda0 Decay. *Phys. Rev. Lett.* 19 (1967), pp. 391–393. DOI: 10.1103/PhysRevLett.19.391.

[112] J.W. Cronin and O.E. Overseth. Measurement of the decay parameters of the Lambda0 particle. *Phys. Rev.* 129 (1963), pp. 1795–1807. DOI: 10.1103/PhysRev.129.1795.

[113] M. Ablikim et al. Σ^+ and $\bar{\Sigma}^-$ polarization in the J/ψ and $\psi(3686)$ decays. *Phys. Rev. Lett.* 125.5 (2020), p. 052004. DOI: 10.1103/PhysRevLett.125.052004.

[114] F. Harris et al. Proton polarization in sigma+ —> p pi0. *Phys. Rev. Lett.* 24 (1970), pp. 165–168. DOI: 10.1103/PhysRevLett.24.165.

[115] N.H. Lipman et al. A test of the delta-i=1/2 rule and the lee-sugawara relation in the decay sigma+ —> p pi0. *Phys. Lett. B* 43 (1973), pp. 89–92. DOI: 10.1016/0370-2693(73)90551-0.

[116] V. Cirigliano et al. Isospin breaking in K —> pi pi decays. *Eur. Phys. J. C* 33 (2004), pp. 369–396. DOI: 10.1140/epjc/s2003-01579-3.

[117] M. Hoferichter et al. Roy–Steiner-equation analysis of pion–nucleon scattering. *Phys. Rept.* 625 (2016), pp. 1–88. DOI: 10.1016/j.physrep.2016.02.002.

[118] R. Nath and A. Kumar. The effect of final-state interactions on the asymmetry parameter in cascade decay processes. *Nuovo Cim* 36 (1965), pp. 669–671. DOI: 10.1007/BF02751336.

[119] M. Lu, M.B. Wise, and M.J. Savage. Strong Lambda pi phase shifts for CP violation in weak Xi —> Lambda pi decay. *Phys. Lett. B* 337 (1994), pp. 133–136. DOI: `10.1016/0370-2693(94)91456-7`.

[120] A.N. Kamal. pi Lambda scattering phase shifts and CP violation in Xi —> pi Lambda decay. *Phys. Rev. D* 58 (1998), p. 077501. DOI: `10.1103/PhysRevD.58.077501`.

[121] A. Datta, P. O'Donnell, and S. Pakvasa. Lambda - pi phase shifts in chiral perturbation theory. June 1998. arXiv: `hep-ph/9806374`.

[122] J. Tandean, A.W. Thomas, and G.E Valencia. Can the Lambda pi scattering phase shifts be large? *Phys. Rev. D* 64 (2001), p. 014005. DOI: `10.1103/PhysRevD.64.014005`.

[123] U.-G. Meissner and J.A. Oller. The S wave Lambda pi phase shift is not large. *Phys. Rev. D* 64 (2001), p. 014006. DOI: `10.1103/PhysRevD.64.014006`.

[124] B.-L. Huang et al. Meson-baryon scattering to one-loop order in heavy baryon chiral perturbation theory. *Phys. Rev. D* 96.1 (2017), p. 016021. DOI: `10.1103/PhysRevD.96.016021`.

[125] K.M. Watson. Some general relations between the photoproduction and scattering of pi mesons. *Phys. Rev.* 95 (1954), pp. 228–236. DOI: `10.1103/PhysRev.95.228`.

[126] J. Tandean. New physics and CP violation in hyperon nonleptonic decays. *Phys. Rev. D* 69 (2004), p. 076008. DOI: `10.1103/PhysRevD.69.076008`.

[127] D. Chang, X.-G. He, and S. Pakvasa. CP violation in hyperon decays due to left-right mixing. *Phys. Rev. Lett.* 74 (1995), pp. 3927–3930. DOI: `10.1103/PhysRevLett.74.3927`.

[128] X.-G. He and G. Valencia. CP violation in Lambda —> p pi- beyond the Standard Model. *Phys. Rev. D* 52 (1995), pp. 5257–5268. DOI: `10.1103/PhysRevD.52.5257`.

[129] A.J. Buras et al. Connections between epsilon-prime / epsilon and rare kaon decays in supersymmetry. *Nucl. Phys. B* 566 (2000), pp. 3–32. DOI: `10.1016/S0550-3213(99)00645-8`.

[130] X.-G. He et al. CP violation in hyperon decays from supersymmetry. *Phys. Rev. D* 61 (2000), p. 071701. DOI: `10.1103/PhysRevD.61.071701`.

[131] C.-H. Chen. CP violation in hyperon decays from SUSY with Hermitian Yukawa and A matrices. *Phys. Lett. B* 521 (2001), pp. 315–319. DOI: `10.1016/S0370-2693(01)01236-9`.

[132] V. Cirigliano et al. Isospin-violating contributions to ϵ'/ϵ. *JHEP* 02 (2020), p. 032. DOI: `10.1007/JHEP02(2020)032`.

[133] Joachim Brod, Martin Gorbahn, and Emmanuel Stamou. Standard-Model Prediction of ϵ_K with Manifest Quark-Mixing Unitarity. *Phys. Rev. Lett.* 125.17 (2020), p. 171803. DOI: `10.1103/PhysRevLett.125.171803`.

[134] J. Aebischer, A.J. Buras, and J. Kumar. Another SMEFT story: Z facing new results on ϵ'/ϵ, ΔM_K and $K \to \pi\nu\bar{\nu}$. *JHEP* 12 (2020), p. 097. DOI: `10.1007/JHEP12(2020)097`.

[135] S.R. Beane et al. Exploring hyperons and hypernuclei with lattice QCD. *Nucl. Phys. A* 747 (2005), pp. 55–74. DOI: `10.1016/j.nuclphysa.2004.09.081`.

[136] C.G. White et al. Search for direct CP violation in Lambda and Xi hyperon decays. *Nucl. Phys. B Proc. Suppl.* 71 (1999). Ed. by G. Capon et al., pp. 451–456. DOI: 10.1016/S0920-5632(98)00377-6.

[137] C. Materniak. Search for CP violation in Xi and Lambda hyperon decays with the HyperCP spectrometer at Fermilab. *Nucl. Phys. B Proc. Suppl.* 187 (2009). Ed. by Marco Bozzo et al., pp. 208–215. DOI: 10.1016/j.nuclphysbps.2009.01.030.

[138] M. Ablikim et al. Study of J/ψ and $\psi(3686)$ decay to $\Lambda\bar{\Lambda}$ and $\Sigma^0\bar{\Sigma}^0$ final states. *Phys. Rev. D* 95.5 (2017), p. 052003. DOI: 10.1103/PhysRevD.95.052003.

[139] M. Ablikim et al. First measurements of J/Psi decays into Sigma+ anti-Sigma- and Xi0 anti-Xi0. *Phys. Rev. D* 78 (2008), p. 092005. DOI: 10.1103/PhysRevD.78.092005.

[140] M. Ablikim et al. Study of J/ψ and $\psi(3686) \rightarrow \Sigma(1385)^0\bar{\Sigma}(1385)^0$ and $\Xi^0\bar{\Xi}^0$. *Phys. Lett.* B770 (2017), pp. 217–225. DOI: 10.1016/j.physletb.2017.04.048.

[141] S.J. Brodsky and G.P. Lepage. Helicity Selection Rules and Tests of Gluon Spin in Exclusive QCD Processes. *Phys. Rev. D* 24 (1981), p. 2848. DOI: 10.1103/PhysRevD.24.2848.

[142] R.A. Fisher and E.J. Russell. On the mathematical foundations of theoretical statistics. *Philosophical Transactions of the Royal Society of London. Series A.* 222.594-604 (1922), pp. 309–368. DOI: 10.1098/rsta.1922.0009. URL: https://royalsocietypublishing.org/doi/abs/10.1098/rsta.1922.0009.

[143] I.I. Bigi, X.-W. Kang, and H.-B. Li. CP Asymmetries in Strange Baryon Decays. *Chin. Phys. C* 42.1 (2018), p. 013101. DOI: 10.1088/1674-1137/42/1/013101.

[144] M. Ablikim et al. Study of ψ decays to the $\Xi^-\bar{\Xi}^+$ and $\Sigma(1385)^\mp\bar{\Sigma}(1385)^\pm$ final states. *Phys. Rev. D* 93.7 (2016), p. 072003. DOI: 10.1103/PhysRevD.93.072003.

[145] Y.B. Li et al. Measurements of the branching fractions of the semileptonic decays $\Xi_c^0 \rightarrow \Xi^-\ell^+\nu_\ell$ and the asymmetry parameter of $\Xi_c^0 \rightarrow \Xi^-\pi^+$. *Phys. Rev. Lett.* 127.12 (2021), p. 121803. DOI: 10.1103/PhysRevLett.127.121803.

[146] O.E. Overseth and S. Pakvasa. Final-state interactions in nonleptonic hyperon decay. *Phys. Rev.* 184 (1969), pp. 1663–1667. DOI: 10.1103/PhysRev.184.1663.

[147] M. Suzuki. Helicity conservation in inclusive nonleptonic decay $B \rightarrow VX$: Test of long distance final state interaction. *Phys. Rev. D* 66 (2002), p. 054018. DOI: 10.1103/PhysRevD.66.054018.

[148] J.-P. Dedonder et al. S-, P- and D-wave final state interactions and CP violation in B+- –> pi+- pi-+ pi+- decays. *Acta Phys. Polon. B* 42 (2011), p. 2013. DOI: 10.5506/APhysPolB.42.2013.

[149] D.-L. Yao et al. A review on partial-wave dynamics with chiral effective field theory and dispersion relation. *Rept. Prog. Phys.* 84.7 (2021), p. 076201. DOI: 10.1088/1361-6633/abfa6f.

[150] L.-Y. Dai and M.R. Pennington. Comprehensive amplitude analysis of $\gamma\gamma \rightarrow \pi^+\pi^-, \pi^0\pi^0$ and $\overline{K}K$ below 1.5 GeV. *Phys. Rev. D* 90.3 (2014), p. 036004. DOI: 10.1103/PhysRevD.90.036004.

[151] Y.-J. Shi, U.-G. Meißner, and Z.-X. Zhao. Resonance contributions in $B^- \to K^+K^-\pi^-$ within the light-cone sum rule approach. *Eur. Phys. J. C* 82.2 (2022), p. 113. DOI: 10.1140/epjc/s10052-022-10062-0.

[152] J.T. Daub, C. Hanhart, and B. Kubis. A model-independent analysis of final-state interactions in $\overline{B}^0_{d/s} \to J/\psi\pi\pi$. *JHEP* 02 (2016), p. 009. DOI: 10.1007/JHEP02(2016)009.

[153] R. Omnes. On the Solution of certain singular integral equations of quantum field theory. *Nuovo Cim.* 8 (1958), pp. 316–326. DOI: 10.1007/BF02747746.

[154] W. Detmold, C. Lehner, and S. Meinel. $\Lambda_b \to p\ell^-\bar{\nu}_\ell$ and $\Lambda_b \to \Lambda_c\ell^-\bar{\nu}_\ell$ form factors from lattice QCD with relativistic heavy quarks. *Phys. Rev. D* 92.3 (2015), p. 034503. DOI: 10.1103/PhysRevD.92.034503.

[155] E. Goudzovski et al. New physics searches at kaon and hyperon factories. *Rept. Prog. Phys.* 86.1 (2023), p. 016201. DOI: 10.1088/1361-6633/ac9cee.

[156] J.G. Korner and G.A. Schuler. Exclusive Semileptonic Heavy Meson Decays Including Lepton Mass Effects. *Z. Phys. C* 46 (1990), p. 93. DOI: 10.1007/BF02440838.

[157] J.G. Korner and M. Kramer. Polarization effects in exclusive semileptonic Λ_c and Λ_b charm and bottom baryon decays. *Phys. Lett. B* 275 (1992), pp. 495–505. DOI: 10.1016/0370-2693(92)91623-H.

[158] A. Kadeer, J.G. Korner, and U. Moosbrugger. Helicity analysis of semileptonic hyperon decays including lepton mass effects. *Eur. Phys. J.* C59 (2009), pp. 27–47. DOI: 10.1140/epjc/s10052-008-0801-5.

[159] M. Ablikim et al. Probing CP symmetry and weak phases with entangled double-strange baryons. *Nature* 606.7912 (2022), pp. 64–69. DOI: 10.1038/s41586-022-04624-1.

[160] R.L. Workman et al. Review of Particle Physics. *PTEP* 2022 (2022), p. 083C01. DOI: 10.1093/ptep/ptac097.

[161] J. Adler et al. Measurement of the Branching Fractions for D0 —> pi- e+ electron-neutrino and D0 —> K- e+ electron-neutrino and Determination of (V (c d) / V (c s))**2. *Phys. Rev. Lett.* 62 (1989), p. 1821. DOI: 10.1103/PhysRevLett.62.1821.

[162] M. Ablikim et al. Number of J/ψ events at BESIII. *Chin. Phys. C* 46.7 (2022), p. 074001. DOI: 10.1088/1674-1137/ac5c2e.

[163] Y.S. Amhis et al. Averages of b-hadron, c-hadron, and τ-lepton properties as of 2018. *Eur. Phys. J. C* 81.3 (2021), p. 226. DOI: 10.1140/epjc/s10052-020-8156-7.

[164] D. Becirevic and A.B. Kaidalov. Comment on the heavy —> light form-factors. *Phys. Lett. B* 478 (2000), pp. 417–423. DOI: 10.1016/S0370-2693(00)00290-2.

[165] S. Weinberg. Charge symmetry of weak interactions. *Phys. Rev.* 112 (1958), pp. 1375–1379. DOI: 10.1103/PhysRev.112.1375.

[166] P.H. Frampton and W.-K. Tung. Hyperon beta decay. *Phys. Rev. D* 3 (1971), pp. 1114–1121. DOI: 10.1103/PhysRevD.3.1114.

[167] M. Bourquin et al. Measurements of Hyperon Semileptonic Decays at the CERN Super Proton Synchrotron. 2. The $\Lambda \to pe$ Anti-neutrino, Xi- $\to \Lambda e$ Anti-neutrino, and

Xi- → $\Sigma^0 e$ Anti-neutrino Decay Modes. *Z. Phys.* C21 (1983), p. 1. DOI: 10.1007/BF01648771.

[168]   Riazuddin Marshak R.E. and Ryan C.P. *Theory of weak interactions in particle physics*. New York Wiley Interscience, 1969.

[169]   M.L. Goldberger and S.B. Treiman. Form-factors in Beta decay and muon capture. *Phys. Rev.* 111 (1958), pp. 354–361. DOI: 10.1103/PhysRev.111.354.

[170]   J.M. Gaillard and G. Sauvage. Hyperon Beta Decays. *Ann. Rev. Nucl. Part. Sci.* 34 (1984), pp. 351–402. DOI: 10.1146/annurev.ns.34.120184.002031.

[171]   M. Ablikim et al. Σ^+ and $\bar{\Sigma}^-$ polarization in the J/ψ and $\psi(3686)$ decays. *Phys. Rev. Lett.* 125.5 (2020), p. 052004. DOI: 10.1103/PhysRevLett.125.052004.

[172]   M. Ablikim et al. Study of J/ψ and $\psi(3686) \to \Sigma(1385)^0 \bar{\Sigma}(1385)^0$ and $\Xi^0 \bar{\Xi}^0$. *Phys. Lett. B* 770 (2017), pp. 217–225. DOI: 10.1016/j.physletb.2017.04.048.

[173]   M. Ablikim et al. Precise Measurements of the Decay Parameters and *CP* Asymmetries with Entangled $\Xi^0 - \bar{\Xi}^0$ Pairs (May 2023). arXiv: 2305.09218 [hep-ex].

[174]   M. Ablikim et al. Precise Measurements of Decay Parameters and *CP* Asymmetry with Entangled $\Lambda - \bar{\Lambda}$ Pairs Pairs. *Phys. Rev. Lett.* 129.13 (2022), p. 131801. DOI: 10.1103/PhysRevLett.129.131801.

[175]   S. Groote, J.G. Körner, and B. Melić. A new angle on an old problem: Helicity approach to neutron beta decay in the Standard Model. *Eur. Phys. J. C* 79.11 (2019), p. 948. DOI: 10.1140/epjc/s10052-019-7453-5.

[176]   A. Sirlin and A. Ferroglia. Radiative corrections in precision electroweak physics: A historical perspective. *Rev. Mod. Phys.* 85 (1 Feb. 2013), pp. 263–297. DOI: 10.1103/RevModPhys.85.263. URL: https://link.aps.org/doi/10.1103/RevModPhys.85.263.

[177]   A. Garcia and P. Kielanowski. THE BETA DECAY OF HYPERONS. *Lect. Notes Phys.* 222 (1985). Ed. by A. Bohm, pp. 1–173. DOI: 10.1007/3-540-15184-2.

[178]   E. Barberio and Z. Was. PHOTOS: A Universal Monte Carlo for QED radiative corrections. Version 2.0. *Comput. Phys. Commun.* 79 (1994), pp. 291–308. DOI: 10.1016/0010-4655(94)90074-4.

[179]   LHCb. Λ_c^+ polarimetry using the dominant hadronic mode (Jan. 2023). arXiv: 2301.07010 [hep-ex].

[180]   C.F. Perdrisat, V. Punjabi, and M. Vanderhaeghen. Nucleon Electromagnetic Form Factors. *Prog. Part. Nucl. Phys.* 59 (2007), pp. 694–764. DOI: 10.1016/j.ppnp.2007.05.001.

[181]   Xiao-Rui Lyu. Charmed baryon decays at BESIII. *PoS* CHARM2020 (2021), p. 016. DOI: 10.22323/1.385.0016.

[182]   J. Bijnens, H. Sonoda, and Mark B. Wise. On the Validity of Chiral Perturbation Theory for Weak Hyperon Decays. *Nucl. Phys. B* 261 (1985), pp. 185–198. DOI: 10.1016/0550-3213(85)90569-3.